

**Anatomical and functional characterization of the  
orientation network in the central and lateral  
complex of the desert locust *Schistocerca gregaria***

**Kumulative Dissertation**

zur Erlangung des Grades eines

Doktor der Naturwissenschaften

(Dr. rer. nat.)

des Fachbereichs Biologie der Philipps-Universität Marburg

Vorgelegt von

**Ronja Melanie Hensgen**

aus Köln

Marburg an der Lahn, 2022





Die vorliegende Dissertation wurde von Dezember 2015 bis April 2022 am Fachbereich der Biologie unter Leitung von Prof. Dr. Uwe Homberg angefertigt.

Vom Fachbereich Biologie der Philipps-Universität Marburg (Hochschulkennziffer 1180) als Dissertation angenommen am:

Erstgutachter: Prof. Dr. Keram Pfeiffer

Zweitgutachter: Prof. Dr. Uwe Homberg

Tag der mündlichen Prüfung:



# Content

|  |    |
|--|----|
| <b>Erklärung über eigene Beiträge und veröffentlichte Teile der Arbeit</b> ..... | 1  |
| <b>Abstract</b> .....  | 5  |
| <b>Zusammenfassung</b> .....   | 7  |
| Kapitel I.....   | 9  |
| Kapitel II.....  | 11 |
| Kapitel III .....  | 14 |
| Referenzen.....  | 16 |
| <b>Introduction</b> .....  | 21 |
| Spatial orientation and navigation in insects .....                              | 21 |
| The central complex .....  | 22 |
| Neuroanatomy of the central complex.....   | 22 |
| Neurochemistry of the central complex.....                                       | 25 |
| The head direction system .....  | 26 |
| The lateral complex .....  | 28 |
| Polarization Vision .....  | 30 |
| Polarized light .....  | 31 |
| The sky polarization pattern.....  | 32 |
| The neural pathway for polarization vision in insects .....                      | 33 |
| Scope of this work .....   | 34 |
| References .....   | 37 |
| <b>Chapter I</b> .....   | 51 |
| Abstract.....  | 53 |
| Introduction .....   | 53 |
| Materials and methods .....  | 55 |
| Results .....  | 57 |
| Discussion.....  | 61 |
| References .....   | 68 |
| <b>Chapter II</b> .....  | 71 |
| Abstract.....  | 74 |
| Introduction .....   | 75 |
| Materials and methods .....  | 77 |
| Results .....  | 82 |

|                                |     |
|--------------------------------|-----|
| Discussion.....                | 92  |
| References .....               | 101 |
| <b>Chapter III</b> .....       | 107 |
| Abstract.....                  | 109 |
| Introduction .....             | 110 |
| Materials and methods .....    | 110 |
| Results .....                  | 120 |
| Discussion.....                | 130 |
| References .....               | 133 |
| <b>Appendix</b> .....          | 137 |
| Zusätzliche Publikationen..... | 137 |
| Curriculum vitae .....         | 139 |
| <b>Danksagung</b> .....        | 143 |
| <b>Erklärung</b> .....         | 144 |

## **Erklärung über eigene Beiträge und veröffentlichte Teile der Arbeit**

Im Folgenden sind meine eigenen Beiträge zu den gemeinsam verfassten Veröffentlichungen/Manuskripten (Kapitel I bis III) aufgeführt.

### **Kapitel I: Performance of polarization-sensitive neurons of the locust central complex at different degrees of polarization**

Dieses Kapitel wurde in der hier vorliegenden Form beim *Journal of Comparative Physiology A* veröffentlicht: Hensgen, R., Zittrell, F., Pfeiffer, K., Homberg, U. (2022) Performance of polarization-sensitive neurons of the locust central complex at different degrees of polarization. DOI: 10.1007/s00359-022-01545-2

- Konzeption der Studie in Zusammenarbeit mit Prof. Dr. Uwe Homberg und Prof. Dr. Keram Pfeiffer
- Durchführung aller 49 Experimente (Präparation, intrazelluläre Ableitung, histologische Aufarbeitung und Auswertung mittels konfokaler Mikroskopie)
- Konzeption der Auswertung und statistischen Analyse der physiologischen Daten zusammen mit Dr. Frederick Zittrell und Prof. Dr. Uwe Homberg
- Durchführung der Auswertung der physiologischer Daten mittels der von Dr. Frederick Zittrell verfassten MATLAB-Kodierung
- Anfertigung der Abbildungen, wobei die Graphen in Figure 4-7 durch die von Dr. Frederick Zittrell erstellten MATLAB-Kodierung generiert wurden
- Anfertigung es Manuskripts in Zusammenarbeit mit Prof. Dr. Uwe Homberg und Dr. Frederick Zittrell

### **Kapitel II: Myoinhibitory peptides in the central complex of the locust *Schistocerca gregaria* and colocalization with locustatachykinin-related peptides**

Dieses Kapitel wurde am 18.01.2022 zur Veröffentlichung beim *Journal of Comparative Neurology* eingereicht als: Hensgen, R., Dippel, S., Hümmert, S., Jahn, S., Seyfarth, J., Homberg, U. Myoinhibitory peptides in the central complex of the locust *Schistocerca gregaria* and colocalization with locustatachykinin-related peptides

- Konzeption der Studie in Zusammenarbeit mit Prof. Dr. Uwe Homberg

- Durchführung aller Einzelzellmarkierungen für Figure 5, 9 und 12
- Durchführung der immunzytochemischen Färbungen für Figure 5, 9, 11 und 12 sowie deren Auswertung mittels konfokaler Mikroskopie
- Anfertigung der 3-dimensionalen Rekonstruktionen für Figure 3
- Anfertigung der 2-dimensionalen Rekonstruktion für Figure 9a
- Betreuung und Anleitung der Studierenden Sophie Hümmert und Stefanie Jahn, die im Rahmen ihrer Bachelorarbeiten einen Teil der immunzytochemischen Färbungen anfertigten
- Auswertung und Interpretation aller immunzytochemischer Daten in Zusammenarbeit mit Prof. Dr. Uwe Homberg
- Anfertigung der Abbildungen für Figure 3-12
- Anfertigung des Manuskriptes in Zusammenarbeit mit Prof. Dr. Uwe Homberg und Dr. Stefan Dippel

### **Kapitel III: Organization and neural connections of the lateral complex in the brain of the desert locust**

Dieses Kapitel wurde in der hier vorliegenden Form beim *Journal of Comparative Neurology* veröffentlicht: Hensgen, R., Göthe, J., Jahn, S., Hümmert, S., Schneider, K. L., Takahashi, N., Pegel, U., Gotthardt, S., Homberg, U. (2021) Organization and neural connections of the lateral complex in the brain of the desert locust. DOI: 10.1002/cne.25209

- Konzeption der Studie in Zusammenarbeit mit Prof. Dr. Uwe Homberg
- Durchführung der Einzelzellmarkierungen für Figure 2c, 3 und 4f
- Anfertigung der 3-dimensionalen Rekonstruktionen für Figure 1, 3, 4f, 6f, 9,12, 14 und 15d
- Anfertigung der 2-dimensionalen Rekonstruktion für Figure 10d
- Analyse und Überarbeitung der 2-dimensionalen Rekonstruktionen für Figure 7 und 8
- Betreuung, Anleitung und teilweise praktische Unterstützung des Studierenden Jonas Göthe, der im Rahmen seiner Bachelorarbeit die Einzelzellmarkierungen und die immunzytochemische Aufarbeitung der Präparate für Figure 6, 8d-f, 13 und 14 durchführte, sowie die 3-dimensionalen Rekonstruktionen für Figure 6a, 8d, 10a, 13a und 15a anfertigte
- Betreuung und Anleitung der Studierenden Stefanie Jahn, Sophie Hümmert und Kim Lucia Schneider, die im Rahmen ihrer Bachelorarbeit immunzytochemische

Färbungen für Figure 1a,c, 2, 4b,c, 5f und 15e,f durchführten und 3-dimensionale Rekonstruktionen für Figure 2 und 4d anfertigten

- Aufnahme der Daten für Figure 3, 4e,g, und 5 mittels konfokaler Mikroskopie sowie Anleitung und Betreuung der Aufnahme der Daten für Figure 1a,c, 2b,d, 4b,c, 6, 8e,f, 12b,c, 13, 14, 15e,f mittels konfokaler Mikroskopie
- Auswertung der Daten und Anfertigung aller Abbildungen
- Anfertigung des Manuskripts in Zusammenarbeit mit Prof. Dr. Uwe Homberg





## Abstract

Spatial orientation is an indispensable basis of many behaviors that ensure the survival of an individual or a species. Foraging, finding mating partners, avoiding predators or developing new habitats rely on this ability. Insects show sophisticated skills for spatial orientation and navigation. These abilities require integration of external and internal stimuli that provide information about the animal's own position in space or relative to an object. Under the open sky the sun is – even for humans – a prominent orientation cue that can be utilized for orientation by many insect species. Additionally, other celestial cues - that are not perceptible by humans - can be detected and used by insects. One of these is the polarization pattern of the sky that results from scattering of unpolarized sunlight in the earth's atmosphere. It is characterized by the systematic arrangement of the prevailing plane of oscillation of polarized light (angle of polarization, AoP) and depends on the position of the sun. The degree of polarization (DoP) that indicates the percentage of polarized light within a light beam also depends on the sun's position. In the insect brain, the AoP is encoded by the activity of polarization-sensitive neurons that transmit this information from the compound eyes into the central brain, where it is used to generate an internal compass. The internal compass is represented by the activity of neuronal populations of the central complex (CX), a navigation center that processes orientation-relevant information and is involved in the generation of appropriate locomotor responses. The CX comprises four midline spanning neuropils in the center of the brain; the protocerebral bridge (PB), the lower division of the central body (CBL; also known as ellipsoid body, EB, in flies) the upper division of the central body (CBU; also known as fan-shaped body, FB, in flies) and the paired noduli (NO). The neuropils are characterized by vertical columns (or slices) and horizontal layers that result from the neuronal projections of the neuron systems that constitute the CX. Arborizations of tangential neurons establish distinct layers and arborizations of columnar and pontine neurons result in distinct columns. Beside polarization information the neuronal network of the CX also integrates other information that underlies context- and experience dependent behavior. Another brain region, the lateral complex (LX) plays a major role in mediating information flow to and from the CX. The LX is located in both hemispheres laterally from the CX and consists of the lateral accessory lobe (LAL) with the associated gall and the bulb. A variety of neuron types connects the LX and the CX and provides connections between the LX and other brain regions as well as the thoracic ganglia.

The present thesis investigates the physiology of polarization-sensitive neurons of the CX and the anatomical organization of the CX and the LX of the desert locust *Schistocerca*

*gregaria* (Figure I). Electrophysiological experiments were performed to investigate the influence of the DoP on the coding of the AoP by polarization-sensitive neurons of the CX (**Chapter I**). They revealed that even low DoPs allow a reliable coding of AoPs in the locust brain. However, DoPs under a certain threshold result in a strong modulation of the activity of neurons at the input stage of the CX. Neuron types within the CX are characterized in addition to their physiology and morphology by the expression of neurotransmitters and neuropeptides. Immunocytochemical stainings revealed the expression pattern of myoinhibitory peptide (MIP) in the CX (**Chapter II**). We identified and characterized five MIP-expressing neuronal systems comprising cell types that have so far been identified mainly based on single-cell labeling. The combination of single-cell labelings and immunocytochemical stainings revealed potential feedback loops between cell types of the CX and the LX and were used to identify and describe novel cell types of the LAL (**Chapter III**).

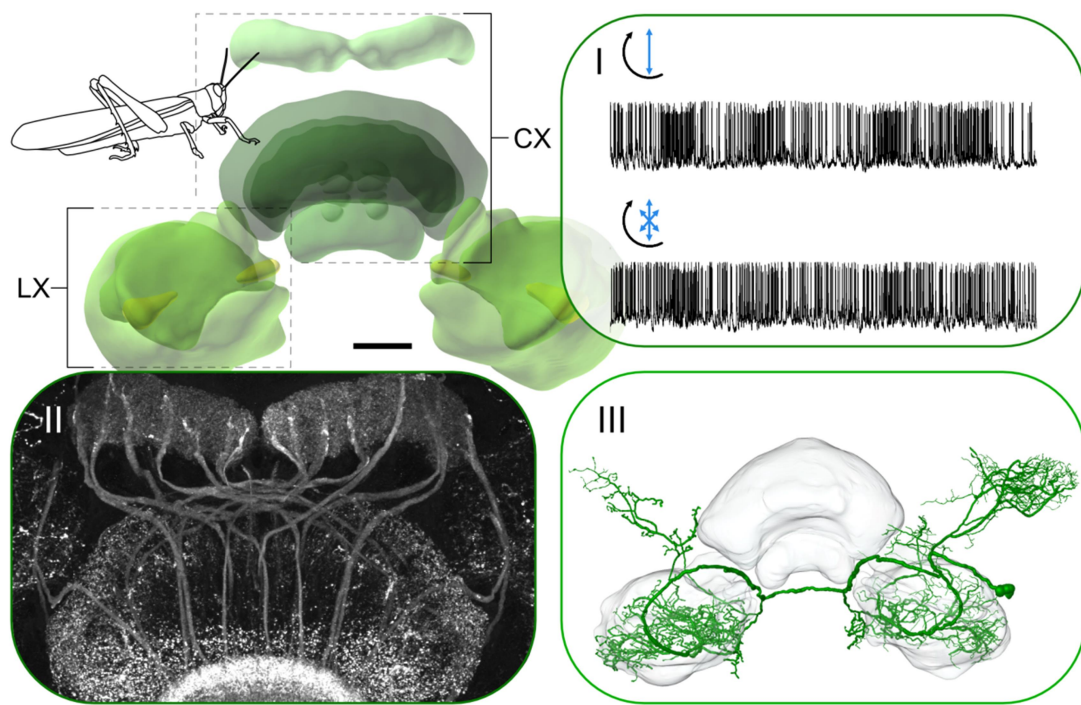


**Figure I** Schematic summary of chapters **I-III**. This thesis examines the neural networks of the central complex (CX) and the lateral complex (LX) that underlie spatial orientation in the desert locust *Schistocerca gregaria*. Chapter **I** investigates the physiological properties of CX neurons upon stimulation with polarized light of different degrees of polarization. Chapter **II** focuses on the morphology of specific neuron sets that comprise the CX. Chapter **III** explores connectivity motifs between the CX and the LX as well as the intrinsic organization of the lateral accessory lobe of the LX. Scale bar = 100  $\mu\text{m}$

## Zusammenfassung

Die räumliche Orientierung bildet eine unverzichtbare Grundlage vieler Verhaltensweisen, die das Überleben eines Individuums oder einer Art sichern. Die Suche nach Nahrung, nach Artgenossen zur Fortpflanzung, das Vermeiden von Fressfeinden oder das Erschließen neuer Lebensräume basieren auf dieser Fähigkeit. Insekten verfügen über ausgeprägte Fertigkeiten zur räumlichen Orientierung und Navigation. Diese setzen die Verarbeitung externer und interner Stimuli voraus, welche Aufschluss über die eigene Position im Raum oder relativ zu einem Objekt geben. Unter freiem Himmel stellt die Sonne - auch für uns Menschen - einen markanten Stimulus dar, der vielen Insekten zur Orientierung dient. Aber auch andere Himmelssignale, die für uns nicht wahrnehmbar sind, können von Insekten genutzt werden. Dazu zählt das Polarisationsmuster des Himmels, das durch die Streuung des Sonnenlichts in der Atmosphäre entsteht. Es ist von der Sonnenposition abhängig und durch die systematische Anordnung der vorherrschenden Schwingungsrichtungen des polarisierten Lichts, der Polarisationswinkel (*angle of polarization*, AoP), gekennzeichnet. Der Polarisationsgrad (*degree of polarization*, DoP) variiert ebenfalls in Abhängigkeit von der Sonnenposition und gibt das Verhältnis der Intensität polarisierten Lichts zur Gesamtintensität des Lichts an. Im Insektengehirn wird der AoP in der Aktivität polarisations-sensitiver Zellen kodiert und über mehrere Verarbeitungsstationen vom Komplexauge bis in das Zentralhirn geleitet, in dem die Polarisationsinformation zur Generierung eines internen Kompasses genutzt wird. Dieser Kompass spiegelt sich in der Aktivität von Neuronenpopulationen des Zentralkomplexes (*central complex*, CX) wider, einem Navigationszentrum, das Orientierungsreize verarbeitet und an der Generierung adäquater motorischer Antworten beteiligt ist. Der CX umfasst vier im Zentralhirn gelegene Neuropile, die Protozerebralbrücke (PB), die obere Einheit des Zentralkörpers (CBU; in Fliegen auch als fächerförmiger Körper, FB, bezeichnet), die untere Einheit des Zentralkörpers (CBL; in Fliegen auch als Ellipsoid-Körper, EB, bezeichnet), sowie die paarigen Noduli (NO). Die Neuropile des CX sind in vertikalen Kolumnen und horizontalen Schichten organisiert, die sich durch die Projektionen unterschiedlicher Neuronensysteme ergeben. Durch die Verzweigungen tangentialer Neurone ergeben sich die Schichten, und durch die Verzweigungen kolumnärer und pontiner Neurone ergeben sich die Kolumnen. Im CX werden neben der Polarisationsinformation auch andere Informationen verarbeitet, die kontext- und erfahrungsabhängigem Verhalten zu Grunde liegen. Eine Vielzahl der Eingänge und Ausgänge des CX wird dabei durch eine weitere Struktur im Gehirn, den lateralen Komplex (LX) vermittelt. Der LX liegt in beiden Gehirnhemisphären

lateral zum CX, er umfasst den lateralen akzessorischen Lobus (LAL) mit dem *gall*, sowie den Bulbus. Unterschiedliche Neuronensysteme verbinden den LX mit dem CX, sowie den LX mit umliegenden Gehirnarealen und auch den Thorakalganglien.

Die vorliegende Arbeit beschäftigt sich mit der Physiologie polarisations-sensitiver Neurone des CX, sowie der anatomischen Organisation des CX und des LX der Wüstenheuschrecke, *Schistocerca gregaria* (Abbildung I). In **Kapitel I** wurden elektrophysiologische Methoden verwendet, um zu untersuchen, welchen Einfluss der DoP auf die Kodierung des AoP durch polarisations-sensitive Zellen des CX hat. Wir konnten zeigen, dass auch niedrige DoPs eine verlässliche Kodierung des AoP im Heuschreckengehirn ermöglichen. Unter einer bestimmten Schwelle liegende DoPs allerdings führen zu einer starken Modulation der Aktivität in der Eingangsebene des CX. Zelltypen des CX sind nicht nur durch ihre Physiologie und Morphologie, sondern auch durch ihre Neurotransmitter- und Peptidzusammensetzung gekennzeichnet. In **Kapitel II** wurde das Expressionsmuster des myoinhibitorischen Peptids (MIP) im CX untersucht. Es konnten fünf MIP-exprimierende Neuronensysteme identifiziert und genauer charakterisiert werden, die bisher vorwiegend auf der Basis von Einzelzellmarkierungen beschrieben waren. **Kapitel III** befasst sich mit der anatomischen Organisation des LX und untersucht spezifische Verbindungen zwischen LX und CX. Durch die Kombination von Einzelzellmarkierungen mit immunzytochemischen Färbungen wurden potentielle Rückkopplungsschleifen zwischen CX und LX bestimmt, sowie neue Zelltypen des LAL identifiziert und morphologisch charakterisiert.

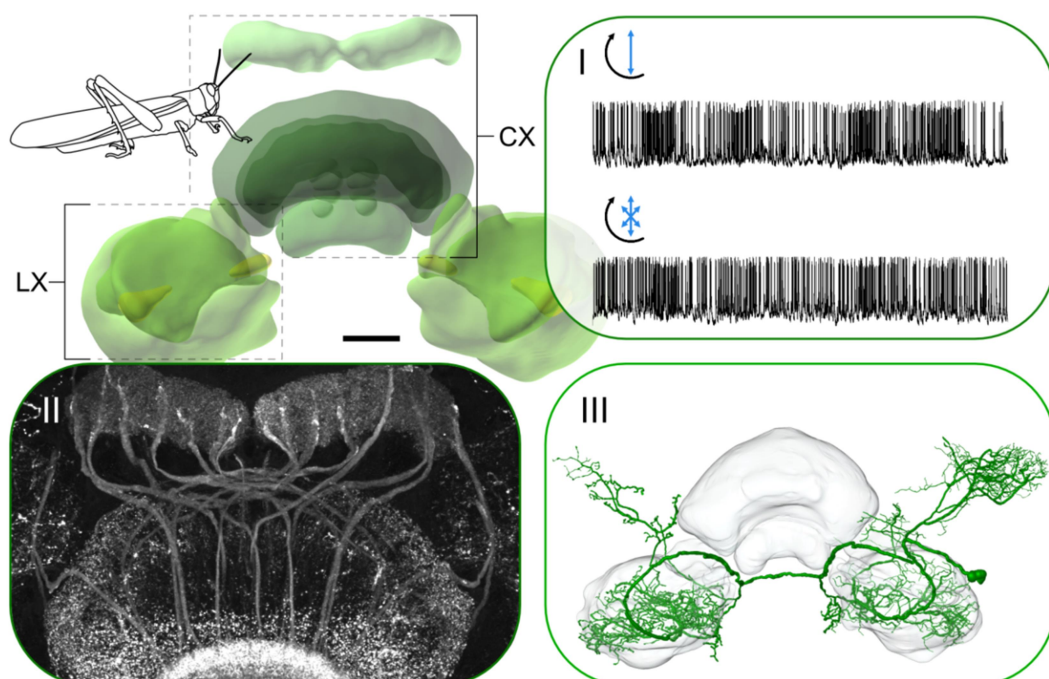


**Abbildung I** Schematische Zusammenfassung von Kapitel I-III. Diese Arbeit untersucht die neuronalen Netzwerke des Zentralkomplexes (CX) und lateralen Komplexes (LX), die der räumlichen Orientierung in der Wüstenheuschrecke *Schistocerca gregaria* zugrunde liegen. Kapitel I untersucht physiologische Eigenschaften von Neuronen des CX während der Stimulation mit polarisiertem Licht unterschiedlicher Polarisationsgrade. Kapitel II konzentriert sich auf die Morphologie spezifischer Neuronentypen des CX. Kapitel III erforscht Verbindungen zwischen dem CX und dem LX, sowie die intrinsische Organisation des lateralen akzessorischen Lobus des LX. Maßstabsbalken = 100  $\mu\text{m}$

## Kapitel I

Das Polarisationsmuster des Himmels, das durch die Streuung von unpolarisiertem Sonnenlicht in der Atmosphäre entsteht, bietet vielen Insekten die Möglichkeit zur Orientierung (Übersichtsartikel: Wehner, 1989; Homberg et al., 2011; Horváth, 2014). Zwei Parameter polarisierten Lichts sind seine Schwingungsebene (der Polarisationswinkel, *angle of polarization*, AoP) und der Polarisationsgrad (*degree of polarization*, DOP; Brines & Gould, 1982; Pomozi et al., 2001). Am Himmel variieren beide Parameter systematisch in Abhängigkeit von der Sonnenposition und lassen so einen Rückschluss auf diese zu. Die Aktivität polarisations-sensitiver Neurone im Insektengehirn ändert sich in Abhängigkeit vom AoP des einfallenden Lichts. Die Stimulation mit Licht, das durch einen linearen Polarisator zu ca. 99 % polarisiert wird, führt bei Drehung des Polarisators und damit einhergehender, sukzessiver Änderung des AoP zu einer sinusförmigen Modulation der Aktivität dieser Neurone. Das Aktivitätsmaximum und Aktivitätsminimum liegen dabei um  $90^\circ$  auseinander (Labhart, 1988; Vitzthum et al., 2002). Der AoP, bei dem die Aktivität eines Neurons ihr Maximum erreicht, wird als bevorzugter AoP ( $\Phi_{\text{max}}$ ) bezeichnet. Im Zentralkomplex (CX) des Insektengehirns variiert der  $\Phi_{\text{max}}$  zwischen einzelnen Neuronen systematisch, sodass sich in dieser Gehirnregion eine kompassartige Repräsentation unterschiedlicher AoPs ergibt (Heinze & Homberg, 2007). Der DoP des Himmelslichts nimmt mit zunehmendem Winkelabstand von der Sonne bis zu einem Abstand von  $90^\circ$  zu und anschließend wieder ab (Pomozi et al., 2001; Foster et al., 2018). Dabei erreicht er nur unter blauem, wolkenlosem Himmel einen Maximalwert von etwa 75 % (DoP = 0,75; Brines & Gould, 1982). Während die AoPs des Himmelspolarisationsmusters größtenteils unabhängig von Wetterbedingungen sind, sinkt der DoP der Lichtstrahlen durch beispielsweise Bewölkung, Nebel oder Dunst (Heinze & Labhart, 2007). Dies führt dazu, dass realistische DoPs oft weit niedriger sind als 0.75. Viele Insekten sind in der Lage sich auch an polarisiertem Licht mit niedrigen DoPs zu

orientieren (von Frisch, 1967; Henze & Labhart, 2007; Foster et al., 2019), was eine entsprechende Sensitivität der an der Verarbeitung dieser Informationen beteiligten neuronalen Systeme voraussetzt.

In der vorliegenden Studie haben wir uns die Frage gestellt, wie polarisations-sensitive Neurone des CX der Wüstenheuschrecke *Schistocerca gregaria* auf polarisiertes Licht mit unterschiedlichen DoPs reagieren. Mithilfe intrazellulärer Ableitungen untersuchten wir die Reaktionen von Neuronen des CX auf im Zenit präsentierte, sich kontinuierlich ändernde AoPs bei unterschiedlichen DoPs. Wir verwendeten maximal polarisiertes Licht (DoP = 0,99), so wie es bei bisherigen Experimenten im Regelfall getan wurde, wenn Reaktionen auf sich ändernde AoPs untersucht wurden. Zudem präsentierten wir nahezu unpolarisiertes Licht (DoP = 0,002), sowie Licht mit drei dazwischenliegenden DoPs (0,35; 0,1; 0,05). In einigen Experimenten übermalten wir die dorsale Randregion (DRA) des Heuschrecken Auges. Da über die DRA der Hauptteil der Polarisationsinformation detektiert wird, sollte das Übermalen zum Ausbleiben der neuronalen Antwort während der Stimulus-Präsentation führen. In allen Experimenten wurde Licht mit einer Wellenlänge von 452 nm verwendet, da die polarisations-sensitiven Photorezeptoren der DRA von *S. gregaria* für Licht im blauen Spektrum empfindlich sind (Schmeling et al., 2014). Während jeder Ableitung wurde ein Marker in die Zelle injiziert, sodass ihre Morphologie im Anschluss an die physiologische Untersuchung durch immunzytochemische Aufarbeitung des Gehirns bestimmt werden konnte.

Im Rahmen der Experimentreihe konnten wir die Reaktionen von Zelltypen der unterschiedlichen Verarbeitungsebenen des CX untersuchen. Tangentiale Neurone der unteren Einheit des Zentralkörpers (TL2- und TL3 Neurone) leiten Polarisationsinformation zu kolumnären Neuronen der unteren Einheit des Zentralkörpers und der Protozerebralbrücke (CL1a Neurone) weiter. In der Protozerebralbrücke findet die Verarbeitung der Information durch einen weiteren Typ tangentialer Neurone (TB Neurone) statt, die ihrerseits auf Ausgangsneurone des CX verschalten. Dabei handelt es sich um kolumnäre Neurone der oberen Einheit des Zentralkörpers (CPU1- und CPU2 Neurone). Zunächst interessierte uns, ab welchem DoP eine verlässliche Kodierung des AoP durch die unterschiedlichen Neuronentypen möglich ist. Unsere Messungen ergaben einen DoP-Schwellenwert von 0.05 und 0.35 für TL2- und TL3 Neurone, einen DoP-Schwellenwert von 0.35 und 0.1 für CL1a- und TB1 Neurone und einen DoP-Schwellenwert von 0.35 für CPU1- und CPU2 Neurone. Generell zeigt die Studie, dass der DoP durchaus einen Einfluss auf die durch Änderungen des AoP hervorgerufene neuronale Antwort hat. So führten steigende DoPs in allen Zelltypen zur

Zunahme der Modulationsstärke der Antworten. In TL2- und CL1a Neuronen bewirkten Änderungen des DoP außerdem eine Veränderung der mittleren Aktivität der Zellen während der Stimulus-Präsentation. Dabei stand die Aktivität von TL2 Neuronen in einem positiven und die von CL1a Neuronen in einem negativen linearen Zusammenhang mit dem DoP. Diese entgegengesetzten Antworteigenschaften unterstützen die Annahme, dass CL1a Neurone durch  $\gamma$ -Aminobuttersäure exprimierende TL2- und TL3 Neurone inhibiert werden. In einzelnen TL2- und TL3 Neuronen führte die Präsentation von unpolarisiertem Licht der gleichen Wellenlänge (452 nm) zu einer starken, tonischen Inhibition oder Exzitation. Das Übermalen der DRA führte zu einem Ausbleiben der Reaktionen auf polarisiertes wie auch unpolarisiertes Licht und bestätigt, dass beide Antworten durch diesen Bereich des Komplexauges vermittelt werden. Das Antwortverhalten der einzelnen TL Neurone könnte durch einen unbalancierten exzitatorischen und inhibitorischen Eingang entstehen und einer Modulation des Eingangs der Polarisationsinformation in den CX dienen. In CL1a Neuronen führte die Präsentation von unpolarisiertem Licht in neun von 13 Zellen zu einer leicht erhöhten Aktivität im Vergleich zur Hintergrundaktivität. Dies könnte auf das Nachlassen der Inhibition durch TL2- und TL3 Neurone zurückzuführen sein. Sowohl TB1- als auch CPU1- und CPU2 Neurone reagierten sehr individuell auf die Präsentation von unpolarisiertem Licht, und Änderungen in der Aktivität waren weniger deutlich. Die geringe Reaktion auf unpolarisiertes Licht resultiert möglicherweise aus der gegenseitigen Inhibition von TB1 Neuronen der beiden Gehirnhemisphären, die zur Abschwächung identischer Informationen führt.

Zusammengefasst zeigt die Studie, dass eine verlässliche Kodierung des AoP in bestimmten Zelltypen bis zu einem DoP von nur 0.05 möglich ist, sodass dieses System für die auf dem Polarisationsmuster des Himmels basierte Orientierung auch unter nicht optimalen Wetterbedingungen, wie Bewölkung oder Nebel, geeignet ist. Der starke Einfluss unpolarisierten blauen Lichts auf die Eingangsneurone des CX (TL2- und TL3 Neurone) deutet zudem darauf hin, dass die Polarisationsinformation im CX entsprechend ihrer Verfügbarkeit gewichtet wird und bei unzureichendem Informationsgehalt zu Gunsten der Verarbeitung anderer Stimuli unterdrückt werden könnte.

## Kapitel II

Der CX spielt eine Hauptrolle bei der Integration sensorischer Stimuli zur zielgerichteten Orientierung, aber auch bei der Schlafregulation und der zustandsabhängigen Modulation von

Verhalten (Pfeiffer & Homberg, 2014; Honkanen et al., 2019; Hulse et al., 2021). Seine Anatomie wird durch eine Vielzahl unterschiedlicher Neuronentypen bestimmt, die sich durch ihre Morphologie, ihre Physiologie aber auch ihre Neurotransmitter und Peptidzusammensetzung charakterisieren lassen. Die Expressionsmuster von einigen neuroaktiven Substanzen wie  $\gamma$ -Aminobuttersäure oder Histamin sind in vielen Insektenpezies deutlich konserviert, sie können sich aber für andere Substanzen, vor allem für Neuropeptide, stark unterscheiden (Pfeiffer & Homberg, 2014) und sollten daher für jede Art individuell bestimmt werden. Die Funktion vieler neuroaktiver Substanzen im CX ist bisher nicht geklärt, trotzdem ist die Analyse ihrer Verteilung neuroanatomisch aufschlussreich.

In der vorliegenden Studie haben wir die Verteilung des myoinhibitorischen Peptids (MIP) im CX von *S. gregaria* untersucht. MIP-exprimierende Neurone konnten bereits im Gehirn anderer Insekten identifiziert werden. Zunächst stellten wir uns die Frage, ob MIP-verwandte Peptide im Genom von *S. gregaria* kodiert sind. Wir führten eine *in silico* Analyse des Genoms und Transkriptom von *S. gregaria* durch, deren Ergebnis die Existenz von acht unterschiedlichen, neuroaktiven MIPs (Scg-MIP) nahelegt. Die Aminosäuresequenzen der Scg-MIPs zeigen starke Ähnlichkeiten zu den Aminosäuresequenzen der MIPs aus der Wanderheuschrecke, *Locusta migratoria*, sowie zu der Aminosäuresequenz des MIP aus der Amerikanischen Großschabe, *Periplaneta americana* (Pea-MIP-1). Durch immunzytochemische Färbungen mit einem gegen Pea-MIP-1 gerichteten Antiserum an Gehirnpräparaten von *S. gregaria* visualisierten wir die Expression von MIP im CX. Wir führten außerdem Färbungen mit Antiseren gegen Locustatachykinin II und Serotonin durch. Die Färbemuster dieser beiden Antiseren wurden in *S. gregaria* bereits beschrieben und erlaubten uns daher eine detailliertere Auswertung des MIP-Expressionsmusters. Pea-MIP-1-Färbungen an Präparaten, in denen zuvor einzelne Zellen spezifisch markiert worden waren, ermöglichten zudem eine präzisere Bestimmung der Identität der MIP-exprimierenden Zelltypen und ihrer Morphologie.

Unsere Ergebnisse zeigen, dass fünf Systeme von Zentralkomplexneuronen in *S. gregaria* MIP exprimieren. Bei zwei Systemen handelt es sich CL1b- und CL2 Neurone, kolumnäre Neurone der unteren Einheit des Zentralkörpers (CBL). CL2 Neurone verbinden ausschließlich Untereinheiten des CX miteinander während CL1b Neurone zusätzlich Verbindungen mit dem gall des LX herstellen. In *S. gregaria* sind beide Zelltypen polarisations-sensitiv und spielen wahrscheinlich eine Rolle bei der Orientierung anhand des Himmelpolarisationsmusters. Die homologen Zelltypen aus der Fruchtfliege, *Drosophila*



*melanogaster*, sind essentielle Elemente eines Ring-Attraktor Netzwerkes, dessen Aktivität die Kopfrichtung des Tieres signalisiert. Die starke Konservierung der neuronalen Elemente des CX über verschiedene Insektenarten hinweg deutet darauf hin, dass die Nutzung eines Ring-Attraktor Systems zur Orientierung in all diesen Arten realisiert ist. Unsere Studie zeigt, dass das System von CL1b Neuronen in *S. gregaria* nicht wie bisher angenommen aus acht Zellen, sondern aus neun Zellen pro Gehirnhemisphäre besteht. Damit stimmt ihre Anzahl mit der Anzahl der homologen Zellen in *D. melanogaster* überein. Wir führten daraufhin die Reevaluation eines weiteren Subtyps von CL1 Neuronen (CL1a Neurone) durch, die auch für diesen Zelltyp eine Zahl von neun anstelle von acht Zellen pro Hirnhemisphäre nahelegt.

Zwei weitere Systeme MIP-exprimierender Zellen umfassen ebenfalls kolumnäre Zelltypen, die CU2x- und CU2y Neurone. Diese besitzen Verzweigungen in der oberen Einheit des Zentralkörpers (CBU). Die Morphologie der CU2x Neurone konnte anhand der anti-Pea-MIP-1-Färbung rekonstruiert werden und offenbarte ein System von nur vier Neuronen pro Hirnhemisphäre, welche die CBU mit einem anderen Gehirnareal, der *crepine*, verbinden. Die Rekonstruktion von zwei individuellen CU2y Neuronen erfolgte auf der Basis von Färbungen an Präparaten mit Einzelzellmarkierungen. Auch diese Neurone stellen Verbindungen zwischen der CBU und der *crepine* her, sie bilden allerdings ein System von etwa 19 Zellen pro Gehirnhemisphäre. Über die Funktion dieser Neuronentypen ist nur wenig bekannt, es wird allerdings angenommen, dass potentiell homologe Neurone aus *D. melanogaster* mit anderen Neuronen der CBU lokale Netzwerke bilden (FC1 neurons, Hulse et al., 2021).

Das fünfte MIP-exprimierende Neuronensystem besteht aus einem Typ tangentialer Neurone der CBU (TU Neurone). Aufgrund der schwachen Markierung dieses Zelltyps konnten die Verzweigungsbereiche außerhalb des CX nicht charakterisiert werden. Generell vermittelt eine Vielzahl unterschiedlicher TU Neurone aus distinkten Gehirnarealen Eingang in den CX, wobei die Qualität der übermittelten Informationen weitestgehend unbekannt ist. Während in CL1b-, CU2x- und CU2y Neuronen MIP und Locustatachykinin II kolokalisiert sind, werden die CL2- und die TU Neurone nur durch das Antiserum gegen Pea-MIP-1 markiert. Serotonin und MIP zeigen keine Kolokalisation innerhalb des CX.

Ein Vergleich der Verteilung von MIP im CX von *S. gregaria* mit der in *L. migratoria*, *D. melanogaster*, sowie der Madeira Schabe, *Rhyparobia maderae*, beschriebenen Verteilung legt nahe, dass sie zwischen *S. gregaria* und *L. migratoria* konserviert ist, während zwischen der MIP-Verteilung in *S. gregaria* und *R. maderae* sowie *D. melanogaster* sowohl Gemeinsamkeiten als auch Unterschiede bestehen.

Zusammengefasst zeigt die Studie das Vorkommen von mindestens acht MIP Peptidsequenzen in *S. gregaria*. Die Expression von MIP konnte in fünf Neuronensystemen des CX nachgewiesen werden und erlaubte die genauere Analyse der Morphologie einiger dieser Zellen sowie die Bestimmung ihrer Anzahl. Das Expressionsmuster von MIP konnte mit dem von Locustatachykinin II und Serotonin verglichen werden. Darüber hinaus ermöglicht die Studie einen Vergleich des MIP-Expressionsmusters zwischen verschiedenen Spezies.

### Kapitel III

Der Zentralkomplex (CX) ist - wie sein Name vermuten lässt - im Zentrum des Insektengehirns lokalisiert und dient der Integration verhaltensrelevanter Stimuli und der Generierung von Verhalten. Bei der Kommunikation des CX mit anderen Gehirnarealen und den Thorakalganglien spielt eine weitere Gehirnregion, der laterale Komplex (LX), eine wichtige Rolle. Der LX liegt lateral zu beiden Seiten des CX und besteht aus dem lateralen akzessorischen Lobus (LAL) und dem Bulbus (Ito et al., 2014). Der LAL macht den größten Teil des LX aus und ist in vielen Spezies in einen oberen (ULAL) und einen unteren (LLAL) LAL unterteilt. Zudem lässt sich ein weiterer, kleiner Bereich des LAL abgrenzen, der *gall*. Der Bulbus besteht aus bis zu drei Untereinheiten, die speziesspezifisch fusioniert oder räumlich separiert vorliegen. Tangentiale Neurone des CX leiten unterschiedliche sensorische Informationen aus dem Bulbus und dem LAL in die Neuropile des CX. Dabei gelangen Signale aus dem Bulbus in die CBL (Träger et al., 2008; Held et al., 2016; Omoto et al., 2017), während Signale aus dem LAL vorwiegend in die CBU und die Noduli (NO) des CX weitergeleitet werden (Stone et al., 2017; von Hadeln et al., 2020). Der Bulbus fungiert vor allem als Einbahnstraße in den CX, während der LAL auch Informationen aus dem CX erhält, die größtenteils über kolumnäre Neurone der Protozerebralbrücke (PB) und der CBU übermittelt werden (Heinze & Homberg, 2008; Hulse et al., 2021). Es liegt nahe, dass über diese Verbindungen motorische Befehle aus dem CX in die Motorzentren weitergeleitet werden (Adden et al., 2020; Rayshubskiy et al., 2020). Die Neurone des LAL Netzwerkes sind in vielen Insektenarten an der Steuerung von Bewegungsabläufen beteiligt (Übersichtsartikel: Namiki & Kanzaki, 2016). Der *gall* ist eine distinkte Region des LAL, der vor allem durch die Verzweigungen von CL1 Neuronen charakterisiert ist. In *Drosophila* bilden Neurone des CX und LX, darunter CL1 Neurone, Rückkopplungsschleifen über den *gall* (Franconville et al., 2018; Hulse et al., 2021).

Die vorliegende Studie widmet sich der Organisation des LX in *S. gregaria*. In *S. gregaria* sind bereits zahlreiche Verbindungen zwischen CX und LX beschrieben (Heinze & Homberg, 2008; von Hadeln et al., 2020). Der Fokus dieser Arbeit lag daher auf der Identifizierung potentieller Rückkopplungsschleifen zwischen den beiden Gehirnarealen, sowie auf der Untersuchung von Neuronen, die den LAL des LX mit anderen Gehirnregionen verbinden. Wir führten Einzelzellmarkierungen durch, um neue Zelltypen zu identifizieren und nutzten immunzytochemische Methoden, um die Morphologie bereits bekannter Zelltypen genauer zu analysieren.

*S. gregaria* ist eines der ersten Insekten, bei dem die Grenzen des LAL definiert wurden (el Jundi et al., 2010). Um eine bessere Vergleichbarkeit zu Insektenarten zu schaffen, in denen der LAL in jüngerer Zeit charakterisiert worden ist, definierten wir seine Grenzen in *S. gregaria* neu. Dadurch verlor der ULAL Bereiche an eine andere Gehirnregion, die *crepine*. Die Grenze zwischen ULAL und LLAL wurde zudem so verschoben, dass sie nun hauptsächlich durch den Verlauf eines prominenten Fasertraktes, der LAL Kommissur, definiert wird (Iwano et al., 2010; Heinze & Reppert, 2012).

Die genauere Analyse der Verzweigungsbereiche von polarisations-sensitiven kolumnären und tangentialen Neuronen innerhalb des LX führte zur Identifikation von potentiellen Rückkopplungsschleifen im *gall*. CL1 Neurone verbinden die PB und die CBL mit dem *gall*. Es stellte sich heraus, dass auch CP2 Neurone, die in der PB verzweigen, und TL1 Neurone, die in der CBL verzweigen, Innervationsbereiche im *gall* besitzen. Daher könnten Informationen im *gall* durch CL1- und CP2 Neurone aus dem CX an TL1 Neurone weitergeleitet werden, die diese Information wiederum zurück zur CBL leiten. Darüber hinaus liegt nahe, dass im *gall* auch zwischen individuellen Neuronen des gleichen Zelltyps ein Informationsaustausch stattfindet (Hulse et al., 2021). Die Verzweigungen von CL1 Neuronen im LX beschränken sich auf den *gall*, die Verzweigungsbereiche von CP2- und TL1 Neuronen erstrecken sich auch noch in umliegende Regionen, was auf größere Überlappungsbereiche zwischen den Verzweigungen dieser beiden Zelltypen hindeutet.

Eine zweite potentielle Rückkopplungsschleife identifizierten wir im *ovoid body*, einer Region im LX, die im Rahmen dieses Projekts erstmalig beschrieben wurde. CP1 Neurone, die in der PB verzweigen, ziehen in eine distinkte, eiförmige Region, den *ovoid body*. Neu identifizierte TL3c Neurone verzweigen ebenfalls in diesem Areal und verbinden es mit der CBL. Im *ovoid body* könnten daher Informationen aus der PB durch CP1 Neurone über TL3c Neurone zurück in die CBL gelangen. Durch Immunfärbungen konnte außerdem das Vorkommen von Leucokinin, Serotonin und Orcokinin im *ovoid body* nachweisen werden.

Im Rahmen der Studie charakterisierten wir fünfzehn Zelltypen des LAL auf der Basis von Einzelzellmarkierungen und einen weiteren Zelltyp basierend auf der Markierung mehrerer Zellen des gleichen Typs. Acht der beschriebenen Neuronentypen verbinden die LALs beider Gehirnhälften miteinander, während die übrigen Neurone im LAL nur einer Gehirnhemisphäre verzweigen. Bei zwei Neuronen aus der letztgenannten Gruppe handelt es sich um absteigende Neurone, die aus dem Gehirn Richtung Thorax ziehen. Während ein Neuron exklusiv die LALs innerviert, besitzen die übrigen Neurone zusätzliche Verzweigungen in anderen Gehirnarealen. Darunter finden sich Neuropile wie die anteriore Lobula der optischen Loben und die obere Einheit des anterioren optischen Tuberkels, die an der Weiterleitung visueller Informationen beteiligt sind, sowie die *wedge*, die in *D. melanogaster* in die Verarbeitung von Windrichtungsinformationen involviert ist. Ein Gehirnareal, das über auffallend viele Neurone mit dem LAL verbunden ist, ist die *crepine*. Über die Funktion dieses Neuropils ist bisher kaum etwas bekannt, allerdings besitzt es zahlreiche Verbindungen zu den Pilzkörpern, die eine essentielle Rolle beim assoziativen Lernen und bei der Gedächtnisbildung spielen. Verbindungen zwischen LAL und *crepine* könnten daher dazu dienen, erlernte Assoziationen oder Erfahrungen in das Orientierungsnetzwerk zu integrieren. Über die Hälfte der hier beschriebenen Neurone, einschließlich der beiden absteigenden Neurone, verbindet den LAL mit der *posterior slope*. Da ein Großteil der absteigenden Neurone des Gehirns in der *posterior slope* verzweigt, vermitteln diese Verbindungen wahrscheinlich die Kommunikation zwischen dem LAL und den Motorzentren der Thorakalganglien.

Zusammengefasst zeigt die Studie, dass polarisations-sensitive Neurone des CX im *gall* und im *ovoid body* des LX Rückkopplungsschleifen formen könnten. Die umliegende Region des *gall* könnte dabei in die Kommunikation zwischen zwei der Neuronentypen ebenso involviert sein. Die hier identifizierten Zelltypen stützen die auf vorausgehenden Studien basierende Annahme, dass der LAL über verschiedene Gehirnregionen sensorische Informationen erhält und zudem direkt und indirekt mit thorakalen Motorzentren verbunden ist.

## Referenzen

Adden, A., Stewart, T. C., Webb, B., & Heinze, S. (2020). A neural model for insect steering applied to olfaction and path integration. *BioRxiv*, 2020.08.25.266247. <https://doi.org/10.1101/2020.08.25.266247>

- Brines, M. L., & Gould, J. L. (1982). Skylight polarization patterns and animal orientation. *Journal of Experimental Biology*, *96*(1), 69-91. <https://doi.org/10.1242/jeb.96.1.69>
- el Jundi, B., Heinze, S., Lenschow, C., Kurylas, A., Rohlfing, T., & Homberg, U. (2010). The locust standard brain: a 3D standard of the central complex as a platform for neural network analysis. *Frontiers in Systems Neuroscience*, *3*. <https://doi.org/10.3389/neuro.06.021.2009>
- Foster, J. J., Kirwan, J. D., el Jundi, B., Smolka, J., Khaldy, L., Baird, E., Byrne, M. J., Nilsson, D.-E., Johnsen, S., & Dacke, M. (2019). Orienting to polarized light at night - matching lunar skylight to performance in a nocturnal beetle. *Journal of Experimental Biology*, *222*(2), jeb.188532. <https://doi.org/10.1242/jeb.188532>
- Foster, J. J., Temple, S. E., How, M. J., Daly, I. M., Sharkey, C. R., Wilby, D., & Roberts, N. W. (2018). Polarisation vision: overcoming challenges of working with a property of light we barely see. *The Science of Nature*, *105*(3-4), 27. <https://doi.org/10.1007/s00114-018-1551-3>
- Franconville, R., Beron, C., & Jayaraman, V. (2018). Building a functional connectome of the *Drosophila* central complex. *eLife*, *7*, e37017. <https://doi.org/10.7554/eLife.37017>
- Heinze, S., & Homberg, U. (2007). Maplike representation of celestial *E*-vector orientations in the brain of an insect. *Science*, *315*, 995-997. <https://doi.org/10.1126/science.1135531>
- Heinze, S., & Homberg, U. (2008). Neuroarchitecture of the central complex of the desert locust: intrinsic and columnar neurons. *Journal of Comparative Neurology*, *511*(4), 454-478. <https://doi.org/10.1002/cne.21842>
- Heinze, S., & Reppert, S. M. (2012). Anatomical basis of sun compass navigation I: the general layout of the monarch butterfly brain. *Journal of Comparative Neurology*, *520*(8), 1599-1628. <https://doi.org/10.1002/cne.23054>
- Held, M., Berz, A., Hensgen, R., Muenz, T. S., Scholl, C., Rössler, W., Homberg, U., & Pfeiffer, K. (2016). Microglomerular synaptic complexes in the sky-compass network of the honeybee connect parallel pathways from the anterior optic tubercle to the central complex. *Frontiers in Behavioral Neuroscience*, *10*. <https://doi.org/10.3389/fnbeh.2016.00186>
- Henze, M. J., & Labhart, T. (2007). Haze, clouds and limited sky visibility: polarotactic orientation of crickets under difficult stimulus conditions. *Journal of Experimental Biology*, *210*(18), 3266-3276. <https://doi.org/10.1242/jeb.007831>
- Homberg, U., Heinze, S., Pfeiffer, K., Kinoshita, M., & el Jundi, B. (2011). Central neural coding of sky polarization in insects. *Philosophical Transactions of the Royal Society B: Biological Sciences*, *366*(1565), 680-687. <https://doi.org/10.1098/rstb.2010.0199>

- Honkanen, A., Adden, A., da Silva Freitas, J., & Heinze, S. (2019). The insect central complex and the neural basis of navigational strategies. *Journal of Experimental Biology*, 222(Suppl\_1), jeb188854. <https://doi.org/10.1242/jeb.188854>
- Horváth, G. (2014). Polarized light and polarization vision in animal sciences. Springer Berlin Heidelberg. <https://doi.org/10.1007/978-3-642-54718-8>
- Hulse, B. K., Haberkern, H., Franconville, R., Turner-Evans, D. B., Takemura, S., Wolff, T., Noorman, M., Dreher, M., Dan, C., Parekh, R., Hermundstad, A. M., Rubin, G. M., & Jayaraman, V. (2021). A connectome of the *Drosophila* central complex reveals network motifs suitable for flexible navigation and context-dependent action selection. *eLife*, e66039. <https://doi.org/10.7554/eLife.66039>
- Ito, K., Shinomiya, K., Ito, M., Armstrong, J. D., Boyan, G., Hartenstein, V., Harzsch, S., Heisenberg, M., Homberg, U., Jenett, A., Keshishian, H., Restifo, L. L., Rössler, W., Simpson, J. H., Strausfeld, N. J., Strauss, R., & Vosshall, L. B. (2014). A systematic nomenclature for the insect brain. *Neuron*, 81(4), 755–765. <https://doi.org/10.1016/j.neuron.2013.12.017>
- Iwano, M., Hill, E. S., Mori, A., Mishima, T., Mishima, T., Ito, K., & Kanzaki, R. (2010). Neurons associated with the flip-flop activity in the lateral accessory lobe and ventral protocerebrum of the silkworm moth brain. *Journal of Comparative Neurology*, 518(3), 366–388. <https://doi.org/10.1002/cne.22224>
- Namiki, S., & Kanzaki, R. (2016). Comparative neuroanatomy of the lateral accessory lobe in the insect brain. *Frontiers in Physiology*, 7. <https://doi.org/10.3389/fphys.2016.00244>
- Omoto, J. J., Keleş, M. F., Nguyen, B.-C. M., Bolanos, C., Lovick, J. K., Frye, M. A., & Hartenstein, V. (2017). Visual input to the *Drosophila* central complex by developmentally and functionally distinct neuronal populations. *Current Biology*, 27(8), 1098–1110. <https://doi.org/10.1016/j.cub.2017.02.063>
- Labhart, T. (1988). Polarization-opponent interneurons in the insect visual system. *Nature*, 331, 435–437. <https://doi.org/10.1038/331435a0>
- Pfeiffer, K., & Homberg, U. (2014). Organization and functional roles of the central complex in the insect brain. *Annual Review of Entomology*, 59(1), 165–184. <https://doi.org/10.1146/annurev-ento-011613-162031>
- Pomozi, I., Horváth, G., & Wehner, R. (2001). How the clear-sky angle of polarization pattern continues underneath clouds: full-sky measurements and implications for animal orientation. *Journal of Experimental Biology*, 204, 2933–2942. <https://doi.org/10.1242/jeb.204.17.2933>
- Rayshubskiy, A., Holtz, S. L., D'Alessandro, I., Li, A. A., Vanderbeck, Q. X., Haber, S., Gibb, P. W., & Wilson, R. I. (2020). Neural circuit mechanisms for steering control in

walking *Drosophila*. *bioRxiv* 2020.04.04.024703; <https://doi.org/10.1101/2020.04.04.024703>

- Schmeling, F., Wakakuwa, M., Tegtmeier, J., Kinoshita, M., Bockhorst, T., Arikawa, K., & Homberg, U. (2014). Opsin expression, physiological characterization and identification of photoreceptor cells in the dorsal rim area and main retina of the desert locust, *Schistocerca gregaria*. *Journal of Experimental Biology*, jeb.108514. <https://doi.org/10.1242/jeb.108514>
- Stone, T., Webb, B., Adden, A., Weddig, N. B., Honkanen, A., Templin, R., Wcislo, W., Scimeca, L., Warrant, E., & Heinze, S. (2017). An anatomically constrained model for path integration in the bee brain. *Current Biology*, 27(20), 3069-3085.e11. <https://doi.org/10.1016/j.cub.2017.08.052>
- Träger, U., Wagner, R., Bausenwein, B., & Homberg, U. (2008). A novel type of microglomerular synaptic complex in the polarization vision pathway of the locust brain. *Journal of Comparative Neurology*, 506(2), 288–300. <https://doi.org/10.1002/cne.21512>
- Vitzthum, H., Müller, M., & Homberg, U. (2002). Neurons of the central complex of the locust *Schistocerca gregaria* are sensitive to polarized light. *Journal of Neuroscience*, 22(3), 1114–1125. <https://doi.org/10.1523/JNEUROSCI.22-03-01114.2002>
- von Frisch, K. (1967). The dance language and orientation of bees. Harvard University Press, Cambridge, MA
- von Hadeln, J., Hensgen, R., Bockhorst, T., Rosner, R., Heidasch, R., Pegel, U., Quintero Pérez, M., & Homberg, U. (2020). Neuroarchitecture of the central complex of the desert locust: tangential neurons. *Journal of Comparative Neurology*, 528(6), 906–934. <https://doi.org/10.1002/cne.24796>
- Wehner, R. (1989). Neurobiology of polarization vision. *Trends in Neurosciences*, 12(9), 353-359. [10.1016/0166-2236\(89\)90043-x](https://doi.org/10.1016/0166-2236(89)90043-x)





## Introduction

### Spatial orientation and navigation in insects

Spatial orientation is a prerequisite for most vital behaviors, including the search for food, finding mating partners or the avoidance of predators (Jain et al., 2017; Harootonian et al., 2022). In all those cases, spatial orientation requires a sense for the own location and heading in space that is acquired and continuously updated by the integration of multisensory information (Varga et al., 2017; Harootonian et al., 2022). This information is provided by cues that derive from the environment (allothetic cues) and can be of different modalities, like visual, auditory, olfactory, or magnetic cues, and by cues that derive from the animals own movement (idiothetic cues) including proprioception and optic flow (Varga et al., 2017; Jain et al., 2017). Because idiothetic cues are prone to accumulate errors over time the additional use of allothetic cues is essential (Bernard & Wehner, 1977). Finally, the information gathered by the integration of relevant cues has to be utilized to initiate appropriate locomotion.

Despite their small brains insects show an impressive behavioral repertoire of navigational strategies (reviewed in Heinze, 2017), ranging from short-distance straight-line orientation in dung beetles that escape from a point of origin (Byrne et al., 2003; Dacke et al., 2013), path integration in bees and ants that find a straight way back home after a tortuous foraging trip (Wehner, 2003; Srinivasan, 2015; Collett, 2019), to long-distance migration undertaken by monarch butterflies and desert locusts between habitats separated by hundreds to thousands of kilometers (reviewed in Reppert et al., 2016 and Homberg, 2015, respectively). The use of multimodal information and multimodal strategies enables insects not only to gain more precise information from several cues but also to switch between cues depending on their availability (reviewed in Buehlmann et al., 2020). Previous experiences and the internal state of the animal also shape its orientation behavior further illustrating the complexity of the insect's orientation system (Heinze, 2017). The orientation system needs to be fed with relevant sensory information, manage the integration of a variety of cues and compute appropriate behavioral output. Studies in many insect species revealed two important structures within the insect brain that are involved in those processes; the central complex (CX; reviewed in Pfeiffer & Homberg, 2014; Varga et al., 2017; Honkanen et al., 2019; Sun et al., 2021; Hulse et al., 2021) and the lateral complex (LX) composed of the bulbs (lateral triangle and median olive in Träger et al., 2008; Held et al., 2016) and the lateral accessory

lobes (LAL; reviewed in Namiki & Kanzaki, 2016; Steinbeck et al., 2020). The different chapters (**I-III**) focus on aspects of physiological (**Chapter I**) and anatomical (**Chapter II**) properties of the CX and on the anatomical organization of the LX (**Chapter III**). The following sections provide an overview of the two structures and their role in insect orientation as well as of one specific orientation cue that can be utilized by different insects: the polarization pattern of the sky.

## The central complex

The CX of the insect brain is the main processing region underlying orientation and navigation behaviors (reviewed in Pfeiffer (reviewed in Pfeiffer & Homberg, 2014; Varga et al., 2017; Honkanen et al., 2019). It is considered to integrate multimodal sensory information and to generate behavioral commands that serve goal directed orientation (Stone et al., 2017; Hulse et al., 2021; Sun et al., 2021). Studies that support a function of the CX circuitry in different orientation behaviors range from the discovery of an internal sky-compass in the CX of the desert locust, *Schistocerca gregaria* (Heinze & Homberg, 2007; Pegel et al., 2019; Zittrell et al., 2020), to the role of the CX in locomotor control in the cockroach, *Blaberus discoidalis* (Bender et al., 2010; Martin et al., 2015), and to the discovery of a ring-attractor network formed by CX neurons that encodes heading direction in the fruit fly *Drosophila melanogaster* (Seelig & Jayaraman, 2015). Notably, additional higher functions are attributed to computations within CX circuits (reviewed in Pfeiffer & Homberg, 2014; Hulse et al., 2021), including sleep control (Donlea et al., 2014; Liu et al., 2016; reviewed in Shafer & Keene, 2021), and visual learning and memory (Neuser et al., 2008; Ofstad et al., 2011). Altogether, the CX plays an important role in shaping insect behavior depending on environmental and internal conditions (Heinze & Pfeiffer, 2018; Hulse et al., 2021). The structure of the CX is conserved across insects and thus appears to be optimized to solve different navigational tasks based on a variety of sensory sources (Honkanen et al., 2019; Sun et al., 2021).

### *Neuroanatomy of the central complex*

The CX (Figure 1) is an assembly of midline spanning neuropils in the center of the insect brain (Hanesch et al., 1989; Heinze & Homberg, 2008; Pfeiffer & Homberg, 2014). It

comprises four major neuropils; the handlebar-shaped protocerebral bridge (PB), the upper division of the central body (CBU), the lower division of the central body (CBL), and the paired noduli (NO). The CBL and the CBU together are termed central body. Though the neuropils of the CX correspond between insect species the CBL and CBU are termed ellipsoid body (EB) and fan-shaped body (FB), respectively, in flies. In *D. melanogaster*, the CX also contains the asymmetrical body (Pascual et al., 2004; Wolff & Rubin, 2018). A likely homologous structure is also present in the grey flesh fly *Neobellieria bullata* and the blowfly *Calliphora erythrocephala* (Phillips-Portillo & Strausfeld, 2012) but so far lacks an equivalent in other species. The neuropils of the CX are organized in vertical columns and horizontal layers (Heinze & Homberg, 2008; Pfeiffer & Homberg, 2014; Honkanen et al., 2019). This striking architecture arises from the projections of the neurons that constitute the CX; columnar (Figure 1D), pontine and amacrine neurons (small field neurons) and tangential neurons (large-field neurons; Figure 1E; Hanesch et al., 1989; Heinze & Homberg, 2008; von Hadeln et al., 2020).

Subtypes of columnar and pontine neurons are the main computational elements of the CX network and, in case of columnar neurons, play a direct role in mediating its output (Stone et al., 2017; Sayre et al., 2021; Hulse et al., 2021). Whereas pontine and amacrine neurons are mainly intrinsic to the CBU (Heinze & Homberg, 2008; Hulse et al., 2021), columnar neurons interconnect different CX neuropils and, depending on cell type, provide output to other brain areas. Their cell bodies are located in the pars intercerebralis (Boyan & Liu, 2016), a region that extends from the anterior midline of the brain posterior and dorsally to the CX (Boyan & Williams, 1997; de Velasco et al., 2007). Between the PB and the central body the neurites of the cells run through bilaterally symmetrical tract systems (w, x, y, z, from lateral to medial; Williams, 1975; Williams et al., 2005; Boyan & Reichert, 2011) until they rearrange into discrete fiber bundles that continue ventrally (Williams, 1975). The main types of columnar neurons are distinguished based on the innervated neuropils and can be further divided into subtypes. These subtypes comprise isomorphic sets of different numbers of individual neurons with repetitive projection patterns that establish the vertical stratification of the PB, the CBU and the CBL. Whereas the PB in locusts has so far been reported to comprise 16 columns (8 per hemisphere; Heinze & Homberg, 2008; Pfeiffer & Homberg, 2014), we found that it actually consists of 18 columns (9 per hemisphere; **Chapter II**) similar to the PB in *D. melanogaster* (Wolff et al., 2015; Wolff & Rubin, 2018) and the bumblebee *Bombus terrestris* (Sayre et al., 2021).

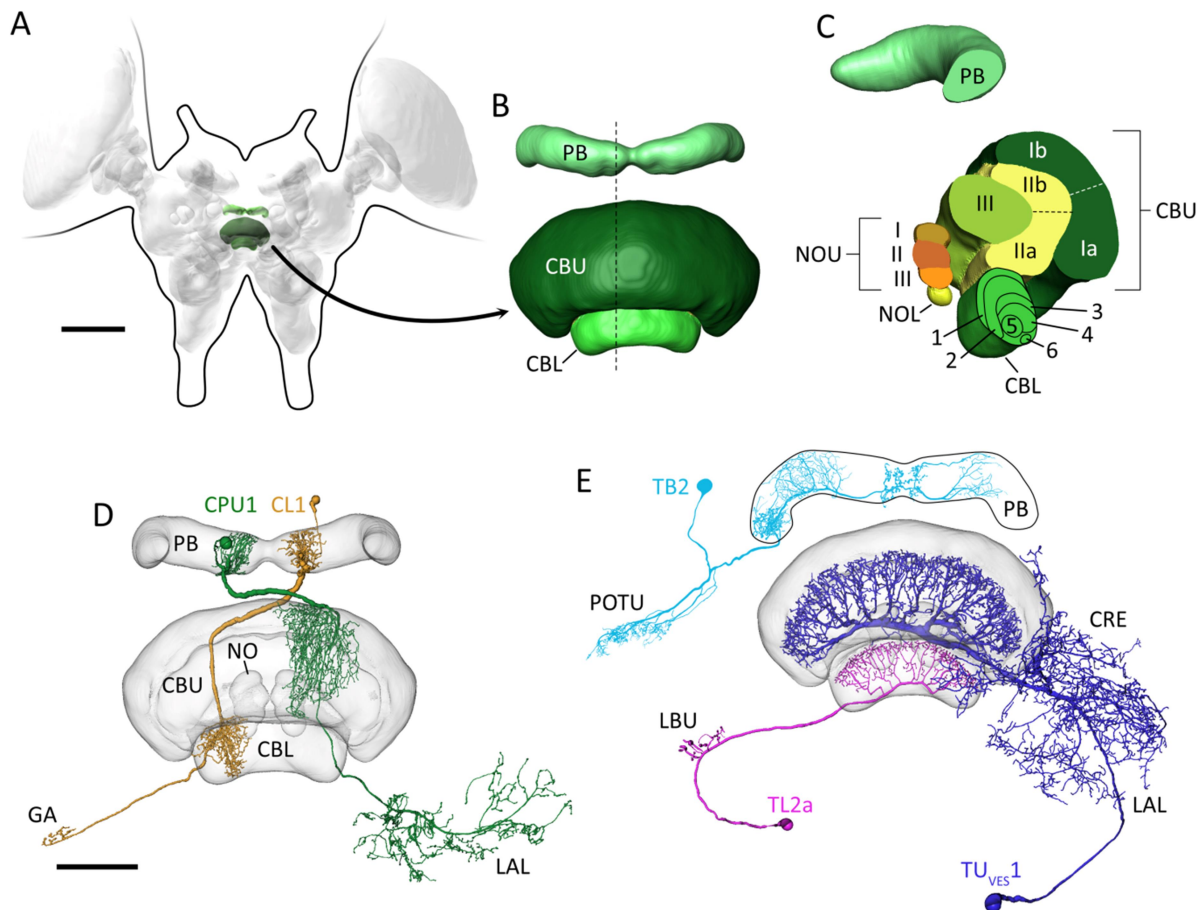


**Figure 1** The central complex (CX) of the desert locust *Schistocerca gregaria*. **(A)** Frontal view of a three-dimensional model of the locust brain with the CX in green. **(B)** Frontal view of the three-dimensional standard of the CX showing the protocerebral bridge (PB), the upper division of the central body (CBU), and the lower division of the central body (CBL). The dotted line indicates the sectional plane for the cross section shown in **C**. **(C)** Cross section through the three-dimensional standard model of the CX illustrating the layering of the CBU, the CBL and the noduli (NO). The CBU consists of three layers and the CBL consists of six layers. The NO can be divided into an upper unit (NOU), subdivided into three layers, and a lower unit (NOL). **(D)** Frontal view of the three-dimensional reconstruction of a columnar neuron of the FB/CBU (CPU1 neuron, green) and a columnar neuron of the CBL (CL1 neuron, beige). **(E)** Frontal view of the three-dimensional reconstruction of a tangential neuron of the CBU (TUves1 neuron, dark blue), a tangential neuron of the CBL (TL2a neuron, magenta), and a tangential neuron of the PB (TB2 neuron, light blue). Scale bars = 500  $\mu\text{m}$  (**A**), 100  $\mu\text{m}$  (**D**). The model in **A** was generated with insectbrainDB.org based on data from Kurylas et al. (2008) and el Jundi et al. (2010). **B** and **C** are adapted from von Hadeln et al. (2021) and generated with data from el Jundi et al. (2010) available on insectbrainDB.org. The CX models, the CPU1-, TUves1-, and TL2a neuron in **D** and **E** were generated with data from el Jundi et al. (2010) and von Hadeln et al. (2021) available on insectbrainDB.org. The TB2 neuron is adapted from von Hadeln et al. (2021).

Tangential neurons provide the main input to the CX network (Franconville et al., 2018; von Hadeln et al., 2020; Hulse et al., 2021). They connect areas outside the CX to specific layers or regions of the four CX neuropils. Even though the cell bodies of tangential neurons are more distributed throughout the brain than those of columnar neurons, many of them can be found in distinct clusters. In locusts, eleven clusters have been identified (von Hadeln et al., 2020). Based on the innervated CX neuropil different types of tangential neurons can be distinguished. Within each type further subtypes were identified based on more detailed morphological features. The arborization areas of tangential neurons establish the horizontal stratification of the CBL and the CBU and establish subunits of the NO (*D. melanogaster*: Wolff & Rubin, 2018; *S. gregaria*: von Hadeln et al., 2020; Hensgen et al., 2021). Tangential neurons of the PB differ from the remaining types as their arborizations follow, to some extent, a columnar organization, and do not establish an obvious stratification of the PB.

### *Neurochemistry of the central complex*

Investigating the distribution of neurotransmitters and neuropeptides has greatly contributed to reveal the organization of the CX, either through the identification of subregions (mostly layers) defined by expression patterns or through identification and characterization of individual cell types. A variety of neuroactive substances occurs in the CX, ranging from classical neurotransmitters like  $\gamma$ -aminobutyric acid (GABA) and acetylcholine, to biogenic amines like serotonin and dopamine to neuropeptides like orckinins and tachykinins (reviewed in Homberg, 2002 and Nässel & Homberg, 2006; Kahsai & Winther, 2011; reviewed in Pfeiffer & Homberg, 2014). The distribution of some neuroactive substances is highly conserved between insect species but can also vary for others, especially for neuropeptides. One striking example for a conserved distribution is GABA (Bernard & Wehner, 1977; Hanesch et al., 1989; Homberg et al., 1999, 2018), the main inhibitory neurotransmitter of the insect brain, which is present in tangential neurons of the CBL (TL neurons, or ring neurons in flies) and also in two systems of tangential neurons of the CBU (TU neurons, or FB neurons in flies). In *S. gregaria* studies on the distribution of neuroactive substances include the characterization of neurons containing the biogenic amine serotonin (5-HT; Homberg, 1991) and the neuropeptide locustatachykinin II (LomTK-II; Vitzthum & Homberg, 1998). Except for the CBL, all neuropils of the CX are innervated by 5-HT immunoreactive neurons (Homberg, 1991). The presence of 5-HT in one type of columnar neuron (neurons of group S1 in Homberg, 1991; CPU4b neurons) and different types of

tangential neurons (neurons of groups S3-S5 in Homberg, 1991; TU neurons) visualizes the different layers of the CBU (Figure 2A; Homberg, 1991). In contrast to 5-HT, LomTK-II is expressed by neurons of all CX neuropils, including the CBL (Figure 2B), which is innervated by two types of columnar neurons (LTCI & LTCII in Vitzthum & Homberg, 1998) and one type of tangential neuron (LTTI in Vitzthum & Homberg, 1998). In **Chapter III** we perform immunostaining for 5-HT and LomTK-II in combination with immunostaining for the myoinhibitory peptide (MIP) to characterize the expression pattern of the latter within the CX in more detail.

Although the distribution of neuroactive substances and also of some of their receptors has been analyzed in great detail in some species only a few studies have focused on their function within the CX network (Pfeiffer & Homberg, 2014). In the grasshopper, *Chorthippus biguttulus*, cholinergic, GABAergic, and nitric oxide-releasing neurons are thought to play a role in sound production (Kunst et al., 2011). In *D. melanogaster* dopaminergic CX neurons play a role in regulating sleep and arousal (Kong et al., 2010; Liu et al., 2012; Tomita et al., 2021) and tachykinin- and short neuropeptide F expressing neurons have been shown to play a role in different aspects of locomotor behavior (Kahsai et al., 2010). Recent work (Turner-Evans et al., 2020) confirmed an excitatory role of cholinergic neurons and an inhibitory role of GABAergic and glutamatergic neurons within the network that encodes heading direction in *D. melanogaster*. In general, neuropeptides are likely to serve as co-transmitters in several neurons as they are often co-localized with classical transmitters and biogenic amines (reviewed in Nässel & Homberg, 2006).

### *The head direction system*

Already two decades ago studies pointed to the CX as an internal compass and navigation center (reviewed in Homberg, 2004; Pisokas et al., 2020) and indeed in 2007, Heinze and Homberg found that the activity of CX neurons in *S. gregaria* encodes the angle of polarization of polarized light presented in the zenith of the animal in a compass-like fashion. In 2015, Seelig and Jayaraman showed that the activity of CX neurons in *D. melanogaster* encodes the fly's azimuth relative to its environment based on visual and self-motion cues and that this activity is maintained even when those cues are absent. They suggested that the underlying network acts as a ring-attractor, similar to what has been proposed for head direction cells in mammals (Skaggs et al., 1995; Seelig & Jayaraman, 2015). Until now the

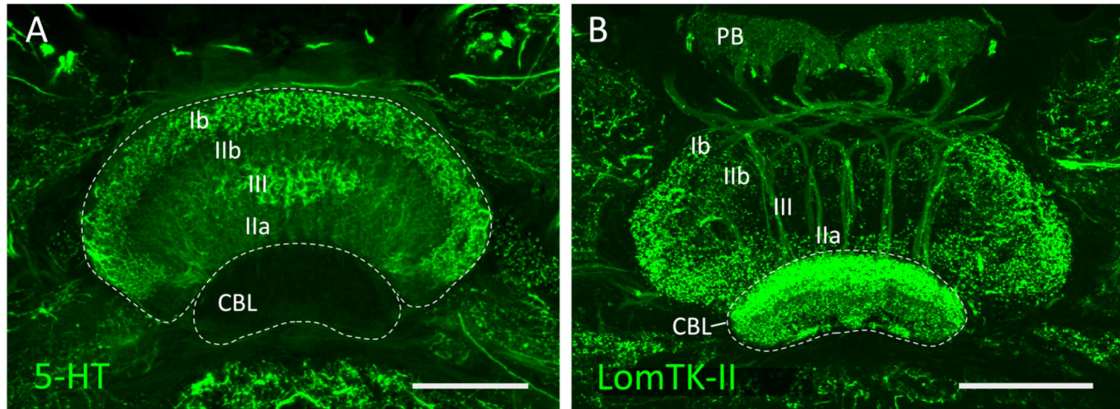


**Figure 2** Serotonin (5-HT) and locustatachykinin II (LomTK-II) in the central complex of *Schistocerca gregaria*. **(A)** Frontal section showing 5-HT-immunoreactivity in the central body. Staining is not present in lower division of the central body (CBL). Differences in 5-HT-immunoreactive staining in the upper division of the central body (CBU) visualize the different layers Ib, IIb, III and IIa. **(B)** Frontal section showing LomTK-II-immunoreactivity in the protocerebral bridge (PB) and the central body. Staining is prominent in all layers of the CBL and in the PB. Layer III of the CBU lacks LomTK-II-immunoreactivity, whereas immunoreactive staining is visible in layers Ib, IIb and IIa. Scale bars: 100  $\mu\text{m}$ . Images were generated from data included in the publication of **Chapter II**.

compass- or head direction system is most extensively studied and best understood in *D. melanogaster* (reviewed in Green & Maimon, 2018 and Hulse & Jayaraman, 2020). Briefly, the fly's heading is represented in the population activity of E-PG neurons (CL1a neurons in *S. gregaria*) resulting in a bump of activity in the EB (CBL) and two to three periodically spaced bumps of activity in the PB (Figure 3; Green et al., 2017; reviewed in Green & Maimon, 2018). When the fly turns, the activity bump is shifted along the EB and the PB signaling a change in heading direction. This update of the bump's location is based on the integration of multimodal information. The major input that anchors the activity bump to environmental cues, including information about visual features and wind direction, is mediated by ring neurons (TL neurons in *S. gregaria*) that get input in the LX (Omoto et al., 2017; Fisher et al., 2019; Okubo et al., 2020; Hardcastle et al., 2021). The input that updates the location of the bump based on idiothetic cues indicating self-motion (i.e. rotational velocity) is mediated by P-EN neurons (CL2 neurons in *S. gregaria*; Green et al., 2017; Turner-Evans et al., 2017, 2020). An offset between the projections of E-PG and P-EN neurons in the EB (CBL) allows the activity bump to be shifted in clockwise or counterclockwise direction based on P-EN input. Moreover, most models of the ring-attractor

network postulate that the activity bump is shaped by inhibitory input which appears to be mediated by glutamatergic  $\Delta 7$  neurons (TB neurons in *S. gregaria*) and types of GABAergic ring neurons (reviewed in Green & Maimon, 2018; Hulse & Jayaraman, 2020; Pisokas et al., 2020; Turner-Evans et al., 2020).

Not only the EB (CBL) circuitry, but also circuits of the FB (CBU) are part of the orientation network. Neurons of the FB (CBU) encode heading and turning behavior (Shiozaki et al., 2020) as well as airflow direction (Currier et al., 2020). Importantly, neurons of the CBU and the NO are suggested to provide information about the desired heading of the animal and to allow the comparison between desired heading and current heading to generate compensatory steering signals that are encoded by another type of CBU neuron (called PFL or CPU neurons depending on species; sweat bee, *Megalopta genalis*: Stone et al., 2017; Honkanen et al., 2019; *D. melanogaster*: Shiozaki et al., 2020; Sun et al., 2021). These neurons connect the CBU to the LAL of the LX (Hanesch et al., 1989; Heinze & Homberg, 2008; Hulse et al., 2021) where they synapse onto descending neurons that are involved in the control of steering (Rayshubskiy et al., 2020).

The cell types that constitute the core circuitry as well as the basic layout of the heading direction system are largely conserved across insect species. However, detailed analyses of the CX circuitry in species other than *D. melanogaster* began to also unravel differences as indicated by the identification of species-specific cell types that lack counterparts in other species (Sayre et al., 2021), differences in neurotransmitter expression (Timm et al., 2021), and differences in connectivity patterns that establish the ring attractor dynamics (Pisokas et al., 2020).

## The lateral complex

It already becomes apparent from the previous section that the LX (Figure 4) is associated with the CX in several ways. The term lateral complex was introduced by Ito et al. (2014) to refer to two structures, the bulb and the lateral accessory lobe (LAL) that lie anterior-laterally to either side of the CX. The bulb consists of functional subregions that are spatially segregated or lie close to each other depending on insect species. In the locust, the bulb constitutes two spatially separated structures, the lateral bulb (LBU) and the medial bulb (MBU) (formerly known as lateral triangle and median olive, respectively, Träger et al., 2008). The LAL constitutes the largest volume of the LX and is also called inferior



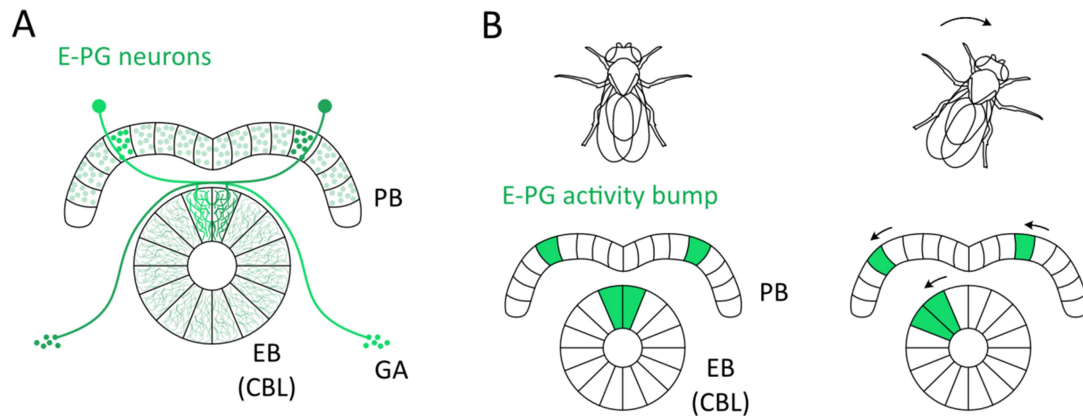


**Figure 3** Simplified illustration of the head direction mechanism in *Drosophila melanogaster*. **(A)** Schematic of columnar neurons of the ellipsoid-body (EB), the protocerebral bridge (PB) and the gall (GA) called E-PG neurons (CL1a in *Schistocerca gregaria*). Individual E-PG neurons innervate a single glomerulus of the PB, a wedge in the EB and the contralateral GA. **(B)** Schematic illustrating the shift of the E-PG activity bump as the fly turns. A single bump of activity in the EB corresponds to two bumps of activity in the PB due to the wiring pattern of E-PG neurons. Turning of the fly leads to a shift in the position of the bump. **A** and **B** are adapted from Turner-Evans et al. (2017)

dorsofrontal protocerebrum (IDFP) or ventral body in Diptera (Hanesch et al., 1989; Chiang et al., 2011). It is further divided into upper LAL (ULAL) and lower LAL (LLAL) in most species (silkworm, *Bombyx mori*: Iwano et al., 2010; monarch butterfly, *Danaus plexippus*: Heinze & Reppert, 2012; *S. gregaria*: von Hadeln et al., 2018; *D. melanogaster*: Hulse et al., 2021). Also part of the LAL is a small, distinct region, the gall (GA; Ito et al., 2014).

The bulbs are part of the anterior sky-compass pathway (el Jundi et al., 2014; Hulse et al., 2021) and house dendritic arborizations of TL neurons that project into the CBL. These neurons carry sky-compass signals, including information about the angle of polarization or the azimuth of an unpolarized light spot in different insect species (*S. gregaria*: el Jundi et al., 2011; Pegel et al., 2017; Takahashi et al., 2022; dung beetles: el Jundi et al., 2015; *D. plexippus*: Heinze & Reppert, 2011; Nguyen et al., 2021; *D. melanogaster*: Hardcastle et al., 2021). One notable feature of the bulb is the microglomerular organization of synapses formed by its input- and output neurons. They are highly conserved and particularly prominent in immunostainings across insect species (Träger et al., 2008; Held et al., 2016; Mota et al., 2016; Homberg et al., 2018).

The LAL houses a variety of neuron types that provide connections to different brain areas and thoracic motor centers. Descending LAL neurons that connect the brain to the thoracic

ganglia and bilateral LAL interneurons that connect the LALs of both hemispheres have been extensively studied in the silkworm *B. mori*. The activity of those neurons is linked to motor patterns displayed during pheromone orientation in walking silkworm and during phonotactic steering in crickets (*B. mori*: Kanzaki et al., 1994; Iwano et al., 2010; *Gryllus bimaculatus*: Zorović & Hedwig, 2011; reviewed in Namiki & Kanzaki, 2016). Studies in other insects also link the LAL to locomotor control (reviewed in Namiki & Kanzaki, 2016). Additionally, the LAL receives a variety of sensory information (reviewed in Steinbeck et al., 2020), some of which is transmitted into the CX via different types of tangential neurons: TN neurons (optic flow: Stone et al., 2017; airflow: Currier et al., 2020), TL neurons (wind information: Okubo et al., 2020) and likely TU neurons (von Hadeln et al., 2020; Hulse et al., 2021). Information flow from the CX to the LAL is mediated via CPU neurons. Consequently, the LAL is a good candidate to mediate steering commands resulting from computations in the CX toward motor centers in the thoracic ganglia. Computational models support this assumption by illustrating that CX generated output can be utilized by the LAL circuitry to induce appropriate steering (Adden et al., 2020). Indeed, recent findings in *D. melanogaster* show that descending LAL neurons are involved in the control of steering driven by the CX and are directly contacted by types of CPU neurons (Rayshubskiy et al., 2020). However, the LAL also mediates locomotor commands based on sensory input that bypasses the CX (Steinbeck et al., 2020; Rayshubskiy et al., 2020; Franzke et al., 2021).

The GA is a small, distinct region of the LAL and can be divided into subregions in some species (Bogong moth, *Agrotis infusa*: de Vries et al., 2017; dung beetles, *Scarabaeus lamarcki* and *S. satyrus*: Immonen et al., 2017; *D. melanogaster*: Wolff & Rubin, 2018). In *D. melanogaster*, the GA primarily, but not exclusively, hosts recurrent connections between subtypes of CL1- and TL neurons (Hulse et al., 2021). However, the functions of these connections are currently unknown. Because some types of CX neurons target an undefined region surrounding the GA this area has been defined as the gall surround (GAs) in *D. melanogaster* (Wolff et al., 2015; Hulse et al., 2021).

## Polarization Vision

The sky provides several cues that can be used for spatial orientation and navigation. The most prominent one is the sun, but also the moon and the Milky Way provide orientation

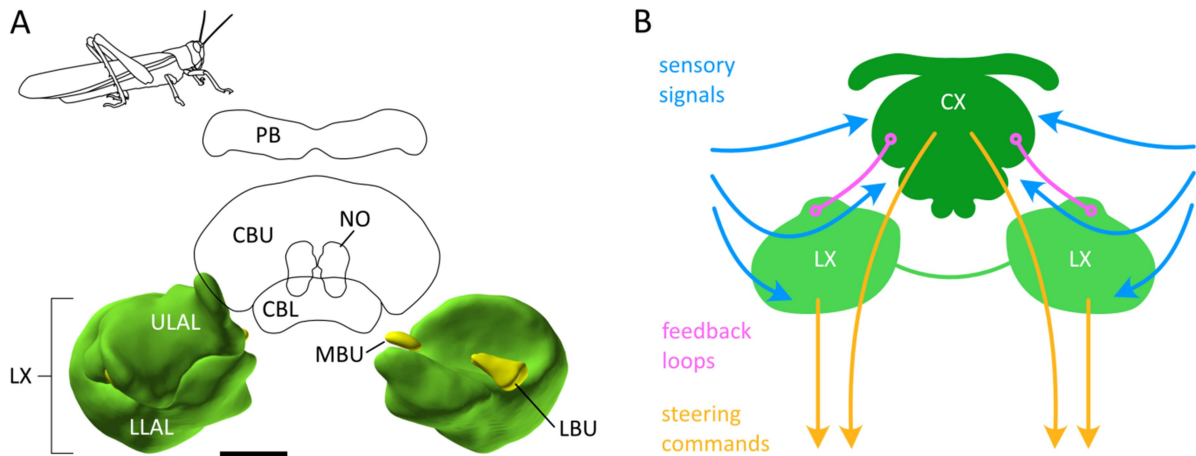


**Figure 4** The lateral complex (LX). **(A)** Frontal view of the three-dimensional standard of the locust LX showing the upper lateral accessory lobe (ULAL), the lower lateral accessory lobe (LLAL), the medial bulb (MBU), and the lateral bulb (LBU) located to both sides of the upper division of the central body (CBU) and the lower division of the central body (CBL). **(B)** Schematic illustrating the connectivity of the CX and the LX. The CX and the LX both receive sensory input (blue) from other brain regions. Some of these signals enter the CX through the LX. The LX contains descending neurons that transmit steering commands (yellow) to motor centers, some of which are generated in the CX. Additionally, LX and CX are connected via feedback loops. Three-dimensional model in **A** was generated with insectbrainDB.org based on data from el Jundi et al. (2010). **B** is adapted and modified based on Homberg (2004), Rayshubskiy (2021), Steinbeck et al. (2020) and Hulse et al. (2021)

information (Dacke et al., 2013, 2019). In addition to celestial objects, many insects can also use the sky light intensity gradient and the polarization pattern of the sky for orientation (el Jundi et al., 2014).

### *Polarized light*

Light consists of transverse electromagnetic waves with electric and magnetic fields oscillating at right angles to the direction of propagation. If the electric field waves oscillate in all planes perpendicular to the direction of travel, the light is unpolarized (Foster et al., 2018). If all electric field waves oscillate in the same plane, the light is 100% polarized. By convention the polarization of light concerns the orientation of the electric not the magnetic field waves, because it is mostly the electric field that exerts an effect on the matter the light interacts with (Foster et al., 2018). The prevailing axis in which the waves oscillate is the

angle of polarization (AoP) that can vary between  $0^\circ$  and  $180^\circ$  (Wehner, 2001; Foster et al., 2018). The percentage of an electromagnetic wave that is polarized is indicated by the degree of polarization (DoP; Pfeiffer et al., 2011), or more precisely: the DoP is the ratio between the intensity of the polarized portion to the total intensity of a light beam (Ellis et al., 2005; Foster et al., 2018). Furthermore, linearly (or plane) polarized light can be distinguished from circularly or elliptically polarized light. In linearly polarized light the electric fields oscillate in a single axis as the wave travels, whereas in circular or elliptical polarized light the axis changes as the light propagates (Mathejczyk & Wernet, 2017; Foster et al., 2018).

Polarized light is a common feature of our natural environment resulting from reflection of sunlight by different surfaces, including still water or vegetation, and from scattering of light in the atmosphere and hydrosphere (Wehner, 2001; Cronin & Marshall, 2011). Naturally occurring polarized light is most often linearly polarized, whereas elliptically polarized light is rare in nature, but can be used for visual communication in some species like the mantis shrimp (Cronin et al., 2009; Gagnon et al., 2015). For many insects the linearly polarized sky light provides a useful cue for spatial orientation and navigation.

### *The sky polarization pattern*

The polarization pattern in the sky (Figure 4A) results from Rayleigh scattering (Strutt, 1871) of unpolarized sunlight at small scattering centers (e.g. atoms, molecules, aerosols) in the atmosphere (Cronin & Marshall, 2011; Foster et al., 2018). The AoP of the scattered light is perpendicular to the scattering plane between the position of the sun, the observer, and the observed point (Zhang et al., 2015; Zhao et al., 2018). Additionally, from the point of view of the observer, the DoP increases with the angular distance from the sun reaching its maximum at  $90^\circ$  and then decreases again (Bernard & Wehner, 1977; Foster et al., 2018). Thus, the systematic pattern of DoP and AoP across the sky depends on and therefore indicates the sun's position and can serve as an orientation cue.

Felix Santschi discovered in the early 20<sup>th</sup> century that insects are able to orient properly even under sun-free skies (Wehner, 1982). He found that desert ants returning from a feeding source were able to maintain their homeward courses even when the sun was obscured (Wehner, 1982; Horváth, 2014). However, it was not until later in 1948 that Karl von Frisch performed similar experiments in dancing honeybees and identified the polarization of sky light to provide the orientation information (von Frisch, 1949; reviewed in Wehner, 1982 and Horváth, 2014). Since then a variety of studies in different insect species focused on their

ability to exploit polarized light information for orientation, including behavioral, physiological, and neuroanatomical studies.

### *The neural pathway for polarization vision in insects*

Insects have oddly beautiful eyes consisting of numerous individual light-detecting units, the ommatidia, that consist of usually eight photoreceptors (Strausfeld, 1976; Tomioka et al., 1990). The detection of polarized light is mainly mediated by a specific region of the compound eye, the dorsal rim area (DRA; reviewed in Labhart & Meyer, 1999). The visual pigments in the microvillar membrane of each photoreceptor in the DRA are aligned in a way to maximally absorb light that oscillates in a plane that is parallel to the microvilli long axis, i.e. light with a certain AoP, thus working as polarization analyzers (Labhart & Meyer, 1999). Each ommatidium within the DRA contains two groups of photoreceptor cells with orthogonal microvilli orientations resulting in a tuning of the photoreceptors to orthogonal AoPs (Homberg & Paech, 2002; Labhart & Meyer, 1999, 2002). The sets of photoreceptors within the DRA are homochromatic and blue sensitive in locusts and crickets (crickets, *Gryllus campestris*: Labhart et al., 1984; *S. gregaria*: Schmeling et al., 2014) and UV sensitive in monarch butterflies (Stalleicken et al., 2006), the fruit fly, desert ants, and honey bees (reviewed in Horváth, 2014 and Labhart, 2016). Polarization-sensitive neurons, whose activity shows a sinusoidal modulation when stimulated with a continuously rotating polarizer (Labhart, 1988; Vitzthum et al., 2002; Pfeiffer et al., 2005), mediate information flow from the optic lobes to the central brain. The main layout of this anterior polarization vision pathway (or sky-compass pathway) is conserved across insect species (reviewed in el Jundi et al., 2014; Heinze & Reppert, 2011; Heinze et al., 2013; Held et al., 2016; Hardcastle et al., 2021). Detailed insights are based on studies in *S. gregaria* and some of the general features are outlined in the following paragraph.

The photoreceptors of the locust DRA project to the dorsal rim area of the lamina and medulla of the optic lobe (Homberg & Paech, 2002; reviewed in el Jundi et al., 2014). Anatomically identified transmedulla neurons transmit information from the optic lobe to the lower unit of the anterior optic tubercle (AOTU-LU; Homberg et al., 2003; el Jundi et al., 2011) and likely integrate polarization signals and sky-compass associated unpolarized light information (el Jundi et al., 2011). Neurons of the AOTU-LU pass the information to TL neurons that project from the bulbs of the LX to the CBL (Pfeiffer et al., 2005; reviewed in el Jundi et al., 2014). TL neurons therefore constitute the input stage of the putative hierarchy

for polarized light processing in the CX (Vitzthum et al., 2002; Heinze & Homberg, 2009). From the CBL, information is carried via CL1a neurons to TB neurons of the PB (Heinze & Homberg, 2009). TB neurons pass information onto CPU neurons of the output stage. AoPs presented in the animal's zenith are represented topographically along the PB by the activity of TB and CPU neurons indicating that this cue can be utilized for compass orientation (Heinze & Homberg, 2007). Recent studies showed that the azimuth of a green light spot, likely representing the sun, is also represented in a compass-like fashion by the activity of neurons in the PB (Pegel et al., 2019) and that this sun compass is also encoded based on a whole-sky polarization pattern via matched-filter coding (Zittrell et al., 2020).

Additional elements of the polarization-vision network that have been extensively studied, are neurons that connect the AOTU-LU of both hemispheres (LoTu and TuTu neurons; Pfeiffer & Homberg, 2007; Kinoshita et al., 2007; Pfeiffer et al., 2011). These neurons are suggested to play a role in distinguishing the solar and the anti-solar hemisphere, and to compensate for changes in sky-compass information based on changing solar elevation during the day (reviewed in Homberg et al., 2011 and el Jundi et al., 2014).

## Scope of this work

Insects have demonstrated astonishing capabilities of spatial orientation and navigation with the CX and the LX playing a major role in the underlying neuronal network. The desert locust *Schistocerca gregaria*, a long-distance migrator, has been well studied in this regard revealing aspects of the intrinsic organization of the CX and the LX as well as an internal sky-compass in the CX. However, the complex architecture of the CX and the physiological properties of its components and especially the organization of the LX still required further investigations. We aimed to contribute insights into how CX neurons process the polarization pattern of the sky (**Chapter I**), and into the architecture of the CX (**Chapter II**) as well as into the network that is formed by the CX and the LX (**Chapter III**).

The utilization of polarized light has been intensely investigated in this context and a rich repertoire of studies exists tackling behavioral aspects as well as the underlying neuronal components. However, the degree of polarization (DoP) - although an important feature of the sky's polarization pattern - has been taken into account only by a few behavioral studies (von Frisch, 1967; Henze & Labhart, 2007; Foster et al., 2019), and even fewer physiological studies (Labhart, 1996; Sakura et al., 2008; Pfeiffer et al., 2011). To close this knowledge gap,

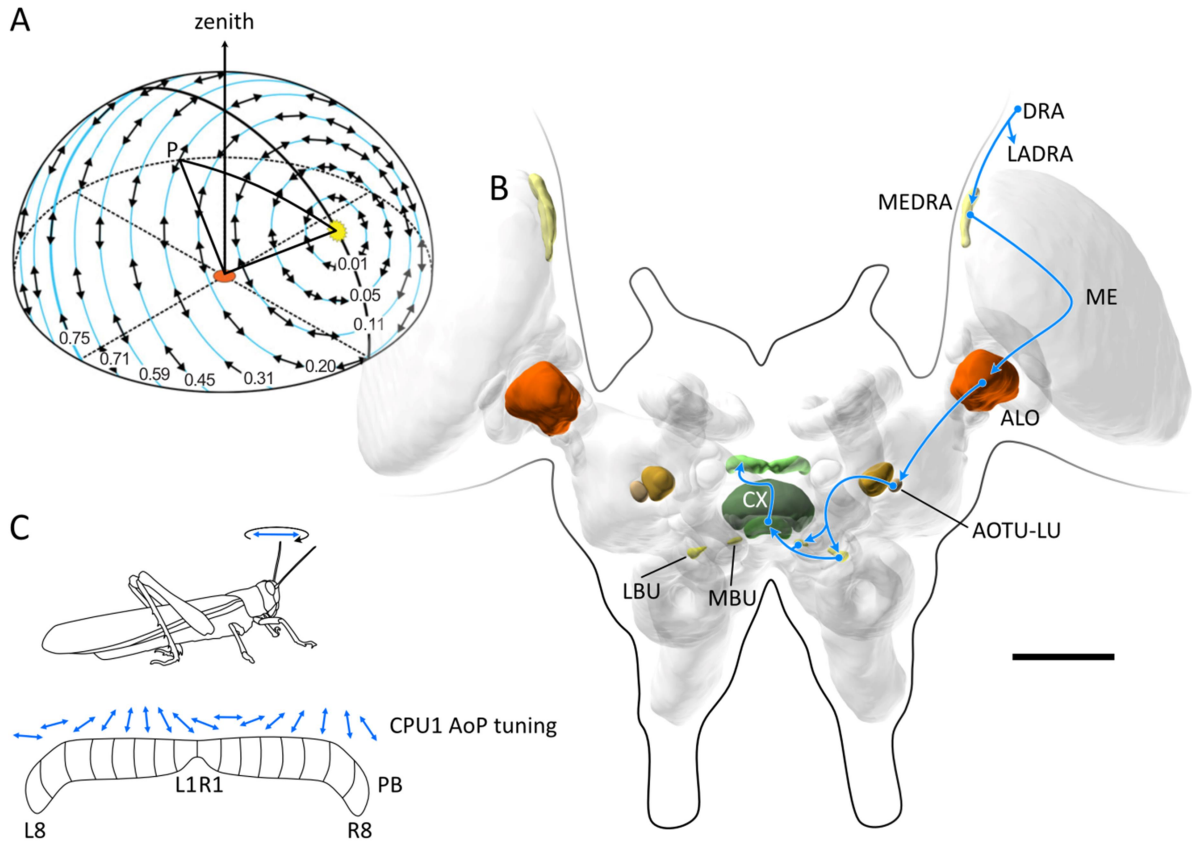


**Figure 5** The polarization compass in the locust. **(A)** Schematic of the sky's polarization pattern relative to an observer (orange spot) at a solar elevation of  $40^\circ$ . Double-arrows indicate the angle of polarization (AoP) which is perpendicular to the scattering plane defined by the observed point (P), the observer, and the sun (yellow spot). The numbers indicate the degree of polarization that is highest (0.75) at an angular distance of  $90^\circ$  from the sun. **(B)** The anterior polarization vision pathway (blue) from the dorsal rim area (DRA) of the compound eye to the central complex (CX). **(C)** The AoP of blue polarized light presented in the zenith of the locust is represented topographically across the columns (L8 to R8) of the protocerebral bridge (PB) in the activity of CPU1 neurons. **A** adapted and modified from Pfeiffer et al. (2011) and Zhao et al. (2018). **B** adapted and modified from Homberg (2004). The brain model in **B** was generated with insectbrainDB.org. **C** adapted and modified from Pegel et al. (2019) and Zittrell et al. (2020). ALO, anterior lobe of the lobula complex; AOTU-LU, lower unit of the anterior optic tubercle; LBU, lateral bulb of the lateral complex; LADRA, dorsal rim area of the lamina; ME, medulla; MEDRA, dorsal rim area of the medulla; MBU, medial bulb of the lateral complex. Scale bar = 500  $\mu\text{m}$ .

we recorded intracellularly from neurons of the CX of the locust to analyze how they perform at different degrees of polarization (**Chapter I**). We show that a reliable coding of the angle of polarization is also possible at low DoPs (0.05-0.35, depending on cell type). However, the

neuronal responses are influenced by the DoP, suggesting that this feature is actually integrated when the sky's polarization pattern is used for navigation.

Insights into the neuroarchitecture of the locust CX are drawn from different experimental approaches, extending from the visualization of neuropils and fiber tracts and the investigation of the distribution of neuroactive substances to single-cell dye-injections. Despite these efforts many cell types and potential wiring schemes remain obscure. To complement this knowledge, we performed immunocytochemical stainings using antisera against myoinhibitory peptide (MIP) in the CX (**Chapter II**). We identified four different types of columnar neurons and one type of tangential neuron as MIP-positive. Amongst those, two types of columnar neurons are known to be core elements of the sky-compass network in the locust and the head-direction network in *D. melanogaster*. We show that, of these, CL1b neurons are similar in cell number when compared to the homologous neurons in *D. melanogaster*. Moreover, we found that specific types of columnar neurons of the upper division of the central body appear to be particularly high in number (CUy neurons), another finding that corresponds to what has been described for the fruit fly and for likely homologous cell types in the cockroach (*Rhyarobia maderae*). Aside from these anatomical findings our study suggests a function of MIP in the networks of CX.

The CX is closely associated with the LX that comprises the bulb and the LAL. Extensive connections exist between both brain regions, and especially in *S. gregaria* the input routes from the bulbs to the CX are well described. However, the target structures of some polarization-sensitive columnar and tangential cells in the LX remained undefined and needed to be determined. To this end we analyzed the arborization patterns of these cells in more detail using immunocytochemical stainings and three-dimensional reconstructions, thereby revealing two potential feedback loops between the CX and the LX. Similar computational motifs are known also in *D. melanogaster* (**Chapter III**). The LAL is the largest portion of the LX and houses a variety of cells most of which are described based on studies in the silkworm *B. mori* and *D. melanogaster*. We performed single-cell stainings and three-dimensional reconstructions to identify neuron types of the LAL in *S. gregaria* (**Chapter III**). We described neurons that likely provide sensory input to the LAL and neurons that could contribute to the communication between the LAL and thoracic motor centers, complementing the picture of the LAL as a general steering network that mediates sensory-driven behavior in insects as proposed by Steinbeck et al. (2020).



## References

- Adden, A., Stewart, T. C., Webb, B., & Heinze, S. (2020). A neural model for insect steering applied to olfaction and path integration. *BioRxiv*, 2020.08.25.266247. <https://doi.org/10.1101/2020.08.25.266247>
- Bender, J. A., Pollack, A. J., & Ritzmann, R. E. (2010). Neural activity in the central complex of the insect brain is linked to locomotor changes. *Current Biology*, 20(10), 921–926. <https://doi.org/10.1016/j.cub.2010.03.054>
- Bernard, G. D., & Wehner, R. (1977). Functional similarities between polarization vision and color vision. *Vision Research*, 17(9), 1019–1028. [https://doi.org/10.1016/0042-6989\(77\)90005-0](https://doi.org/10.1016/0042-6989(77)90005-0)
- Boyan, G. S., & Liu, Y. (2016). Development of the neurochemical architecture of the central complex. *Frontiers in Behavioral Neuroscience*, 10. <https://doi.org/10.3389/fnbeh.2016.00167>
- Boyan, G. S., & Reichert, H. (2011). Mechanisms for complexity in the brain: generating the insect central complex. *Trends in Neurosciences*, 34(5), 247–257. <https://doi.org/10.1016/j.tins.2011.02.002>
- Boyan, G. S., & Williams, J. L. D. (1997). Embryonic development of the pars intercerebralis/central complex of the grasshopper. *Development Genes and Evolution*, 207(5), 317–329. <https://doi.org/10.1007/s004270050119>
- Brines, M. L., & Gould, J. L. (1982). Skylight polarization patterns and animal orientation. *Journal of Experimental Biology*, 96(1), 69–91. <https://doi.org/10.1242/jeb.96.1.69>
- Buehlmann, C., Mangan, M., & Graham, P. (2020). Multimodal interactions in insect navigation. *Animal Cognition*, 23(6), 1129–1141. <https://doi.org/10.1007/s10071-020-01383-2>
- Byrne, M., Dacke, M., Nordström, P., Scholtz, C., & Warrant, E. (2003). Visual cues used by ball-rolling dung beetles for orientation. *Journal of Comparative Physiology A: Sensory, Neural, and Behavioral Physiology*, 189(6), 411–418. <https://doi.org/10.1007/s00359-003-0415-1>
- Chiang, A.-S., Lin, C.-Y., Chuang, C.-C., Chang, H.-M., Hsieh, C.-H., Yeh, C.-W., Shih, C.-T., Wu, J.-J., Wang, G.-T., Chen, Y.-C., Wu, C.-C., Chen, G.-Y., Ching, Y.-T., Lee, P.-C., Lin, C.-Y., Lin, H.-H., Wu, C.-C., Hsu, H.-W., Huang, Y.-A., ... Hwang, J.-K. (2011). Three-dimensional reconstruction of brain-wide wiring networks in *Drosophila* at single-cell resolution. *Current Biology*, 21(1), 1–11. <https://doi.org/10.1016/j.cub.2010.11.056>

- Collett, T. S. (2019). Path integration: how details of the honeybee waggle dance and the foraging strategies of desert ants might help in understanding its mechanisms. *Journal of Experimental Biology*, 222(11), jeb205187. <https://doi.org/10.1242/jeb.205187>
- Cronin, T. W., Chiou, T.-H., Caldwell, R. L., Roberts, N., & Marshall, J. (2009). Polarization signals in mantis shrimps. *Proc. SPIE 7461, Polarization Science and Remote Sensing IV*, 74610C; <https://doi.org/10.1117/12.828492>
- Cronin, T. W., & Marshall, J. (2011). Patterns and properties of polarized light in air and water. *Philosophical Transactions of the Royal Society B: Biological Sciences*, 366(1565), 619–626. <https://doi.org/10.1098/rstb.2010.0201>
- Currier, T. A., Matheson, A. M., & Nagel, K. I. (2020). Encoding and control of orientation to airflow by a set of *Drosophila* fan-shaped body neurons. *eLife*, 9, e61510. <https://doi.org/10.7554/eLife.61510>
- Dacke, M., Baird, E., Byrne, M., Scholtz, C. H., & Warrant, E. J. (2013). Dung beetles use the Milky Way for orientation. *Current Biology*, 23(4), 298–300. <https://doi.org/10.1016/j.cub.2012.12.034>
- Dacke, M., Bell, A. T. A., Foster, J. J., Baird, E. J., Strube-Bloss, M. F., Byrne, M. J., & el Jundi, B. (2019). Multimodal cue integration in the dung beetle compass. *Proceedings of the National Academy of Sciences*, 116(28), 14248–14253. <https://doi.org/10.1073/pnas.1904308116>
- Dacke, M., Byrne, M., Smolka, J., Warrant, E., & Baird, E. (2013). Dung beetles ignore landmarks for straight-line orientation. *Journal of Comparative Physiology A*, 199(1), 17–23. <https://doi.org/10.1007/s00359-012-0764-8>
- de Velasco, B., Erclik, T., Shy, D., Sclafani, J., Lipshitz, H., McInnes, R., & Hartenstein, V. (2007). Specification and development of the pars intercerebralis and pars lateralis, neuroendocrine command centers in the *Drosophila* brain. *Developmental Biology*, 302(1), 309–323. <https://doi.org/10.1016/j.ydbio.2006.09.035>
- de Vries, L., Pfeiffer, K., Trebels, B., Adden, A. K., Green, K., Warrant, E., & Heinze, S. (2017). Comparison of navigation-related brain regions in migratory versus non-migratory noctuid moths. *Frontiers in Behavioral Neuroscience*, 11, 158. <https://doi.org/10.3389/fnbeh.2017.00158>
- Donlea, J. M., Pimentel, D., & Miesenböck, G. (2014). Neuronal machinery of sleep homeostasis in *Drosophila*. *Neuron*, 81(4), 860–872. <https://doi.org/10.1016/j.neuron.2013.12.013>
- el Jundi, B., Heinze, S., Lenschow, C., Kurylas, A., Rohlfing, T., & Homberg, U. (2010). The locust standard brain: a 3D standard of the central complex as a platform for neural network analysis. *Frontiers in Systems Neuroscience*, 3. <https://doi.org/10.3389/neuro.06.021.2009>

- el Jundi, B., Pfeiffer, K., Heinze, S., & Homberg, U. (2014). Integration of polarization and chromatic cues in the insect sky compass. *Journal of Comparative Physiology A*. <https://doi.org/10.1007/s00359-014-0890-6>
- el Jundi, B., Pfeiffer, K., & Homberg, U. (2011). A distinct layer of the medulla integrates sky compass signals in the brain of an insect. *PLoS ONE*, *6*(11), e27855. <https://doi.org/10.1371/journal.pone.0027855>
- el Jundi, B., Smolka, J., Baird, E., Byrne, M. J., & Dacke, M. (2014). Diurnal dung beetles use the intensity gradient and the polarization pattern of the sky for orientation. *Journal of Experimental Biology*, jeb.101154. <https://doi.org/10.1242/jeb.101154>
- el Jundi, B., Warrant, E. J., Byrne, M. J., Khaldy, L., Baird, E., Smolka, J., & Dacke, M. (2015). Neural coding underlying the cue preference for celestial orientation. *Proceedings of the National Academy of Sciences*, *112*(36), 11395–11400. <https://doi.org/10.1073/pnas.1501272112>
- Ellis, J., Dogariu, A., Ponomarenko, S., & Wolf, E. (2005). Degree of polarization of statistically stationary electromagnetic fields. *Optics Communications*, *248*(4–6), 333–337. <https://doi.org/10.1016/j.optcom.2004.12.050>
- Fisher, Y. E., Lu, J., D’Alessandro, I., & Wilson, R. I. (2019). Sensorimotor experience remaps visual input to a heading-direction network. *Nature*, *576*(7785), 121–125. <https://doi.org/10.1038/s41586-019-1772-4>
- Foster, J. J., Kirwan, J. D., el Jundi, B., Smolka, J., Khaldy, L., Baird, E., Byrne, M. J., Nilsson, D.-E., Johnsen, S., & Dacke, M. (2019). Orienting to polarized light at night - matching lunar skylight to performance in a nocturnal beetle. *Journal of Experimental Biology*, *222*(2), jeb.188532. <https://doi.org/10.1242/jeb.188532>
- Foster, J. J., Temple, S. E., How, M. J., Daly, I. M., Sharkey, C. R., Wilby, D., & Roberts, N. W. (2018). Polarisation vision: overcoming challenges of working with a property of light we barely see. *The Science of Nature*, *105*(3–4), 27. <https://doi.org/10.1007/s00114-018-1551-3>
- Franconville, R., Beron, C., & Jayaraman, V. (2018). Building a functional connectome of the *Drosophila* central complex. *eLife*, *7*, e37017. <https://doi.org/10.7554/eLife.37017>
- Franzke, M., Kraus, C., Gayler, M., Dreyer, D., Pfeiffer, K., & el Jundi, B. (2022). Stimulus-dependent orientation strategies in monarch butterflies. *Journal of Experimental Biology*, *225*(3), jeb243687. <https://doi.org/10.1242/jeb.243687>
- Gagnon, Y. L., Templin, R. M., How, M. J., & Marshall, N. J. (2015). Circularly polarized light as a communication signal in mantis shrimps. *Current Biology*, *25*(23), 3074–3078. <https://doi.org/10.1016/j.cub.2015.10.047>

- Green, J., Adachi, A., Shah, K. K., Hirokawa, J. D., Magani, P. S., & Maimon, G. (2017). A neural circuit architecture for angular integration in *Drosophila*. *Nature*, *546*(7656), 101–106. <https://doi.org/10.1038/nature22343>
- Green, J., & Maimon, G. (2018). Building a heading signal from anatomically defined neuron types in the *Drosophila* central complex. *Current Opinion in Neurobiology*, *52*, 156–164. <https://doi.org/10.1016/j.conb.2018.06.010>
- Hanesch, U., Fischbach, K.-F., & Heisenberg, M. (1989). Neuronal architecture of the central complex in *Drosophila melanogaster*. *Cell and Tissue Research*, *257*(2), 343–366. <https://doi.org/10.1007/BF00261838>
- Hardcastle, B. J., Omoto, J. J., Kandimalla, P., Nguyen, B.-C. M., Keleş, M. F., Boyd, N. K., Hartenstein, V., & Frye, M. A. (2021). A visual pathway for skylight polarization processing in *Drosophila*. *eLife*, *10*, e63225. <https://doi.org/10.7554/eLife.63225>
- Harootonian, S. K., Ekstrom, A. D., & Wilson, R. C. (2022). Combination and competition between path integration and landmark navigation in the estimation of heading direction. *PLOS Computational Biology*, *18*(2), e1009222. <https://doi.org/10.1371/journal.pcbi.1009222>
- Heinze, S. (2017). Unraveling the neural basis of insect navigation. *Current Opinion in Insect Science*, *24*, 58–67. <https://doi.org/10.1016/j.cois.2017.09.001>
- Heinze, S., Florman, J., Asokaraj, S., el Jundi, B., & Reppert, S. M. (2013). Anatomical basis of sun compass navigation II: The neuronal composition of the central complex of the monarch butterfly. *Journal of Comparative Neurology*, *521*(2), 267–298. <https://doi.org/10.1002/cne.23214>
- Heinze, S., & Homberg, U. (2007). Maplike representation of celestial E-vector orientations in the brain of an insect. *Science*, *315*, 995–997. <https://doi.org/10.1126/science.1135531>
- Heinze, S., & Homberg, U. (2008). Neuroarchitecture of the central complex of the desert locust: intrinsic and columnar neurons. *Journal of Comparative Neurology*, *511*(4), 454–478. <https://doi.org/10.1002/cne.21842>
- Heinze, S., & Homberg, U. (2009). Linking the input to the output: new sets of neurons complement the polarization vision network in the locust central complex. *Journal of Neuroscience*, *29*(15), 4911–4921. <https://doi.org/10.1523/JNEUROSCI.0332-09.2009>
- Heinze, S., & Pfeiffer, K. (2018). The insect central complex - from sensory coding to directing movement. *Frontiers in Behavioral Neuroscience*, *12*, 156. <https://doi.org/10.3389/fnbeh.2018.00156>

- Heinze, S., & Reppert, S. M. (2011). Sun compass integration of skylight cues in migratory monarch butterflies. *Neuron*, *69*(2), 345-358. <https://doi.org/10.1016/j.neuron.2010.12.025>
- Heinze, S., & Reppert, S. M. (2012). Anatomical basis of sun compass navigation I: the general layout of the monarch butterfly brain. *Journal of Comparative Neurology*, *520*(8), 1599–1628. <https://doi.org/10.1002/cne.23054>
- Held, M., Berz, A., Hensgen, R., Muenz, T. S., Scholl, C., Rössler, W., Homberg, U., & Pfeiffer, K. (2016). Microglomerular synaptic complexes in the sky-compass network of the honeybee connect parallel pathways from the anterior optic tubercle to the central complex. *Frontiers in Behavioral Neuroscience*, *10*. <https://doi.org/10.3389/fnbeh.2016.00186>
- Hensgen, R., England, L., Homberg, U., & Pfeiffer, K. (2021). Neuroarchitecture of the central complex in the brain of the honeybee: neuronal cell types. *Journal of Comparative Neurology*, *529*(1), 159–186. <https://doi.org/10.1002/cne.24941>
- Henze, M. J., & Labhart, T. (2007). Haze, clouds and limited sky visibility: polarotactic orientation of crickets under difficult stimulus conditions. *Journal of Experimental Biology*, *210*(18), 3266–3276. <https://doi.org/10.1242/jeb.007831>
- Homberg, U. (1991). Neuroarchitecture of the central complex in the brain of the locust *Schistocerca gregaria* and *S. americana* as revealed by serotonin immunocytochemistry. *Journal of Comparative Neurology*, *303*(2), 245–254. <https://doi.org/10.1002/cne.903030207>
- Homberg, U. (2002). Neurotransmitters and neuropeptides in the brain of the locust. *Microscopy Research and Technique*, *56*(3), 189–209. <https://doi.org/10.1002/jemt.10024>
- Homberg, U. (2004). In search of the sky compass in the insect brain. *Naturwissenschaften*, *91*(5), 199–208. <https://doi.org/10.1007/s00114-004-0525-9>
- Homberg, U. (2015). Sky compass orientation in desert locusts - evidence from field and laboratory studies. *Frontiers in Behavioral Neuroscience*, *9*. <https://doi.org/10.3389/fnbeh.2015.00346>
- Homberg, U., Heinze, S., Pfeiffer, K., Kinoshita, M., & el Jundi, B. (2011). Central neural coding of sky polarization in insects. *Philosophical Transactions of the Royal Society B: Biological Sciences*, *366*(1565), 680–687. <https://doi.org/10.1098/rstb.2010.0199>
- Homberg, U., Hofer, S., Pfeiffer, K., & Gebhardt, S. (2003). Organization and neural connections of the anterior optic tubercle in the brain of the locust, *Schistocerca gregaria*. *Journal of Comparative Neurology*, *462*(4), 415–430. <https://doi.org/10.1002/cne.10771>

- Homberg, U., Humberg, T.-H., Seyfarth, J., Bode, K., & Pérez, M. Q. (2018). GABA immunostaining in the central complex of dicondylian insects. *Journal of Comparative Neurology*, 526(14), 2301–2318. <https://doi.org/10.1002/cne.24497>
- Homberg, U., & Paech, A. (2002). Ultrastructure and orientation of ommatidia in the dorsal rim area of the locust compound eye. *Arthropod Structure & Development*, 30(4), 271–280. [https://doi.org/10.1016/S1467-8039\(02\)00010-5](https://doi.org/10.1016/S1467-8039(02)00010-5)
- Homberg, U., Vitzthum, H., Müller, M., & Binkle, U. (1999). Immunocytochemistry of GABA in the central complex of the locust *Schistocerca gregaria*: Identification of immunoreactive neurons and colocalization with neuropeptides. *Journal of Comparative Neurology*, 409(3), 495–507. [https://doi.org/10.1002/\(SICI\)1096-9861\(19990705\)409:3<495::AID-CNE12>3.0.CO;2-F](https://doi.org/10.1002/(SICI)1096-9861(19990705)409:3<495::AID-CNE12>3.0.CO;2-F)
- Honkanen, A., Adden, A., da Silva Freitas, J., & Heinze, S. (2019). The insect central complex and the neural basis of navigational strategies. *Journal of Experimental Biology*, 222(Suppl\_1), jeb188854. <https://doi.org/10.1242/jeb.188854>
- Horváth, G. (2014). Polarized light and polarization vision in animal sciences. Springer Berlin Heidelberg. <https://doi.org/10.1007/978-3-642-54718-8>
- Hulse, B. K., Haberkern, H., Franconville, R., Turner-Evans, D. B., Takemura, S., Wolff, T., Noorman, M., Dreher, M., Dan, C., Parekh, R., Hermundstad, A. M., Rubin, G. M., & Jayaraman, V. (2021). A connectome of the *Drosophila* central complex reveals network motifs suitable for flexible navigation and context-dependent action selection. *eLife*, e66039. <https://doi.org/10.7554/eLife.66039>
- Hulse, B. K., & Jayaraman, V. (2020). Mechanisms underlying the neural computation of head direction. *Annual Review of Neuroscience*, 43(1), 31–54. <https://doi.org/10.1146/annurev-neuro-072116-031516>
- Immonen, E.-V., Dacke, M., Heinze, S., & el Jundi, B. (2017). Anatomical organization of the brain of a diurnal and a nocturnal dung beetle. *Journal of Comparative Neurology*, 525(8), 1879–1908. <https://doi.org/10.1002/cne.24169>
- Ito, K., Shinomiya, K., Ito, M., Armstrong, J. D., Boyan, G., Hartenstein, V., Harzsch, S., Heisenberg, M., Homberg, U., Jenett, A., Keshishian, H., Restifo, L. L., Rössler, W., Simpson, J. H., Strausfeld, N. J., Strauss, R., & Vosshall, L. B. (2014). A systematic nomenclature for the insect brain. *Neuron*, 81(4), 755–765. <https://doi.org/10.1016/j.neuron.2013.12.017>
- Iwano, M., Hill, E. S., Mori, A., Mishima, T., Mishima, T., Ito, K., & Kanzaki, R. (2010). Neurons associated with the flip-flop activity in the lateral accessory lobe and ventral protocerebrum of the silkworm moth brain. *Journal of Comparative Neurology*, 518(3), 366–388. <https://doi.org/10.1002/cne.22224>

- Jain, D., Jakhalekar, I. R., & Deshmukh, S. S. (2017). Navigational strategies and their neural correlates. *Journal of the Indian Institute of Science*, 97(4), 511–525. <https://doi.org/10.1007/s41745-017-0053-1>
- Kahsai, L., Martin, J.-R., & Winther, Å. M. E. (2010). Neuropeptides in the *Drosophila* central complex in modulation of locomotor behavior. *Journal of Experimental Biology*, 213(13), 2256–2265. <https://doi.org/10.1242/jeb.043190>
- Kahsai, L., & Winther, Å. M. E. (2011). Chemical neuroanatomy of the *Drosophila* central complex: distribution of multiple neuropeptides in relation to neurotransmitters. *Journal of Comparative Neurology*, 519(2), 290–315. <https://doi.org/10.1002/cne.22520>
- Kanzaki, R., Ikeda, A., & Shibuya, T. (1994). Morphological and physiological properties of pheromone-triggered flipflopping descending interneurons of the male silkworm moth, *Bombyx mori*. *Journal of Comparative Physiology A*, 175(1). <https://doi.org/10.1007/BF00217431>
- Kinoshita, M., Pfeiffer, K., & Homberg, U. (2007). Spectral properties of identified polarized-light sensitive interneurons in the brain of the desert locust *Schistocerca gregaria*. *Journal of Experimental Biology*, 210(8), 1350–1361. <https://doi.org/10.1242/jeb.02744>
- Kong, E. C., Woo, K., Li, H., Lebestky, T., Mayer, N., Sniffen, M. R., Heberlein, U., Bainton, R. J., Hirsh, J., & Wolf, F. W. (2010). A pair of dopamine neurons target the D1-Like dopamine receptor DopR in the central complex to promote ethanol-stimulated locomotion in *Drosophila*. *PLoS ONE*, 5(4), e9954. <https://doi.org/10.1371/journal.pone.0009954>
- Kunst, M., Pförtner, R., Aschenbrenner, K., & Heinrich, R. (2011). Neurochemical architecture of the central complex related to its function in the control of grasshopper acoustic communication. *PLoS ONE*, 6(9), e25613. <https://doi.org/10.1371/journal.pone.0025613>
- Labhart, T. (1988). Polarization-opponent interneurons in the insect visual system. *Nature*, 331, 435–437. <https://doi.org/10.1038/331435a0>
- Labhart, T. (1996). How polarization-sensitive interneurons of crickets perform at low degrees of polarization. *Journal of Experimental Biology*, 199(7), 1467–1475. <https://doi.org/10.1242/jeb.199.7.1467>
- Labhart, T. (2016). Can invertebrates see the e-vector of polarization as a separate modality of light? *Journal of Experimental Biology*, 219(24), 3844–3856. <https://doi.org/10.1242/jeb.139899>

- Labhart, T., Hodel, B., & Valenzuela, I. (1984). The physiology of the cricket's compound eye with particular reference to the anatomically specialized dorsal rim area. *Journal of Comparative Physiology A*, 155(3), 289–296. <https://doi.org/10.1007/BF00610582>
- Labhart, T., & Meyer, E. P. (1999). Detectors for polarized skylight in insects: a survey of ommatidial specializations in the dorsal rim area of the compound eye. *Microscopy Research and Technique*, 47(6), 368–379. [https://doi.org/10.1002/\(SICI\)1097-0029\(19991215\)47:6<368::AID-JEMT2>3.0.CO;2-Q](https://doi.org/10.1002/(SICI)1097-0029(19991215)47:6<368::AID-JEMT2>3.0.CO;2-Q)
- Labhart, T., & Meyer, E. P. (2002). Neural mechanisms in insect navigation: polarization compass and odometer. *Current Opinion in Neurobiology*, 12(6), 707–714. [https://doi.org/10.1016/S0959-4388\(02\)00384-7](https://doi.org/10.1016/S0959-4388(02)00384-7)
- Liu, Liu, S., Kodama, L., Driscoll, M. R., & Wu, M. N. (2012). Two dopaminergic neurons signal to the dorsal fan-shaped body to promote wakefulness in *Drosophila*. *Current Biology*, 22(22), 2114–2123. <https://doi.org/10.1016/j.cub.2012.09.008>
- Liu, S., Liu, Q., Tabuchi, M., & Wu, M. N. (2016). Sleep drive is encoded by neural plastic changes in a dedicated circuit. *Cell*, 165(6), 1347–1360. <https://doi.org/10.1016/j.cell.2016.04.013>
- Martin, J. P., Guo, P., Mu, L., Harley, C. M., & Ritzmann, R. E. (2015). Central-complex control of movement in the freely walking cockroach. *Current Biology*, 25(21), 2795–2803. <https://doi.org/10.1016/j.cub.2015.09.044>
- Mathejczyk, T. F., & Wernet, M. F. (2017). Sensing polarized light in insects. In *Oxford Research Encyclopedia of Neuroscience*. Oxford Academy Press. <https://doi.org/10.1093/acrefore/9780190264086.013.109>
- Mota, T., Kreissl, S., Carrasco Durán, A., Lefer, D., Galizia, G., & Giurfa, M. (2016). Synaptic organization of microglomerular clusters in the lateral and medial bulbs of the honeybee brain. *Frontiers in Neuroanatomy*, 10. <https://doi.org/10.3389/fnana.2016.00103>
- Namiki, S., & Kanzaki, R. (2016). Comparative neuroanatomy of the lateral accessory lobe in the insect brain. *Frontiers in Physiology*, 7. <https://doi.org/10.3389/fphys.2016.00244>
- Nässel, D. R., & Homberg, U. (2006). Neuropeptides in interneurons of the insect brain. *Cell and Tissue Research*, 326(1), 1–24. <https://doi.org/10.1007/s00441-006-0210-8>
- Neuser, K., Triphan, T., Mronz, M., Poeck, B., & Strauss, R. (2008). Analysis of a spatial orientation memory in *Drosophila*. *Nature*, 453(7199), 1244–1247. <https://doi.org/10.1038/nature07003>
- Nguyen, T. A. T., Beetz, M. J., Merlin, C., & el Jundi, B. (2021). Sun compass neurons are tuned to migratory orientation in monarch butterflies. *Proceedings of the Royal*



*Society B: Biological Sciences*, 288(1945), 20202988.  
<https://doi.org/10.1098/rspb.2020.2988>

- Ofstad, T. A., Zuker, C. S., & Reiser, M. B. (2011). Visual place learning in *Drosophila melanogaster*. *Nature*, 474(7350), 204–207. <https://doi.org/10.1038/nature10131>
- Okubo, T. S., Patella, P., D'Alessandro, I., & Wilson, R. I. (2020). A neural network for wind-guided compass navigation. *Neuron*, 107(5), 924–940. <https://doi.org/10.1016/j.neuron.2020.06.022>
- Omoto, J. J., Keleş, M. F., Nguyen, B.-C. M., Bolanos, C., Lovick, J. K., Frye, M. A., & Hartenstein, V. (2017). Visual input to the *Drosophila* central complex by developmentally and functionally distinct neuronal populations. *Current Biology*, 27(8), 1098–1110. <https://doi.org/10.1016/j.cub.2017.02.063>
- Pascual, A., Huang, K.-L., Neveu, J., & Pr eat, T. (2004). Brain asymmetry and long-term memory. *Nature*, 427(6975), 605–606. <https://doi.org/10.1038/427605a>
- Pegel, U., Pfeiffer, K., & Homberg, U. (2017). Integration of celestial compass cues in the central complex of the locust brain. *Journal of Experimental Biology*, jeb.171207. <https://doi.org/10.1242/jeb.171207>
- Pegel, U., Pfeiffer, K., Zittrell, F., Scholtyssek, C., & Homberg, U. (2019). Two compasses in the central complex of the locust brain. *Journal of Neuroscience*, 39(16), 3070–3080. <https://doi.org/10.1523/JNEUROSCI.0940-18.2019>
- Pfeiffer, K., & Homberg, U. (2007). Coding of azimuthal directions via time-compensated combination of celestial compass cues. *Current Biology*, 17(11), 960–965. <https://doi.org/10.1016/j.cub.2007.04.059>
- Pfeiffer, K., & Homberg, U. (2014). Organization and functional roles of the central complex in the insect brain. *Annual Review of Entomology*, 59(1), 165–184. <https://doi.org/10.1146/annurev-ento-011613-162031>
- Pfeiffer, K., Kinoshita, M., & Homberg, U. (2005). Polarization-sensitive and light-sensitive neurons in two parallel pathways passing through the anterior optic tubercle in the locust brain. *Journal of Neurophysiology*, 94(6), 3903–3915. <https://doi.org/10.1152/jn.00276.2005>
- Pfeiffer, K., Negrello, M., & Homberg, U. (2011). Conditional perception under stimulus ambiguity: polarization- and azimuth-sensitive neurons in the locust brain are inhibited by low degrees of polarization. *Journal of Neurophysiology*, 105(1), 28–35. <https://doi.org/10.1152/jn.00480.2010>
- Phillips-Portillo, J., & Strausfeld, N. J. (2012). Representation of the brain's superior protocerebrum of the flesh fly, *Neobellieria bullata*, in the central body. *Journal of Comparative Neurology*, 520(14), 3070–3087. <https://doi.org/10.1002/cne.23094>

- Pisokas, I., Heinze, S., & Webb, B. (2020). The head direction circuit of two insect species. *eLife*, *9*, e53985. <https://doi.org/10.7554/eLife.53985>
- Pomozi, I., Horváth, G., & Wehner, R. (2001). How the clear-sky angle of polarization pattern continues underneath clouds: full-sky measurements and implications for animal orientation. *Journal of Experimental Biology*, *204*, 2933-2942. <https://doi.org/10.1242/jeb.204.17.2933>
- Rayshubskiy, A., Holtz, S. L., D'Alessandro, I., Li, A. A., Vanderbeck, Q. X., Haber, S., Gibb, P. W., & Wilson, R. I. (2020). Neural circuit mechanisms for steering control in walking *Drosophila*. *bioRxiv* 2020.04.04.024703; <https://doi.org/10.1101/2020.04.04.024703>
- Reppert, S. M., Guerra, P. A., & Merlin, C. (2016). Neurobiology of monarch butterfly migration. *Annual Review of Entomology*, *61*(1), 25–42. <https://doi.org/10.1146/annurev-ento-010814-020855>
- Sakura, M., Lambrinos, D., & Labhart, T. (2008). Polarized skylight navigation in insects: model and electrophysiology of e-vector coding by neurons in the central complex. *Journal of Neurophysiology*, *99*(2), 667–682. <https://doi.org/10.1152/jn.00784.2007>
- Sayre, M. E., Templin, R., Chavez, J., Kempnaers, J., & Heinze, S. (2021). A projectome of the bumblebee central complex. *eLife*, *10*, e68911. <https://doi.org/10.7554/eLife.68911>
- Schmeling, F., Wakakuwa, M., Tegtmeier, J., Kinoshita, M., Bockhorst, T., Arikawa, K., & Homberg, U. (2014). Opsin expression, physiological characterization and identification of photoreceptor cells in the dorsal rim area and main retina of the desert locust, *Schistocerca gregaria*. *Journal of Experimental Biology*, jeb.108514. <https://doi.org/10.1242/jeb.108514>
- Seelig, J. D., & Jayaraman, V. (2015). Neural dynamics for landmark orientation and angular path integration. *Nature*, *521*(7551), 186–191. <https://doi.org/10.1038/nature14446>
- Shafer, O. T., & Keene, A. C. (2021). The regulation of *Drosophila* sleep. *Current Biology*, *31*(1), R38–R49. <https://doi.org/10.1016/j.cub.2020.10.082>
- Shiozaki, H. M., Ohta, K., & Kazama, H. (2020). A multi-regional network encoding heading and steering maneuvers in *Drosophila*. *Neuron*, *106*(1), 126-141.e5. <https://doi.org/10.1016/j.neuron.2020.01.009>
- Skaggs, W. E., Knierim, J. J., Kudrimoti, H. S., & McNaughten, B. L. (1995). A model of neural basis of the rat's sense of direction. *Advances in Neural Information Processing Systems*, *7*, 173-180.
- Srinivasan, M. V. (2015). Where paths meet and cross: navigation by path integration in the desert ant and the honeybee. *Journal of Comparative Physiology A*, *201*(6), 533–546. <https://doi.org/10.1007/s00359-015-1000-0>

- Stalleicken, J., Labhart, T., & Mouritsen, H. (2006). Physiological characterization of the compound eye in monarch butterflies with focus on the dorsal rim area. *Journal of Comparative Physiology A*, 192(3), 321–331. <https://doi.org/10.1007/s00359-005-0073-6>
- Steinbeck, F., Adden, A., & Graham, P. (2020). Connecting brain to behaviour: a role for general purpose steering circuits in insect orientation? *Journal of Experimental Biology*, 223(5), jeb212332. <https://doi.org/10.1242/jeb.212332>
- Stone, T., Webb, B., Adden, A., Weddig, N. B., Honkanen, A., Templin, R., Wcislo, W., Scimeca, L., Warrant, E., & Heinze, S. (2017). An anatomically constrained model for path integration in the bee brain. *Current Biology*, 27(20), 3069-3085.e11. <https://doi.org/10.1016/j.cub.2017.08.052>
- Strausfeld, N. J. (1976). Atlas of an insect brain. Springer-Verlag.
- Strutt, J. W. (1871). XV. On the light from the sky, its polarization and colour. *The London, Edinburgh, and Dublin Philosophical Magazine and Journal of Science*, 41(271), 107–120. <https://doi.org/10.1080/14786447108640452>
- Sun, X., Yue, S., & Mangan, M. (2021). How the insect central complex could coordinate multimodal navigation. *eLife*, 10, e73077. <https://doi.org/10.7554/eLife.73077>
- Takahashi, N., Zittrell, F., Hensgen, R., & Homberg, U. (2022). Receptive field structure for two celestial compass cues at the input stage of the central complex in the locust brain. *Journal of Experimental Biology*, 225(4): jeb243858. <https://doi.org/10.1242/jeb243858>
- Timm, J., Scherner, M., Matschke, J., Kern, M., & Homberg, U. (2021). Tyrosine hydroxylase immunostaining in the central complex of dicondylian insects. *Journal of Comparative Neurology*, 529(12), 3131–3154. <https://doi.org/10.1002/cne.25151>
- Tomioka, K., Okada, Y., & Chiba, Y. (1990). Distribution of circadian photoreceptors in the compound eye of the cricket *Gryllus bimaculatus*. *Journal of Biological Rhythms*, 5(4), 303–313. <https://doi.org/10.1177/074873049000500403>
- Tomita, J., Ban, G., Kato, Y. S., & Kume, K. (2021). Protocerebral bridge neurons that regulate sleep in *Drosophila melanogaster*. *Frontiers in Neuroscience*, 15, 647117. <https://doi.org/10.3389/fnins.2021.647117>
- Träger, U., Wagner, R., Bausenwein, B., & Homberg, U. (2008). A novel type of microglomerular synaptic complex in the polarization vision pathway of the locust brain. *Journal of Comparative Neurology*, 506(2), 288–300. <https://doi.org/10.1002/cne.21512>
- Turner-Evans, D. B., Jensen, K. T., Ali, S., Paterson, T., Sheridan, A., Ray, R. P., Wolff, T., Lauritzen, J. S., Rubin, G. M., Bock, D. D., & Jayaraman, V. (2020). The

- neuroanatomical ultrastructure and function of a biological ring attractor. *Neuron*, 108(1), 145-163. <https://doi.org/10.1016/j.neuron.2020.08.006>
- Turner-Evans, Wegener, S., Rouault, H., Franconville, R., Wolff, T., Seelig, J. D., Druckmann, S., & Jayaraman, V. (2017). Angular velocity integration in a fly heading circuit. *eLife*, 6, e23496. <https://doi.org/10.7554/eLife.23496>
- Varga, A. G., Kathman, N. D., Martin, J. P., Guo, P., & Ritzmann, R. E. (2017). Spatial navigation and the central complex: sensory acquisition, orientation, and motor control. *Frontiers in Behavioral Neuroscience*, 11. <https://doi.org/10.3389/fnbeh.2017.00004>
- Vitzthum, H., & Homberg, U. (1998). Immunocytochemical demonstration of locust tachykinin-related peptides in the central complex of the locust brain. *Journal of Comparative Neurology*, 390(4), 455–469. [https://doi.org/10.1002/\(SICI\)1096-9861\(19980126\)390:4<455::AID-CNE1>3.0.CO;2-%23](https://doi.org/10.1002/(SICI)1096-9861(19980126)390:4<455::AID-CNE1>3.0.CO;2-%23)
- Vitzthum, H., Müller, M., & Homberg, U. (2002). Neurons of the central complex of the locust *Schistocerca gregaria* are sensitive to polarized light. *Journal of Neuroscience*, 22(3), 1114–1125. <https://doi.org/10.1523/JNEUROSCI.22-03-01114.2002>
- von Frisch, K. (1949). Die Polarisation des Himmelslichtes als orientierender Faktor bei den Tänzen der Bienen. *Experientia* 5, pp142-148
- von Frisch, K. (1967). The dance language and orientation of bees. Harvard University Press, Cambridge, MA
- von Hadeln, J., Althaus, V., Häger, L., & Homberg, U. (2018). Anatomical organization of the cerebrum of the desert locust *Schistocerca gregaria*. *Cell and Tissue Research*, 374(1), 39–62. <https://doi.org/10.1007/s00441-018-2844-8>
- von Hadeln, J., Hensgen, R., Bockhorst, T., Rosner, R., Heidasch, R., Pegel, U., Quintero Pérez, M., & Homberg, U. (2020). Neuroarchitecture of the central complex of the desert locust: tangential neurons. *Journal of Comparative Neurology*, 528(6), 906–934. <https://doi.org/10.1002/cne.24796>
- Wehner, R. (1989). Neurobiology of polarization vision. *Trends in Neurosciences*, 12(9), 353-359. [10.1016/0166-2236\(89\)90043-x](https://doi.org/10.1016/0166-2236(89)90043-x)
- Wehner, R. (1982). Himmelsnavigation bei Insekten. *Neurophysiologie und Verhalten. Neujahrsblatt der Naturforschenden Gesellschaft Zürich*, pp1-123
- Wehner, R. (2001). Polarization vision – a uniform sensory capacity? *Journal of Experimental Biology*, 204(14), 2589-2596. <https://doi.org/10.1242/jeb.204.14.2589>
- Wehner, R. (2003). Desert ant navigation: how miniature brains solve complex tasks. *Journal of Comparative Physiology A: Sensory, Neural, and Behavioral Physiology*, 189(8), 579–588. <https://doi.org/10.1007/s00359-003-0431-1>

- Williams, J. L. D. (1975). Anatomical studies of the insect central nervous system: a ground-plan of the midbrain and an introduction to the central complex in the locust, *Schistocerca gregaria* (Orthoptera). *Journal of Zoology*, 176(1), 67–86. <https://doi.org/10.1111/j.1469-7998.1975.tb03188.x>
- Williams, J. L. D., Güntner, M., & Boyan, G. S. (2005). Building the central complex of the grasshopper *Schistocerca gregaria*: temporal topology organizes the neuroarchitecture of the w, x, y, z tracts. *Arthropod Structure & Development*, 34(1), 97–110. <https://doi.org/10.1016/j.asd.2004.11.001>
- Wolff, T., Iyer, N. A., & Rubin, G. M. (2015). Neuroarchitecture and neuroanatomy of the *Drosophila* central complex: a GAL4-based dissection of protocerebral bridge neurons and circuits. *Journal of Comparative Neurology*, 523(7), 997–1037. <https://doi.org/10.1002/cne.23705>
- Wolff, T., & Rubin, G. M. (2018). Neuroarchitecture of the *Drosophila* central complex: a catalog of nodulus and asymmetrical body neurons and a revision of the protocerebral bridge catalog. *Journal of Comparative Neurology*, 526(16), 2585–2611. <https://doi.org/10.1002/cne.24512>
- Zhang, W., Cao, Y., Zhang, X., & Liu, Z. (2015). Sky light polarization detection with linear polarizer triplet in light field camera inspired by insect vision. *Applied Optics*, 54(30), 8962. <https://doi.org/10.1364/AO.54.008962>
- Zhao, H., Xu, W., Zhang, Y., Li, X., Zhang, H., Xuan, J., & Jia, B. (2018). Polarization patterns under different sky conditions and a navigation method based on the symmetry of the AOP map of skylight. *Optics Express*, 26(22), 28589. <https://doi.org/10.1364/OE.26.028589>
- Zittrell, F., Pfeiffer, K., & Homberg, U. (2020). Matched-filter coding of sky polarization results in an internal sun compass in the brain of the desert locust. *Proceedings of the National Academy of Sciences*, 117(41), 25810–25817. <https://doi.org/10.1073/pnas.2005192117>
- Zorović, M., & Hedwig, B. (2011). Processing of species-specific auditory patterns in the cricket brain by ascending, local, and descending neurons during standing and walking. *Journal of Neurophysiology*, 105(5), 2181–2194. <https://doi.org/10.1152/jn.00416.2010>



## **Chapter I**

Performance of polarization-sensitive neurons  
of the locust central complex at different  
degrees of polarization







# Performance of polarization-sensitive neurons of the locust central complex at different degrees of polarization

Ronja Hensgen<sup>1</sup> · Frederick Zittrell<sup>1</sup> · Keram Pfeiffer<sup>2</sup> · Uwe Homberg<sup>1</sup>

Received: 8 September 2021 / Revised: 18 January 2022 / Accepted: 25 January 2022  
© The Author(s) 2022

## Abstract

The polarization pattern of the sky is exploited by many insects for spatial orientation and navigation. It derives from Rayleigh scattering in the atmosphere and depends directly on the position of the sun. In the insect brain, the central complex (CX) houses neurons tuned to the angle of polarization (AoP), that together constitute an internal compass for celestial navigation. Polarized light is not only characterized by the AoP, but also by the degree of polarization (DoP), which can be highly variable, depending on sky conditions. Under a clear sky, the DoP of polarized sky light may reach up to 0.75 but is usually much lower especially when light is scattered by clouds or haze. To investigate how the polarization-processing network of the CX copes with low DoPs, we recorded intracellularly from neurons of the locust CX at different stages of processing, while stimulating with light of different DoPs. Significant responses to polarized light occurred down to DoPs of 0.05 indicating reliable coding of the AoP even at unfavorable sky conditions. Moreover, we found that the activity of neurons at the CX input stage may be strongly influenced by nearly unpolarized light, while the activity of downstream neurons appears less affected.

**Keywords** Polarization vision · Central complex · Sky compass coding · Intracellular recordings · Desert locust

## Abbreviations

|             |   |
|-------------|---|
| AoP         | Angle of polarization   |
| CBL         | Lower division of the central body  |
| CBU         | Upper division of the central body  |
| CL neurons  | Columnar neurons of the protocerebral bridge and lower division of the central body |
| CPU neurons | Columnar neurons of the protocerebral bridge and upper division of the central body |
| CX          | Central complex   |
| DRA         | Dorsal rim area   |
| DoP         | Degree of polarization  |

|            |  |
|------------|--|
| TB neurons | Tangential neurons of the protocerebral bridge               |
| TL neurons | Tangential neurons of the lower division of the central body |

## Introduction

Spatial orientation and navigation require the perception and integration of environmental stimuli. For estimating spatial directions, many animals rely on sky compass cues, including celestial bodies such as the sun or moon, the chromatic gradient and the polarization pattern of the sky. Linear polarization of skylight mainly derives from Rayleigh scattering in the atmosphere (Strutt 1871) and results in a polarization pattern across the sky that directly depends on the position of the sun or moon (Fig. 1a). Orientation to polarized light has been demonstrated for several insect species in the field (honey bees, *Apis mellifera*: von Frisch 1949; Evangelista et al. 2014; desert ants, *Cataglyphis fortis*: Sommer and Wehner 2005; dung beetles, *Scarabaeus satyrus*: Dacke et al. 2013) and in the laboratory (desert locusts, *Schistocerca gregaria*: Mappes and Homberg 2004; field crickets, *Gryllus campestris*: Brunner and Labhart 1987; monarch butterflies,

Handling Editor: Friedrich G Barth.

✉ Uwe Homberg  
homberg@biologie.uni-marburg.de

<sup>1</sup> Department of Biology, Animal Physiology and Center for Mind Brain and Behavior (CMBB), Philipps-University of Marburg and Justus Liebig University of Giessen, 35032 Marburg, Germany

<sup>2</sup> Behavioral Physiology and Sociobiology (Zoology II), Biocenter, University of Würzburg, 97074 Würzburg, Germany

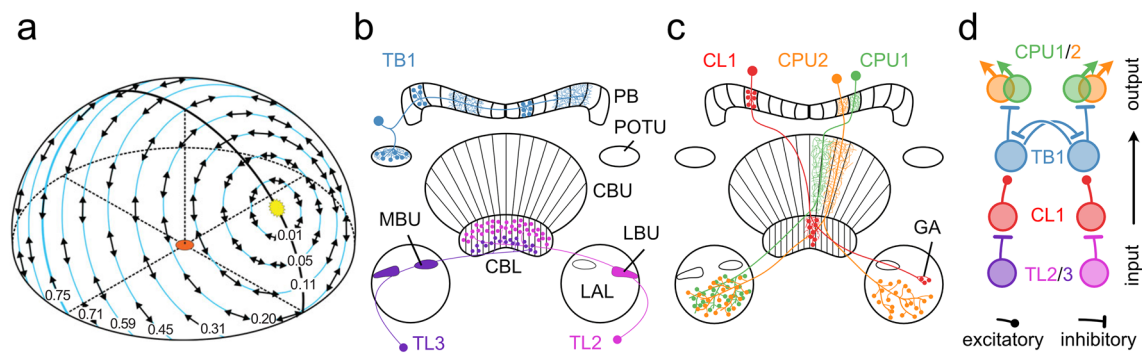


**Fig. 1** **a** Schematic representation of the polarization pattern of the sky as seen from the center of the sphere (orange) at a solar elevation of  $40^\circ$ . Double arrows indicate angles of polarization (AoP) that are arranged tangentially along concentric circles around the sun (yellow). Numbers indicate the degree of polarization (DoP). Under optimal atmospheric conditions the DoP increases with angular distance from the sun up to a maximum value of 0.75 at  $90^\circ$  from the sun. **b, c** Schematic illustration of tangential neurons (**b**) and columnar neurons (**c**) of the locust central complex. Fine branches indicate dendritic arborizations and small dots indicate axonal terminals. **b** TL2- and TL3 neurons provide input from the lateral bulb (LBU) and medial bulb (MBU) to the lower division of the central body (CBL). TB1 neurons connect the posterior optic tubercle (POTU) to the pro-

tocerebral bridge (PB). **c** CL1a neurons connect the CBL to the PB and the gall (GA). CPU1- and CPU2 neurons connect the PB to the upper division of the central body (CBU) and the lateral accessory lobes (LAL). **d** Putative processing hierarchy of the major types of polarization-sensitive neurons shown in **b, c**. TL2/TL3 neurons provide input to the central complex by synapsing onto intermediate-stage CL1a neurons. CL1a neurons transmit the information to TB1 neurons. Here, oppositely tuned neurons inhibit each other and finally synapse onto CPU1/CPU2 output neurons. **a** From Homberg et al. (2011) and Pfeiffer et al. (2011), **b, c** modified from Pegel et al. (2019) and Zittrell et al. (2020). **d** modified from Bockhorst and Homberg (2017)

*Danaus plexippus*: Reppert et al. 2004). The neural pathways that mediate transmission of polarization information from the eye to the central brain have been studied particularly well in locusts (Homberg et al. 2003, 2011; Kinoshita et al. 2007), crickets (Labhart 1988; Sakura et al. 2007; Labhart et al. 2001) and fruit flies (Hardcastle et al. 2021) but also in other insects including monarch butterflies (Heinze and Reppert 2011) and dung beetles (el Jundi et al. 2015). Specialized photoreceptors of a small, dorsal region of the compound eye, the dorsal rim area (DRA), are particularly sensitive to the oscillation angle of polarized light (Labhart and Meyer 1999). Signals from dorsal rim photoreceptors are transmitted via the optic lobe, the anterior optic tubercle, and the bulb of the lateral complex to the central complex (CX) of the brain. The CX is an assembly of midline spanning neuropils, including the protocerebral bridge, the lower (CBL) and upper (CBU) division of the central body (corresponding to the ellipsoid body and the fan-shaped body in *Drosophila*, respectively), and the paired noduli. The CX houses a neural network signaling head-direction (Seelig and Jayaraman 2015; Green and Maimon 2018; Green et al. 2019; Pisokas et al. 2020; Hulse and Jayaraman 2020; Shiozaki et al. 2020) and as such integrates various sensory cues to generate appropriate behavioral output and guidance during navigation (Varga et al. 2017; Honkanen et al. 2021). The architecture of the CX is characterized by the projections of tangential and columnar neurons (Fig. 1b, c) that provide connectivity within the CX and between the CX and other brain regions (Hanesch et al. 1989; Heinze and

Homberg 2008; Heinze et al. 2013; von Hadeln et al. 2020; Hulse et al. 2021).

As in other insects, many neurons of the CX of the locust *S. gregaria* are sensitive to the angle of polarization (AoP) of light from the sky. Physiological studies revealed a putative processing hierarchy for polarized light information in the CX (Fig. 1d; Heinze and Homberg 2009; Bockhorst and Homberg 2015): tangential neurons of the CBL (TL2, TL3 neurons, ER neurons or ring neurons in *Drosophila*) provide input from the bulbs of the lateral complex to the CX (Fig. 1b). Columnar neurons of the PB and CBU (CPU neurons, PFL neurons in *Drosophila*). The latter provide output from the CX to the lateral accessory lobes (Fig. 1c). Consistent with the role of the CX as an internal compass, the orientation of the pattern of AoPs across the sky and the azimuth of a simulated sun are represented topographically in the neuronal activity across the protocerebral bridge (Heinze and Homberg 2007; Pegel et al. 2019; Zittrell et al. 2020).

Linearly polarized light is characterized, in addition to its AoP, by the degree of polarization (DoP) which indicates the percentage of polarized light within a light beam. The DoP depends on the angular distance from the sun and is lowest for direct sunlight (DoP=0) and highest at  $90^\circ$  from the sun (DoP=0.75 under optimal sky conditions; Fig. 1a). The DoP decreases under haze or clouds resulting in lower

values. Several behavioral studies accounted for the natural occurrence of low DoPs by testing the performance of animals under matching conditions. For *A. mellifera* a detection threshold was proposed at a DoP between 0.07 and 0.1 (von Frisch 1967), and field crickets (*Gryllus campestris*) showed behavioral responses at DoPs even lower than 0.07 (Henze and Labhart 2007). Findings for the nocturnal dung beetle (*Scarabaeus satyrus*) indicated a behavioral threshold for polarized lunar skylight between 0.04 and 0.32 (Foster et al. 2019). These studies show that certain insect species can utilize polarization information for orientation even under highly unfavorable conditions. However, the majority of physiological experiments on neuronal responses to polarized light have been conducted with substantially higher DoPs (of 0.99). Only few studies examined the influence of low DoPs on neuronal responses. Among these are experiments performed in *G. campestris* that revealed a threshold DoP of 0.05 for polarization-opponent interneurons of the optic lobes (Labhart 1996) and an insensitivity of CX neurons of *G. bimaculatus* to changes in the DoP between 0.99 and 0.18 (Sakura et al. 2007). These findings fit the results from behavioral experiments. In contrast, neuronal responses of interneurons of the anterior optic tubercle of *S. gregaria* indicated a much higher DoP threshold of 0.3 and additionally demonstrated increasing neuronal inhibition upon stimulation with decreasing DoPs (Pfeiffer et al. 2011).

In this study, we investigated how different DoPs affect the responses of CX neurons of *S. gregaria* to polarized blue light. We show that reliable coding of AoPs is present in certain cell types down to DoPs of 0.05. Moreover, the activity of some neurons of the CX input is strongly affected by nearly unpolarized blue light, and this response is also mediated by the DRA.

## Materials and methods

### Animals and preparation

Male and female gregarious desert locusts were obtained from colonies reared at Philipps-Universität Marburg. Animals were kept at a constant temperature of 28 °C under a 12 h:12 h light/dark cycle. Animals were mounted onto a metal holder and legs and wings were cut off. A window was cut frontally into the head capsule, and fat tissue and air sacs were removed to get access to the brain. The esophagus was cut and the gut was removed via the abdomen, which was sealed afterwards with dental wax. The brain was stabilized from posterior with a small twisted metal wire inserted into the window of the head. Finally, the neural sheath of the brain was partly removed to allow penetration of the recording electrode. The brain was kept submerged in locust saline

(Clements and May 1974) during preparation, recording and dissection.

### Electrophysiology

Intracellular recordings were performed with sharp microelectrodes drawn from borosilicate capillaries (Hilgenberg, Malsfeld, Germany), with a Flaming/Brown horizontal puller (P-97, Sutter Instrument, Novato, CA). The tip of the electrodes was loaded with 4% Neurobiotin (Vector Laboratories, Burlingame, CA) in 1 mol l<sup>-1</sup> KCl and the shanks were loaded with 1 mol l<sup>-1</sup> KCl. Signals were amplified 10× with a BA-01× amplifier (npi electronic instruments, Tamm, Germany), and monitored with a custom-built audio monitor (University of Marburg) and an oscilloscope (Hameg, Frankfurt/Main, Germany). Data were digitized with a Power1401-mkII (Cambridge Electronic Design, Cambridge, GB) and stored on a PC using Spike2 (Cambridge Electronic Design, Cambridge, UK) with a sampling rate of 20 kHz. After the recording, Neurobiotin was injected into the cell by application of a positive current of 0.5–2 nA for at least 2 min.

### Histology and image acquisition

Brains were dissected and fixed in 4% paraformaldehyde, 0.25% glutaraldehyde, and 2% saturated picric acid diluted in 0.1 mol l<sup>-1</sup> phosphate buffered saline (PBS) at 4 °C overnight. Following rinses in PBS (4×15 min) brains were incubated in Cy3-conjugated streptavidin (1:1000) in PBS containing 0.3% Triton X-100 (PBT) at 4 °C for 3 days. Following rinses in PBT (2×20 min) and PBS (3×20 min) brains were dehydrated in an ascending ethanol series (30%, 50%, 70%, 90%, 95%, 100%, 15 min each) and cleared in a 1:1 mixture of 100% ethanol and methyl salicylate (Merck, Darmstadt, Germany) for 15 min and in pure methyl salicylate for 1 h. Finally, they were mounted in Permount (Fisher Scientific, Pittsburgh, PA) between two coverslips. Samples were scanned with a confocal laser scanning microscope (Leica, TCS SP5, Leica Microsystems, Wetzlar, Germany) with a 20× immersion objective (HC PL APO 20×/0.75 Imm Corr CS2, Leica). A diode pumped solid state laser (561 nm) was used to excite Cy3. Scanning frequency was 400 Hz and the voxel size was 0.54×0.54×2.0 μm<sup>3</sup>.

### Stimulation

Animals were stimulated from the zenith by light from a blue light emitting diode (LED; Oslon SSL 80, LDCQ7P, 452 nm, Osram Opto Semiconductors GmbH, Regensburg, Germany). The light was linearly polarized by a dichroic polarizer sheet (HNP'B, Polaroid, Cambridge, MA). To generate degrees of polarization between 0.002 and 0.9, diffusor

sheets were placed in different combinations between the LED and the polarizer or between the animal and the polarizer (Fig. 2a). At the highest degree of polarization, all four diffusor sheets were placed between the LED and the polarizer, while at the lowest degree of polarization, the four diffusor sheets were placed between the animal and the polarizer. With the different arrangements, five stimuli could be tested: DoP=0.99 (maximally polarized light,  $1.9 \times 10^{13}$

photons  $\text{cm}^{-2} \text{s}^{-1}$ ), DoP=0.35 ( $1.6 \times 10^{13}$  photons  $\text{cm}^{-2} \text{s}^{-1}$ ), DoP=0.1 and DoP=0.05 ( $1.5 \times 10^{13}$  photons  $\text{cm}^{-2} \text{s}^{-1}$ ), and DoP=0.002 ( $1.7 \times 10^{13}$  photons  $\text{cm}^{-2} \text{s}^{-1}$ ). The stimuli covered a visual angle of  $12.6^\circ$ . To monitor the angle and the degree of polarization, a HNP'B polarization filter was placed in front of an OPT101 photodiode/transimpedance amplifier (Texas Instruments, Dallas, TX) positioned close to the animal's head (Fig. 2a). The output of the OPT101

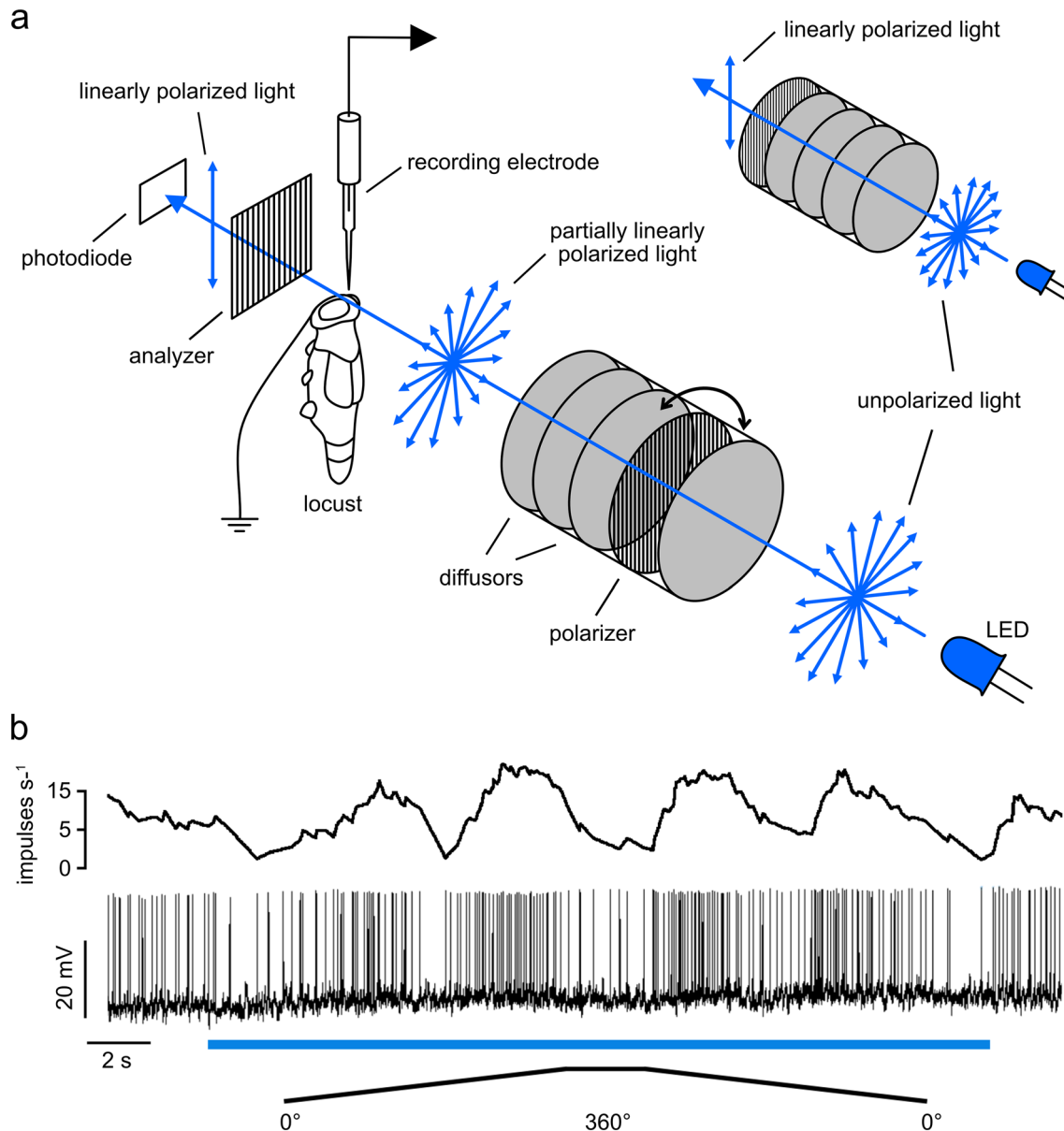


**Fig. 2** **a** Schematic illustration of the stimulus setup. Unpolarized light emitted by a light-emitting diode (LED) was linearly polarized by a polarizer. Diffusors were placed between the LED and the polarizer or between the polarizer and the animal to achieve different degrees of polarization (DoPs). With four diffusors between the LED and the polarizer (small image inset) maximally polarized light (DoP=0.99) was generated. The degree and angle of polarization

were measured via a photodiode/transimpedance amplifier placed behind a polarization filter. **b** Spike train showing the response of a CL1a neuron to two full rotations of the polarizer in clockwise and counterclockwise direction ( $0^\circ$ – $360^\circ$ ,  $360^\circ$ – $0^\circ$ ). The blue bar indicates the time window during which polarized blue light was presented. The mean spiking frequency is indicated as moving average with a window size of 1 s above the spike train

was continuously recorded via the digitizer. The stimulation device rotated 360° clockwise and counterclockwise at 40°/s. In four recordings from TL neurons, we painted the DRAs of the animal during the recording with acrylic black paint using a fine paintbrush. Removing the paint was also done while recording and was either done with forceps or with a paintbrush, depending on whether the paint was already dry or not.

## Data evaluation

Recording data were only analyzed when the recorded neuron was successfully labeled and the stained cell type unequivocally identified. Physiological data were preprocessed using Spike2 and exported as mat-files for further analysis in MATLAB (Version 2020a, The MathWorks, Natick, MA, USA) using custom scripts. Circular histograms were created with the CircHist package (Zittrell 2019). Confocal image stacks were processed in Amira 5.6 (ThermoFisher Scientific, Waltham, MA; RRID:SCR\_007353). Images showing raw data were exported from Spike2 and processed with Affinity photo and Affinity Designer (Serif, Nottingham, UK; RRID:SCR\_016951). Diagrams were generated with Microsoft Excel or MATLAB and were exported to Affinity photo to create figure panels.

## Background activity

Owing to fluctuations of background activity (BA) in some neurons we calculated the BA for comparison with firing activity during stimulation within a time window of 5 s preceding the respective stimulus. Spikes were binned in 1 s bins and these spike counts were used to calculate the median and the 2.5th and 97.5th percentile of BA.

## Stimulus responsiveness

We used linear-circular correlation analysis (*CircStat*; Berens 2009) to determine whether the modulation of spike rate was correlated to changes in AoP. Time points of action potentials during each 360° rotation were assigned to the respective orientation of the polarizer and these angles were doubled to allow using circular statistics on these axial data (Zar 1999). The resulting angles were averaged and the result was halved, yielding the preferred AoP ( $\Phi_{\max}$ ) in circular space. At least one clockwise and one counterclockwise rotation of the polarizer were included to measure the responsiveness to a stimulus with a particular DoP. To determine a correlation between firing rate and AoP, spike angles were binned in 10° bins and counts were tested for correlation with bin angles. A resulting  $P$  value  $< 0.05$  indicated significant modulation by AoP. To specify properties of significant responses, we calculated the mean resultant vector

length  $r$  and the response amplitude  $A$ . The vector length  $r$  describes the directedness of the response and ranges from 0 to unity, with unity indicating that all vectors are of the same direction (Batschelet 1981). It was calculated with the *CircStat* toolbox (Berens 2009).  $A$  describes the absolute amplitude of spike frequency modulation during stimulation, with higher  $A$  values indicating stronger modulation.  $A$  was calculated as follows according to Labhart (1996) and Pfeiffer et al. (2011):

$$A = \sum_{i=1}^{i=18} |n_i - \bar{n}|,$$

where  $n_i$  is the number of spikes in bin  $i$  and  $\bar{n}$  is the number of spikes during the 360° rotation divided by the number of bins. Firing rates at  $\Phi_{\max}$  and  $\Phi_{\min}$  were estimated by fitting a bimodal von Mises distribution model to the binned data (Fitak and Johnsen 2017) and taking the model's firing rate at the respective angles.

## Regression analysis

To test whether modulation amplitude  $A$ , length of the mean vector  $r$ , and mean spiking activity were dependent on the DoP, respective data were pooled and tested for linear regression. Only cells that were stimulated with at least three different DoPs were included for this analysis. If the resulting residuals were not normally distributed (based on the Lilliefors test), the data were logarithmically transformed and the regression was done again. If the residuals of this regression were not normally distributed, the two linear models were compared regarding their  $R^2$  values and the one with the higher value was chosen.

## Threshold for reliable coding of the AoP

To estimate the DoP threshold for reliable coding of the AoP we compared the mean resultant vector length  $r$  obtained during the stimulus with the upper 95% confidence limit of  $r$  obtained without stimulation (Pfeiffer et al. 2011). We defined the threshold as the lowest DoP at which the  $r$  values of all responses exceeded the upper 95% confidence limit of the estimated average  $r$  value of the no-stimulus controls.

## Results

We recorded intracellularly from 49 AoP-sensitive neurons in the CX, including 8 TL2 neurons, 5 TL3 neurons, 14 CL1a neurons, 10 TB1 neurons, 8 CPU1 neurons, and 4 CPU2 neurons. We investigated the influence of blue light with different DoPs on the mean vector length  $r$ , the response amplitude  $A$ , and the firing activity of the neurons. Based on



the data, we determined a DoP threshold for reliable AoP signaling.

The recorded neurons showed characteristic sinusoidal modulation of activity during 360° rotation of the polarizer (Fig. 2b). The AoP that results in maximal activity during stimulus presentation is referred to as preferred AoP (or preferred  $E$ -vector orientation,  $\Phi_{\max}$ ). The AoP perpendicular to the  $\Phi_{\max}$  is called anti-preferred AoP ( $\Phi_{\min}$ ).

### Threshold for reliably signaling the angle of polarization

All recordings ( $N=49$ ) included stimulation with blue light of the highest DoP (0.99). Depending on recording stability and duration additional stimuli were tested (DoP=0.35,  $N=41$ ; DoP=0.1,  $N=34$ ; DoP=0.05,  $N=33$ ; DoP=0.002,  $N=45$ ). Figure 3 illustrates the responses of a CL1a neuron that was tested with all five stimuli.

All neurons (TL2=5, TL3=5, CL1a=11, TB1=9, CPU=11) tested with polarized blue light at a DoP of 0.35 showed a significant modulation of firing activity by AoP

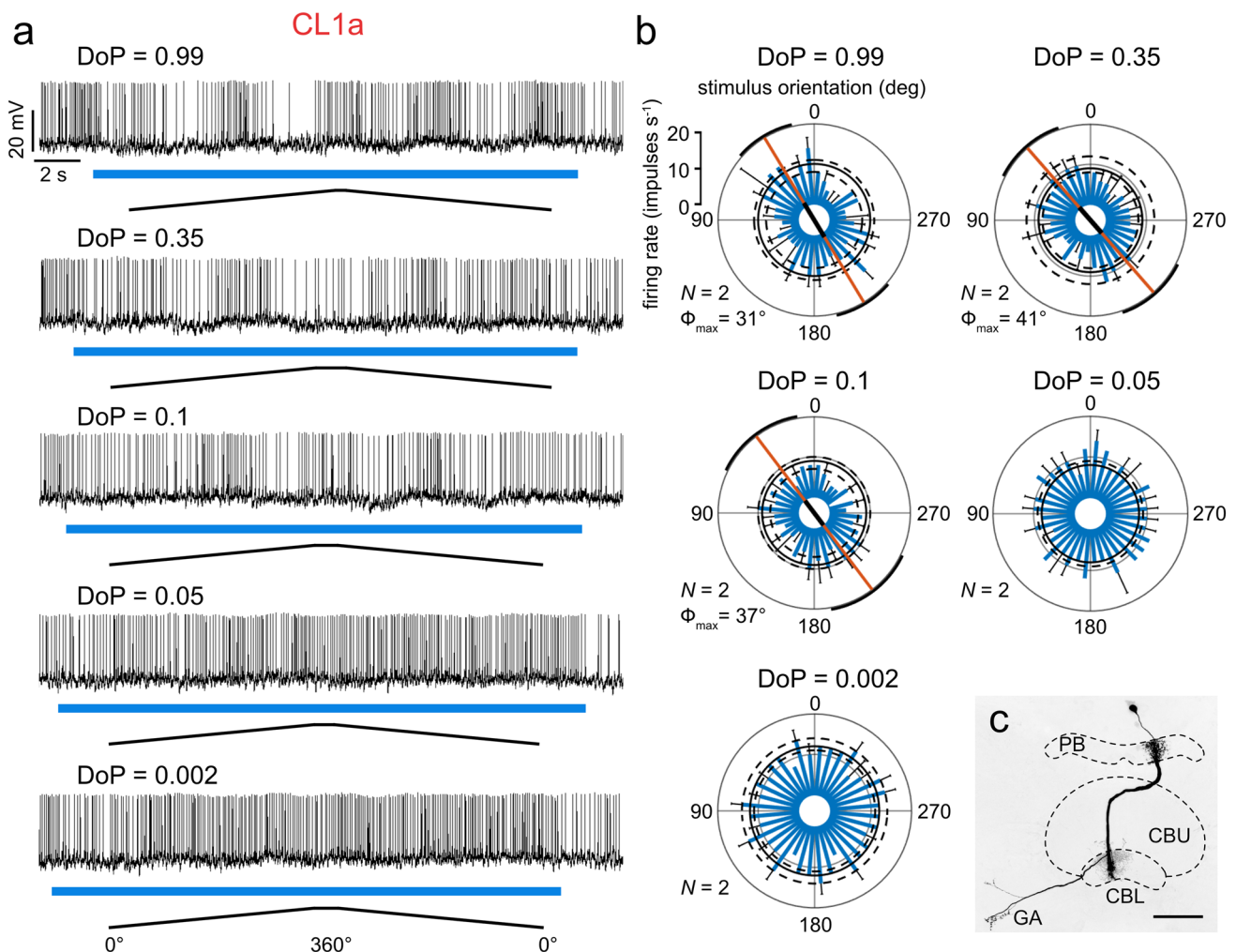


**Fig. 3** **a** Spike trains of a CL1a neuron in response to full clockwise- and counterclockwise polarizer rotations when stimulated with different degrees of polarization (DoP). The duration of the light stimulus is indicated by the blue bars. Ramps indicate 360° rotations of the polarizer, the angle of polarization (AoP) is not indicated by the ramps, as it is shifted depending on the arrangement of diffusors. **b** Circular histograms showing the firing rate (blue bars) during two polarizer rotations at five different DoPs. Black bars indicate standard deviations. If the firing rate was statistically significantly correlated

with the AoP, the orange line indicates the preferred angle of polarization with the black portion indicating the resultant vector length. Black circles indicate median background activity (solid line) and the lower and upper 2.5 percentile (dashed lines) of the background activity. **c** Projection view of the recorded CL1a neuron with arborizations in the protocerebral bridge (PB), the lower division (CBL) of the central body and the gall (GA). CBU, upper division of the central body. Scale bar = 50  $\mu$ m

(Fig. 4a). All three TL2 neurons and all four TL3 neurons tested with a DoP of 0.1 still responded significantly to the stimulus. Most of the CL1a neurons (6 out of 8), TB1 neurons (6 out of 8), CPU1 neurons (7 out of 8), and CPU2 neurons (2 out of 3) also showed significant responses at 0.1 DoP. At a DoP of 0.05 less than half of the tested neurons responded significantly to the stimulus (TL2, 3 out of 4; TL3, 1 out of 5; CL1a, 2 out of 6; TB1, 3 out of 7; CPU1, 2 out of 7; CPU2, 2 out of 4). The lowest DoP of 0.002, which should equal unpolarized light, did not elicit a significant response in any of the neurons tested. These results (summarized in Fig. 4a) point to a threshold for reliable coding of the AoP between a DoP of 0.1 and 0.05.

Pfeiffer et al. (2011) used the mean vector length  $r$  to calculate the threshold for reliable AoP coding (see “Materials and Methods”). In TL2 neurons all  $r$  values at DoP values  $\geq 0.05$  exceeded the upper 95% confidence level (Fig. 4b). TB1 neurons showed reliable coding at DoP values  $\geq 0.1$ . In all other cell types stimuli with a DoP  $\geq 0.35$  resulted in reliable coding of the AoP (Fig. 4b).

### Response amplitude and firing activity at different degrees of polarization

The response amplitude  $A$  was positively correlated with increasing DoPs in all types of neuron tested (Fig. 5). Testing for linear regression revealed that the dependence of  $A$  on the DoP in TL2 neurons and CPU2 neurons was best described when using non-logarithmically transformed data, whereas the dependence of  $A$  on the DoP in the other neurons was best described by a linear model based on logarithmically transformed data (see “Materials and Methods”, Fig. 5). This indicates that the relationship between the response amplitude  $A$  and the DoP is linear in TL2 neurons and CPU2 neurons but logarithmic in the remaining cell types. However, individual neurons of each type could show an either linear or logarithmic relationship between the response amplitude  $A$  and the DoP (not shown). Similar to Pfeiffer et al. (2011) we calculated whether the mean spiking activity during a 360° rotation of the polarizer was influenced by the presented DoP. We found that the mean spiking activity was positively correlated with increasing DoPs in TL2 neurons, negatively correlated in CL1a neurons and not linearly correlated in TL3-, TB1- and CPU neurons (Fig. 6). To further explore the cell-type-specific results, we calculated the minimum and maximum activity of neurons at  $\Phi_{\max}$  and  $\Phi_{\min}$  for different DoPs (Fig. 7). The results show that both, inhibition and excitation, increased in all types of neuron with an increase in DoP, and that activity during low DoPs was clustered around background activity in TL3, TB1 and CPU neurons (Fig. 7). In contrast, activity of CL1a neurons at  $\Phi_{\max}$  and  $\Phi_{\min}$  at low DoPs was increased above background activity, whereas in TL2 neurons activity at low

DoPs was lower than background activity, except for one cell (Fig. 7, TL2, Fig. 8a).

### Influence of unpolarized blue light on firing activity

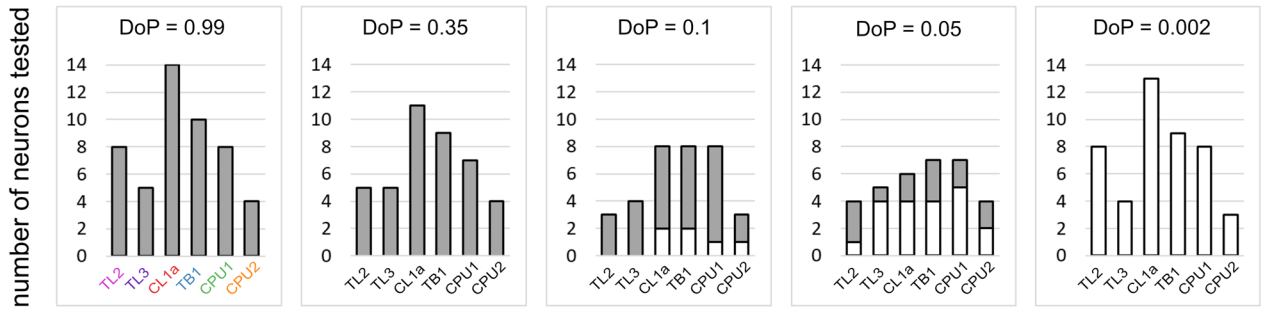
The activity of six neurons (5 TL2, 1 TL3) was strongly affected by unpolarized blue light. Reducing the DoP revealed an overall inhibition or excitation of the neurons during stimulus presentation with strongest effects at the lowest DoP of 0.002 (Fig. 8). Excitatory and inhibitory responses were followed by rebound inhibition or excitation, respectively, at stimulus offset. These effects were observed primarily in TL neurons, especially TL2 cells, but could also be observed, however to a lesser extent, in CL1a-, TB1- and CPU neurons.

Five out of eight TL2 neurons were inhibited and two were excited at 0.002 DoP, and among four TL3 neurons one was inhibited. The strength of inhibition and excitation varied between individual cells and could be very pronounced or rather mild. The remaining neurons (one TL2 and three TL3) did not show obvious changes in firing activity upon stimulation with unpolarized blue light.

The strong excitatory response of a TL2 neuron to stimulation with the lowest DoP as well as the responses to higher degrees of polarization were followed by strong inhibition upon stimulus offset which lasted up to 20 s (Fig. 8a, arrowheads). These inhibitions at lights off were abolished after the DRAs were covered with black paint (Fig. 8a) but were restored when uncovering the DRAs again (Fig. 8a). Painting the DRAs resulted, in addition, in higher overall activity of the neuron, perhaps owing to the lack of inhibition following each stimulus. The opposite response, again in a TL2 neuron, is illustrated in Fig. 8b. Here the TL2 neuron responded to low DoPs with inhibition and rebound excitation at lights off. Both responses were abolished when the DRAs were covered (Fig. 8b). Uncovering the DRAs restored the polarization response at high DoPs, the inhibition at low DoPs (unpolarized blue light) and the excitation at lights off (Fig. 8b). Covering the DRA with black paint during the recording from one TL3 neuron and another TL2 neuron (data not shown) showed the same results.

In 12 out of 13 CL1a neurons we observed phasic inhibition after stimulus offset (lights off) that varied in strength. Nine of these neurons displayed phasic inhibition also at stimulus onset (lights on) that gave way to slightly elevated activity (Fig. 9a). Three neurons did not show phasic lights on inhibition but only excitation during stimulation with the lowest DoP (Fig. 9b). Although the strength and duration of phasic inhibition at lights on, the following sustained excitation, and the rebound inhibition upon lights off varied between individual neurons, only one CL1a neuron showed a completely different response characterized by phasic excitation upon lights on (Fig. 9c).

**a**



■ significant response    □ non significant response

**b**

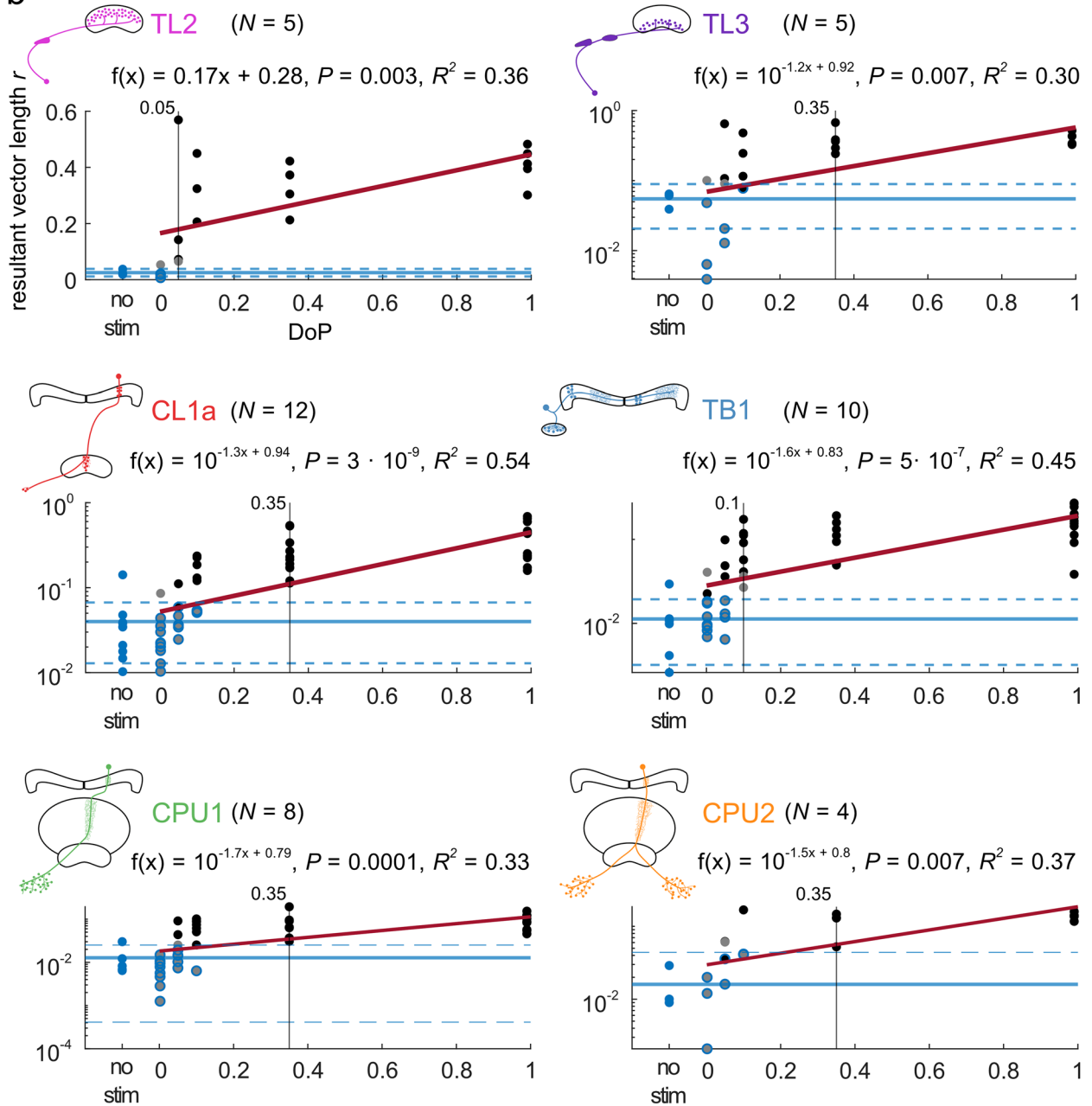




**Fig. 4 a** Summary of significant (grey portion of bars) versus non-significant (white portion of bars) responses of different cell types at different degrees of polarization (DoP). All neurons responded significantly at DoPs of 0.99 and 0.35. At DoPs of 0.1 and 0.05 some neurons of each cell type showed significant responses, whereas others did not respond. At a DoP of 0.002 no neuron showed a significant response. **b** The mean vector length  $r$ , i.e., the directedness of responses increased with increasing DoP in all cell types. The regression lines are shown in red. The solid blue lines indicate the means of the no-stimulus data, the dashed blue lines indicate the respective lower and the upper 95% confidence limits. Vertical black lines mark the stimulus at which the  $r$  values of all responses exceed the upper 95% confidence limit of the estimated average  $r$  value of the no-stimulus controls. Blue dots are no-stimulus data points, grey dots are non-significant responses, grey dots with blue outline indicate non-significant responses that lie within the confident limits of the no-stimulus data. Black dots are significant-responses. Black dots with blue outline indicate significant-responses that lie within the confident limits of the no-stimulus data

Nine TB1 neurons showed more variable responses. One neuron showed slight excitation followed by rebound inhibition (Fig. 10a). Two neurons showed slight inhibition during stimulation followed by rebound excitation (Fig. 10b), three neurons showed only excitation upon stimulus offset (Fig. 10c), and one neuron showed slight inhibition after stimulus offset (Fig. 10d). Two neurons showed slight excitation during stimulation but lacked rebound inhibition (Fig. 10e).

Of the 11 CPU neurons one CPU2 neuron showed slight excitation during stimulus presentation followed by rebound inhibition (Fig. 10f). Four CPU neurons (two CPU1, two CPU2) showed inhibition during stimulation with a DoP = 0.002 and rebound excitation upon stimulus offset (Fig. 10g). One CPU1 neuron displayed rebound excitation at lights off but no activity change during stimulation (Fig. 10h). Four CPU neurons (three CPU1, one CPU2) showed no obvious change in activity during stimulation (Fig. 10i). The remaining CPU1 neuron showed phasic excitation upon stimulus onset and rebound excitation upon stimulus offset (Fig. 10j).

## Discussion

### Threshold for reliable AoP signaling

Intracellular recordings from AoP-sensitive neurons of the locust CX revealed that AoP signaling in these neurons is reliable down to DoPs of 0.35 in TL3-, CL1a-, and CPU neurons, 0.1 in TB1 neurons and 0.05 in TL2 neurons. Because our estimation of reliable coding does not account for DoPs between the discrete values that were tested (0.35, 0.1 and 0.05), and based on the significance of responses of individual neurons, we assume that at least for TL3-, CL1a- and CPU neurons the actual threshold for AoP coding might be

lower than the estimated threshold and might lie between 0.35 and 0.1. The low thresholds found in TL2 and TB1 neurons are similar to thresholds that have been determined for polarotactic behavior in honeybees, crickets, and dung beetles (von Frisch 1967; Henze and Labhart 2007; Foster et al. 2019) and for neuronal responses of polarization-opponent interneurons in the optic lobes of crickets (Labhart 1996). Prior to this study, neurons of the CX have been tested with different DoPs only in crickets (CNL neurons, Sakura et al. 2007). Those neurons are homologous to TL2/TL3 neurons in locusts. They showed responses to polarized light with modulation amplitudes independent of the DoP, ranging from 0.99 to 0.18. Lower DoPs, however, were not tested. In contrast to the data in crickets, the modulation amplitude in all types of locust CX neurons increased with increasing DoP (Fig. 5). This should be advantageous for encoding sun positions through matched-filter coding of sky polarization patterns as shown by Zittrell et al. (2020). Locust CX neurons integrate polarization information not only from the zenith but across the entire sky and respond best to polarization patterns that match a particular position of the sun. Because each point in the sky is not only characterized by polarization angle, but also by DoP depending on distance from the sun (Fig. 1a), both parameters should ideally be considered and integrated in coding of sky polarization patterns.

For two cell types of the anterior optic tubercle of the locust (LoTu1- and TuTu1 neurons), Pfeiffer et al. (2011) determined a DoP threshold for reliable AoP signaling of 0.3. This threshold is similar to the threshold we determined for TL3-, CL1a-, and CPU neurons but higher than the threshold determined for TL2 and TB1 neurons. When comparing these different types of neuron one has to take into account that LoTu1- and TuTu1 neurons are not directly involved in the polarization vision pathway to the CX, but rather provide integration between the right and left tubercle in the locust brain.

### Effect of unpolarized blue light on polarization-sensitive neurons

In LoTu1 neurons dorsally presented polarized blue light increases spiking activity irrespective of the angle of polarization, whereas dorsally presented unpolarized light decreases overall spiking activity (Pfeiffer et al. 2011). Because unpolarized light consists of all possible angles of polarization these results appeared puzzling and led to a hypothetical model of the underlying mechanisms. The authors suggested that the temporal and spatial pattern of histamine release by polarization-sensitive photoreceptors leads to inhibition and rebound excitation of lamina neurons which becomes visible in LoTu1 neurons. In TL neurons we found similar, but also opposite responses, with pronounced inhibition upon presentation of unpolarized

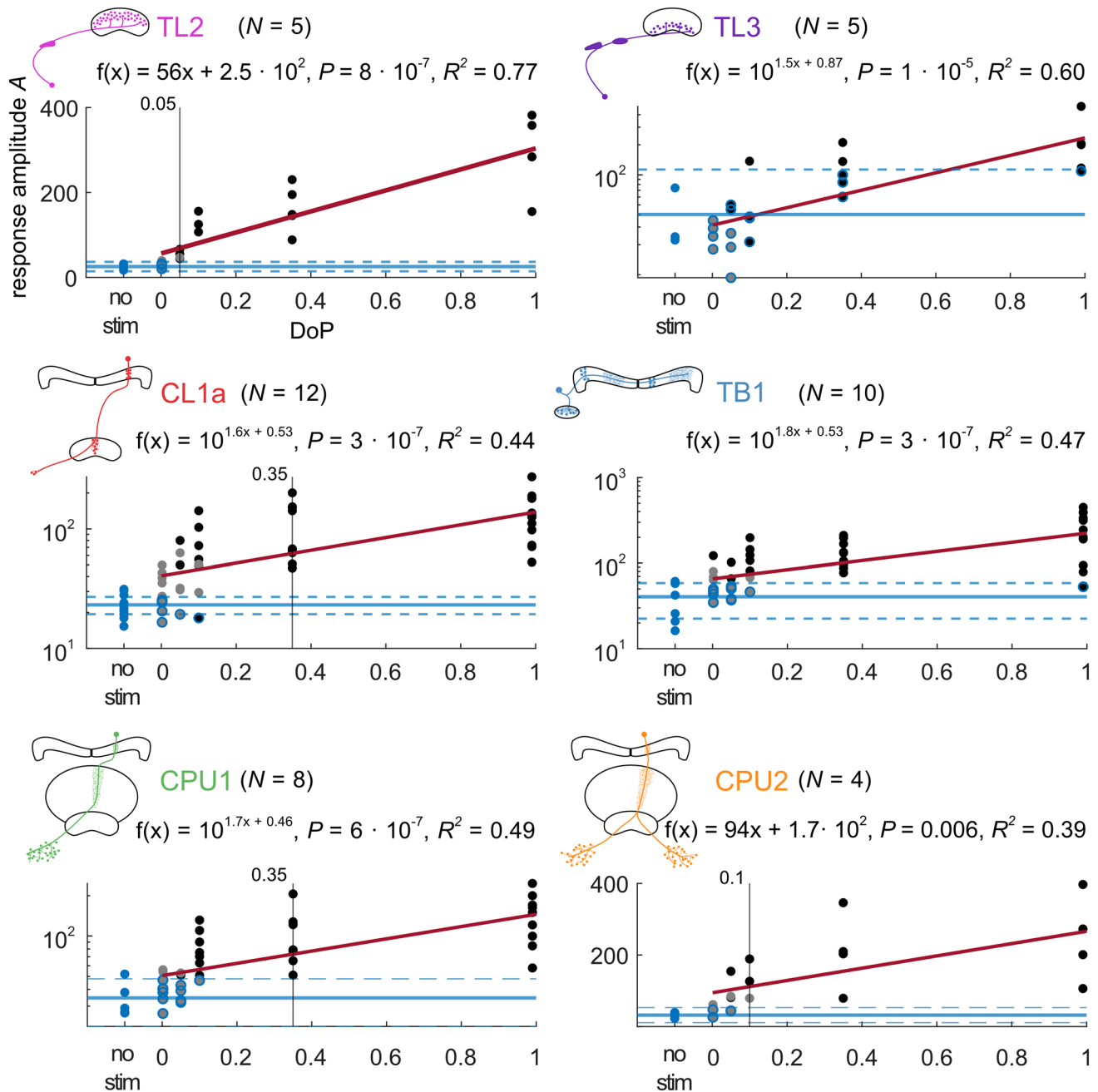


**Fig. 5** The absolute response amplitude  $A$  increases with increasing degree of polarization in all cell types. The regression lines are shown in red. The solid blue lines indicate the means of the no-stimulus data, the dashed blue lines indicate the respective lower and the upper 95% confidence limits. Blue dots are no-stimulus data points, grey dots are non-significant responses, grey dots with blue outline indicate non-significant responses that lie within the confident limits

of the no-stimulus data. Black dots are significant responses. Black dots with blue outline indicate significant responses that lie within the confident limits of the no-stimulus data. Vertical black lines mark the stimulus at which the  $A$  values of all responses exceed the upper 95% confidence limit of the estimated average  $A$  value of the no-stimulus controls

blue light (Fig. 8b) in five cells, but also pronounced excitation upon stimulation with unpolarized blue light (Fig. 8a) in one cell. Although these responses are reminiscent of those described for LoTu1 neurons, we propose that the

underlying mechanism is different. Whereas DRA-mediated inhibition and excitation in LoTu1 neurons are suggested to be driven by only one input, we suggest that TL2 and TL3 neurons receive inhibitory and excitatory input. This

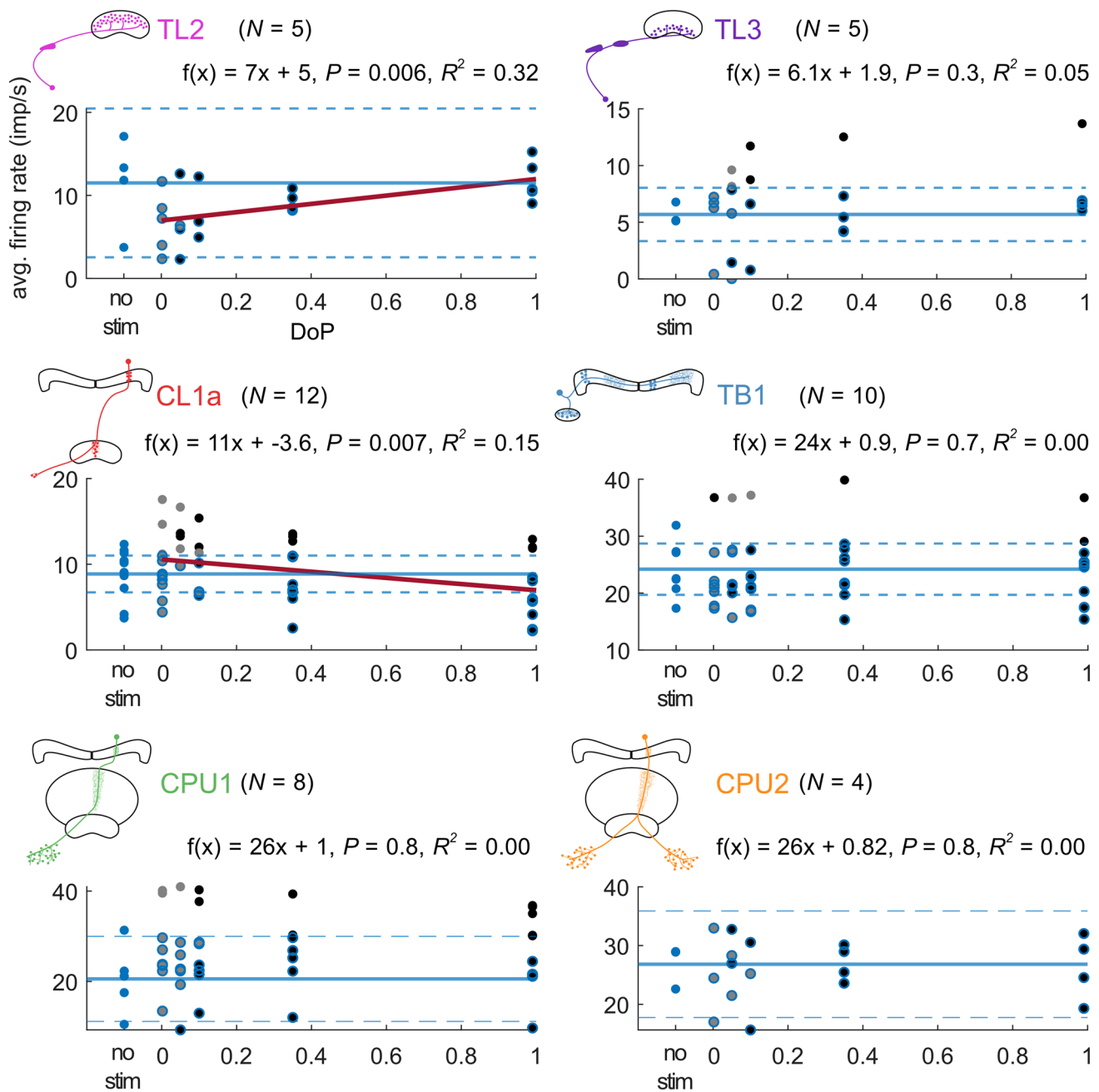


**Fig. 6** The average firing activity during stimulation with a rotating polarizer was positively correlated with the degree of polarization (DoP) in TL2 neurons and negatively correlated with the DoP in CL1a neurons. In TL3, TB1 and CPU neurons the average firing activity was not correlated with the DoP. The regression lines are shown in red. The solid blue lines indicate the mean of the no-stimulus data, the dashed blue lines indicate the respective lower and the

upper 95% confidence limits. Blue dots are no-stimulus data points, grey dots are non-significant responses, grey dots with blue outline indicate non-significant responses that lie below the upper confidence limit of the no-stimulus data. Black dots are significant-responses. Black dots with blue outline indicate significant-responses that lie below the upper confident limit of the no-stimulus data

assumption is supported by polarization opponency in TL2 and TL3 neurons (Pegel et al. 2018) which would result from inhibitory input at  $\Phi_{\min}$  and excitatory input at  $\Phi_{\max}$ .

Pronounced inhibition or excitation at low DoP values in TL neurons might, therefore, result from unbalanced inhibitory and excitatory inputs leading to an overall excitation or

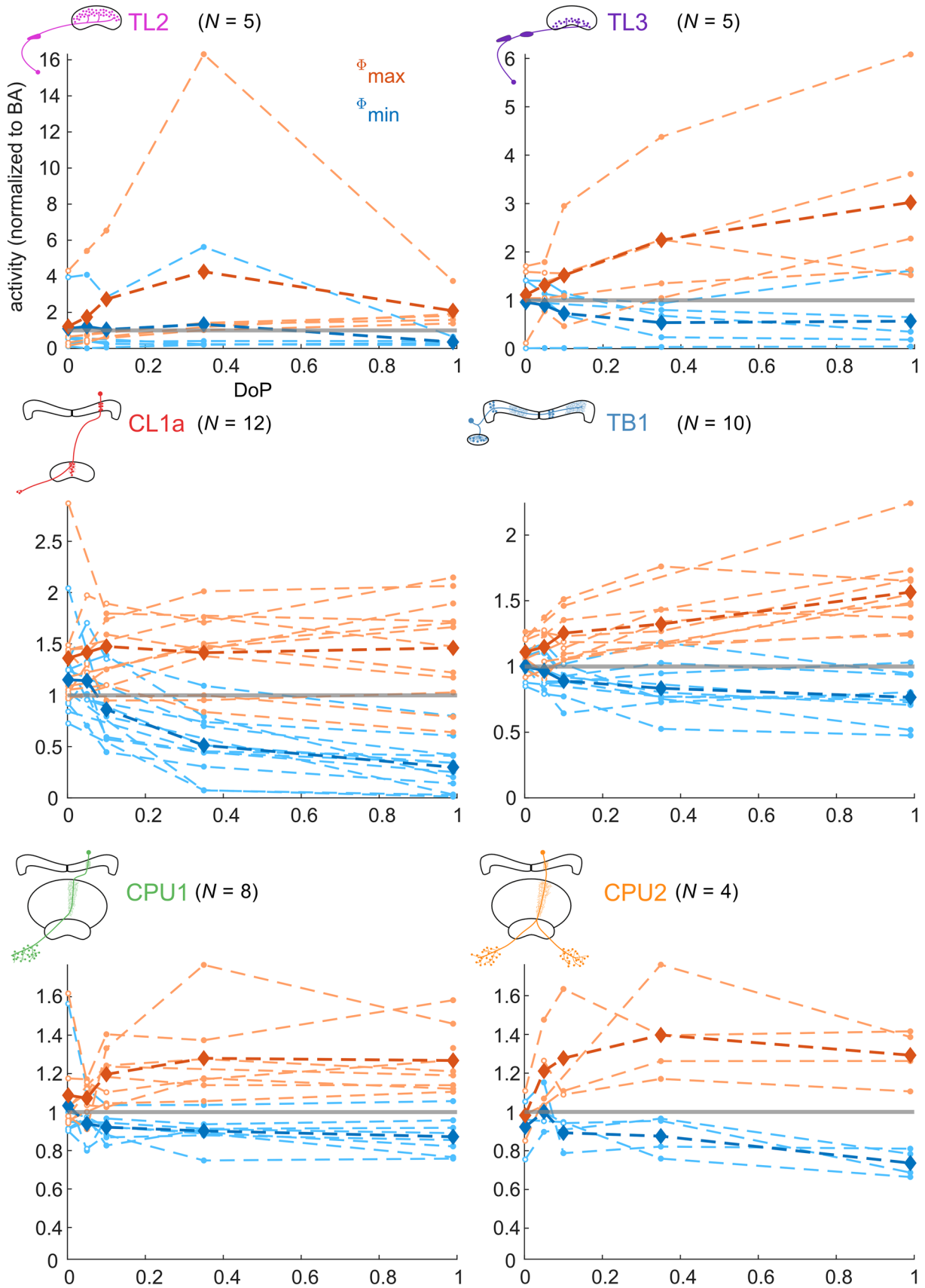


**Fig. 7** Activity of individual neurons at  $\Phi_{\max}$  (orange) and  $\Phi_{\min}$  (blue) during responses to a rotating polarizer at different degrees of polarization (DoP). Activity is normalized to background activity of a 5 s interval (median value of 1-s-binned spike rate averages) preceding each stimulus. The grey lines indicate background activity. Dots indicate significant responses, whereas circles indicate non-significant responses. The bold lines indicate the averaged activity of all neurons at  $\Phi_{\max}$  and  $\Phi_{\min}$ , respectively

inhibition when reducing the DoP. In accordance with the hypothetical model provided by Pfeiffer et al. (2011), unpolarized light would equally excite all polarization-sensitive photoreceptors and would lead to either inhibition or excitation in TL neurons depending on whether the inhibitory input outweighs the excitatory input or vice versa. Balanced inhibitory and excitatory input would result in unaltered neuronal activity upon presentation of low DoPs. Pfeiffer et al. (2011) plotted the average firing rate of LoTu1- and TuTu1 neurons over the DoP to illustrate the increase in average

firing rate with increasing DoPs. We found a similar trend in TL2 neurons but for TL3 neurons we found no correlation (Fig. 6). These findings indicate that TL2 and TL3 neurons serve slightly different purposes.

The suppression of activity in LoTu1 neurons might prevent signaling of ambiguous information deriving from low DoPs (Pfeiffer et al. 2011). Unbalanced input to TL neurons that results in either pronounced excitation or inhibition might serve to modulate the TL network activity according to available stimuli, i.e. silencing the polarization-processing pathway when respective stimuli are absent, clearing the way for other navigational relevant stimuli, such as wind (Okubo et al. 2020) or proprioceptive feedback. Pfeiffer et al. (2011) assumed that the inhibition by low DoP in LoTu1- and TuTu1 neurons is caused by the same set of polarization-sensitive photoreceptors that signal relevant AoP stimuli. Here, we demonstrate that photoreceptors of the DRA, indeed, mediate the inhibitory and excitatory responses to

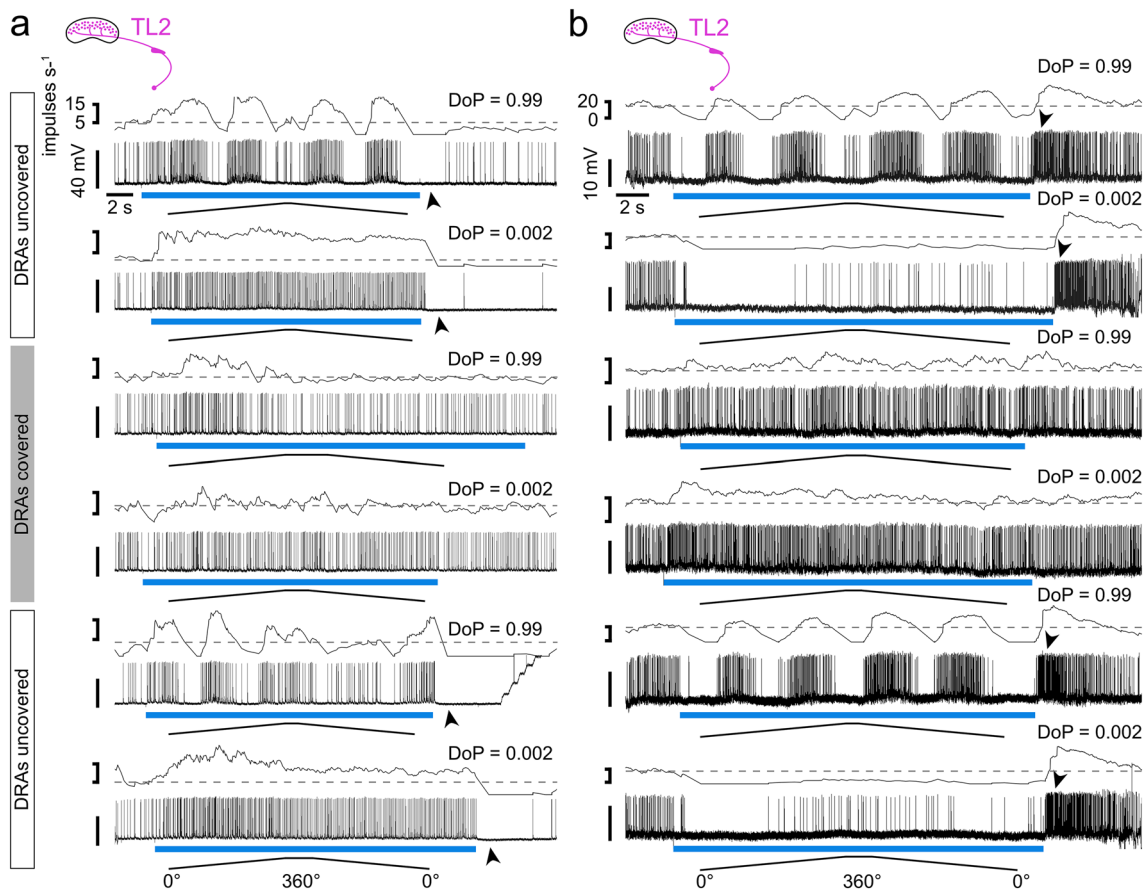


**Fig. 8** Responses of two different TL2 neurons to polarizer rotations with the lowest degree of polarization (DoP=0.002) and the highest degree of polarization (DoP=0.99). The blue bars indicate the time windows during which polarized blue light was presented. Ramps indicate 360° rotations of the polarizer. Dashed lines indicate median background activity during 5 s preceding each stimulus. While the

neuron in **a** is excited by low DoPs, the neuron in **b** gets inhibited. Covering the DRA of both eyes abolished the polarization response, the excitation (**a**) or inhibition (**b**) during low DoPs, and the inhibitory rebound (**a**) or excitatory rebound (**b**) at lights off (arrowheads). Uncovering the DRAs restored the responses

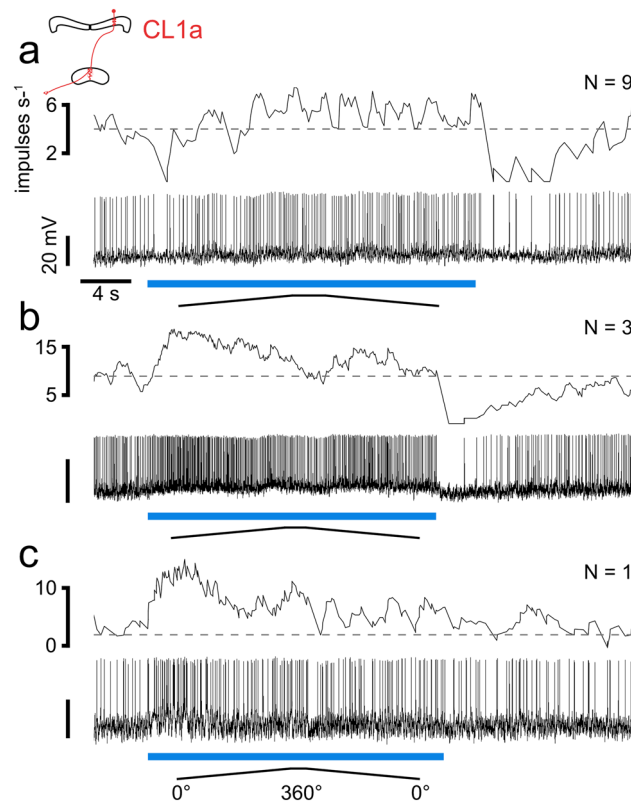


**Fig. 9** Responses of three different CL1a neurons to the lowest degree of polarization (DoP=0.002). The blue bars indicate the time windows during which polarized blue light was presented. Ramps indicate 360° rotations of the polarizer. Dashed lines indicate median background activity during 5 s preceding each stimulus. **a** This CL1a neuron responded with slightly elevated activity preceded by phasic

inhibition at lights on. Phasic rebound inhibition occurs at lights off. **b** This CL1a neuron responded with excitation to the stimulus, followed by rebound inhibition at lights off. **c** This CL1a neuron displayed phasic excitation at lights on. *N* indicates how many of the recorded cells showed similar responses to the lowest DoP

dorsally presented unpolarized blue light in TL neurons (Fig. 8), whereas other eye regions have only a marginal, if any, effect.

Unpolarized blue light had similar but less prominent effects in the downstream cell types of the CX. In CL1a neurons consistent increase in firing rate during stimulus presentation corresponded to rebound inhibition after stimulus offset. This response pattern is opposite to that found in most TL2 neurons (Fig. 8b). In accordance with that, the average firing activity of CL1a neurons was negatively correlated with an increase in the DoP. All of these properties support the assumption that CL1a neurons are inhibited by

the GABAergic TL neurons. Because the activity of CL1a neurons is likely modulated by global inhibition from many TL neurons, their excitation during low DoP is less pronounced likely by convergent input from many TL neurons, some of which are excited as well (Fig. 8a).

The responses in TB1- and CPU neurons to unpolarized blue light were weaker and more variable than those of CL1a neurons. This may be a result of mutual inhibition of heterolateral TB1 neurons proposed by Bockhorst and Homberg (2017) illustrated in Fig. 1d. Slight inhibition observed in several CPU neurons might point to a net inhibitory input to CPU neurons from CL1a neurons. In both, TB1- and CPU





neurons, the average firing activity appears to be independent of the DoP.

## Conclusions

The data show that the CX in desert locusts is capable of reliable AoP coding and thus sky-compass dependent head-direction signaling even under highly unfavorable sky conditions. As our stimulus device only covered a visual angle of 12.5°, even lower effective degrees of polarization in the sky may suffice to generate head-direction signals by integration of inputs across the full sky as shown by Zittrell et al. (2020). This might allow to still exploit skylight polarization at a sky fully overcast by thin clouds showing effective degrees of polarization just above 0.05 (Labhart 1996, 1999).

**Acknowledgements** We are grateful to Martina Kern for maintaining laboratory cultures of desert locusts.

**Author contributions** Study concept and design: UH, KP, RH; acquisition of data: RH; data analysis and interpretation: RH, FZ; analysis code: FZ; drafting the manuscript: RH; review and editing: UH, RH, KP.

**Funding** Open Access funding enabled and organized by Projekt DEAL. This work was supported by the Deutsche Forschungsgemeinschaft, Grant number HO 950/24-1 and HO 950/28-1.

## Declarations

**Conflict of interest** The authors declare no conflict of interest.

**Availability of data and materials** All data that support the findings of this study are available from the corresponding author.

**Code availability** MATLAB analysis code is available upon request.

**Open Access** This article is licensed under a Creative Commons Attribution 4.0 International License, which permits use, sharing, adaptation, distribution and reproduction in any medium or format, as long as you give appropriate credit to the original author(s) and the source, provide a link to the Creative Commons licence, and indicate if changes were made. The images or other third party material in this article are included in the article's Creative Commons licence, unless indicated otherwise in a credit line to the material. If material is not included in the article's Creative Commons licence and your intended use is not permitted by statutory regulation or exceeds the permitted use, you will need to obtain permission directly from the copyright holder. To view a copy of this licence, visit <http://creativecommons.org/licenses/by/4.0/>.

## References

- Batschelet E (1981) Circular statistics in biology. Academic Press, New York
- Berens P (2009) CircStat: a MATLAB toolbox for circular statistics. *J Stat Soft* 31:1–21
- Bockhorst T, Homberg U (2015) Amplitude and dynamics of polarization-plane signaling in the central complex of the locust brain. *J Neurophysiol* 113:3291–3311. <https://doi.org/10.1152/jn.00742.2014>
- Bockhorst T, Homberg U (2017) Interaction of compass sensing and object-motion detection in the locust central complex. *J Neurophysiol* 118:496–506
- Brunner D, Labhart T (1987) Behavioral evidence for polarization vision in crickets. *Physiol Entomol* 12:1–10. <https://doi.org/10.1111/j.1365-3032.1987.tb00718.x>
- Clements AN, May TE (1974) Studies on locust neuromuscular physiology in relation to glutamic acid. *J Exp Biol* 60:6730–7705. <https://doi.org/10.1242/jeb.60.3.673>
- Dacke M, Baird E, Byrne M, Scholtz CH, Warrant EJ (2013) Dung beetles use the milky way for orientation. *Curr Biol* 23:298–300. <https://doi.org/10.1016/j.cub.2012.12.034>
- el Jundi B, Warrant EJ, Byrne MJ, Khaldy L, Baird E, Smolka J, Dacke M (2015) Neural coding underlying the cue preference for celestial orientation. *Proc Natl Acad Sci USA* 112:11395–11400. <https://doi.org/10.1073/pnas.1501272112>
- Evangelista C, Kraft P, Dacke M, Labhart T (2014) Honeybee navigation: critically examining the role of the polarization compass. *Philos Trans R Soc B* 369:20130037. <https://doi.org/10.1098/rstb.2013.0037>
- Fitak RR, Johnsen S (2017) Bringing the analysis of animal orientation data full circle: model-based approaches with maximum likelihood. *J Exp Biol* 220:3878–3882. <https://doi.org/10.1242/jeb.167056>
- Foster JJ, Kirwan JD, el Jundi B, Smolka J, Khaldy L, Baird E, Byrne MJ et al (2019) Orienting to polarized light at night—matching lunar skylight to performance in a nocturnal dung beetle. *J Exp Biol* 222:jeb188532. <https://doi.org/10.1242/jeb.188532>
- Green J, Maimon G (2018) Building a heading signal from anatomically defined neuron types in the *Drosophila* central complex. *Curr Opin Neurobiol* 52:156–164. <https://doi.org/10.1016/j.conb.2018.06.010>
- Green J, Vijayan V, Pires PM, Adachi A, Maimon G (2019) A neural heading estimate is compared with an internal goal to guide oriented navigation. *Nat Neurosci* 22:1460–1468
- Hanesch U, Fischbach KF, Heisenberg M (1989) Neuronal architecture of the central complex in *Drosophila melanogaster*. *Cell Tissue Res* 257:343–366. <https://doi.org/10.1007/BF00261838>
- Hardcastle BJ, Omoto JJ, Kandimalla P, Nguyen BCM, Keleş MF, Boyd NK, Hartenstein V, Frye MA (2021) A visual pathway for skylight polarization processing in *Drosophila*. *ELife* 10:e63225. <https://doi.org/10.7554/eLife.63225>
- Heinze S, Homberg U (2007) Maplike representation of celestial *E*-vector orientations in the brain of an insect. *Science* 315:995–997. <https://doi.org/10.1126/science.1135531>
- Heinze S, Homberg U (2008) Neuroarchitecture of the central complex of the desert locust: intrinsic and columnar neurons. *J Comp Neurol* 511:454–478. <https://doi.org/10.1002/cne.21842>
- Heinze S, Homberg U (2009) Linking the input to the output: new sets of neurons complement the polarization vision network in the locust central complex. *J Neurosci* 29:4911–4921. <https://doi.org/10.1523/JNEUROSCI.0332-09.2009>
- Heinze S, Reppert M (2011) Sun compass integration of skylight cues in migratory monarch butterflies. *Neuron* 69:345–358. <https://doi.org/10.1016/j.neuron.2010.12.025>
- Heinze S, Florman J, Asokaraj A, el Jundi B, Reppert SM (2013) Anatomical basis of sun compass navigation II: the neuronal composition of the central complex of the monarch butterfly. *J Comp Neurol* 521:267–298. <https://doi.org/10.1002/cne.23214>
- Henze MJ, Labhart T (2007) Haze, clouds and limited sky visibility: polarotactic orientation of crickets under difficult stimulus



- conditions. *J Exp Biol* 210:3266–3276. <https://doi.org/10.1242/jeb.007831>
- Homberg U, Hofer S, Pfeiffer K, Gebhardt S (2003) Organization and neural connections of the anterior optic tubercle in the brain of the locust, *Schistocerca gregaria*. *J Comp Neurol* 468:415–430. <https://doi.org/10.1002/cne.10771>
- Homberg U, Heinze S, Pfeiffer K, Kinoshita M, el Jundi B (2011) Central neural coding of sky polarization in insects. *Philos Trans R Soc B* 366:680–687. <https://doi.org/10.1098/rstb.2010.0199>
- Honkanen AE, Adden A, da Silva Freitas J, Heinze S (2021) The insect central complex and the neural basis of navigational strategies. *J Exp Biol* 222:jeb188854. <https://doi.org/10.1242/jeb.188854>
- Hulse BK, Jayaraman V (2020) Mechanisms underlying the neural computation of head direction. *Annu Rev Neurosci* 43:31–54
- Hulse BK, Haberkern H, Franconville R, Turner-Evans DB, Takemura S, Wolff T et al (2021) A connectome of the *Drosophila* central complex reveals network motifs suitable for flexible navigation and context-dependent action selection. *Elife* 10:e66039. <https://doi.org/10.1101/2020.12.08.413955>
- Kinoshita M, Pfeiffer K, Homberg U (2007) Spectral properties of identified polarized-light sensitive interneurons in the brain of the desert locust *Schistocerca gregaria*. *J Exp Biol* 210:1350–1361. <https://doi.org/10.1242/jeb.02744>
- Labhart T (1988) Polarization-opponent interneurons in the insect visual system. *Nature* 331:435–437. <https://doi.org/10.1038/331435a0>
- Labhart T (1996) How polarization-sensitive interneurons of crickets perform at low degrees of polarization. *J Exp Biol* 199:1467–1475. <https://doi.org/10.1242/jeb.199.7.1467>
- Labhart T (1999) How polarization-sensitive interneurons of crickets see the polarization pattern of the sky: a field study with an opto-electronic model neurone. *J Exp Biol* 201:757–770
- Labhart T, Meyer EP (1999) Detectors for polarized skylight in insects: a survey of ommatidial specializations in the dorsal rim area of the compound eye. *Microsc Res Tech* 47:368–379. [https://doi.org/10.1002/\(SICI\)1097-0029\(19991215\)47:6%3c368::AID-JEMT2%3e3.0.CO;2-Q](https://doi.org/10.1002/(SICI)1097-0029(19991215)47:6%3c368::AID-JEMT2%3e3.0.CO;2-Q)
- Labhart T, Petzold J, Helbling H (2001) Spatial integration in polarization-sensitive interneurons of crickets: a survey of evidence, mechanisms and benefits. *J Exp Biol* 204:2423–2430. <https://doi.org/10.1242/jeb.204.14.2423>
- Mappes M, Homberg U (2004) Behavioral analysis of polarization vision in tethered flying locusts. *J Comp Physiol A* 190:61–68. <https://doi.org/10.1007/s00359-003-0473-4>
- Okubo TS, Patella P, D'Alessandro I, Wilson RI (2020) A neural network for wind-guided compass navigation. *Neuron* 107:924–940. e18. <https://doi.org/10.1016/j.neuron.2020.06.022>
- Pegel U, Pfeiffer K, Homberg U (2018) Integration of compass cues in the central complex of the locust brain. *J Exp Biol* 221:jeb171207
- Pegel U, Pfeiffer K, Zittrell F, Scholtyssek C, Homberg U (2019) Two compasses in the central complex of the locust brain. *J Neurosci* 39:3070–3080. <https://doi.org/10.1523/JNEUROSCI.0940-18.2019>
- Pfeiffer K, Negrello M, Homberg U (2011) Conditional perception under stimulus ambiguity: polarization- and azimuth-sensitive neurons in the locust brain are inhibited by low degrees of polarization. *J Neurophysiol* 105:28–35. <https://doi.org/10.1152/jn.00480.2010>
- Pisokas I, Heinze S, Webb B (2020) The head direction circuit of two insect species. *Elife* 9:e53985. <https://doi.org/10.7554/eLife.53985>
- Reppert SM, Zhu H, White RH (2004) Polarized light helps monarch butterflies to navigate. *Curr Biol* 14:155–158. <https://doi.org/10.1016/j.cub.2003.12.034>
- Sakura M, Lambrinos D, Labhart T (2007) Polarized skylight navigation in insects: model and electrophysiology of e-vector coding by neurons in the central complex. *J Neurophysiol* 99:667–682. <https://doi.org/10.1152/jn.00784.2007>
- Seelig JD, Jayaraman V (2015) Neural dynamics for landmark orientation and angular path integration. *Nature* 521:186–191. <https://doi.org/10.1038/nature14446>
- Shiozaki HM, Otha K, Kazama H (2020) A multi-regional network encoding heading and steering maneuvers in *Drosophila*. *Neuron* 106:1–16
- Sommer S, Wehner R (2005) Vector navigation in desert ants, *Cataglyphis fortis*: celestial compass cues are essential for the proper use of distance information. *Naturwissenschaften* 92:468–471. <https://doi.org/10.1007/s00114-005-0020-y>
- Strutt JW (1871) XV. On the light from the sky, its polarization and colour. *Philos Mag* 41:107–120 (274–279)
- Varga AG, Kathman ND, Martin JP, Guo P, Ritzmann RE (2017) Spatial navigation and the central complex: sensory acquisition, orientation, and motor control. *Front Behav Neurosci* 11:4. <https://doi.org/10.3389/fnbeh.2017.00004>
- von Frisch K (1949) Die Polarisation des Himmelslichtes als orientierender Faktor bei den Tänzern der Bienen. *Experientia* 5:142–148. <https://doi.org/10.1007/bf02174424>
- von Frisch K (1967) The dance language and orientation of bees. Harvard University Press, Cambridge
- von Hadeln J, Hensgen R, Bockhorst T, Rosner R, Heidasch R, Pegel U, Pérez MQ, Homberg U (2020) Neuroarchitecture of the central complex of the desert locust: tangential neurons. *J Comp Neurol* 528:906–934. <https://doi.org/10.1002/cne.24796>
- Zar JH (1999) Biostatistical analysis, 4th edn. Prentice Hall, Upper Saddle River
- Zittrell F (2019) CircHist: circular histogram in MATLAB. <https://github.com/zifredder/CircHist>.
- Zittrell F, Pfeiffer K, Homberg U (2020) Matched-filter coding of sky polarization results in an internal sun compass in the brain of the desert locust. *Proc Natl Acad Sci USA* 117:25810–25817. <https://doi.org/10.1073/pnas.2005192117>

**Publisher's Note** Springer Nature remains neutral with regard to jurisdictional claims in published maps and institutional affiliations.



## Chapter II

Myoinhibitory peptides in the central complex of the locust *Schistocerca gregaria* and colocalization with locustatachykinin-related peptides



# **Myoinhibitory peptides in the central complex of the locust *Schistocerca gregaria* and colocalization with locustatachykinin-related peptides**

Running title: Myoinhibitory peptides in the central complex

Ronja Hensgen<sup>1</sup>, Stefan Dippel<sup>2</sup>, Sophie Hümmert<sup>1</sup>, Stefanie Jahn<sup>1</sup>, Jutta Seyfarth<sup>1</sup>, Uwe Homberg<sup>1,3\*</sup>

<sup>1</sup>Department of Biology, Animal Physiology, Philipps-Universität Marburg, D-35032 Marburg, Germany

<sup>2</sup>Department of Biology, Institut für Allgemeine Zoologie und Entwicklungsbiologie, Justus Liebig University of Giessen, 35392 Giessen, Germany

<sup>3</sup>Center for Mind, Brain and Behavior (CMBB), University of Marburg and Justus Liebig University Giessen

\*Correspondence to: Uwe Homberg, Fachbereich Biologie, Tierphysiologie, Philipps-Universität Marburg, D-35032 Marburg, Germany, Tel. +49-6421-2823402, Fax +49-6421-2828941, E-mail: homberg@staff.uni-marburg.de

## **Acknowledgments**

We are grateful to Drs. Hans Agricola (University of Jena), Manfred Eckert (University of Jena), Erich Buchner and Christian Wegener (University of Würzburg) for donating antibodies. Funding was obtained from Deutsche Forschungsgemeinschaft, grant number: HO 950/26-1 and HO 950/28-1.

## **Data availability statement**

All data that support the findings of this study are available from the corresponding author.

## **Conflict of interest disclosure**

The authors declare no conflict of interest.

## **Author contributions**

Study concept and design: U.H., R.H.; acquisition of data: R.H., S.D., S.H., S.J., J.S.; data analysis and interpretation: R.H., U.H., S.D.; drafting the manuscript: R.H.; review and editing: U.H., R.H.

**ABBREVIATIONS:** AA, amino acid; CBL, lower division of the central body; CBU, upper division of the central body; CX, central complex; LAL, lateral accessory lobe; LX, lateral complex; NO, noduli; PB, protocerebral bridge

## Abstract

The central complex in the brain of insects provides a neuronal network for sensorimotor processing that is essential for spatial navigation and locomotion and plays a role in sleep control. Studies on the neurochemical architecture of the central complex aid in identification of neuronal cell types and an understanding of how they interact. In addition to various neurotransmitters, several neuropeptides are distributed in the neuron population of the central complex. Here, we investigate the distribution of myoinhibitory peptides (MIPs) in the central complex of the desert locust *Schistocerca gregaria*. *In silico* transcript analysis suggests the presence of eight different MIPs in the desert locust. Through immunolabeling, we identified five systems of central-complex neurons that express MIP-like peptides. Two systems constitute columnar neurons of the protocerebral bridge and the lower division of the central body, while the other three systems are columnar neurons (2 systems) and tangential neurons (1 system) of the upper division of the central body. The innervation pattern and cell count of at least two systems of columnar neurons revealed the existence of 18 instead of 16 columns of the protocerebral bridge. Immunostaining of preparations containing intracellularly stained single cells allowed us to further specify subtypes of labeled columnar neurons. Double label experiments showed that three systems of MIP-immunostained columnar neurons are also locustatachykinin-II-immunoreactive. No colocalization was found with serotonin immunostaining. The data provide novel insights into the architecture of the locust central complex and suggest that MIP-like peptides play a role within the central complex network.

**Key words:** neuropeptides; insect brain; neuroanatomy; central complex; spatial orientation

## Introduction

Insect myoinhibitory peptides (MIPs) are a family of W(X<sub>6</sub>)Wamides characterized by tryptophans at positions 2 and 9. Owing to the history of their identification and based on different functions in different insect species they are also known as B-allatostatins (AST-B, cricket type) or prothoracicostatic peptides (PTSP). The first member of this peptide family was identified in the migratory locust, *Locusta migratoria*, based on inhibitory effects on hindgut and oviduct contractions and was therefore termed Lom-MIP (Schoofs et al., 1991). Later, four related peptides were found to inhibit juvenile hormone synthesis in the field cricket, *Gryllus bimaculatus*. Although they showed high sequence similarity to Lom-MIP they were termed Grb-Allatostatins-B1-4 according to their function in the cricket (Lorenz et al., 1995). Additional MIPs have since been identified in various insect species, i.e. the moth *Manduca sexta* (Mas-MIP-I-VI; Blackburn et al., 1995), the fruit fly *Drosophila melanogaster* (drostatin-B1-5, Williamson et al., 2001) and the American cockroach, *Periplaneta americana* (Pea-MIP; Predel et al., 2001). In the larvae of the silkworm *Bombyx mori*, a peptide with the same sequence as Mas-MIP-I was identified and found to inhibit prothoracicotropic hormone-stimulated ecdysteroidogenesis in the prothoracic gland and was, therefore, termed prothoracicostatic peptide (Bom-PTSP, Hua et al., 1999). Additionally, MIP has been shown to be a ligand of the sex peptide receptor (SPR) in *Drosophila* and of its ortholog in *Bombyx* (Jang et al., 2017; Poels et al., 2010; Yamanaka et al., 2010). In *Drosophila* MIP and SPR are involved in a sleep-stabilizing pathway (Oh et al., 2014). According to their various functions in different insect species, the distribution of MIPs in neurons innervating the heart, oviduct and hindgut, but also the corpora cardiac and corpora allata has been demonstrated. More recently, MIP expression in visual neurons and their putative association with neurons of the circadian clock has been demonstrated in *D. melanogaster* (Kolodziejczyk & Nässel, 2011a), the blowfly *Calliphora vomitoria* (Kolodziejczyk & Nässel, 2011b) and the cockroach *Rhyparobia maderae* (Schulze et al., 2012). Finally, several studies have reported MIP expression in various brain regions, including the central complex (CX; *L. migratoria*, Schoofs et al., 1996; *R. maderae*; Schulze et al., 2012; *D. melanogaster*, Kahsai & Winther, 2011).

The CX is an assembly of midline spanning neuropils involved in spatial orientation and navigation but also in sleep control (Hulse et al., 2021, Donlea et al., 2018). Signal processing in the CX serves the generation of flexible behavior adapted to sensorimotor information and motivational state of the animal (Hulse et al., 2021). In addition to physiological studies that

reveal properties of the CX network, anatomical studies of neuronal connectivity patterns also help to identify the underlying circuitry. The four neuropils that comprise the CX are the protocerebral bridge (PB), the upper division of the central body (CBU), also termed fan-shaped body, the lower division of the central body (CBL), also termed ellipsoid body, and a pair of noduli (NO). Two major types of neuron, columnar and tangential neurons, establish a characteristic organization of these neuropils into vertical slices and horizontal layers, respectively. Although the overall organization of the CX is highly conserved across insect species, some variation in the number of columns and layers has been reported. The PB, for example, consists of 18 columns (glomeruli) in *D. melanogaster* (Wolff et al., 2015) and the bumblebee *Bombus terrestris* (Sayre et al., 2021), while only 16 columns have been reported in the desert locust *Schistocerca gregaria* (Heinze & Homberg, 2008) and the dung beetle *Scarabeus satyrus* (el Jundi et al., 2018). The columns of the PB are defined by distinct sets of columnar neurons (termed CL1, CL2, CPU, CU, and CP in the locust) and tangential (TB) neurons. CL1 neurons (CCI neurons of Williams, 1975; E-PG/P-EG neurons in *D. melanogaster*) arborize in individual slices of the PB and the CBL and in the contralateral gall of the lateral complex. In contrast to CL1 neurons, CL2 neurons connect the PB and the CBL to the contralateral lower unit of the NO. Their interhemispheric wiring scheme has an offset of one slice within the CBL, compared to that of CL1 neurons (Heinze & Homberg, 2008). Homologues of CL1 and CL2 neurons in *D. melanogaster* (types E-PG/P-EG, resp. P-EN) are key elements of a ring attractor network within the CX that encodes the animal's heading direction (Seelig & Jayaraman, 2015; Turner-Evans, et al., 2020).

Identification of neurotransmitter substances provides additional insights into the properties of neural networks. In the locust CX, candidate neurotransmitters and neuromodulators include GABA, serotonin, dopamine, octopamine, and tyramine but also neuropeptides related to tachykinins, allatostatins, allatotropins and orcokininins (Homberg, 2002; Pfeiffer & Homberg, 2014; Homberg et al., 2021). Whereas some of these substances, e.g. GABA, are present in homologous types of neuron across different insects and thus appear to have a highly conserved function (Homberg et al., 2018), others, such as neuropeptides might serve to modulate core networks in a species-specific way. As MIPs have been shown to be expressed in CX neurons of the several insects, we investigated their expression pattern in *S. gregaria* aiming to identify and characterize individual cell types.

The present study provides *in silico* transcript analysis of MIPs in the desert locust. Using an antiserum against MIP we identify MIP-expressing neurons and reveal novel insights into the neuroarchitecture and neurochemical organization of the locust CX. Double label



experiments show substantial colocalization of MIP- and locustatachykinin II-related peptides, but no colocalization with serotonin.

## Materials and methods

### **Animals**

Adult male and female desert locusts (*S. gregaria*) were obtained from crowded colonies at Philipps-University Marburg. Animals were raised at 28 °C, about 60% relative humidity, and a 12 h/12 h light/dark cycle.

### **MIP immunolabeling**

The indirect immunoperoxidase-technique was used to label myoinhibitory peptides (MIPs) on vibratome sections. Animals were cold anesthetized at 4 °C, heads were cut off and the brains were dissected. Brains were fixed in Zamboni's fixative (4% paraformaldehyde and 7.5% picric acid in phosphate buffered saline (PBS, 0.1 mol l<sup>-1</sup>, pH 7.4)) at 4 °C overnight. Following rinses in sodium phosphate buffer (NaPi, 0.1 mol l<sup>-1</sup>, pH 7.4) brains were embedded in gelatin/albumin and fixed in 8% formaldehyde in NaPi at 4 °C overnight. Brains were sectioned in frontal plane with a vibrating-blade microtome (VT1000 S, Leica Microsystems, Wetzlar, Germany) into 30-µm slices. After thorough rinses in saline-substituted Tris buffer (SST, 0.1 mol l<sup>-1</sup> Tris-HCl/0.3 mol l<sup>-1</sup> NaCl, pH 7.4) containing 0.1% Triton X-100 (TrX) the sections were preincubated in 5% normal goat serum (NGS, Dianova, Hamburg, Germany) in SST with 0.5% TrX at room temperature for 1 h. Preincubation was followed by incubation with polyclonal rabbit antiserum against Pea-MIP-1 diluted at 1:12,000 to 1:20,000 in SST containing 0.5% TrX and 2% NGS at room temperature overnight. Following rinses in SST, sections were incubated with secondary antiserum, horseradish-peroxidase-conjugated goat-anti-rabbit (Jackson ImmunoResearch, cat#, RRID: AB\_2313567) diluted at 1:300 in SST containing 0.5% TrX and 1% NGS at room temperature for 1 h. After thorough rinses, the sections were treated with 3,3'-diaminobenzidine tetrahydrochloride (0.33 mg/ml, Sigma Aldrich) with 0.3% nickel ammonium sulfate and 0.05% H<sub>2</sub>O<sub>2</sub> in 0.05 mol l<sup>-1</sup> Tris buffer (Tris-HCl, pH 7.4). Enzymatic reaction was stopped by rinses in Tris buffer, and the sections were mounted on chrome alum-

gelatin coated glass slides. After dehydration sections were cleared in xylene and embedded in Entellan (Merck, Darmstadt, Germany).

### **Double label experiments**

Labeling of MIP and locustatachykinin II (LomTK-II) or serotonin (5-HT) was performed on 130- $\mu\text{m}$  vibratome sections. Preparation and fixation of brains followed the protocol described above except that 4% paraformaldehyde in NaPi was used for the first fixation step. Brains were sectioned in 130- $\mu\text{m}$  slices using a vibrating-blade microtome (VT1200 S, Leica Biosystems, Wetzlar, Germany).

For MIP and LomTK-II double labeling, sections were rinsed with PBS ( $0.1 \text{ mol l}^{-1}$ , pH 7.4) and PBT (PBS with 0.3% TrX) and incubated in 5% normal donkey serum (NDS) in PBT at 4 °C overnight. After several rinses with PBT, sections were incubated with primary rabbit antiserum against Pea-MIP-1 diluted at 1:12,000 in PBT and 2% NDS at 4 °C for 2 d. Following, sections were washed and incubated with unconjugated goat anti-rabbit Fab fragments (Jackson ImmunoResearch, cat# 111007-003; RRID: AB\_2337925) diluted at 1:50 in PBT at 4 °C overnight to mask the primary antibody. After washing, sections were incubated with the secondary antibody, Cy3-conjugated donkey-anti-goat IgG (Jackson ImmunoResearch, cat# 705165-003; RRID: AB\_2340411) diluted at 1:300 in PBT and 2% NDS at 4 °C for 2 d. Thorough rinses in PBT were followed by incubation with biotinylated polyclonal rabbit antiserum against LomTK-II diluted at 1:10,000 in PBT and 2% NDS at 4 °C for 2 d. Following several rinses, sections were incubated with Cy2-conjugated streptavidin (Jackson ImmunoResearch, cat# 016-220-084; RRID AB\_2337246) diluted at 1:1000 in PBT at 4 °C for 2 d. After rinses in PBT and PBS, sections were dehydrated in an ascending ethanol series (30%, 50%, 70%, 90%, 95%, and 100% ethanol, 15 min each) and cleared in a 1:1 mixture of 100% ethanol and methyl salicylate for 20 min, followed by 100% methyl salicylate for 45 min. Finally, sections were embedded between two glass cover slides in Permount (Fisher Scientific, Pittsburgh, PA).

For Pea-MIP-1 and 5-HT double labeling, sections were preincubated in 5% NDS in PBT at 4 °C overnight. Following rinses in PBT, sections were incubated with rabbit antiserum against Pea-MIP-1 and goat antiserum against 5-HT (ImmunoStar, cat# 20079, RRID: AB\_572262) diluted at 1:12,000 and 1:7,500, respectively, in PBT and 2% NDS at 4 °C for 2 d. Thorough rinses were followed by incubation with secondary antibodies, Cy3-conjugated donkey-anti-rabbit IgG (Jackson ImmunoResearch, cat# 711-165-152, RRID: AB\_2307443) and Cy5-conjugated donkey-anti-goat IgG (Jackson ImmunoResearch, cat# 705-175-147,

RRID: AB\_2340415) each diluted at 1:300 in PBT and 2% NGS at 4°C for 2 d. Dehydration and embedding followed the procedure described above.

### **Immunolabeling of rehydrated thick section**

Mounted brains containing Neurobiotin-injected cells from intracellular recordings (as described in Pegel et al., 2018 and Pfeiffer et al., 2005) were demounted by incubation with xylene at room temperature for 2-3 h. Because anti-Pea-MIP-1-immunostaining on brains that were initially fixed with Neurobiotin-fixative (4% paraformaldehyde, 0.25% glutaraldehyde, 0.2% saturated picric acid in 0.1 mol l<sup>-1</sup> in PBS) resulted in poor staining quality, we used brains with Neurobiotin-injected cells for anti-Pea-MIP-1 staining that were previously fixed with 4% paraformaldehyde. Brains were rehydrated in a descending ethanol series (100%, 95%, 90%, 70%, 50%, 30%, 15 min each), rinsed in PBT and embedded in gelatin/albumin. Sectioning and labeling with the primary polyclonal rabbit-antiserum against Pea-MIP-1 or LomTK-II was performed as described above, except that a monoclonal mouse antibody against synapsin (diluted at 1:50, kindly provided by E. Buchner) was added during incubation with the primary antiserum. Cy5-conjugated goat-anti-mouse IgG (Jackson ImmunoResearch, cat# 115-175-146, RRID: AB\_2338713) and Cy2-conjugated goat-anti-rabbit IgG (Jackson ImmunoResearch, cat# 111-225-144, RRID: AB\_2338021) each diluted at 1:300 were used as secondary antibodies.

### **Antibody characterization**

The polyclonal antiserum against Pea-MIP-1 was raised in rabbits against conjugates of *Periplaneta americana* MIP-1 and thyroglobulin (Predel et al., 2001). Antibody specificity was demonstrated in *P. americana* by lack of staining when the antiserum was replaced by pre-immune rabbit serum and when the antiserum was liquid-phase preadsorbed with Pea-MIP-1 (Predel et al., 2001). Specificity in *R. maderae* was demonstrated by liquid-phase preadsorption with Pea-MIP-1 (Schulze et al., 2011), and in *C. vomitoria* and *D. melanogaster* by preadsorption with *Drosophila* MIP-3 (Kolodziejczyk & Nässel, 2011).

The polyclonal rabbit antiserum against LomTK-II (K1-50820091) was a gift from Hans Agricola (University of Jena, Germany). The antiserum was biotinylated as described by Vitzthum & Homberg (1998). Immunostaining with the biotinylated anti-LomTK-II antiserum revealed the same staining pattern as the non-biotinylated antiserum (Vitzthum & Homberg, 1998). Enzyme-linked immunosorbent assay (ELISA) with synthetic LomTK-I and

-II and callitachykinins I and II as antigens was used by Nässel et al. (1995) to test the specificity of the antiserum. Cross reaction of the antiserum with all four tachykinins was found, with a slightly higher affinity to the LomTKs. Specificity of the antiserum on locust brain sections was demonstrated by Vitzthum and Homberg (1998). Liquid-phase preadsorption of the diluted antiserum with  $100 \mu\text{mol l}^{-1}$  GABA-glutaraldehyde conjugate, leucokinin, or substance P did not reduce immunostaining, whereas preadsorption with  $10 \mu\text{mol l}^{-1}$  synthetic LomTK-II abolished all immunostaining in brain sections of *S. gregaria*.

To test cross-reactivity between the Pea-MIP-1 and the LomTK-II antisera, we preadsorbed the diluted antisera with synthetic Pea-MIP-1 (GWQDLQGGWamide, kindly provided by Dr. M. Eckert) and synthetic LomTK-II (Peninsula, Heidelberg, Germany). Preadsorption of the Pea-MIP-1 antiserum with  $0.1 \mu\text{mol l}^{-1}$  of Pea-MIP-1 abolished immunostaining in *S. gregaria* brain sections, whereas  $100 \mu\text{mol l}^{-1}$  LomTK-II did not affect the staining. Preadsorption of the LomTK-II antiserum with  $10 \mu\text{mol l}^{-1}$  LomTK-II peptide abolished immunostaining in *S. gregaria* brain sections, whereas staining was unaffected by preadsorption with  $100 \mu\text{mol l}^{-1}$  Pea-MIP-1.

The antiserum against 5-HT (ImmunoStar, cat# 20079, RRID: AB\_572262) was raised in goat against serotonin coupled to bovine serum albumin (BSA) with paraformaldehyde. The antiserum led to a staining pattern that was indistinguishable from the pattern of immunolabeling resulting from a different 5-HT antiserum (Homberg et al., 2020; Homberg, 1991). Preadsorption of the diluted antiserum with  $100 \mu\text{g/ml}$  serotonin-BSA conjugate abolishes all labeling (ImmunoStar, product information sheet).

The monoclonal antibody against synapsin was raised in mouse against parts of the *Drosophila* synaptic vesicle protein SYN1 fused with glutathione-S-transferase (Klagges et al., 1996). Its specificity has been demonstrated in *Drosophila* by Klagges et al. (1996). The antibody has been used to label synaptic neuropils in different insect species. In *S. gregaria*, neuropil labeling has been demonstrated by Kurylas et al. (2008), el Jundi et al. (2010), von Hadeln et al. (2018, 2020) and Hensgen et al. (2021).

### **Image acquisition and data processing**

Images from peroxidase-labeled brains were obtained by a transmission light microscope (Axioskop, Zeiss, Oberkochen, Germany) with an attached digital camera (ProgRes C12plus, Jenoptik). Images from fluorescence-labeled brain sections were acquired using a confocal laser scanning microscope (Leica, TCS SP5, Leica Microsystems, Wetzlar, Germany). Scans were obtained with a 20x immersion objective (HC PL APO 20x/0.75 Imm Corr CS2), 40x

oil objective (HCX PL APO 40x/1.25 Oil), or 63x oil objective (HCX PL APO 63x/1.40 Oil). An argon laser (488 nm), a diode pumped solid state laser (561 nm), and a helium neon laser (633 nm) were used to excite the fluorophores Cy2, Cy3, and Cy5 respectively. Pinhole size was 1 airy unit and the scanning frequency was 400 Hz. Pixel size in the xy plane ranged from 0.24 x 0.24  $\mu\text{m}$  to 0.75 x 0.75  $\mu\text{m}$  and the z-step size was set to 0.5, 1 or 1.5  $\mu\text{m}$ .

2D reconstructions from peroxidase-labeled neurons were created by manually tracing the neurons through a camera lucida attachment on a compound microscope (Leitz, Wetzlar, Germany). Drawings were digitized with a scanner (CanoScan 9000F, mark II, Canon, Tokyo, Japan) and processed in Adobe Illustrator (Adobe Illustrator, RRID: SCR\_010279).

Primary processing of image stacks from the confocal laser scanning microscope was done in Amira 5.6 (ThermoFisher Scientific, Waltham, MA; RRID: SCR\_007353). Cell bodies (Figure 1b) were marked using the Landmark module and neuropils were reconstructed as described by Hensgen et al. (2021). Briefly, several layers of each neuropil were manually marked in the x-, y-, and z-plane in the segmentation editor. The resulting scaffold was used to compute a 3D structure by applying the wrapping function. Images were optimized and assembled in Affinity Photo (Serif, Nottingham, UK; RRID: SCR\_016951) and Affinity Designer (Serif, Nottingham, UK; RRID: SCR\_016952).

## Sequence analysis

The *S. gregaria* MIP transcript was identified based on the available allatostatin-B sequence from *L. migratoria* (GenBank: AKN21242.1, Hou et al., 2015) by using NCBI's BLAST (NCBI Resource Coordinators, 2016) (tblastn against transcriptome shotgun assembly [TSA] archives). Since the coverage by transcriptome data from *S. gregaria* was not sufficient we used the closely related sister species *Schistocerca americana* to identify the MIP transcript (GenBank: GIOT01126231.1, Foquet, B. and Song, H., unpublished). To eventually obtain the *S. gregaria* sequence we took advantage of the recently released genome sequence (Verlinden et al., 2020) and identified in an iterative process based on BLAST and pairwise alignments the genomic region and thereby the transcript. All alignments and annotations were made with Geneious 10 (Biomatters Ltd., Auckland, New Zealand). The signal peptide was predicted by SignalIP (Petersen et al., 2011).

## Results

### **Analysis of MIP transcript sequences**

The *S. gregaria* MIP gene consists of 5 exons distributed over a genomic region of more than 600 kb (Figure 1a, exon 5 not shown). The transcript is at least 1.201 bp long with an 837 bp open reading frame encoding the 278 amino acid (AA) MIP prepropeptide. The prepropeptide contains a 29 AA signal peptide for secretion and 12 putative bioactive neuropeptides, of which eight are unique. MIP-1 to MIP-5 are 9 AA, MIP-6 and MIP-7 are 11 AA, and MIP-8 is 13 AA long (Figure 1b). The differences between *S. gregaria* and *Locusta migratoria* (Hou et al., 2015) MIPs (AST-B) are minor and only in regions which also differ between the intraspecific isoforms (Figure 2a). There are three isoforms with no differences, four with a single AA exchange, and one with two exchanges. The AA sequence comparison with Pea-MIP-1, that was used to raise the antiserum, reveals high similarity and implicates high specificity of the antiserum for MIPs in *S. gregaria* (Figure 2b).

### **Identification of MIP-immunolabeled cell types**

The CX is innervated by at least four systems of MIP-immunoreactive columnar neurons with somata in the pars intercerebralis (Figure 3). Two systems innervate the CBL and at least two systems innervate the CBU. Additionally, one set of tangential neurons with somata likely located in the super lateral protocerebrum, contributes to staining in the CBU.

One of the two systems of columnar neurons of the CBL consists of 18 neurons (9 per hemisphere) with prominent, large cell bodies (Figure 4). The somata (Figure 4b, arrowheads) give rise to thick fibers that enter the PB and project via the w-, x-, y-, and z-bundles through the posterior chiasma. The z-bundle contains three fibers, whereas two fibers run through each of the other bundles (Figure 4a,c). As described by Williams (1975), fibers of the x-, y-, w-, and z-bundles rearrange themselves into nine fiber fascicles when running toward the CBL. Seven of these groups penetrate the substance of the CBU and are termed lb, lc, ld, e, rd, rc, rb (from left to right), whereas the other two, la and ra, run over the ventro-lateral surface of the CBU (Williams, 1975). Out of the 18 fibers of columnar neurons one fiber of the left and one of the right hemisphere project via la and ra, respectively and two fibers, one of each hemisphere, project via lc, ld, e, rd, and rc. Three fibers, two from the contralateral and one

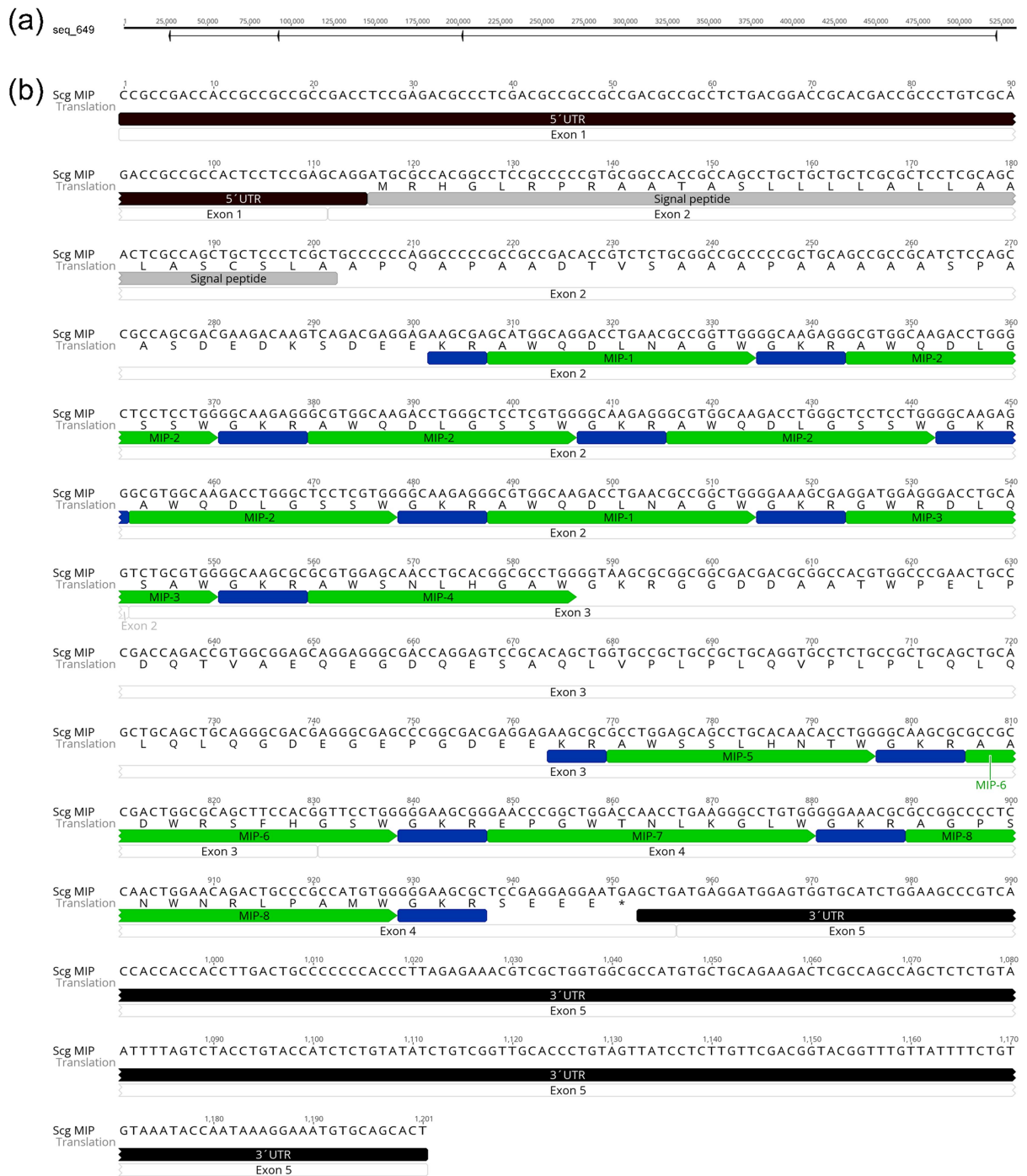


**Figure 1** DNA and protein sequence of *S. gregaria* myoinhibitory peptide (Scg-MIP). (a) Genomic organization of the prepropeptide on contig seq\_649. Arrowheads represent the exons, the numbering above shows base pairs. The exons one to four (arrowheads) span from 522,139 > 522,029; 202,692 > 202,263; 92,674 > 92,386; 27,495 > 27,370 base pairs; exon five was located on contig seq\_1671. (b) DNA sequence of the MIP transcript (top trace), the translation of the open reading frame (second trace), functional characterization (third trace), and its exon structure (bottom trace). Blue boxes mark cleavage sites flanking the putatively bioactive peptides (green).

from the ipsilateral hemisphere, project via lb and rb (Figure 4a, arrowheads). From the CBL, the neurons project together with fibers of CBU columnar neurons (see below) via the isthmus tracts to the gall of the contralateral LX (Figure 4a, dashed lines, Figure 4d, arrowheads).

The neurons arborize in the PB, the CBL and the gall, but as these arborizations intermingle with those of other neurons their processes could not be traced. Judged from cell body position and projection pattern, the immunolabeled neurons correspond to a set of CL1 neurons that has been labeled by an antiserum against locustatachykinin I and II (LTC I neurons, Vitzthum & Homberg, 1998). However, Vitzthum & Homberg (1998) counted only 16 instead of 18 cells of this system.

In locusts, four subtypes of CL1 neurons have been distinguished, CL1a-CL1d (Heinze & Homberg, 2008, 2009). CL1a and CL1b neurons are discriminated based on their opposite polarity and differences in the size of their somata, with CL1a neurons possessing small somata and CL1b neurons possessing large somata. CL1c neurons have large somata but lack axons to the gall. CL1d neurons have small somata and have so far only been colabeled with either CL1c or CL1b neurons (Heinze & Homberg, 2008, 2009). To test whether polarization-sensitive CL1a neurons are labeled by the antiserum against Pea-MIP-1 we performed labeling on brains with individually labeled CL1a neurons from intracellular recordings. The experiments showed that CL1a neurons are not MIP-positive (Figure 5). CL1a neurons have smaller cell bodies than the MIP-positive neurons. Judged from one dye filled preparation showing two CL1 neurons, presumably CL1a and CL1d, colabeled in one column of the PB (Figure 5c,e), we can also exclude that CL1d neurons are MIP-positive. These data suggest that MIP-positive CL1 neurons are CL1b neurons that have larger somata than CL1a neurons and CL1d neurons.

The second set of columnar neurons of the CBL is more faintly stained. It consists of 20-24 neurons with somata of intermediate size in the pars intercerebralis (Figure 6a,b). The neurons send thin neurites into the PB and project via the four bundles through the posterior chiasma. Owing to faint staining and fiber crossings the tracing revealed only an incomplete wiring scheme of 20 cells with at least two fibers projecting via each bundle. The four additional fibers were traced only partly and could not be unambiguously assigned to a bundle. Toward the CBL, fibers become thicker and project into the CBL and the lower unit of the contralateral nodulus (NOL). The staining appearance in the NOL was reconstructed, whereas arborizations in the PB and CBL could not be traced owing to dense staining. The morphology of the cells indicates that they are CL2 neurons, which connect single slices of the PB to slices of the CBL and the contralateral NOL (Heinze & Homberg, 2008).



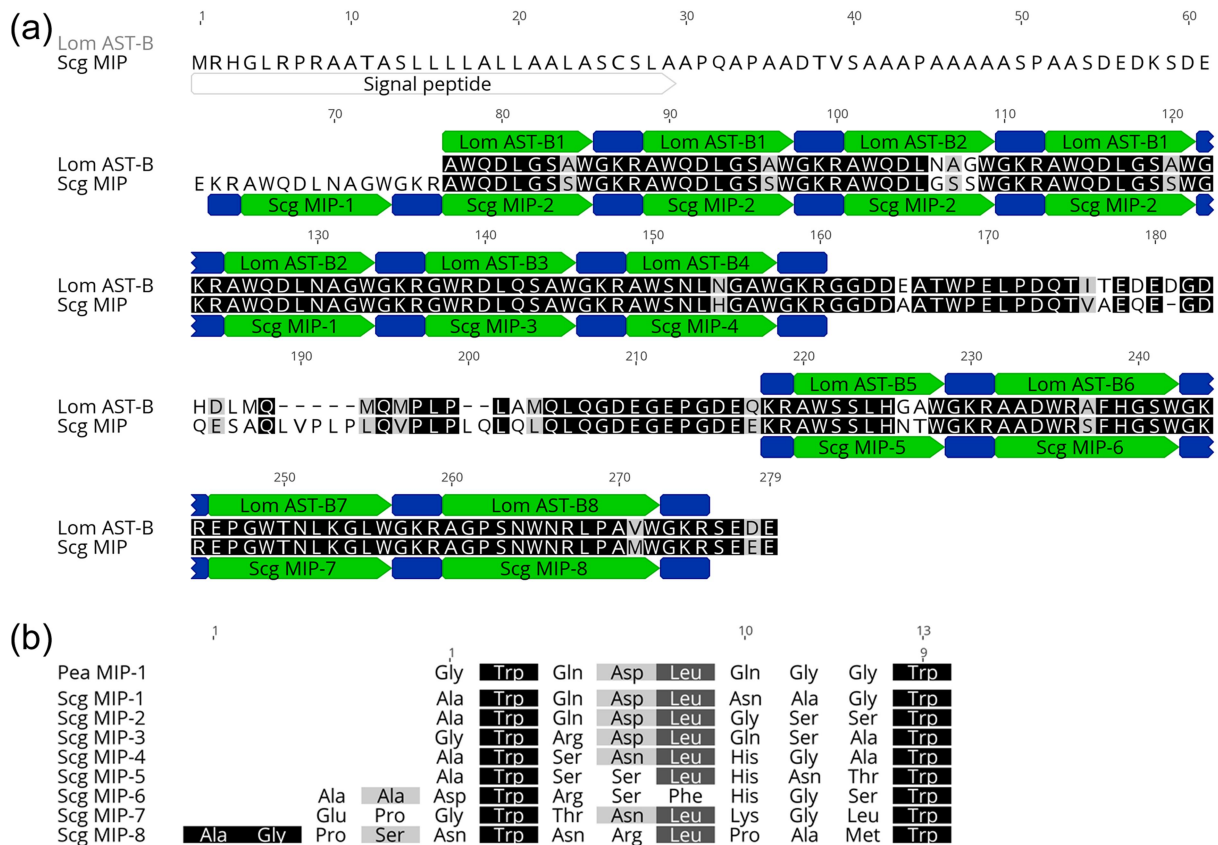


**Figure 2** Protein sequence alignments. (a) Sequence alignment of the myoinhibitory (MIP, allatostatin-B) prepropeptides from *S. gregaria* and *L. migratoria*. Amino acids are highlighted as: black indicating identity; grey indicating close chemical similarity; white, dissimilar. The prepropeptide is highly conserved between the two species, only a few amino acid exchanges affect the bioactive peptides (green). (b) Sequence alignment of the putatively bioactive myoinhibitory peptides of *S. gregaria* (Scg MIP-1 to Scg MIP-8) and the *Periplaneta americana* (Pea MIP-1) epitope used by Predel et al. (2001) to raise the antiserum.

One set of MIP-immunoreactive columnar neurons of the CBU consists of eight cells (Figure 6c,d). Their cell bodies in the pars intercerebralis give rise to fine fibers that project via the w-, x-, y-, and z-bundles to the CBU. Here, neurites become larger and prominent processes innervate layer I. Owing to dense staining in the CBU, areas of terminal ramifications could not be determined. From the CBU neurites continue and give off varicose terminals in the contralateral crepine (Figure 6c,d, arrowheads). According to their projection pattern these neurons correspond to a subtype of CU2 neurons (Heinze & Homberg, 2008). Because their fiber trajectories do not fully correspond to CU2a or CU2b neurons (Heinze & Homberg, 2008), they are termed CU2x.

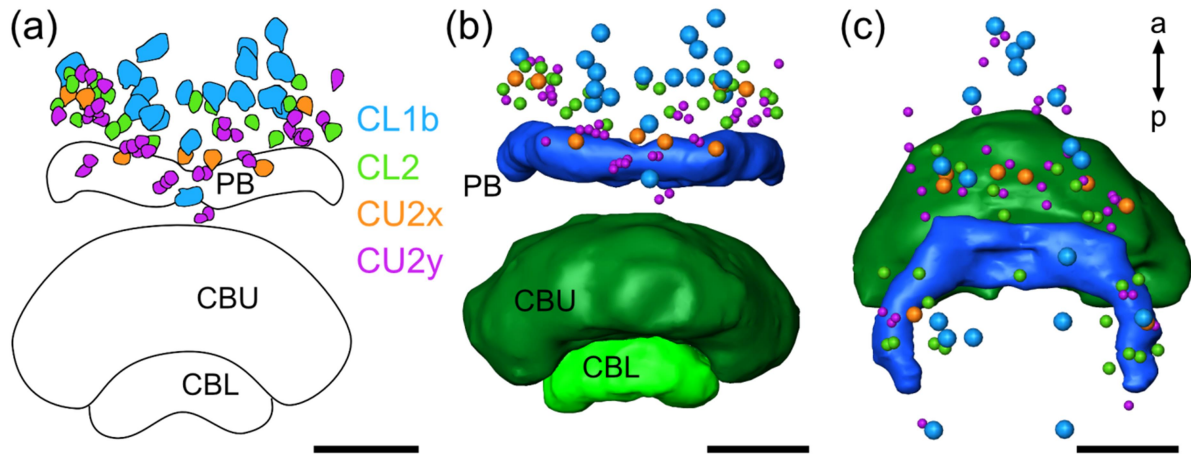


**Figure 3** Somata of myoinhibitory peptide (MIP)-immunoreactive neurons in the pars intercerebralis innervating the central complex of the desert locust. In total, cell bodies of 18 CL1b, 20-24 CL2, 8 CU2x, and 38 CU2y neurons of unidentified subtype could be distinguished. Depending on orientation some cell bodies may be obscured by others. (a) Frontal diagram of the CX illustrating the shape and size of MIP-immunoreactive somata. (b) Frontal and (c) horizontal view of a 3-dimensional reconstruction of the upper division of the central body (CBU), the lower division of the central body (CBL), and the protocerebral bridge (PB) together with spherical landmarks indicating the number and position of MIP-positive somata. Color scheme of somata is similar to that in (a). a, anterior; p, posterior. Scale bars = 100  $\mu\text{m}$

Additional cell bodies within the PI and arborizations in the CBU and crepine suggest that at least one further set of CU neuron is MIP-immunoreactive. Owing to the large number of stained cells their neurites could not be traced but their morphology was analyzed in more detail in double labeling experiments (see below).

### Double label experiments

Vitzthum and Homberg (1998) showed that an antiserum against LomTK-II labels four systems of columnar CX neurons, termed LTC I-IV. Because the morphology of those cells is highly similar to CL1b- (LTCI+II) and CU2x (LTCIII+IV) neurons labeled by the Pea-MIP-1 antiserum, we performed double label experiments with antisera against Pea-MIP-1 and LomTK-II.

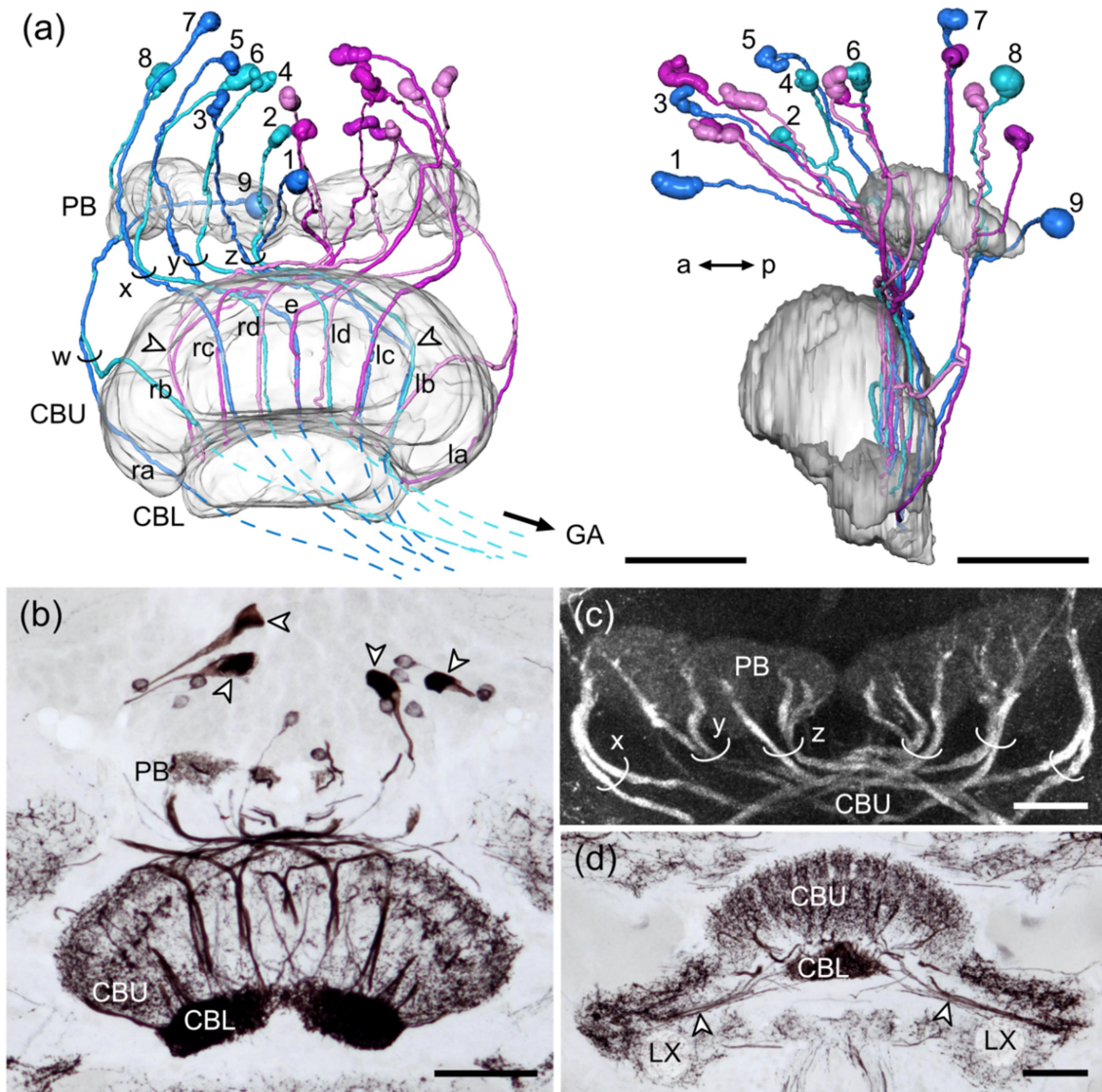


**Figure 4** Myoinhibitory peptide (MIP)-immunoreactive CL1b neurons innervating the lower division of the central body (CBL). (a) Frontal (left) and sagittal (right) view of the 3-dimensional reconstruction of 18 CL1b neurons (9 per hemisphere). The cell bodies are located in the pars intercerebralis and send fibers into the protocerebral bridge (PB). The main neurites project from the PB via the w-, x-, y-, and z-bundles through the posterior chiasma and run in nine distinct fiber groups (ra, rb, rc, rd, e, ld, lc, lb, la) to the CBL. Owing to intense staining in the CBL individual neurites could not be traced further, but the projections toward the gall (GA) are indicated by dashed lines for cells of the right hemisphere. (b) Immunoperoxidase-labeled frontal section illustrating the large cell bodies of CL1b neurons (arrowheads), their projection pattern, and the dense innervation of the CBL by MIP-immunoreactive processes. (c) Maximum intensity projection of a confocal stack of MIP-immunofluorescent images at the level of the PB. Three large fibers of CL1b neurons project via each z-bundle, whereas only two fibers project via each y- and x-bundle. (d) Frontal section illustrating MIP-immunoreactive fibers of CL1b neurons that run from the CBL via the isthmus tracts (arrowheads) to the lateral complex (LX). a, anterior; CBU, upper division of the central body; MAL, medial accessory lobe; p, posterior. Scale bars = 100  $\mu$ m (a,b,d), 40  $\mu$ m (c)

The experiments confirmed double labeling in CL1b/LTC I and CU2x/LTC IV neurons (Figure 7). The large somata of CL1b neurons as well as their neurites are prominently double labeled (Figure 7a-c, arrowheads). Counting of the double labeled, large cell bodies confirmed that this system comprises 18 instead of 16 cells reported by Vitzthum & Homberg (1998). The neurite of the additional cell (one per hemisphere) projects into the innermost column of the PB and continues via the z-bundle and within the b-group of fibers toward the CBL.

Double labeling was also observed in the eight medium-sized cell bodies of CU2x neurons (Figure 7a-c, yellow arrowhead), their large fibers (Figure 7d-f, yellow arrowheads), and varicose arborizations in layer Ia and IIa of the CBU that are likely ramifications of these neurons.

In addition to these two sets of neurons, approximately 38 small somata in the pars intercerebralis are labeled by both antisera (Figure 7a-c, double arrowheads). Because many cells are labeled, the respective neurites could not be fully traced. However, analysis of the staining intensity of the different neuronal processes indicates that at least one subset of these small cell bodies belongs to a second system of CU2 neurons (now termed CU2y, Figure 8, Figure 9a) with the following projection pattern. From the PB, CU2y neurons project via the w-, x-, y- and z-bundles into the CBU (Figure 8a, arrowheads) where they arborize in layer Ib. Their neurites continue through the same fiber bundles as those of CL1b neurons toward the CBL (Figure 8a, double arrowheads) and further via the isthmus tracts toward the crepine (Figure 8b,c arrowheads). The two cell types (CL1b and CU2y) can be distinguished based on staining intensity, with CL1b neurons being more strongly labeled by anti-Pea-MIP-1 and CU2y neurons more strongly by anti-LomTK-II. Arborizations of CU2y neurons likely contribute to double labeling in the crepine (Figure 8c). In general, their projection pattern is highly similar to that of the CU2x neurons, but shows the following differences. Somata of CU2y neurons are smaller than those of CU2x neurons. Neurites of CU2y neurons enter the CBU more dorsally than those of CU2x neurons, and they arborize predominantly in layer Ib of the CBU instead of layer Ia and IIa. Their primary neurites project more posteriorly toward the ventral groove than those of CU2x neurons and their arborizations within the crepine are located slightly more laterally within the neuropil than those of CU2x neurons.

Immunostaining for LomTK-II of a preparation containing one Neurobiotin-labeled CL1a neuron, one CL1b neuron, and two CU2y neurons enabled us to trace the morphology of the CU2y neurons (Figure 9a). Moreover, it revealed that the CL1b neuron and the CU2y neurons but not the CL1a neuron are LomTK-II-positive (Figure 9b-j) and, hence, supports the assumption that CL1b neurons and CU2y neurons are labeled by anti-Pea-MIP-1. Noticeably,

we found that the axonal fiber of the CL1b neuron to the gall is much thinner than the fiber of the CL1a neuron (data not shown).

As expected, MIP-positive CL2 neurons do not show LomTK-II immunoreactivity in the noduli (Figure 10). Correspondingly, around 20-24 somata in the pars intercerebralis were only labeled by anti-Pea-MIP-1 (Figure 7a-c, asterisks). Prominent MIP-positive terminals that also lack LomTK-II immunostaining are present in layer IIb of the CBU (Figure 7d-f). Although their origin could not be traced, MIP-positive fibers that enter the CBU via the anterior bundles (Figure 10d,e, arrowheads) suggest that these might be terminals of tangential neurons with somata in the superior lateral protocerebrum (von Hadeln et al., 2020). Double labeling confirmed that these fibers lack LomTK-II immunoreactivity (Figure 10e, arrowhead).

Columnar neurons with innervation in the NO are also labeled by antisera against 5-HT (Homberg, 1991). To confirm, that the respective system of columnar neurons is different from that labeled by anti-Pea-MIP-1, we performed double label experiments with both antisera (Figure 11). Indeed, the staining revealed no colocalization in the CX (Figure 11). Layer I and layer III of the CBU show intense 5-HT staining, whereas layer II shows weaker 5-HT labeling (Figure 11). In contrast, MIP immunostaining is strongest in layer II, weaker in layer I, and layer III lacks MIP staining (Figure 11). As expected, MIP- and 5-HT immunostainings are confined to different subunits of the NO, with MIP immunoreactivity in the lower units of the noduli (NOL) and 5-HT immunolabeling in layer II of the upper units of the noduli (NOUII).

### **The columns of the protocerebral bridge**

Identification of a system of 18 MIP-positive CL1 neurons, presumably CL1b, prompted us to reinvestigate the number of CL1a neurons, which have been described as a system of 16 neurons (Vitzthum & Homberg, 1998; Heinze & Homberg, 2008). Detailed analysis of CL1a neurons with arborizations in the innermost columns of the PB (Figure 12a-c) suggest that this column consists of two hemicolumns (now termed column 1 and column 0) that together correspond in volume to the other PB columns. Neurites of the CL1a neurons of column 1 and column 0 follow the same trajectory through the CBU but enter the CBL with a slight offset (Figure 12d), indicating that they innervate overlapping, but not identical regions within the CBL. Moreover, we found that axonal fibers of CL1a neurons take different trajectories



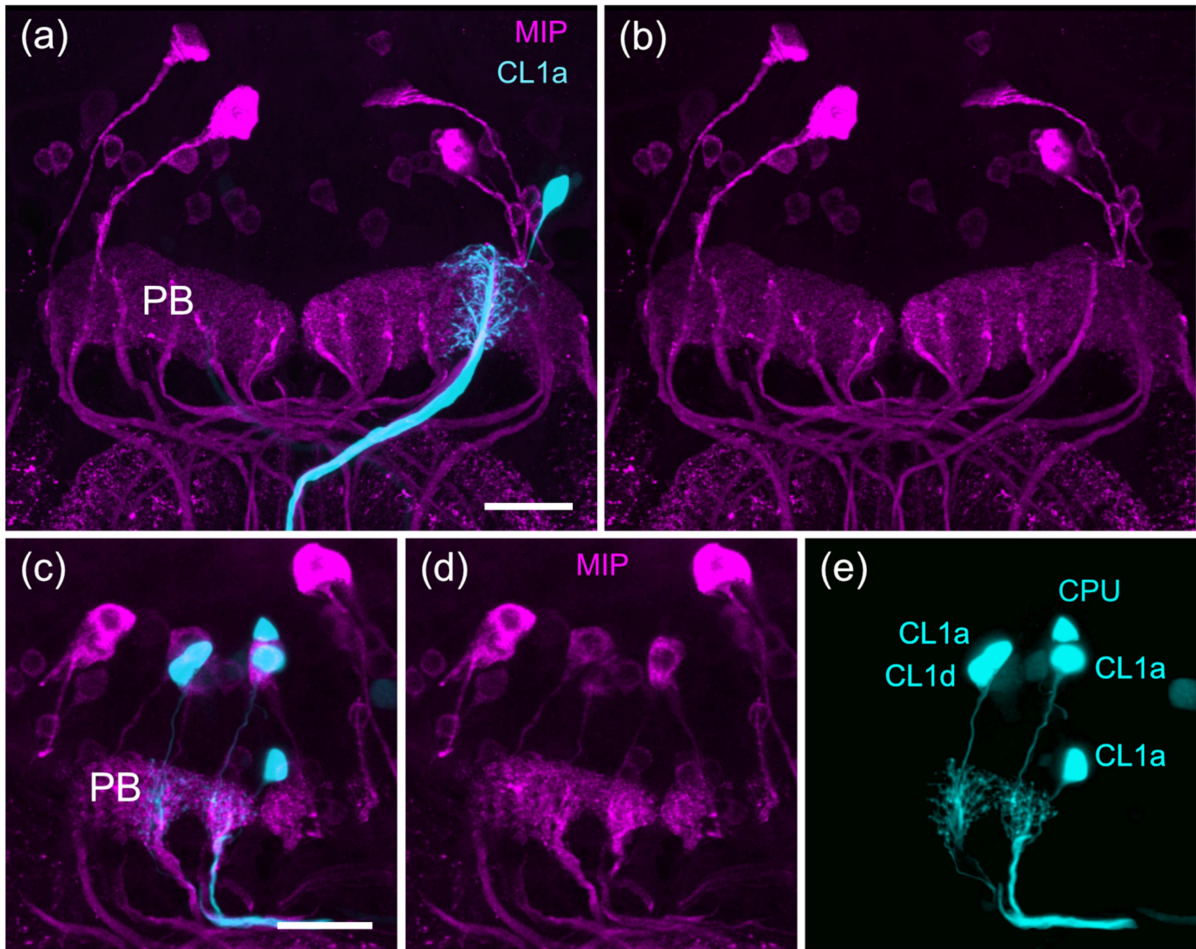


**Figure 5** Double staining of Neurobiotin-injected CL1a neurons (cyan) and myoinhibitory peptide (MIP)-immunoreactive neurons (magenta). (a,b) Maximum intensity projection of several optical slices showing MIP staining at the level of the protocerebral bridge (PB). An intracellularly stained CL1a neuron is not labeled by the Pea-MIP-1 antiserum. (c-e). Maximum intensity projection of several optical slices showing MIP staining at the level of the PB. None of the three intracellularly stained CL1a neurons, nor the putative CL1d neuron or the CPU neuron are labeled by the Pea-MIP-1 antiserum. Scale bars = 50 μm

through the isthmus tracts, depending on which PB column they innervate (Figure 12e,f). CL1a neurons with arborizations in odd numbered columns (1,3,5,7) project more anteriorly and dorsally via the isthmus tracts, whereas CL1a neurons with arborizations in even numbered columns (0,2,4,6,8) take a ventral path through the isthmus tracts. This scheme would be in line with the existence of an additional column (column 0) in the PB, as these neurons project ventrally into the GA. Taken together, these findings indicate the presence of

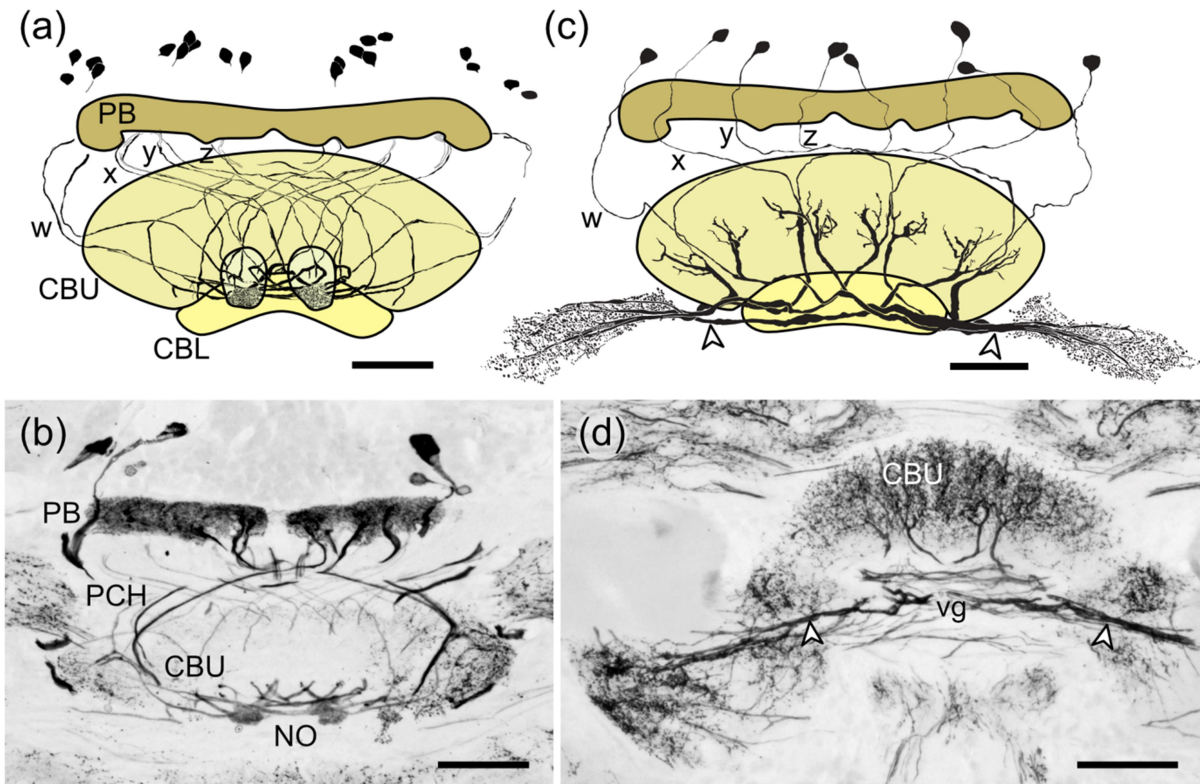


**Figure 6** Myoinhibitory peptide (MIP)-immunoreactive CL2 neurons (a,b) innervating the lower division of the central body (CBL) and the noduli (NO), and CU2x neurons (c,d) innervating the upper division of the central body (CBU) and the crepine. (a) Frontal reconstruction of MIP labeled CL2 neurons. The cell bodies are located in the pars intercerebralis and send fibers into the protocerebral bridge (PB). The main neurites project via the w-, x-, y-, and z-bundles through the posterior chiasma (PCH) to the CBL. Ramifications in the PB and CBL could not be traced due to intense staining. Fine terminals are visible in the lower units of the NO. (b) Immunoperoxidase-labeled frontal section illustrating the small fibers of CL2 neurons and their terminals in the NO. (c) Frontal reconstruction of eight CU2x neurons with somata in the pars intercerebralis. Cell body fibers run through each of the w-, x-, y-, and z-bundles toward the CBU, where not all ramifications could be traced due to dense staining. From the CBU large processes of the CU2x neurons continue to the crepine. (d) Frontal immunoperoxidase-labeled section illustrating large fibers of CU2x neurons and their projections to the crepine. vg, ventral groove. Scale bars = 100  $\mu$ m

18 CL1a neurons, corresponding to the number of 18 CL1b neurons identified based on MIP- and LomTK-II immunoreactivity.



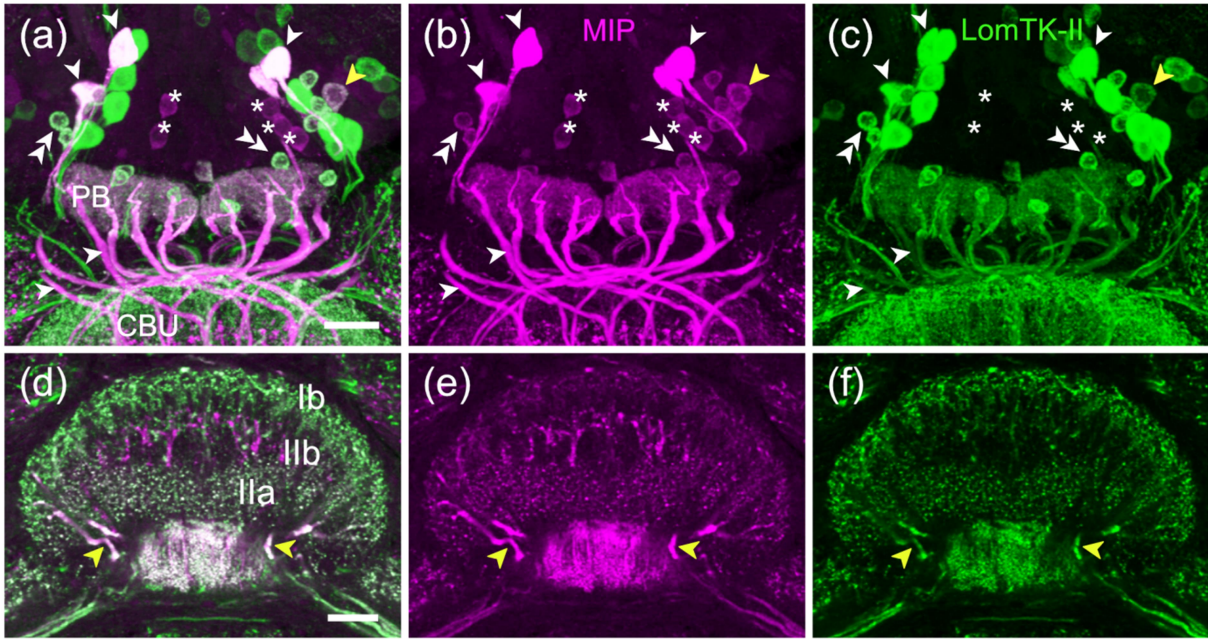


**Figure 7** Double immunofluorescent staining for myoinhibitory peptide (MIP, magenta) and locustatachykinin II (LomTK-II, green) in the central complex and lateral complex. (a-c) Maximum intensity projection of several optical slices at the level of the protocerebral bridge (PB). CL1b neurons (arrowheads) with large somata are double labeled by both antisera. Small somata close to the PB (double arrowhead) are also labeled by both antisera. Some somata of intermediate size are only MIP-immunoreactive (CL2 neurons, asterisks). One soma of a CU2x neuron is double labeled (yellow arrowhead). (d-f) Maximum intensity projection of several optical slices at the level of the central body upper (CBU) and lower division (CBL). The layers of the CBU show a distinct pattern of LomTK-II- and MIP immunoreactivity, resulting from the innervation by different cell types. Double labeled CU2x neurons with large fiber diameter (yellow arrowheads) contribute to staining in layer IIa of the CBU. Several prominent ramifications in layer IIb are only MIP-immunoreactive. Immunoreactivity of CL1b neurons and CL2 neurons contributes to double-labeling in the CBL. Scale bars = 40  $\mu\text{m}$

## Discussion

In the CX of the desert locust brain, neuropeptides of the MIP family are present in at least four systems of columnar neurons and one type of tangential neuron. Based on existing catalogs of neuronal cell types (Heinze & Homberg, 2008, 2009) we identified CL1b and CL2 neurons as MIP-positive neurons of the CBL, and two subtypes of CU2 neurons as MIP-positive in the CBU. Tangential neurons that innervate layer IIb of the CBU could not be identified in detail but likely correspond to  $\text{TU}_{\text{SLP}}$  neurons described by von Hadeln et al. (2020). Double label experiments revealed colocalization of MIP with locustatachykinin II in



CL1b- and CU2 neurons. Detailed analysis of projection patterns showed that CL1 neurons divide the protocerebral bridge into 18 columns and not 16 as reported previously (Williams, 1975; Heinze & Homberg, 2008). Analysis of the MIP transcript, finally, predicts the presence of 8 MIPs with high sequence similarity to 8 MIPs in *L. migratoria* (Hou et al., 2015) as well as to Pea MIP-1 that was used to produce the antiserum (Figure 2b).

### **MIP-positive cells of the CBL**

Four types of CL1 columnar neurons have been distinguished in the locust CX (Heinze & Homberg, 2009). One of these systems, identified as CL1b neurons, is Pea-MIP-1-immunoreactive. In *Drosophila*, E-PG neurons (likely homologous to CL1a neurons of the locust) are key elements of a ring-attractor network, encoding the heading direction of the animal. P-EG (CL1b) cells follow an identical projection pattern but have opposite polarity. Whereas their function first remained unclear and speculative (Franconville et al., 2018; Pisokas et al., 2020), it has recently been shown that they play a role in generating persistent activity in E-PGs and thus serve to stabilize the heading direction circuit even in the absence of external stimuli (Turner-Evans et al., 2020). With the identification of 18 CL1b neurons in the locust their number fits the number of 18 P-EG neurons in *Drosophila* (Scheffer et al., 2020). As in the fly, three fibers of P-EG/CL1b neurons run within each z-bundle while only two fibers run within each of the remaining bundles. The number of 18 CL1a neurons also fits the number of PB glomeruli in *Drosophila*. However, with 46 individual neurons the number of E-PG neurons in *Drosophila* is more than twice as high as the number of CL1a neurons in the locust (Scheffer et al., 2020).

Pisokas et al. (2020) explored the functional consequences of differences between the fruit fly and locust CX. They pointed to three striking differences, the open kidney-shaped CBL in the locust vs. the closed toroidal ellipsoid body of *Drosophila*, the number of 16 vs. 18 PB glomeruli, and the difference in the dendritic distribution of TB1/ $\Delta$ 7 neurons across the PB. Despite these differences they assumed that there is an eight-fold radial symmetric inhibitory and excitatory circuit in both species that arises from the species-specific connectivity patterns between cell types. To which extent the additional hemicolumn changes the circuit functionality is, therefore, also dependent on the cell to cell connectivity and cannot be clarified at this point. Species-specific differences in circuit solution are also supported by recent findings on the bumblebee projectome that suggest an additional strategy to close the loop in insects with an open CBL (Sayre et al., 2021).

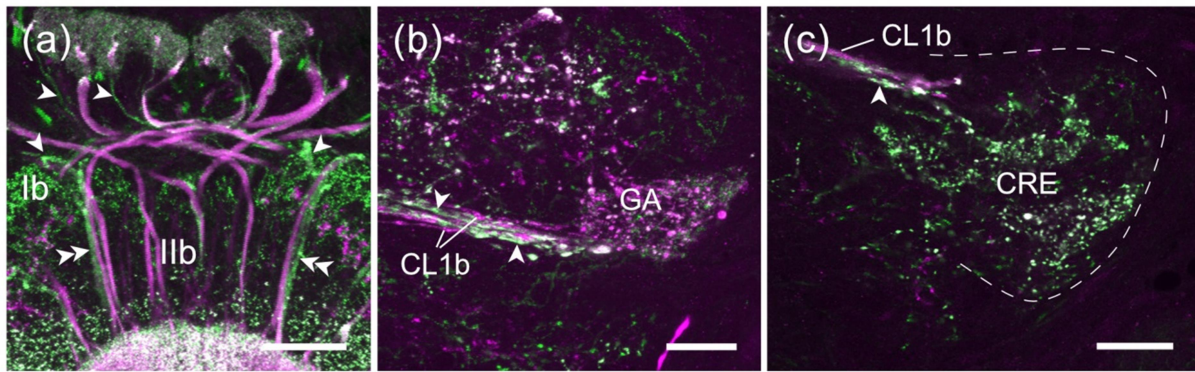


**Figure 8** Double immunofluorescent staining for myoinhibitory peptide (MIP, magenta) and locustatachykinin II (LomTK-II, green) in the central complex, the isthmus tracts and the crepine (CRE). (a) Maximum intensity projection of several optical slices at the level of the posterior chiasma. Neurites of CU2y neurons are strongly labeled by anti-LomTK-II but only weakly by anti-Pea-MIP-1. They run from the PB to the CBU (arrowheads) where they become thicker and innervate layer Ib. They continue ventrally (double arrowheads) in the same fiber bundles as CL1b neurons that are more strongly labeled by anti-Pea-MIP-1. (b) Maximum intensity projection of several optical slices at the level of the isthmus tract and the gall (GA). Both cell types, CL1b and CU2y (arrowheads), project via the isthmus tract toward the GA. Their neurites are distinguishable based on staining intensity, with CL1b neurons in magenta and CU2y neurons in green. (c) Maximum intensity projection of several optical slices at the level of the CRE. Whereas CL1b neurons arborize in the GA (b), CU2y neurons (arrowhead) contribute to staining in the CRE. Scale bars = 50  $\mu\text{m}$  (a), 20  $\mu\text{m}$  (b), 25  $\mu\text{m}$  (c)

In *Drosophila*, two variants of P-EG neurons have been described (Wolff & Rubin, 2018), the ‘tile’ cells (P-EG) and the ‘canal’ cells (P-E<sub>c</sub>G). Whether P-E<sub>c</sub>G neurons or P-EG neurons are more similar to the locusts CL1b neurons remains unclear. E-PG and P-EG neurons are cholinergic in *Drosophila* (Turner-Evans et al., 2020), and at least one subtype of CL1 neurons expresses the muscarinic acetylcholine receptor in the grasshopper *Chorthippus biguttulus* (Kunst et al., 2011). Whether CL1 neurons in *S. gregaria* are cholinergic or express acetylcholine receptors is not known.

The second major type of CL neurons, CL2, is likewise MIP-positive in the locust. In *Drosophila*, P-EN neurons (equivalent to CL2 in the locust) are a second key element of the heading direction circuit. They provide angular velocity input that shifts the activity in the E-PG neuron population when the fly turns (Green et al., 2017, Turner-Evans et al., 2017). Similarly, polarization-sensitive CL2 neurons are elements of the internal compass in locusts (Pegel et al., 2018) and might play a similar role in shifting the activation in CL1 neurons

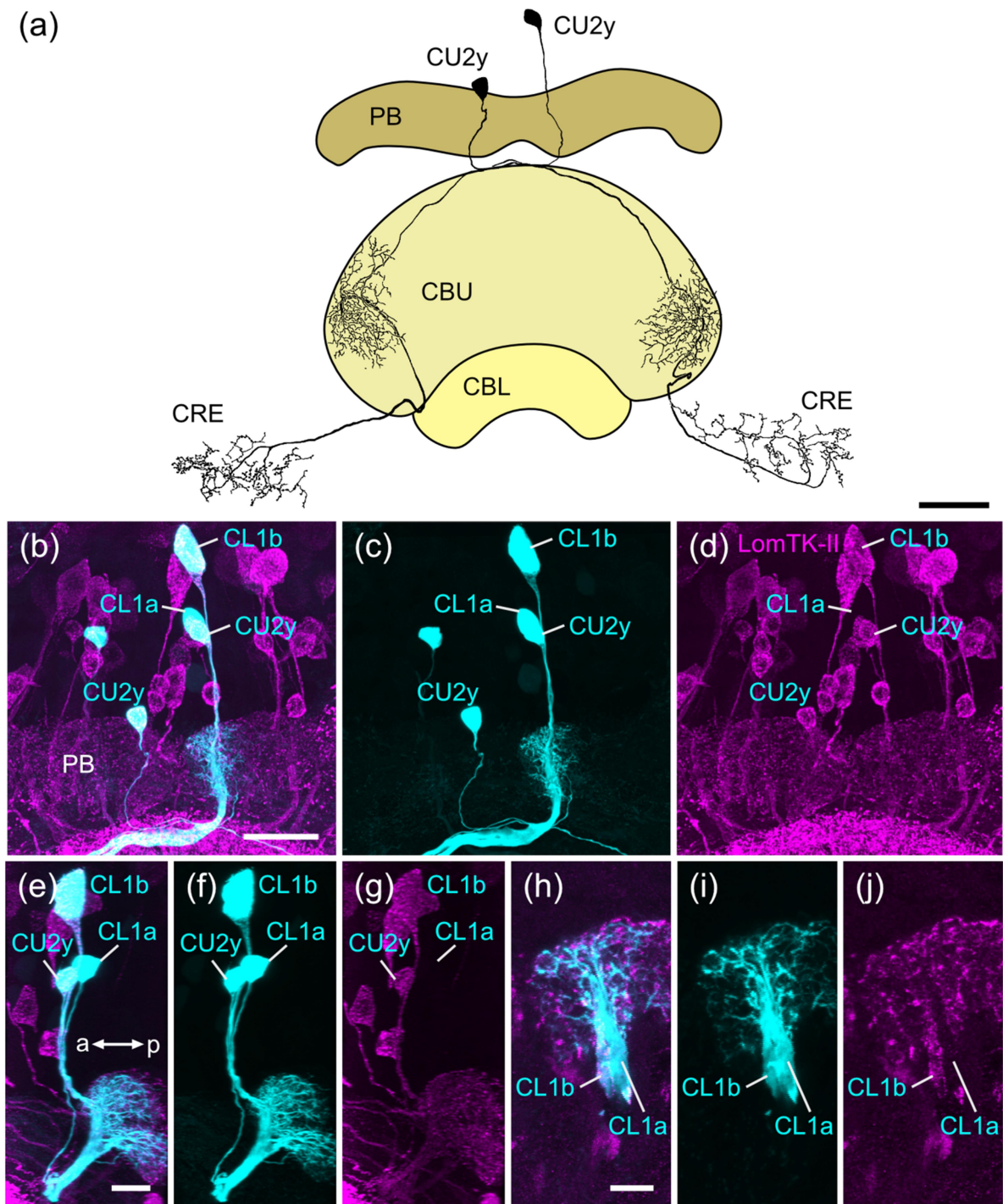


**Figure 9** Double staining of Neurobiotin-injected neurons (cyan) and locustatachykinin II (LomTK-II)-immunoreactive neurons (magenta). (a) Frontal reconstruction of two CU2y neurons shown in (b-g). (b-d) Maximum intensity projection of several optical slices showing LomTK-II staining and the injected individual cells at the level of the protocerebral bridge (PB). An intracellularly stained CL1a neuron is not labeled by the LomTK-II antiserum, whereas the somata of a CL1b neuron and of two CU2y neurons are labeled by the antiserum. (e-g). Sagittal view of the somata and arborizations shown in (a-c) illustrating that the CL1a neuron is not labeled by the LomTK-II antiserum. (h-j) Maximum intensity projection of a stack of optical slices showing LomTK-II staining at the level of the PB. The neurites of the

LomTK-II-positive CL1b neuron and the LomTK-II-negative CL1a neuron run in close proximity to one another. Scale bars = 50  $\mu\text{m}$  (a), 20  $\mu\text{m}$  (b-g), 10  $\mu\text{m}$  (h-j)

when the animal turns. In *Drosophila* two different subtypes of P-EN neurons were distinguished, P-EN\_a (P-EN1) and P-EN\_b (P-EN2). Although they appear morphologically similar, they have different synaptic partners and exhibit cell type specific activity patterns when the animal turns (Scheffer et al. 2020, Green et al., 2017; Turner-Evans et al., 2020). Recently, P-EG and P-EN\_b neurons have been shown to form a second excitatory loop that sustains the activity pattern of E-PG neurons in darkness (Turner-Evans et al., 2020). In the locust a system of 20-22 CL2 neurons expresses orcokinin A-related peptides (Homberg et al., 2020). Analysis of double label experiments with anti-Pea-MIP-1 and anti-orcokinin A antisera, however, remained inconclusive owing to crossreactivity of the antisera (data not shown). The existence of 20-24 Pea-MIP-1-positive CL2 neurons in the locust suggests correspondence rather to the 22 P-EN\_b cells than to the 20 P-EN\_a cells counted in the fly.

### **MIP-positive cells of the CBU**

The Pea-MIP-1 antiserum labeled two subsystems of columnar neurons of the CBU, CU2x (8 somata) and CU2y (up to 38 somata) neurons. Two subtypes, CU2a and CU2b, have already been described by Heinze and Homberg (2008). Based on the trajectory of their main neurites close to those of CL1 neurons and their arborizations in layer Ia of the CBU we assume that CU2y neurons correspond to CU2a neurons. However, the large number of somata (up to 38) suggests that CU2y neurons might actually correspond to two CU2 subtypes. CU2x neurons appear to be different from CU2a and CU2b neurons as their neurites run much more anteriorly along the CBU.

The large number of CU neurons and neuron types corresponds to what has been found in *Drosophila*, where ten distinct types of CU2-like cells (FC and FR neurons, 290 neurons in total) have been described (Hulse et al., 2021). FC neurons connect columns of the fan-shaped body to regions within the crepine, while FR neurons connect columns of the fan-shaped body to the rubus, a distinct, round structure at the anterior and lateral edge of the crepine (Wolff et al., 2018) that has not been identified as a distinct entity in the locust. Hence, a possible homology between CU2 neurons and FC/FR neurons remains to be resolved. Notably, all subtypes of FC- and FR cells, comprise sets of at least 16 neurons, so that neither might



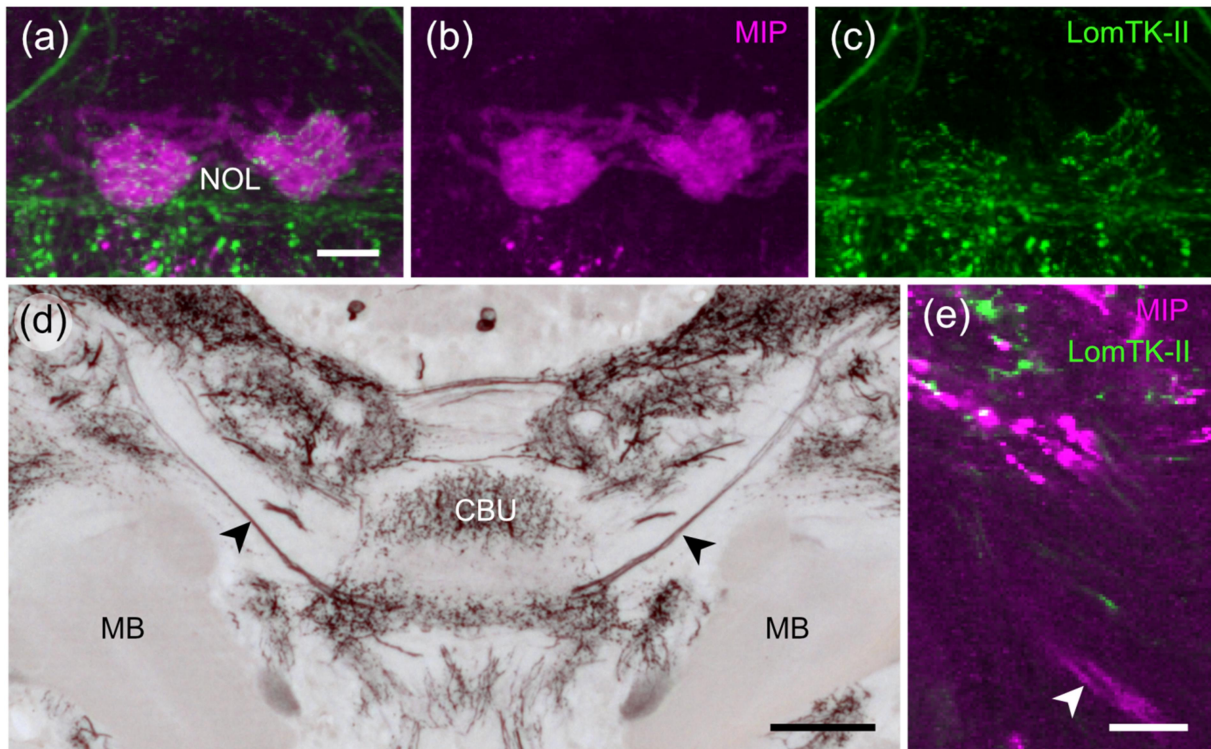


**Figure 10** Double immunofluorescent staining for myoinhibitory peptide (MIP, magenta) and locustatachykinin II (LomTK-II, green) in the noduli (NO, a-c) and anterior protocerebrum (e), and immunoperoxidase labeling of MIP in the anterior protocerebrum (d). (a-c) Maximum intensity projection of several optical slices at the level of the NO. The lower units of the NO are densely innervated by MIP-immunoreactive CL2 neurons, that are not labeled with the LomTK-II antiserum. (d) Frontal immunoperoxidase labeled section illustrating MIP-immunoreactive fibers that project via the anterior bundles toward the central body (arrowheads). Double labeling experiments show that these fibers are only labeled by the antiserum against MIP and do not show LomTK-II-immunoreactivity (e, arrowhead). Scale bars = 20  $\mu\text{m}$  (a,e), 100  $\mu\text{m}$  (d)

correspond to the relatively small number of eight MIP-immunoreactive CU2x neurons in the locust.

In addition to CU neurons, one type of tangential neuron with arborizations in layer IIb of the CBU was MIP-immunolabeled. Their neurites were first visible in the anterior bundles and enter the CBU via the ventral groove. However, owing to faint staining in these neurites and overlap with processes from other neurons, we were not able to identify the arborization regions outside the CX or their somata. So far, two types of TU neuron have been described that arborize within layer IIb of the CBU and whose neurites project along anterior bundle 2; TU<sub>SLP1</sub> and TU<sub>SLP4</sub> neurons (von Hadeln et al., 2020).

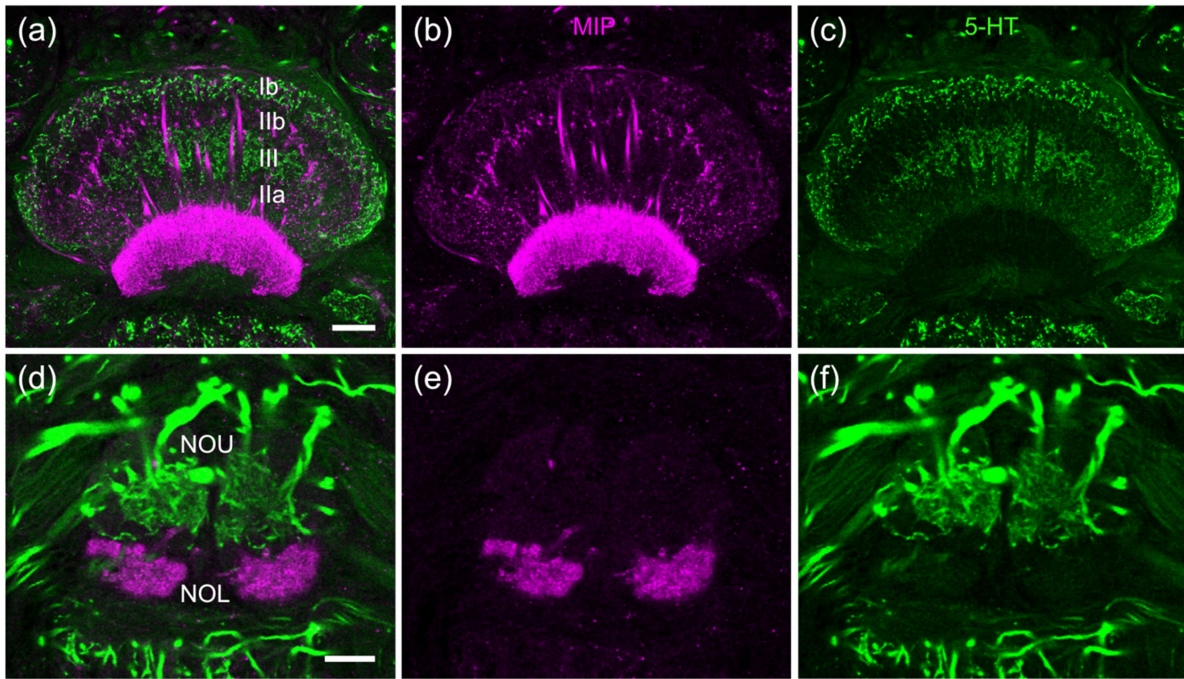


**Figure 11** Double immunofluorescent staining for myoinhibitory peptide (MIP, magenta) and serotonin (5-HT, green) in the central complex. (a-c) Several optical slices at the level of the upper (CBU) and lower division of the central body (CBL). MIP- and 5-HT immunoreactivity are not colocalized in the central body. (d-e) Several optical slices at the level of the noduli (NO). Whereas the lower units of the noduli (NOL) are densely innervated by MIP-immunoreactive fibers, 5-HT-immunoreactive processes are only present in layer II of the upper units of the NO (NOU). Scale bars = 40  $\mu\text{m}$  (a), 20  $\mu\text{m}$  (d)

### Colocalization with LomTK-II

Double label experiments revealed colocalization of LomTK-II in all MIP-positive columnar neurons, except CL2 neurons. Reconstructions of LomTK-II-positive columnar neurons revealed four cell systems, termed LTC I- IV (Vitzthum & Homberg, 1998). LTC I cells correspond to CL1b neurons, but comprise a set of 18 instead of 16 neurons reported by Vitzthum and Homberg (1998). Owing to the small size of the additional innermost PB column (column 0) and the parallel projection of the neurites of cells innervating column 1 and column 0 it is likely that the second cell was overlooked in the past. The CU2x neurons identified here suggest that the large somata of the LTC III system and the fibers and terminals of the LTC IV system are parts of the same set of CU neurons. The small cell bodies of the LTC III system likely correspond to the subset of 38 neurons that we assigned to CU2y neurons.



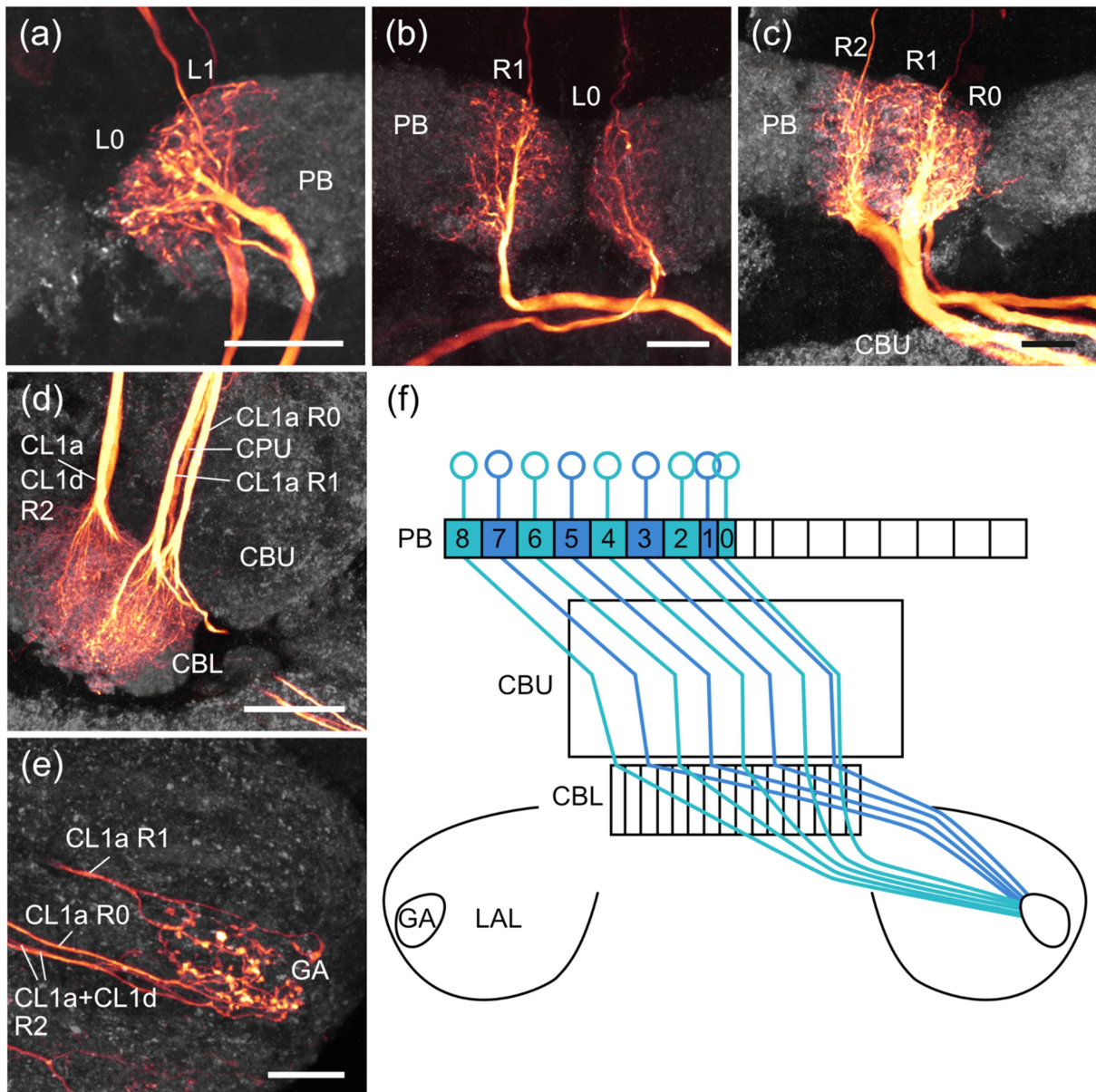


**Figure 12** Projection pattern of CL1a neurons. (a-c) Maximum intensity projections of arborization trees of several intracellularly stained CL1a neurons in the inner columns of the protocerebral bridge (PB). Synapsin staining is shown in grey. (a) Two CL1a neurons stained in the same preparation. Both arborize in the left hemisphere, but one arborizes in column 0 of the PB and the other in column 1. (b) Two CL1a neurons stained in the same preparation. They arborize in different hemispheres and occupy column R1 and column L0 of the PB. (c) Three CL1a neurons, one CL1d neuron, and one CPU neuron stained in the same preparation (see also Figure 5c-e). Two CL1 neurons, CL1a and CL1d, innervate column 2 of the right PB, whereas one CL1a neuron innervates column 1 and another CL1a neuron innervates column R0. (d) Maximum intensity projection of arborizations of the neurons shown in (c) in the lower division of the central body (CBL). The two CL1 neurons from PB column R2 occupy similar regions within the CBL, whereas the CL1a neurons from column R1 and R0 enter the CBL with a slight offset. (e) Maximum intensity projection of arborizations of the neurons shown in (c,d) in the gall (GA). CL1 neurons from even numbered PB columns (2 and 0) project ventrally into the GA, whereas the CL1 neuron from column 1 projects dorsally

into the GA. (f) Putative connectivity scheme of CL1a neurons. CL1a neurons that innervate even-numbered columns of the PB project more ventrally and posteriorly via the isthmus tracts toward the GA than CL1a neurons of odd-numbered PB columns. The innermost column of the PB consists of two hemicolumns. Scale bars = 30  $\mu\text{m}$  (a), 20  $\mu\text{m}$  b,d,e, 40  $\mu\text{m}$ . (f) Modified from Heinze and Homberg (2008)

### **MIPs in the central complex of other insects**

MIP-positive processes in the CX have been reported for *L. migratoria* (Schoofs et al., 1996), *L. maderae* (Schulze et al., 2012), and *D. melanogaster* (Kahsai & Winther, 2011). Lom-MIP-immunoreactivity in the migratory locust is highly similar to MIP immunolabeling in *S. gregaria*, with staining in all subunits of the CX, including the PB, the CBU, the CBL, and the NO. Despite these similarities, Schoofs et al. (1996) reported much lower numbers of immunostained somata, likely because they used relatively insensitive paraffin histology for MIP immunolabeling (Schoof et al. 1996). In the cockroach, Pea-MIP-1-positive fibers innervate the PB, the CBU and the CBL. However, staining in the CBL is only sparse. Cell types that contribute to the staining are tangential neurons of the PB (TB neurons), TU neurons, and CU neurons. Whereas we did not find Pea-MIP-1-positive TB neurons in the locust, the morphology of the MIP-positive CU neurons in both species appears similar. Considering the high number of MIP-positive CU neurons in the cockroach (2 x 16) they might correspond to CU2y neurons rather than CU2x neurons. However, whether these cell types are, indeed, homologous or only express related neuropeptides remains to be resolved. Interestingly, similar to the difficulties in identifying the MIP-positive TU neuron type in the locust, a MIP-positive TU neuron type was also not fully traceable in the cockroach. Except for the innervation in the CBU and the projection via the anterior bundles the morphology of this type of neuron remains uncertain in both insects. MIP immunoreactivity in the *Drosophila* CX was confined to several layers in the fan-shaped body, whereas no MIP immunoreactivity has been reported for the other subunits. The cellular identity of the immunolabeled neurons has not been revealed (Kahsai & Winther, 2010).

### **MIP function in the CX**

The presence of MIPs in several types of CX neurons suggests that these neuropeptides are involved in the modulation of computational processes within the CX network. The expression of MIPs by CL1b and CL2 neurons that are elements of the sky compass in several



insects and of the head direction system in *Drosophila* indicates a role of MIPs in spatial orientation and navigation. Whether MIPs have a direct function linked to the performance of the network or play a modulatory role dependent on different internal states of the animal remains to be resolved. MIP immunostaining of CU neurons might again point to a similar role. Homologs of CU subtypes in *Drosophila* (FC neurons) are likely elements of the orientation network, judged by their synaptic connections (Hulse et al., 2021), but are thought to function in circuits closer to the motor output. With the complete lack of functional studies on CU neurons in the locust as well as FC and FR cells in *Drosophila*, however, our understanding of their functions is still very limited. If, as in *Drosophila*, the central body is also involved in sleep control in the locust, a function in modulating sleep homeostasis is also possible, considering that MIPs are expressed not only in several CU subtypes but also in one type of TU neuron.

## References

- Blackburn, M. B., Wagner, R. M., Kochansky, J. P., Harrison, D. J., Thomas-Laemont, P., & Raina, A. K. (1995). The identification of two myoinhibitory peptides, with sequence similarities to the galanins, isolated from the ventral nerve cord of *Manduca sexta*. *Regulatory Peptides*, *57*(3), 213-219. [https://doi.org/10.1016/0167-0115\(95\)00034-9](https://doi.org/10.1016/0167-0115(95)00034-9)
- Donlea, J. M., Pimentel, D., Talbot, C. B., Kempf, A., Omoto, J. J., Hartenstein, V. & Miesenböck, G. (2018). Recurrent circuitry for balancing sleep need and sleep. *Neuron*, *97*(2), 378-389.e4. <https://doi.org/10.1016/j.neuron.2017.12.016>
- el Jundi, B., Warrant, E. J., Pfeiffer, K., & Dacke, M. (2018). Neuroarchitecture of the dung beetle central complex. *Journal of Comparative Neurology*, *526*(16), 2612–2630. <https://doi.org/10.1002/cne.24520>
- Franconville, R., Beron, C., & Jayaraman, V. (2018). Building a functional connectome of the *Drosophila* central complex. *eLife*, *7*, e37017. <https://doi.org/10.7554/eLife.37017>
- Green, J., Adachi, A., Shah, K. K., Hirokawa, J. D., Magani, P. S., & Maimon, G. (2017). A neural circuit architecture for angular integration in *Drosophila*. *Nature*, *546*(7656), 101–106. <https://doi.org/10.1038/nature22343>
- Heinze, S., & Homberg, U. (2008). Neuroarchitecture of the central complex of the desert locust: Intrinsic and columnar neurons. *Journal of Comparative Neurology*, *511*(4), 454–478. <https://doi.org/10.1002/cne.21842>
- Heinze, S., & Homberg, U. (2009). Linking the input to the output: new sets of neurons complement the polarization vision network in the locust central complex. *Journal of Neuroscience*, *29*(15), 4911–4921. <https://doi.org/10.1523>

- Homberg, U., Humberg, T. H., Seyfarth, J., Bode, K., & Quintero Pérez, M. (2018). GABA immunostaining in the central complex of dicondylarian insects. *Journal of Comparative Neurology*, *526*(14), 2301–2318. <https://doi.org/10.1002/cne.24497>
- Homberg, U., Hensgen, R., Rieber, E., Seyfarth, J., Kern, M., Dippel, S., Dirksen, H., Spänig, L., & Kina, Y. P. (2021). Orcokinin in the central complex of the locust *Schistocerca gregaria*: identification of immunostained neurons and colocalization with other neuroactive substances. *Journal of Comparative Neurology*, *529*, 1876-1894. <https://doi.org/10.1002/cne.25062>
- Hou, L., Jiang, F., Yang, P., Wang, X., & Kang, L. (2015). Molecular characterization and expression profiles of neuropeptide precursors in the migratory locust. *Insect Biochemistry and Molecular Biology*, *63*, 63-71. <https://doi.org/10.1016/j.ibmb.2015.05.014>
- Hua Y. J., Tanaka, Y., Nakamura, K., Sakakibara, M., Nagata, S., & Kataoka, H. (1999). Identification of a prothoracicostatic peptide in the larval brain of the silkworm, *Bombyx mori*. *Journal of Biological Chemistry*, *274*(44), 31169-31173. <https://doi.org/10.1074/jbc.274.44.31169>
- Hulse, B. K., Haberkern, H., Franconville, R., Turner-Evans, D. B., Takemura, S. Y., Wolff, T., Noorman, M., Dreher, M., Dan, C., Parekh, R., Hermundstad, A. M., Rubin, G. M. & Jayaraman, V. (2021). A connectome of the *Drosophila* central complex reveals network motifs suitable for flexible navigation and context-dependent action selection. *eLife*, *10*, e66039. Advance online publication. <https://doi.org/10.7554/eLife.66039>
- Jang, Y. H., Chae, H., & Kim, Y. J. (2017). Female-specific myoinhibitory peptide neurons regulate mating receptivity in *Drosophila melanogaster*. *Nature Communications*, *8*(1), 1630. <https://doi.org/10.1038/s41467-017-01794-9>
- Kahsai, L., & Winther, A. M. (2011). Chemical neuroanatomy of the *Drosophila* central complex: distribution of multiple neuropeptides in relation to neurotransmitters. *Journal of Comparative Neurology*, *519*(2), 290-315. <https://doi.org/10.1002/cne.22520>
- Klagges, B. R., Heimbeck, G., Godenschwege, T. A., Hofbauer, A., Pflugfelder, G. O., Reifegerste, R., Reisch, G., Schaupp, M., Buchner, S. & Buchner, E. (1996). Invertebrate synapsins: A single gene codes for several isoforms in *Drosophila*. *Journal of Neuroscience*, *16*(10), 3154-3165. <https://doi.org/10.1523/JNEUROSCI.16-10-03154.1996>
- Kolodziejczyk, A., & Nässel, D. R. (2011a). A novel wide-field neuron with branches in the lamina of the *Drosophila* visual system expresses myoinhibitory peptide and may be associated with the clock. *Cell and Tissue Research*, *343*(2), 357-369. <https://doi.org/10.1007/s00441-010-1100-7>
- Kolodziejczyk, A., & Nässel, D. R. (2011b). Myoinhibitory peptide (MIP) immunoreactivity in the visual system of the blowfly *Calliphora vomitoria* in relation to putative clock neurons and serotonergic neurons. *Cell and Tissue Research*, *345*(1), 125-135. <https://doi.org/10.1007/s00441-011-1198-2>

- Kunst, M., Pförtner, R., Aschenbrenner, K., & Heinrich, R. (2011). Neurochemical architecture of the central complex related to its function in the control of grasshopper acoustic communication. *PloS one*, 6(9), e25613. <https://doi.org/10.1371/journal.pone.0025613>
- Lorenz, M. W., Kellner, R., & Hoffmann, K. H. (1995). A family of neuropeptides that inhibit juvenile hormone biosynthesis in the cricket, *Gryllus bimaculatus*. *Journal of Biological Chemistry*, 270(36), 21103-21108. <https://doi.org/10.1074/jbc.270.36.21103>
- NCBI Resource Coordinators (2016). Database resources of the National Center for Biotechnology Information. *Nucleic Acids Research*, 44(D1), D7-D19. <https://doi.org/10.1093/nar/gkv1290>
- Oh, Y., Yoon, S. E., Zhang, Q., Chae, H. S., Daubnerová, I., Shafer, O. T., Choe, J., & Kim, Y. J. (2014). A homeostatic sleep-stabilizing pathway in *Drosophila* composed of the sex peptide receptor and its ligand, the myoinhibitory peptide. *PLoS Biology*, 12(10), e1001974. <https://doi.org/10.1371/journal.pbio.1001974>
- Pegel, U., Pfeiffer, K., & Homberg, U. (2018). Integration of celestial compass cues in the central complex of the locust brain. *Journal of Experimental Biology*, 221, jeb171207. <https://doi.org/10.1242/jeb.171207>
- Peterson, T. N., Brunak, S., von Heijne, G., & Nielsen, H. (2011). SignalP 4.0: discriminating signal peptides from transmembrane regions. *Nature Methods*, 8(10), 785-786. <https://doi.org/10.1038/nmeth.1701>
- Pfeiffer, K., & Homberg, U. (2014). Organization and functional roles of the central complex in the insect brain. *Annual Review of Entomology*, 59, 165-184. <https://doi.org/10.1146/annurev-ento-011613-16203>
- Pisokas, I., Heinze, S., & Webb, B. (2020). The head direction circuit of two insect species. *eLife*, 9, e53985. <https://doi.org/10.7554/eLife.53985>
- Poels, J., Van Loy, T., Vandersmissen, H. P., Van Hiel, B., Van Soest, S., Nachman, R. J., & Vanden Broeck, J. (2010). Myoinhibiting peptides are the ancestral ligands of the promiscuous *Drosophila* sex peptide receptor. *Cellular and Molecular Life Sciences*, 67(20), 3511-3522. <https://doi.org/10.1007/s00018-010-0393-8>
- Predel, R., Rapus, J., & Eckert, M. (2001). Myoinhibitory neuropeptides in the American cockroach. *Peptides*, 22(2), 199-208. [https://doi.org/10.1016/S0196-9781\(00\)00383-1](https://doi.org/10.1016/S0196-9781(00)00383-1)
- Sayre, M. E., Templin, R., Chavez, J., Kempnaers, J., & Heinze, S. (2021). A projectome of the bumblebee central complex. *eLife*, 10, e68911. <https://doi.org/10.7554/eLife.68911>
- Seelig, J. D., & Jayaraman, V. (2015). Neural dynamics for landmark orientation and angular path integration. *Nature*, 521(7551), 186-191. <https://doi.org/10.1038/nature14446>
- Scheffer, L. K., Xu, C. S., Januszewski, M., Lu, Z., Takemura, S. Y., Hayworth, K. J., Huang, G. B., Shinomiya, K., Maitlin-Shepard, J., Berg, S., Clements, J., Hubbard, P. M., Katz, W. T., Umayam, L., Zhao, T., Ackerman, D., Blakely, T., Bogovic, J., Dolafi, T., Kainmueller,

- D., ... Plaza, S. M. (2020). A connectome and analysis of the adult *Drosophila* central brain. *eLife*, 9, e57443. <https://doi.org/10.7554/eLife.57443>
- Schoofs, L., Holman, G. M., Hayes, T. K., Nachman, R. J., & De Loof, A. (1991). Isolation, identification and synthesis of locustamyoinhibiting peptide (LOM-MIP), a novel biologically active neuropeptide from *Locusta migratoria*. *Regulatory Peptides*, 36(1), 111-119. [https://doi.org/10.1016/0167-0115\(91\)90199-q](https://doi.org/10.1016/0167-0115(91)90199-q)
- Schoofs, L., Veelaert, D., Broeck, J. V., & De Loof, A. (1996). Immunocytochemical distribution of locustamyoinhibiting peptide (Lom-MIP) in the nervous system of *Locusta migratoria*. *Regulatory Peptides*, 63(2-3), 171-179. [https://doi.org/10.1016/0167-0115\(96\)00040-7](https://doi.org/10.1016/0167-0115(96)00040-7)
- Schulze, J., Neupert, S., Schmidt, L., Predel, R., Lamkemeyer, T., Homberg, U., & Stengl, M. (2012). Myoinhibitory peptides in the brain of the cockroach *Leucophaea maderae* and colocalization with pigment-dispersing factor in circadian pacemaker cells. *Journal of Comparative Neurology*, 520(5), 1078–1097. <https://doi.org/10.1002/cne.22785>
- Turner-Evans, D., Wegener, S., Rouault, H., Franconville, R., Wolff, T., Seelig, J. D., Druckmann, S., & Jayaraman, V. (2017). Angular velocity integration in a fly heading circuit. *eLife*, 6, e23496. <https://doi.org/10.7554/eLife.23496>
- Turner-Evans, D. B., Jensen, K. T., Ali, S., Paterson, T., Sheridan, A., Ray, R. P., Wolff, T., Lauritzen, J. S., Rubin, G. M., Bock, D. D., & Jayaraman, V. (2020). The neuroanatomical ultrastructure and function of a biological ring attractor. *Neuron*, 108(1), 145–163.e10. <https://doi.org/10.1016/j.neuron.2020.08.006>
- Verlinden, H., Sterck, L., Li, J., Li, Z., Yssel, A., Gansemans, Y., Verdonck, R., Holtof, M., Song, H., Behmer, S. T., Sword, G. A., Matheson, T., Ott, S. R., Deforce, D., Van Nieuwerburgh, F., Van de Peer, Y., & Vanden Broeck, J. (2020). First draft genome assembly of the desert locust *Schistocerca gregaria*. *F1000Research*, 9, 775. <https://doi.org/10.12688/f1000research.25148.2>
- Vitzthum, H., & Homberg, U. (1998). Immunocytochemical demonstration of locustatachykinin-related peptides in the central complex of the locust brain. *Journal of Comparative Neurology*, 390(4), 455-469. [https://doi.org/10.1002/\(sici\)1096-9861\(19980126\)390:4<455::aid-cne1>3.0.co;2-#](https://doi.org/10.1002/(sici)1096-9861(19980126)390:4<455::aid-cne1>3.0.co;2-#)
- Williams, J. L. D. (1975). Anatomical studies of the insect central nervous system: a ground-plan of the midbrain and an introduction to the central complex in the locust, *Schistocerca gregaria* (Orthoptera). *Journal of Zoology*, 176(1), 67-86. <https://doi.org/10.1111/j.1469-7998.1975.tb03188.x>
- Williamson, M., Lenz, C., Winther, A. M., Nässel, D. R., & Grimmelikhuijzen, C. J. (2001). Molecular cloning, genomic organization, and expression of a C-type (*Manduca sexta*-type) allatostatin preprohormone from *Drosophila melanogaster*. *Biochemical and Biophysical Research Communications*, 282(1), 124-130. <https://doi.org/10.1006/bbrc.2001.4565>

- Wolff, T., Iyer, N. A., & Rubin, G. M. (2015). Neuroarchitecture and neuroanatomy of the *Drosophila* central complex: A GAL4-based dissection of protocerebral bridge neurons and circuits. *Journal of Comparative Neurology*, 523(7), 997–1037. <https://doi.org/10.1002/cne.23705>
- Wolff, T., & Rubin, G. M. (2018). Neuroarchitecture of the *Drosophila* central complex: A catalog of nodulus and asymmetrical body neurons and a revision of the protocerebral bridge catalog. *Journal of Comparative Neurology*, 526(16), 2585–2611. <https://doi.org/10.1002/cne.24512>
- Yamanaka, N., Hua, Y. J., Roller, L., Spalovská-Valachová, I., Mizoguchi, A., Kataoka, H., & Tanaka, Y. (2010). *Bombyx* prothoracicostatic peptides activate the sex peptide receptor to regulate ecdysteroid biosynthesis. *Proceedings of the National Academy of Sciences of the United States of America*, 107(5), 2060-2065. <https://doi.org/10.1073/pnas.0907471107>



## **Chapter III**

Organization and neural connections of the lateral complex in the brain of the desert locust





## RESEARCH ARTICLE



WILEY

# Organization and neural connections of the lateral complex in the brain of the desert locust

Ronja Hensgen<sup>1</sup> | Jonas Göthe<sup>1</sup> | Stefanie Jahn<sup>1</sup> | Sophie Hümmert<sup>1</sup> |  
 Kim Lucia Schneider<sup>1</sup> | Naomi Takahashi<sup>1</sup> | Uta Pegel<sup>1</sup> | Sascha Gotthardt<sup>1</sup> |  
 Uwe Homberg<sup>1,2</sup>

<sup>1</sup>Department of Biology, Animal Physiology, Philipps-Universität Marburg, Marburg, Germany

<sup>2</sup>Center for Mind, Brain and Behavior (CMBB), University of Marburg and Justus Liebig University Giessen, Marburg, Germany

## Correspondence

Uwe Homberg, Fachbereich Biologie, Tierphysiologie, Philipps-Universität Marburg, D-35032 Marburg, Germany.  
 Email: homberg@staff.uni-marburg.de

## Funding information

Deutsche Forschungsgemeinschaft, Grant/Award Numbers: HO 950/26-1, HO 950/28-1

## Abstract

The lateral complexes (LXs) are bilaterally paired neuropils in the insect brain that mediate communication between the central complex (CX), a brain center controlling spatial orientation, various sensory processing areas, and thoracic motor centers that execute locomotion. The LX of the desert locust consists of the lateral accessory lobe (LAL), and the medial and lateral bulb. We have analyzed the anatomical organization and the neuronal connections of the LX in the locust, to provide a basis for future functional studies. Reanalyzing the morphology of neurons connecting the CX and the LX revealed likely feedback loops in the sky compass network of the CX via connections in the gall of the LAL and a newly identified neuropil termed ovoid body. In addition, we characterized 16 different types of neuron that connect the LAL with other areas in the brain. Eight types of neuron provide information flow between both LALs, five types are LAL input neurons, and three types are LAL output neurons. Among these are neurons providing input from sensory brain areas such as the lobula and antennal neuropils. Brain regions most often targeted by LAL neurons are the posterior slope, the wedge, and the crepine. Two descending neurons with dendrites in the LAL were identified. Our data support and complement existing knowledge about how the LAL is embedded in the neuronal network involved in processing of sensory information and generation of appropriate behavioral output for goal-directed locomotion.

## KEYWORDS

central complex, head direction, insect brain, neuroanatomy, RRID: AB\_2340415, RRID: AB\_2315017, RRID: AB\_2315425, RRID: AB\_2337244, RRID: AB\_2338021, RRID: AB\_2338713, RRID: AB\_2340411, RRID: AB\_2340607, RRID: AB\_2340612, RRID: AB\_572262, RRID: SCR\_007353, RRID: SCR\_016951, RRID: SCR\_016952, spatial orientation

**Abbreviations:** aLALC, anterior lateral accessory lobe commissure; AVLP, anterior ventrolateral protocerebrum; CBL, lower division of the central body; CBU, upper division of the central body; CRE, crepine; CX, central complex; GA, gall; IT, isthmus tract; LAL, lateral accessory lobe; LALC, LAL commissure; LBU, lateral bulb; LLAL, lower LAL; LOX, lobula complex; LX, lateral complex; MAL, medial accessory lobe; MALT, medial antennal lobe tract; MBU, medial bulb; NO, noduli; OB, ovoid body; PB, protocerebral bridge; PS, posterior slope; PVLP, posterior ventrolateral protocerebrum; SIP, superior intermediate protocerebrum; SMP, superior medial protocerebrum; ULAL, upper LAL.

This is an open access article under the terms of the Creative Commons Attribution-NonCommercial License, which permits use, distribution and reproduction in any medium, provided the original work is properly cited and is not used for commercial purposes.

© 2021 The Authors. *The Journal of Comparative Neurology* published by Wiley Periodicals LLC.

## 1 | INTRODUCTION

All animals interact with their environment to survive and reproduce; they have to find food, avoid predators and unfavorable conditions, and need to find mating partners. An important prerequisite for survival is the ability for spatial orientation. Animals not only need to have a sense of where they are in relation to a goal or threat, they also need to be able to approach or to avoid it. These tasks require processing and integration of external cues, like landmarks, odors, and sounds, but also internal and self-generated cues, such as proprioceptive feedback and movement-related sensory flow, in order to generate and execute appropriate behavioral responses.

Studying the underlying neural mechanisms of spatial orientation in insects revealed that a particular brain area, the central complex (CX) plays an important role in spatial orientation and navigation. The CX is composed of the protocerebral bridge (PB), the upper division of the central body (CBU, also termed fan-shaped body), the lower division of the central body (CBL, also termed ellipsoid body), and a pair of globular-shaped noduli (NO). Neurons of the CX receive a multitude of navigation-related sensory input (Honkanen et al., 2019; Pfeiffer & Homberg, 2014) including sky compass signals (el Jundi et al., 2019; Heinze & Reppert, 2012; Pegel et al., 2018; Zittrell et al., 2020), optic flow information (Rosner et al., 2019; Stone et al., 2017), object and visual panorama information (Seelig & Jayaraman, 2013, 2015; Rosner & Homberg, 2013; Bockhorst & Homberg, 2017; Kim et al., 2019), wind direction information (Currier et al., 2020; Okubo et al., 2020), but also internally generated signals on the animal's angular velocity (Green et al., 2019; Shiozaki et al., 2020; Turner-Evans et al., 2017). A role of the CX in directing locomotor activity has been demonstrated in the fly *Drosophila melanogaster* (Strauss, 2002; Triphan et al., 2010) and the cockroach *Blaberus discoidalis* (Bender et al., 2010; Martin et al., 2015).

Communication of the CX with other brain areas largely occurs via the lateral complex (LX), a brain area adjacent to the CX. The LX consists of the lateral accessory lobe (LAL) and the bulb (Ito et al., 2014). In many species both areas are further subdivided, the LAL into upper LAL (ULAL) and lower LAL (LLAL), separated by the LAL commissure, and the gall (GA), the bulb into two (locust, honeybee) or three subdivisions (fly) (Held et al., 2016; Ito et al., 2014; Namiki & Kanzaki, 2016). Large numbers of neurons provide bidirectional connections between the LX and the CX (desert locust *Schistocerca gregaria*: Heinze & Homberg, 2008; von Hadeln et al., 2020; monarch butterfly *Danaus plexippus*: Heinze et al., 2013; dung beetles: el Jundi et al., 2018; *D. melanogaster*: Wolff & Rubin, 2018; Omoto et al., 2018; Hulse et al., 2020; honey bee *Apis mellifera*: Hensgen et al., 2021). Several of these cell types participate in aspects of spatial navigation and goal-directed behavior, like sky-compass orientation in locusts (Heinze & Homberg, 2007; Pegel et al., 2019; Zittrell et al., 2020), optic-flow based speed-encoding in the sweat bee *Megalopta genalis* (Stone et al., 2017), head-direction coding, angular orientation, and visual place learning in *Drosophila* (Ofstad et al., 2011; Seelig & Jayaraman, 2015; Turner-Evans et al., 2017).

Whereas tangential neurons have largely dendritic ramifications in the LX and thus provide input to the CX, columnar neurons with dendrites in single columns of the CX send axonal outputs to the LX (Heinze & Homberg, 2008; Hensgen et al., 2021; Hulse et al., 2020; von Hadeln et al., 2020). Numerous types of neuron mediate output from the LX to other brain areas or to the ventral nerve cord and play a role in locomotor control, such as walking in flies (Rayshubskiy et al., 2020), flight in locusts (Homberg, 1994), pheromone orientation in silk moths (Iwano et al., 2010; Namiki et al., 2014), obstacle negotiation in cockroaches (Harley & Ritzmann, 2010), or phonotactic steering in crickets (Zorović & Hedwig, 2013) as reviewed by Namiki and Kanzaki (2016) and Steinbeck et al. (2020). Based on data from the silk moth, Namiki and Kanzaki (2016) have proposed a role for the ULAL in largely integrating various inputs while the LLAL largely mediates output via descending neurons.

To further understand the functional organization of the LX in the insect brain, we have analyzed arborization patterns and projections of individually labeled LX neurons in the desert locust. Overlap of branching areas of tangential and columnar neurons of the CX in the LX suggest that feedback loops exist between outputs and inputs of the CX. In addition, we describe cell types of the LAL that are suited to provide novel sensory input to the CX and help to unravel the information flow within the LAL and between the LAL and other brain areas.

## 2 | MATERIALS AND METHODS

### 2.1 | Animals

Adult gregarious male and female desert locusts (*S. gregaria*) were obtained from crowded colonies reared at Philipps-University of Marburg. Animals were kept at constant temperature of 28°C on a 12:12 h light/dark cycle.

### 2.2 | Preparation and Neurobiotin injections

Animals were cold-anesthetized at 4°C for 10–20 min. Legs and wings were cut off, and animals were mounted onto a metal holder in an upright position using dental wax. The head capsule was opened from anterior. Fat tissue and tracheal air sacs were removed to expose the brain. The gut was removed to reduce body movement. A wire loop was inserted into the head capsule to support the brain from posterior. The neural sheath was removed from the central brain to allow access of the electrode. During preparation and injection, the brain was immersed in locust saline (Clements & May, 1974). Intracellular Neurobiotin injections were performed with sharp glass microelectrodes drawn from borosilicate capillaries (Hilgenberg, Malsfeld, Germany) using a Flaming/Brown horizontal puller (P-97; Sutter Instrument, Novato, CA). The tips of the electrodes were loaded with 4% Neurobiotin (Vector Laboratories, Burlingame, CA) diluted in 1 mol l<sup>-1</sup> KCl and the shanks were filled with 1 mol l<sup>-1</sup> KCl. By applying a positive current of ~1 nA for 1–5 min

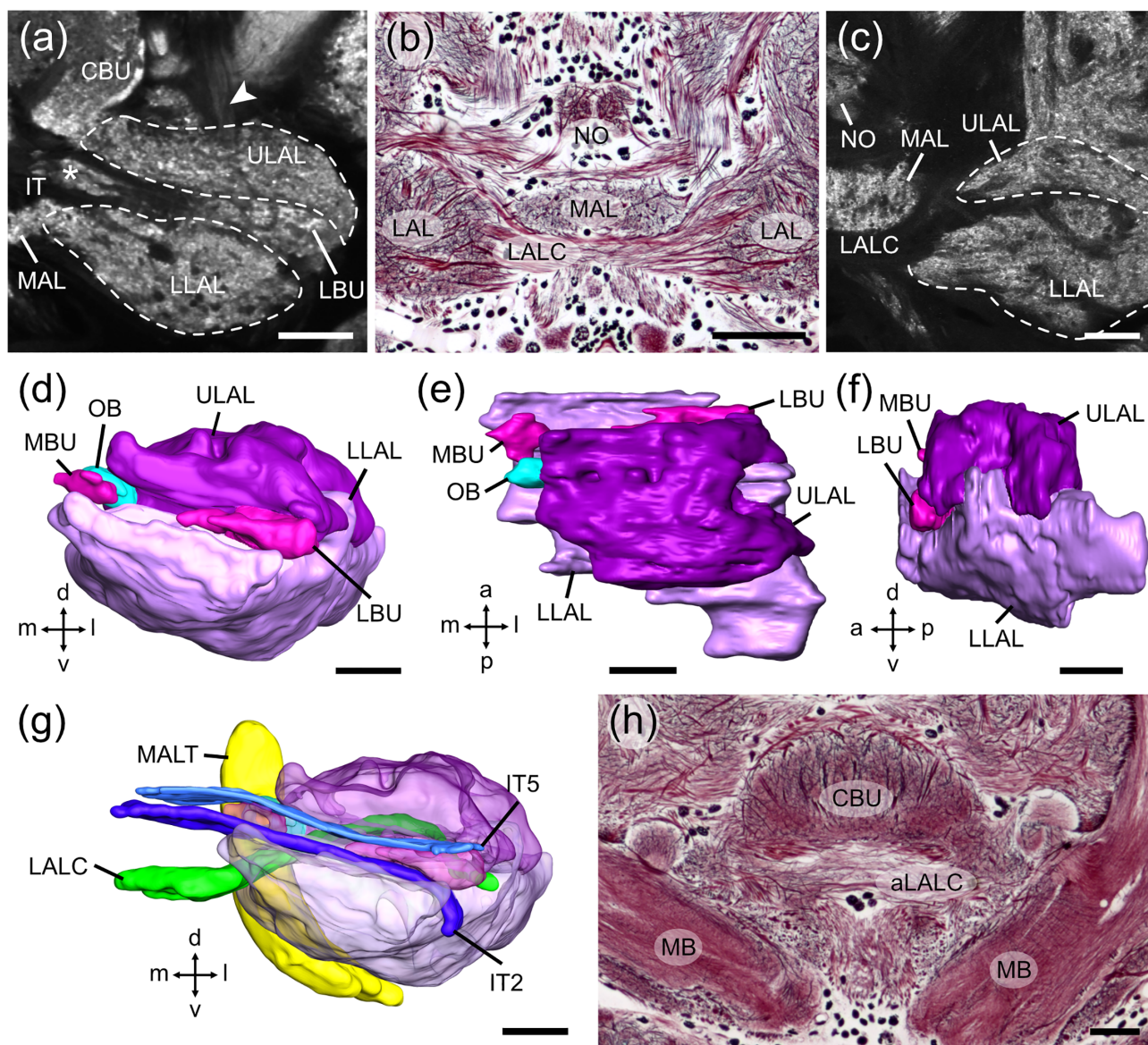


**FIGURE 1** Organization of the lateral complex in the brain of the desert locust. (a) Optical slice showing synapsin immunoreactivity in the central body and the lateral complex. Asterisk indicates the medial bulb. (b) Frontal Bodian-stained paraffin section showing the noduli (NO) and the lateral accessory lobe commissure (LALC) connecting the lateral accessory lobes (LAL) of both hemispheres. (c) Optical slice showing synapsin immunoreactivity in the upper LAL (ULAL) and the lower LAL (LLAL) of one hemisphere. (d–f) 3D-reconstruction of the ULAL and the LLAL, the medial bulb (MBU), the lateral bulb (LBU), and the ovoid body (OB) of the lateral complex of one hemisphere. Frontal view (d), horizontal view (e), and sagittal view (f). (g) 3D-reconstruction of the ULAL, LLAL, MBU and LBU as shown in (d–f) together with parts of the medial antenna lobe tract (MALT), the LALC, and the isthmus tracts 2 and 5 (IT2, IT5). (h) Bodian staining showing the anterior LAL commissure (aLALC) anterior to the lower division of the central body. a, anterior; CBU, upper division of the central body; d, dorsal; l, lateral; m, medial; MAL, medial accessory lobe; MB, mushroom body; p, posterior; v, ventral. Scale bars = 50  $\mu\text{m}$  (a, c, h), 100  $\mu\text{m}$  (b) [Color figure can be viewed at [wileyonlinelibrary.com](http://wileyonlinelibrary.com)]

Neurobiotin was injected into a neuron. In some experiments, Neurobiotin was injected after performing intracellular recordings as described in Pegel et al. (2018) and Pfeiffer et al. (2005). After injections brains were dissected in locust saline and incubated overnight at 4°C in a fixative solution containing 4% paraformaldehyde (Sigma-Aldrich, Steinheim, Germany), 0.25% glutaraldehyde (Carl Roth, Karlsruhe, Germany), and 0.25% saturated picric acid in 0.1 mol l<sup>-1</sup> phosphate-buffered saline (PBS).

Labeling of neurons shown in Figure 10d–g was achieved by electroporation of Neurobiotin (as described in Held et al., 2016 and Hensgen et al., 2021). Briefly, instead of penetrating an individual cell, the microelectrode was positioned in the LAL and a pulsed current of 10 nA (1 Hz, 50% duty cycle) was applied for 20–45 min. Besides ejecting the tracer from the electrode, the electroporating effect of the electric field facilitated the entrance of the tracer into nearby neurons.



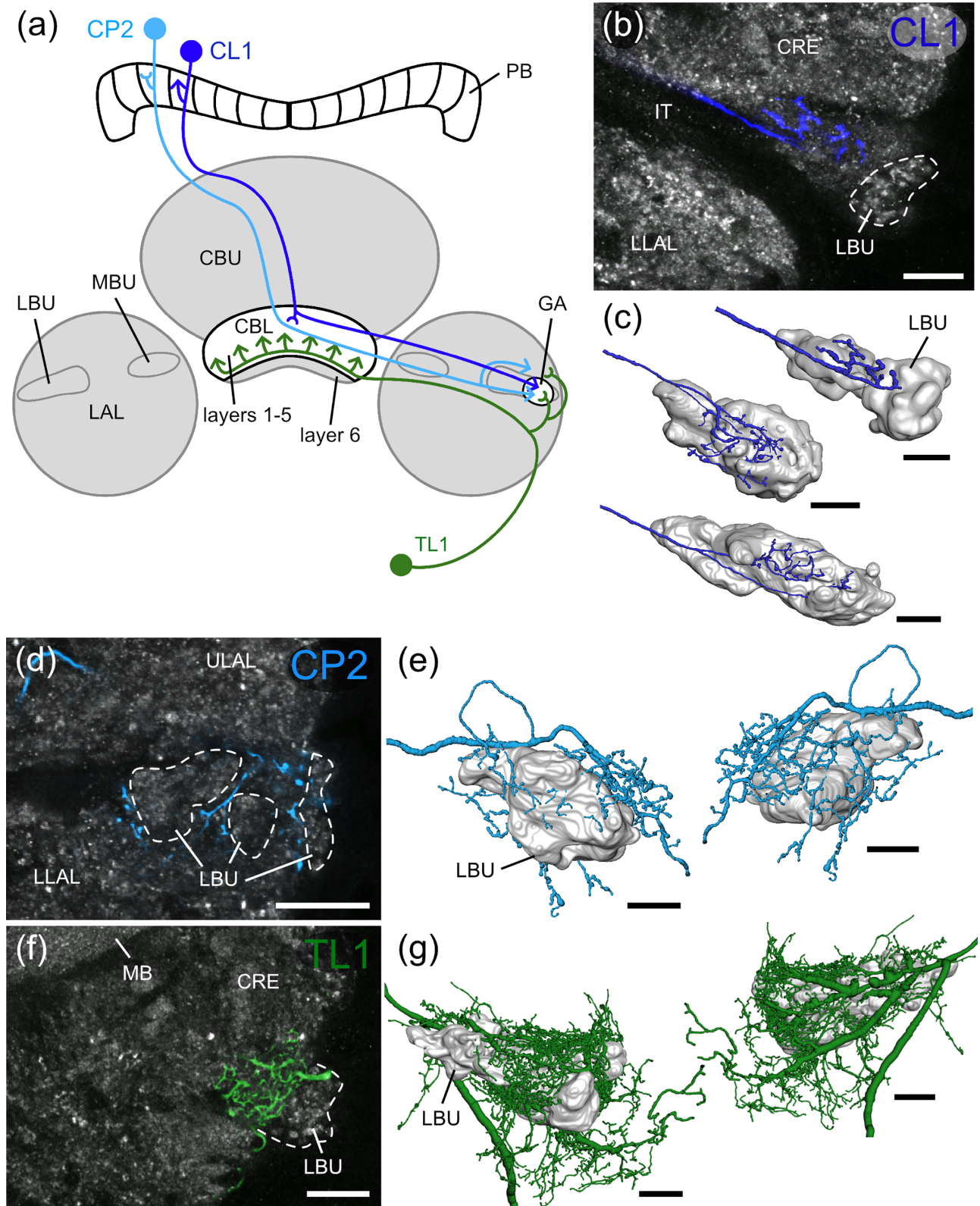


FIGURE 2 Legend on next page.

## 2.3 | Fluorescence labeling of Neurobiotin injected brains

Fixed brains were rinsed with 0.1 mol l<sup>-1</sup> PBS and incubated with Cy3-conjugated streptavidin (1:1000, Jackson ImmunoResearch, RRID: AB\_2337244) in 0.1 mol l<sup>-1</sup> PBT (PBS with 0.3% Triton X-100 [TrX; Sigma, Deisenhofen, Germany]) for 2–3 days at 4°C in the dark. Following thorough rinses in PBT and PBS, brains were dehydrated in an ascending ethanol series (30%, 50%, 70%, 90%, 95%, and 100% ethanol, 15 min each) and cleared in a 1:1 mixture of 100% ethanol and methyl salicylate for 15 min, followed by 100% methyl salicylate for 30 min. Finally, brains were mounted in Permount (Fisher Scientific, Pittsburgh, PA) between two coverslips using reinforcement rings to avoid compression. Fluorescently labeled neurons are shown in Figures 2–4, 5d–f, 6, 8d–f, 9, 10a–c, and 12–15.

## 2.4 | Peroxidase labeling of Neurobiotin injected brains

The protocol for peroxidase labeling of Neurobiotin-injected brains followed the methods described in Vitzthum et al. (2002). In brief, fixed brains were rinsed, embedded in albumin/gelatin (12% ovalbumin, 4.8% gelatin in demineralized water) and fixed overnight at 4°C in 8% formaldehyde in 0.1 mol l<sup>-1</sup> sodium phosphate buffer (NaPi; pH 7.4). Brains were sectioned in frontal plane into 30–40 µm slices using a vibrating-blade microtome (VT1000 S, Leica Microsystems, Wetzlar, Germany). The obtained sections were incubated for 18 h with streptavidin conjugated to horseradish peroxidase (1:200; Amersham Life Science, Little Chalfont, Buckinghamshire, GB) in PBS containing 0.5% TrX. After rinses, sections were treated with a solution of 3,3'-diaminobenzidine tetrahydrochloride (0.3 mg/ml) in 0.05 mol l<sup>-1</sup> Tris-HCl buffer (pH 7.4), with 0.3% nickel ammonium sulfate and 0.015% H<sub>2</sub>O<sub>2</sub> for up to 20 min. After the enzymatic reaction was stopped by rinses, sections were mounted on chrome alum-gelatin coated glass slides, dehydrated, cleared in xylene, and embedded in Entellan (Merck, Darmstadt, Germany). Peroxidase-labeled neurons are shown in Figures 7, 8a–c, 10d–g, and 11.

## 2.5 | Immunolabeling of rehydrated 130- and 80-µm sections

For more detailed analysis of neuronal morphologies, some of the Cy3-labeled brains (Figures 1a,c, 2–4, 5d–f, 9, and 15e,f) were selected for additional immunolabeling as described by von Hadeln et al. (2020). Briefly, brains were incubated in xylene to remove Permount and rehydrated using a decreasing ethanol series. After rinses, brains were embedded in albumin/gelatin, fixed overnight and sectioned in frontal plane into 130-µm slices using a vibrating-blade microtome (VT1200 S, Leica Biosystems, Wetzlar, Germany).

Anti-synapsin labeling was performed as described previously (von Hadeln et al., 2020). Briefly, after preincubation of sections with 5% normal goat serum (NGS), a monoclonal mouse-antibody against synapsin (1:50, SYNORF1, RRID: AB\_2315425, kindly provided by Drs. E. Buchner and C. Wegener, Würzburg, Germany), diluted in PBT and 1% NGS was used as primary antibody. After rinses with PBT, a Cy5-conjugated goat-anti-mouse IgG (1:300, Jackson ImmunoResearch, cat# 115-175-146; RRID: AB\_2338713) diluted in PBT and 1% NGS was used as secondary antibody. After thorough rinses in PBT and PBS, sections were dehydrated, cleared and mounted in Permount as described by von Hadeln et al. (2020).

Double labeling for serotonin and orcokinin and labeling for leucokinin was performed on 80-µm slices from rehydrated wholemounts. After sectioning, slices were rinsed in PBS and PBT. Leucokinin staining followed the protocol for synapsin staining, but with an antibody against leucokinin I (1:1000; 9028-7), kindly provided by D. Nässel (University of Stockholm, Sweden), added to the synapsin antibody solution, and a Cy2-conjugated goat-anti-rabbit IgG (1:300, Jackson ImmunoResearch, cat# 111-225-144, RRID: AB\_2338021) added to the secondary antibody solution.

80-µm sections used for serotonin (5-HT) and orcokinin double labeling were preincubated overnight at 4°C in PBS containing 2% TrX and 5% normal donkey serum (NDS), followed by incubation for 5 days at 4°C with a polyclonal rabbit-antiserum against Asn<sup>13</sup>-orcokinin (1:2500; RRID: AB\_2315017, Bungart et al., 1994) and a polyclonal goat antiserum against 5-HT (1:7500; RRID:

**FIGURE 2** Neurons innervating the gall (GA) and surrounding areas. (a) Schematic drawing of two types of columnar neuron (CP2 and CL1) of the protocerebral bridge (PB) and a tangential neuron (TL1) of the lower division of the central body (CBL), innervating the GA and surrounding areas. The CP2 neuron connects slices of the PB to the GA and regions around the lateral bulb (LBU). The GA is situated anterior to the LBU, not within. The CL1 neuron connects slices of the PB to slices of the CBL and the GA. The TL1 neuron connects the GA and regions around the LBU to layers 1–5 of the CBL. (b) Optical slice showing synapsin immunoreactivity (gray) in the lateral complex and arborizations of a CL1 neuron (dark blue) in the GA anterior to the LBU. (c) Frontal view of 3D-reconstructions of arborizations of three different CL1 neurons in the GA anterior to the LBU. (d) Optical slice showing synapsin immunoreactivity (gray) in the lateral complex and arborizations of a CP2 neuron (light blue) in between the microglomeruli of the LBU. (e) 3D-reconstruction of the arborizations of the CP2 neuron shown in (d) and the LBU. Frontal view (left) and posterior view (right). The neuron arborizes anteriorly, medially, posteriorly and dorsally around the LBU. (f) Optical slice showing synapsin immunoreactivity (gray) in the lateral complex and arborizations of a TL1 neuron (green) in the GA anterior to the LBU. (g) 3D-reconstruction of the arborizations of the TL1 neuron shown in (f) and the LBU. Frontal view (left) and posterior view (right). The neuron arborizes anteriorly, posteriorly, dorsally and ventrally to the LBU. CBU, upper division of the central body; CRE, crepine; IT, isthmus tract; LAL, lateral accessory lobe; LLAL, lower LAL; MBU, medial bulb; ULAL, upper LAL. Scale bars = 20 µm [Color figure can be viewed at [wileyonlinelibrary.com](http://wileyonlinelibrary.com)]

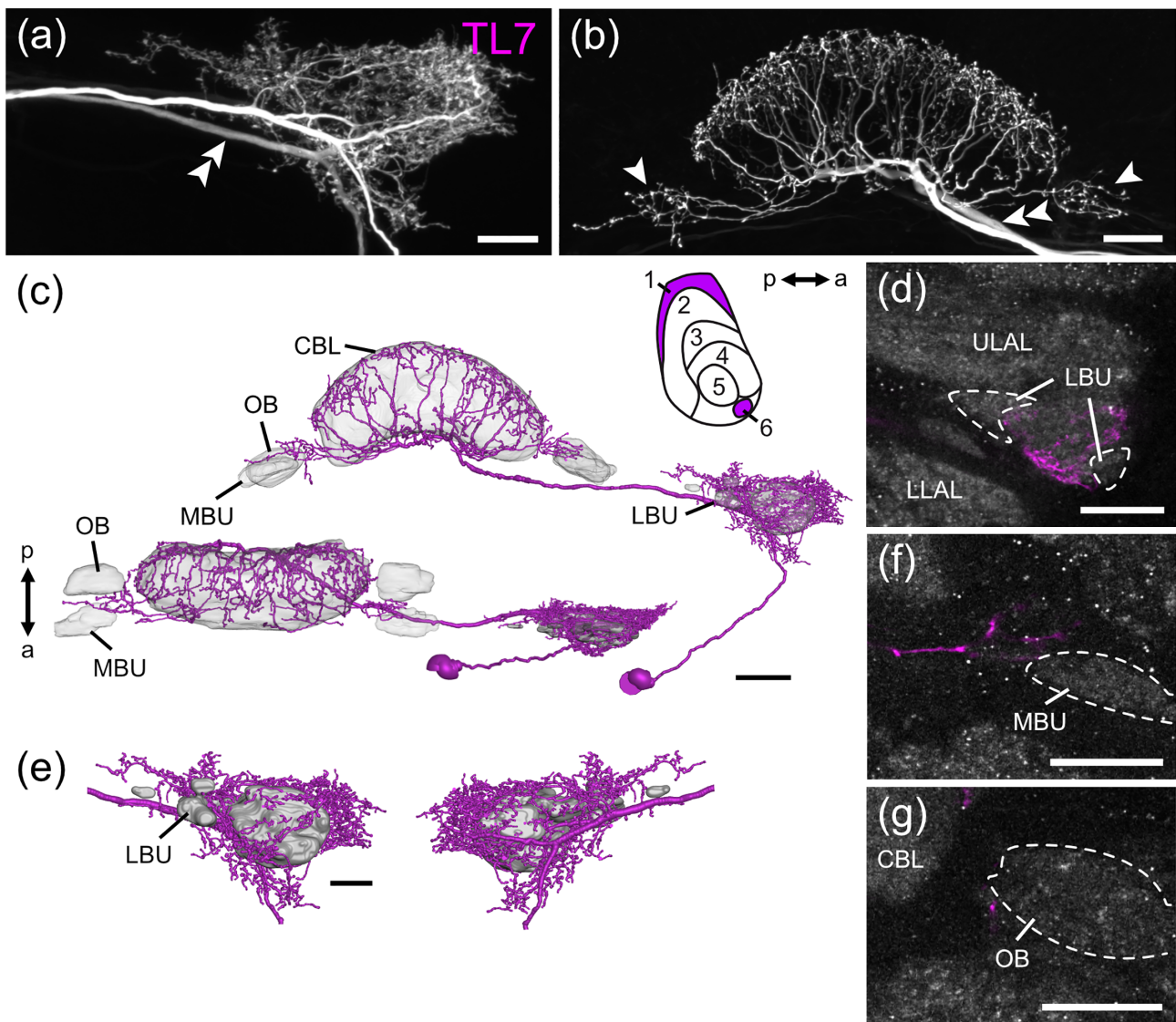


**FIGURE 3** Morphology of a tangential neuron (TL7) of the lower division of the central body (CBL) with arborizations in the lateral complex and the CBL. (a) Merged image stack of arborizations of the TL7 neuron laterally in the lateral complex. (b) Merged image stack of arborizations of the TL7 neuron in the CBL and bilaterally adjacent to the CBL in the lateral complex (arrowheads). Double arrowheads in (a,b) point to the neurite of a colabeled TL2 neuron. (c) 3D-reconstruction of the TL7 neuron. Arborizations in the lateral complex surround the lateral bulb (LBU), especially dorsally, ventrally, posteriorly and dorso-laterally, but also anteriorly (likely in the gall) and medially. Additional, bilateral arborizations invade an area superior-medially to the medial bulb (MBU) and ovoid body (OB). Schematic sagittal view illustrates innervated layers (1 and 6) of the CBL. (d) Optical slice showing synapsin immunoreactivity (gray) in the lateral complex and arborizations of the TL7 neuron (magenta) anterior to the LBU. (e) 3D-reconstruction of arborizations of the TL7 neuron around the LBU from anterior (left) and posterior (right). (f) Optical slice showing synapsin immunoreactivity (gray) in the region of the MBU and arborizations of the TL7 neuron (magenta) in close proximity, medially to the MBU. The MBU is free from ramifications. (g) Optical slice showing synapsin immunoreactivity (gray) in the OB, which is free from ramifications of the TL7 neuron (magenta). a, anterior; LLAL, lower lateral accessory lobe; p, posterior; ULAL, upper lateral accessory lobe. Scale bars = 20  $\mu\text{m}$  (a,d,e), 30  $\mu\text{m}$  (b,f,g), 40  $\mu\text{m}$  (c) [Color figure can be viewed at [wileyonlinelibrary.com](http://wileyonlinelibrary.com)]

AB\_572262, ImmunoStar, cat# 20079) in PBS containing 2% TrX and 1% NDS. After thorough rinses, incubation with the secondary antibodies, Cy2-conjugated donkey-anti-rabbit IgG (1:300, Jackson ImmunoResearch, cat# 711-225-152, RRID: AB\_2340612) and Cy5-conjugated donkey-anti-goat IgG (1:300, Jackson ImmunoResearch, cat# 705-175-147, RRID: AB\_2340415), diluted in PBS containing 2% TrX and 1% NDS followed for 3 days at 4°C. Finally, sections were dehydrated, cleared and mounted in Permount.

## 2.6 | Immunolabeling of 40- $\mu\text{m}$ thin sections

Double-labeling for orckinin and serotonin shown in Figure 5a–c was performed as described by Homberg et al. (2020). In brief, brains were dissected and fixed overnight at 4°C in 4% paraformaldehyde in NaPi. After thorough rinses, brains were embedded in albumin/gelatin, fixed overnight, and sectioned in frontal plane into 40- $\mu\text{m}$  slices using a vibrating-blade microtome (VT1200 S). The sections were



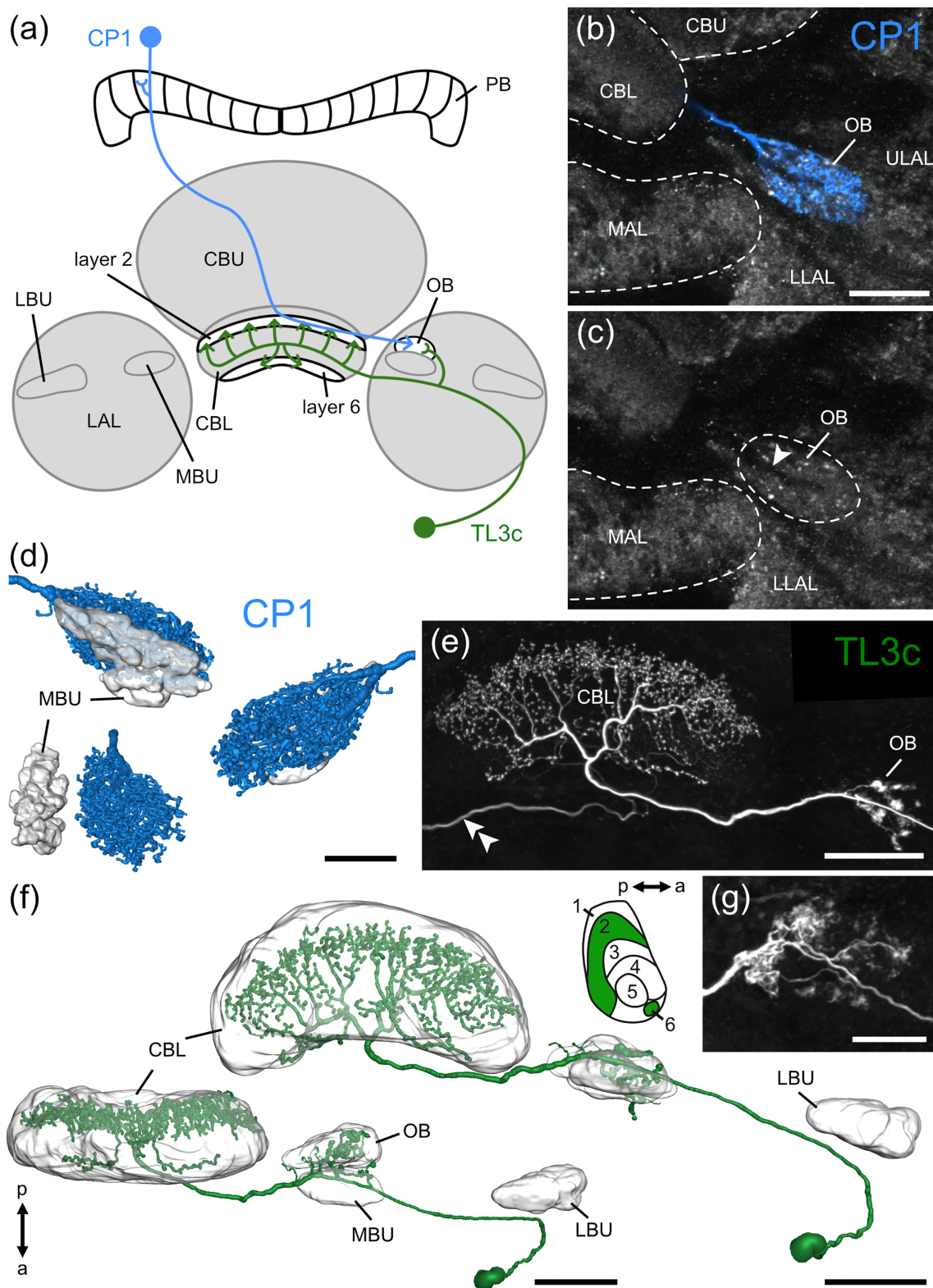


**FIGURE 4** Neurons innervating the ovoid body (OB). (a) Schematic drawing of a columnar neuron (CP1) of the protocerebral bridge (PB) and a tangential neuron (TL3c) of the lower division of the central body (CBL), innervating the OB, located posterior to the MBU of the lateral complex. The CP1 neuron connects a single slice of the PB to the OB. The TL3c neuron connects the OB with layers 2 and 6 of the CBL. (b,c) Optical slice showing synapsin immunoreactivity (gray) in the region of the OB and a CP1 neuron (blue in b) that innervates the OB. Arrowhead in (c) points to a synapsin-free fiber fascicle innervating the OB. (d) 3D-reconstruction of arborizations of the CP1 neuron (blue) and the medial bulb (MBU). Frontal view (upper left), posterior view (right), sagittal view (bottom left). Arborizations of the CP1 neuron are located within the OB, posterior to the MBU. (e) Merged image stack of a TL3c neuron with arborizations in the CBL and OB. Double arrowhead points to a colabeled TL3b neuron. (f) 3D-reconstruction of the TL3c neuron shown in (e). Schematic sagittal view illustrates innervated layers (2 and 6) of the CBL. (g) Merged image stack of arborizations of another TL3c neuron in the OB. a, anterior; CBU, upper division of the central body; LBU, lateral bulb; LLAL, lower lateral accessory lobe; MAL, medial accessory lobe; p, posterior; ULAL, upper lateral accessory lobe. Scale bars = 30  $\mu$ m (b,c), 20  $\mu$ m (d,g), 50  $\mu$ m (e,f) [Color figure can be viewed at [wileyonlinelibrary.com](http://wileyonlinelibrary.com)]

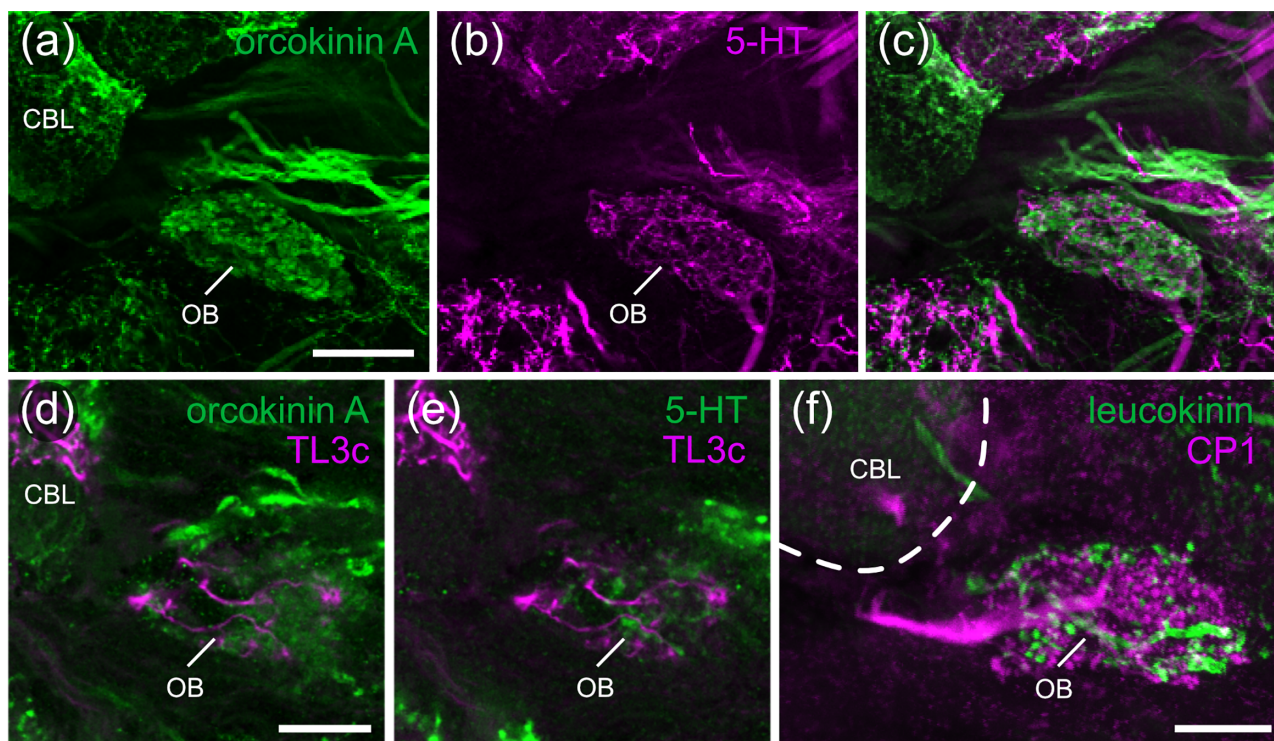


**FIGURE 5** Immunolabeling of the ovoid body (OB) of the lateral complex. (a-c) Optical slices showing orckinin (green) and 5-HT (magenta) immunoreactivity in the OB. (d,e) A labeled TL3c neuron (magenta) together with orckinin- (green in d) and 5-HT (green in e) immunoreactivity in the OB. (f) A labeled CP1 neuron (magenta) together with leucokinin immunoreactivity (green) in the OB. CBL, lower division of the central body. Scale bars = 40  $\mu\text{m}$  (a-c), 20  $\mu\text{m}$  (d-f) [Color figure can be viewed at [wileyonlinelibrary.com](http://wileyonlinelibrary.com)]

preincubated for 2 h at room temperature in 5% NDS and incubated overnight with the rabbit-antiserum against Asn<sup>13</sup>-orckinin (1:3000) and the goat antiserum against 5-HT (1:7500) in saline-substituted Tris buffer (SST; 0.1 mol l<sup>-1</sup> Tris-HCl/0.3 mol l<sup>-1</sup> NaCl, pH 7.4) containing 0.1% TrX and 2% NDS. Following rinses, sections were incubated for 1 h at room temperature with the secondary antibodies, Cy3-conjugated donkey anti-goat IgG (Jackson ImmunoResearch, cat# 705165-003; RRID: AB\_2340411) and Cy5-conjugated donkey anti-rabbit IgG (Jackson ImmunoResearch, cat# 711175-152; RRID: AB\_2340607) in SST containing 0.5% TrX and 2% NDS. Sections were rinsed, mounted on chrome alum-gelatin coated glass slides and left to dry for at least 2 h. Sections were dehydrated, cleared, and embedded in Entellan (Merck, Darmstadt, Germany).

## 2.7 | Bodian staining

Bodian's silver-protein technique was performed as described in Müller et al. (1997), and Heinze and Homberg (2008). Briefly, dissected brains were fixed for 3–4 h in 10% formalin with 5% glacial acetic acid, and 85% ethanol. After dehydration and embedding in Paraplast Plus (Sigma, Deisenhofen, Germany), brains were sectioned into 10- $\mu\text{m}$  slices and stained according to the Bodian-Protargol procedure (Bodian, 1936; Gregory, 1980).

## 2.8 | Image acquisition

Image stacks of fluorescence-labeled brains were obtained using a confocal laser scanning microscope (Leica, TCS SP5, Leica Microsystems, Wetzlar, Germany). A 20 $\times$  objective (HC PL APO 20 $\times$ /0.75 Imm Corr CS2) was used to scan wholemount preparations and acquire overviews of sections with a step size of 1 or 1.5  $\mu\text{m}$  in the z-plane. Detailed scans of brain sections were obtained with a 40 $\times$  objective (HCX PL APO 40 $\times$ /1.25-0.75 Oil) and a 63 $\times$  objective (HCX PL APO 63 $\times$ /1.3 Glyc Corr CS21) with step sizes of 0.5  $\mu\text{m}$  or 1  $\mu\text{m}$ . In the xy plane pixel size ranged from 0.2  $\times$  0.2  $\mu\text{m}$  (63 $\times$  objective) to 0.75  $\times$  0.75  $\mu\text{m}$  (20 $\times$  objective). Scanning frequency was 400 Hz. Excitation of the fluorophores Cy2, Cy3, and Cy5 was induced using an argon laser (488 nm), a diode-pumped solid-state laser (561 nm), and a helium neon laser (633 nm), respectively. Images of peroxidase labeled sections were captured using a digital camera (ProgRes C12plus, Jenoptik) mounted on a transmission light microscope (Axioskop, Zeiss, Oberkochen, Germany).

## 2.9 | Anatomical reconstructions and image processing

Primary processing of image stacks obtained with the confocal laser scanning microscope and 3D-reconstruction of neurons and neuropils was done in Amira 5.6 (ThermoFisher Scientific, Waltham, MA; RRID:



SCR\_007353). Neuropils were reconstructed based on anti-synapsin labeling or background fluorescence. Each neuropil was marked manually in different optical slices of the image stack in the x-, y-, and

z-plane. The wrapping function was used to compute a 3D structure from the resulting scaffold that could be visualized by applying the surface generator module and the surface view. Neurons were

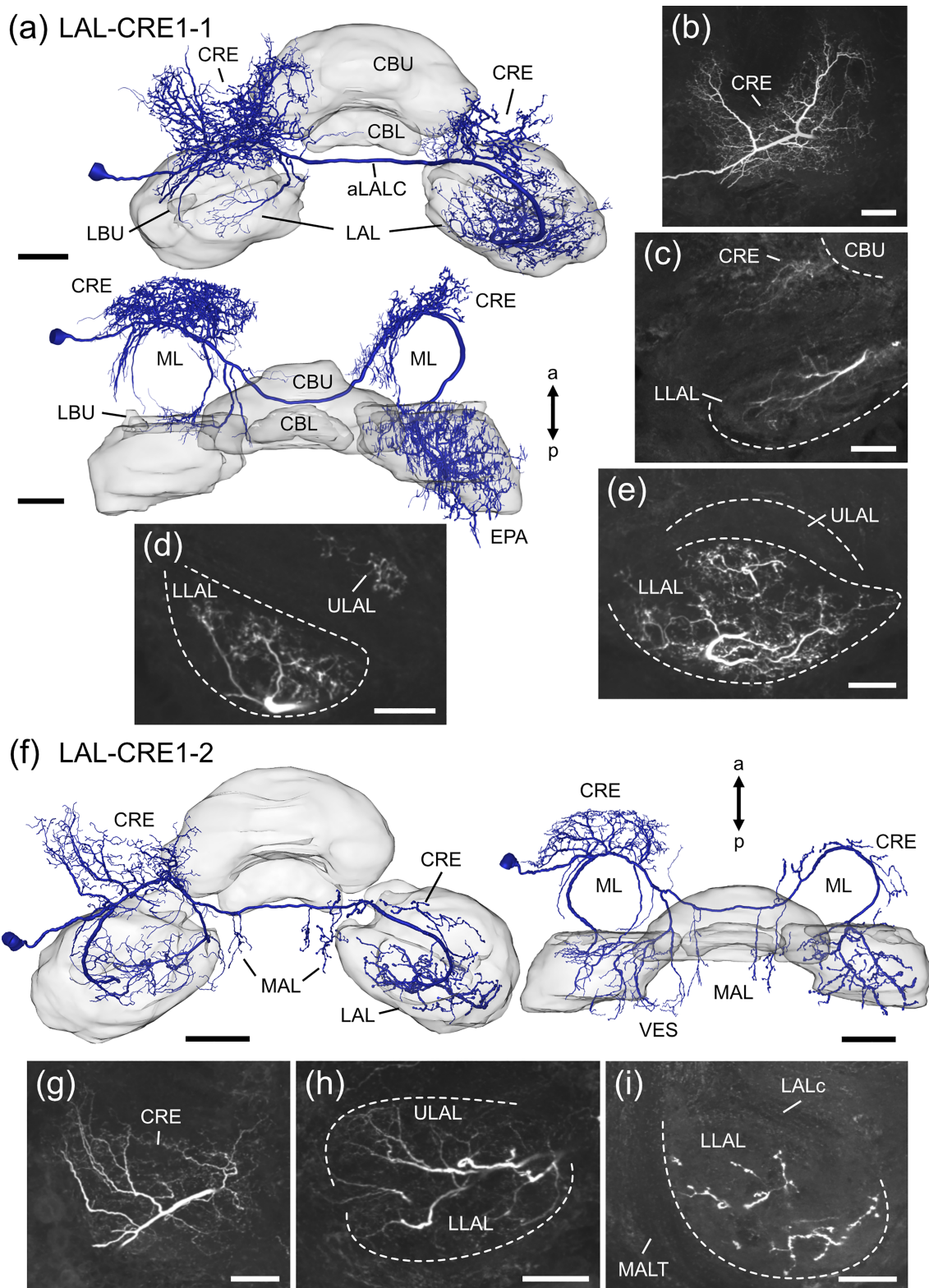
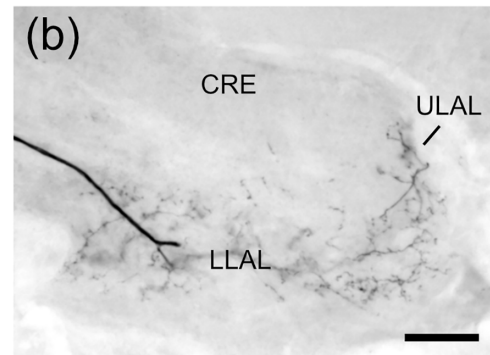
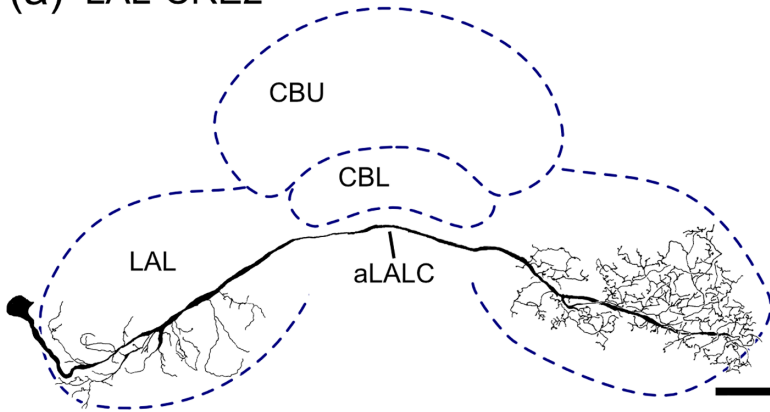


FIGURE 6 Legend on next page.

## (a) LAL-CRE2



**FIGURE 7** Neuron of the lateral accessory lobe (LAL) with soma near the crepine (CRE). (a) 2D-reconstruction of the LAL-CRE2 neuron with fine arborizations in the ipsilateral LAL and varicose arborizations in the contralateral LAL. (b) Merged image stack of varicose ramifications in the contralateral upper LAL (ULAL) and lower LAL (LLAL). aLALC, anterior LAL commissure; CBL, lower division of the central body; CBU, upper division of the central body. Scale bars = 50  $\mu\text{m}$  (a,c–e), 40  $\mu\text{m}$  (b) [Color figure can be viewed at [wileyonlinelibrary.com](http://wileyonlinelibrary.com)]

reconstructed using the skeletonize plugin for Amira (Evers et al., 2005; Schmitt et al., 2004). Processes of each cell were manually traced and path and diameter of each segment were fitted automatically according to the gray values of the image stack. In addition to the 3D-reconstructions of LX neurons presented here, additional 3D views and animated displays of the neurons can be found in the *InsectBrainDatabase* (Heinze et al., 2020). Neurons stained in peroxidase-labeled thin sections were reconstructed using a compound microscope (Leitz, Wetzlar, Germany) with camera lucida attachment and scanned for digitization. The fibers of neurons in Figure 9d–f were traced digitally in Affinity Photo (Serif, Nottingham, UK; RRID: SCR\_016951) based on serial images taken as described for peroxidase-labeled sections. Affinity Photo and Affinity Designer (Serif, Nottingham, UK; RRID: SCR\_016952) were used to optimize contrast and brightness of images and to create final figure panels. All images show frontal views if not indicated otherwise.

## 2.10 | Antibody characterization

The monoclonal antibody against synapsin was raised in mice against fusion proteins consisting of glutathione-S-transferase and parts of

the *Drosophila* synaptic vesicle protein SYN1 (Klagges et al., 1996). The antibody labels synaptic neuropils as shown in different insect species, including *S. gregaria* (Kurylas et al., 2008; Leitinger et al., 2004). Its specificity has been demonstrated in *Drosophila* by Klagges et al. (1996).

The antiserum against 5-HT contains polyclonal antibodies raised in goat against serotonin coupled to bovine serum albumin with paraformaldehyde. Immunostaining with this antiserum was identical to the staining pattern of a different 5-HT antiserum used by Homberg (1991). Preadsorption of the diluted antiserum with 100  $\mu\text{g}/\text{ml}$  serotonin/BSA conjugate completely abolished labeling (ImmunoStar product information sheet).

The polyclonal antiserum against orcokinin was raised in rabbit against  $\text{Asn}^{13}$ -orcokinin from the crayfish *Orconectes limosus* (Bungart et al., 1994). Preadsorption of the diluted antiserum with 1  $\text{nmol l}^{-1}$   $\text{Asn}^{13}$ -orcokinin abolished labeling in *S. gregaria* brain sections (Hofer et al., 2005). Sequence comparison suggest that *S. gregaria* orcokinins A6, A7, and A8 are primarily detected by the antiserum (Homberg et al., 2020). The specificity of the antiserum has been demonstrated in *O. limosus* by Bungart et al. (1994).

The antiserum against leucokinin was raised in rabbit against a conjugate of synthetic leucokinin I and bovine serum albumin with

**FIGURE 6** Neurons of the lateral accessory lobe (LAL) with somata near the crepine (CRE). (a) 3D-reconstruction of the LAL-CRE1-1 neuron with fine arborizations in the ipsilateral and varicose arborizations in the contralateral CRE and LAL and epaulet (EPA). Note projections of the neuron around the medial lobe (ML) of the mushroom body. (b) Merged image stack of fine arborizations in the CRE. (c) Merged image stack of fine arborizations in the ipsilateral CRE and lower LAL (LLAL). (d) Merged image stack of varicose ramifications in the contralateral upper LAL (ULAL) and anterior regions of the LLAL. (e) Merged image stack of varicose arborizations in posterior regions of the ULAL. Posterior regions of the ULAL are free from ramifications. (f) 3D-reconstruction of the LAL-CRE1-2 neuron shown in frontal (left) and dorsal (right) view with fine arborizations in the ipsilateral CRE, LAL, and vest (VES) and varicose ramifications in the contralateral CRE and LAL and the ipsi- and contralateral medial accessory lobe (MAL). Note projections of the neuron around the ML. (g) Merged image stack of fine arborizations in the CRE. (h) Merged image stack of fine arborizations in the anterior ULAL and LLAL. (i) Merged image stack of varicose ramifications in the posterior LLAL. a, anterior; aLALC, anterior LAL commissure; CBL, lower division of the central body; CBU, upper division of the central body; LBU, lateral bulb; MALT, medial antennal lobe tract; p, posterior. Scale bars = 100  $\mu\text{m}$  (a,f), 50  $\mu\text{m}$  (b–e,g–i) [Color figure can be viewed at [wileyonlinelibrary.com](http://wileyonlinelibrary.com)]

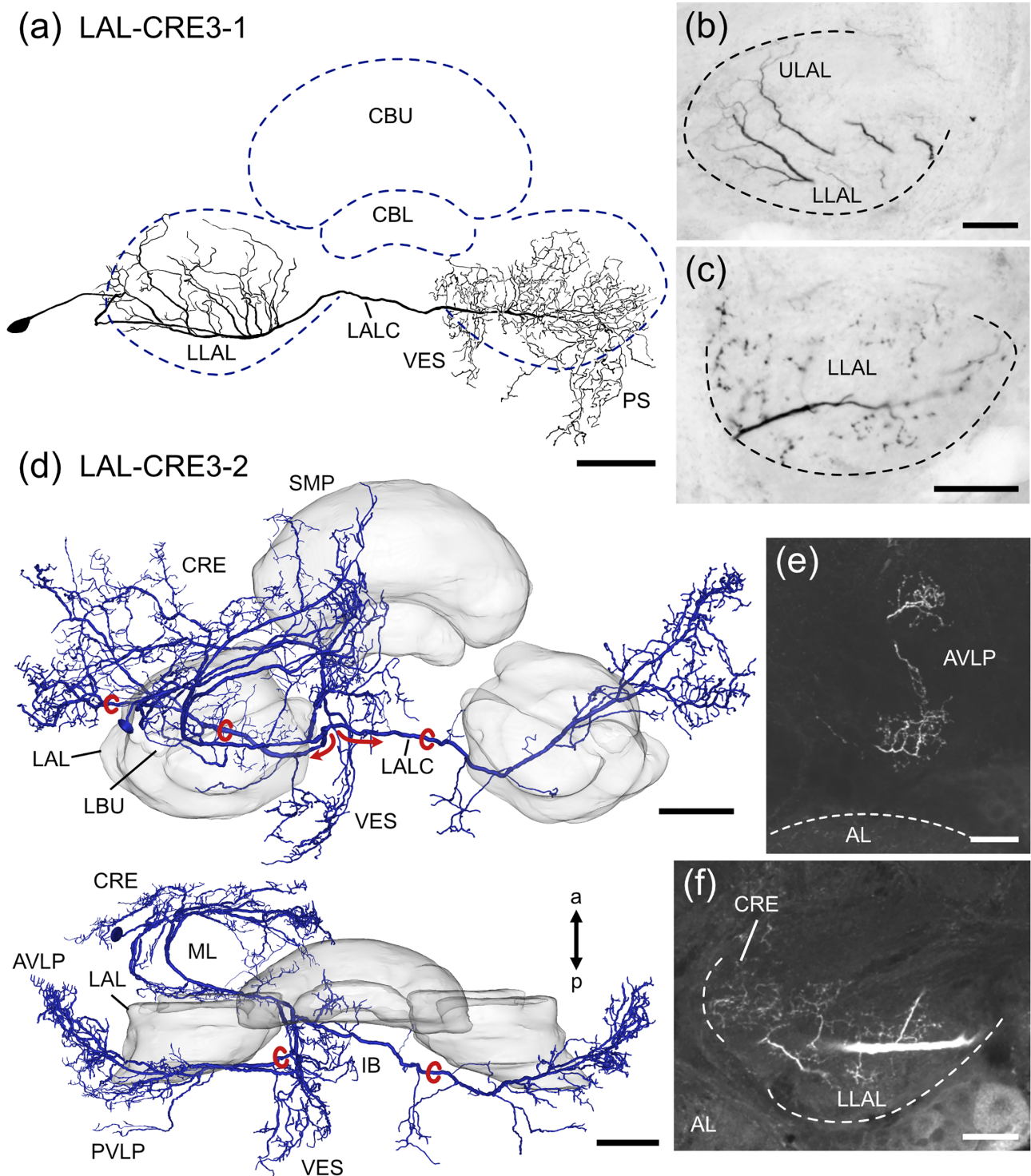


**FIGURE 8** Neurons of the lateral accessory lobe (LAL) with somata near the crepine (CRE). 2D-reconstruction of the LAL-CRE3-1 neuron with fine arborizations in the ipsilateral lower LAL (LLAL) and varicose ramifications in the contralateral LLAL, vest (VES), posterior slope (PS), and wedge. (b) Merged image stack of fine arborizations in the ipsilateral LAL. (c) Merged image stack of varicose ramifications in the contralateral LLAL. (d) 3D-reconstruction of the LAL-CRE3-2 neuron with fine arborizations in the ipsilateral CRE, LLAL, superior medial protocerebrum (SMP), vest (VES), medial accessory lobe, inferior bridge (IB), inferior clamp, and posterior ventrolateral protocerebrum (PVLP) and bilateral varicose ramifications in the VES, PVLP, and anterior ventrolateral protocerebrum (AVLP). Red circles indicate branches that give rise to varicose arborizations in each hemisphere. (e) Merged image stack of varicose ramifications in the AVLP. (f) Merged image stack of fine arborizations in the ipsilateral CRE and LLAL. a, anterior; AL, antennal lobe; CBL, lower division of the central body; CBU, upper division of the central body; LALC, LAL commissure; LBU, lateral bulb; ML, medial lobe of the mushroom body; p, posterior. Scale bars = 100  $\mu\text{m}$  (a,d), 50  $\mu\text{m}$  (b,c,e,f) [Color figure can be viewed at [wileyonlinelibrary.com](http://wileyonlinelibrary.com)]



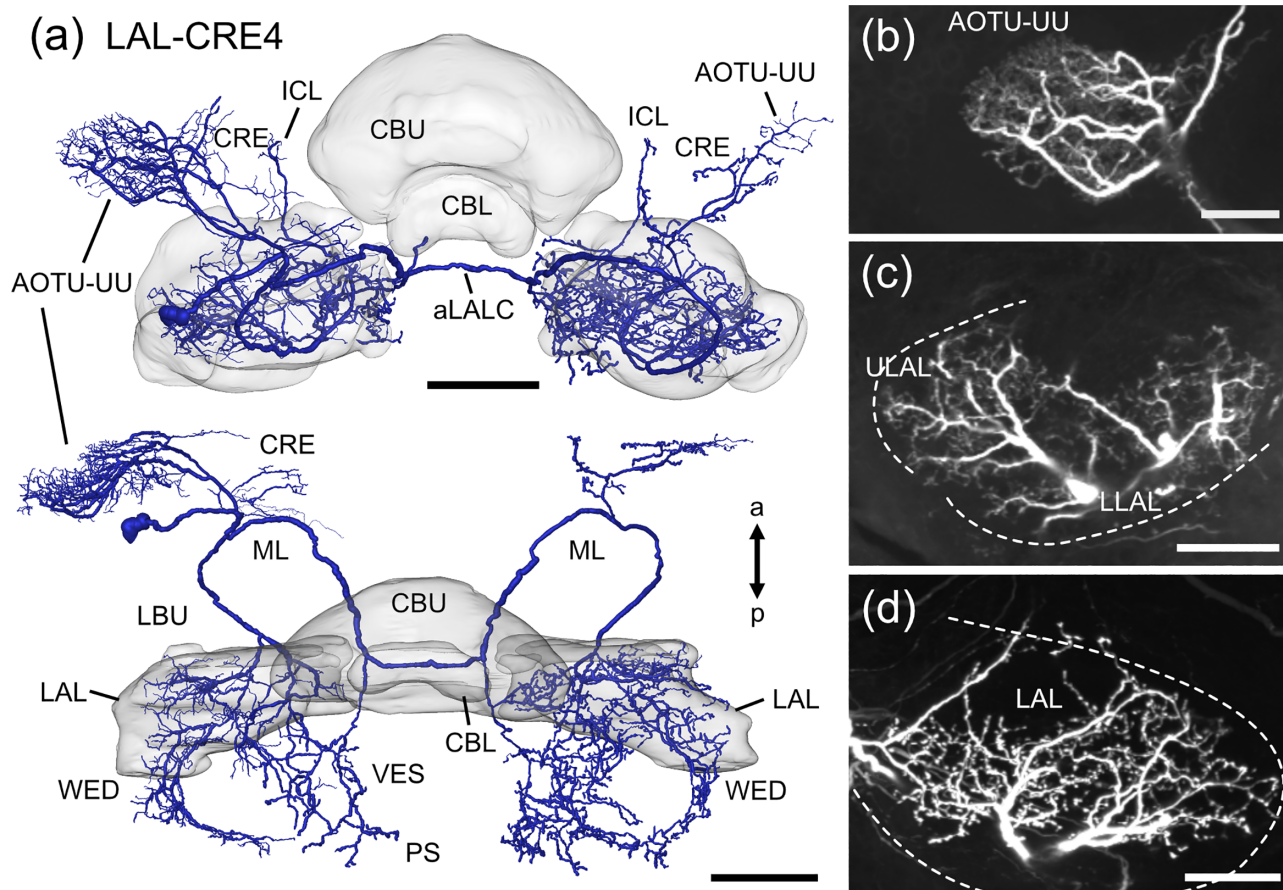


**FIGURE 9** Neuron of the lateral accessory lobe (LAL) with soma near the crepine (CRE). 3D-reconstruction of the LAL-CRE4 neuron with fine arborizations in the ipsilateral upper unit of the anterior optic tubercle (AOTU-UU), CRE, inferior clamp (ICL), LAL, and wedge (WED) and varicose ramifications in the contralateral AOTU-UU, CRE, ICL, LAL, and WED and the ipsi- and contralateral vest (VES) and posterior slope (PS). Note projections of the neuron around the medial lobe (ML) of the mushroom body. (b) Merged image stack of fine arborizations in the ipsilateral AOTU-UU. (c) Merged image stack of fine arborizations in the ipsilateral upper LAL (ULAL) and lower LAL (LLAL). (d) Merged image stack of varicose ramifications in the contralateral LAL. a, anterior; aLALC, anterior LAL commissure; CBL, lower division of the central body; CBU, upper division of the central body; p, posterior. Scale bars = 100  $\mu\text{m}$  (a), 40  $\mu\text{m}$  (b), 50  $\mu\text{m}$  (c,d) [Color figure can be viewed at [wileyonlinelibrary.com](http://wileyonlinelibrary.com)]

1,5-difluoro-2,4-dinitrobenzene (Nässel et al., 1992). It was characterized on brains of the locust *Locusta migratoria* by Nässel (1993) and on *S. gregaria* brains by Vitzthum and Homberg (1998). Preadsorption of the diluted antisera with 10  $\mu\text{m}$  synthetic leucokinin abolished all labeling in brain sections of *S. gregaria* (Vitzthum & Homberg, 1998).

### 3 | RESULTS

#### 3.1 | Nomenclature and general anatomy

We adapted the nomenclature for insect brain neuropils and fiber tracts from Ito et al. (2014), and, for locust-specific brain areas from von Hadeln et al. (2018). CX neurons are named following von Hadeln et al. (2020). LAL neurons were grouped and named according to the position of their cell bodies (see below). The internal organization of the LX (Figure 1) is largely defined by the course of the isthmus tracts (IT1-IT6, von Hadeln et al., 2020) and by two commissures that

connect the LALs bilaterally (Figure 1a,b,c,g,h). The isthmus tracts connect the LX with the CX (von Hadeln et al., 2020) and partly surround the two bulbs of the locust, the medial bulb (MBU) and the lateral bulb (LBU) (Figure 1a,g), which have a microglomerular organization (Träger et al., 2008). To facilitate comparison between the LAL of the locust and the fly *Drosophila*, we readjusted the boundaries of the LAL and its subdivisions, originally established for the locust by el Jundi et al. (2010), to correspond to those in *Drosophila*, established by Ito et al. (2014). First, the most anterior regions of the ULAL that were originally wrapped around the medial lobe of the mushroom body (Figure 3 in el Jundi et al., 2010), are now allocated to the crepine (CRE), and the new anterior border of the ULAL is set further posterior at the level of the tubercle-to-bulb tract (Figure 1a, arrowhead). Thus, the bulbs slightly protrude from the ULAL anteriorly instead of being covered by it (Figure 1e). Second, the plane of separation between ULAL and LLAL, which was previously indicated by the ITs and the bulbs, is now marked by the LAL commissure (LALC), although in general both subdivisions remain highly fused. As a result, the LLAL

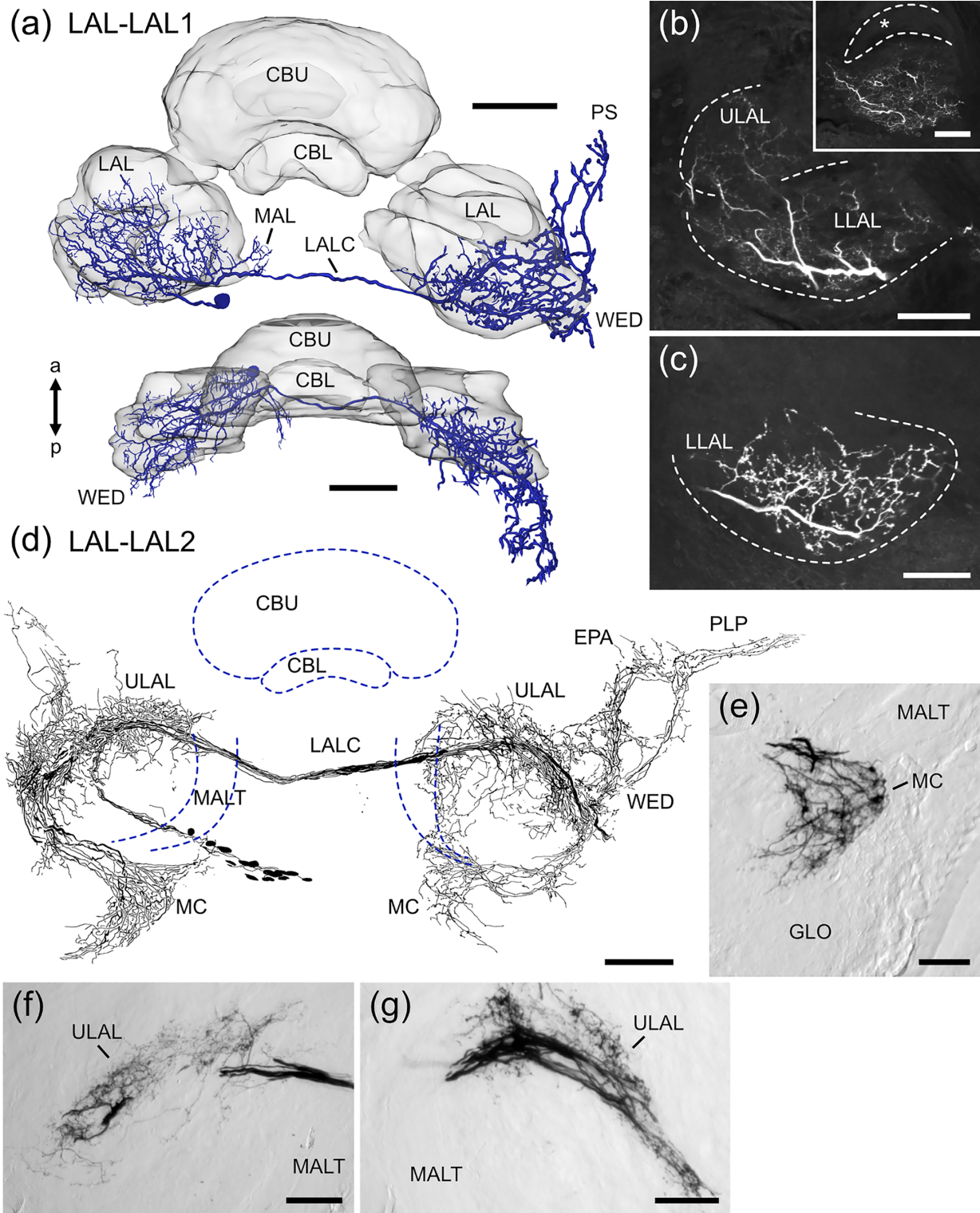


**FIGURE 10** Neurons of the lateral accessory lobe (LAL) with somata near the LAL. (a) 3D-reconstruction of the LAL-LAL1 neuron with fine arborizations in the ipsilateral upper LAL (ULAL) and lower LAL (LLAL), the wedge (WED), and medial accessory lobe (MAL) and varicose ramifications in the contralateral LLAL, WED, and posterior slope (PS). (b) Merged image stack of fine arborizations in the ipsilateral LAL. Asterisk in the inset indicates the ULAL superior to the LAL commissure. (c) Merged image stack of varicose arborizations in the contralateral LLAL. (d) 2D-reconstruction of about 14 neurons of the LAL-LAL2 neuron type with fine arborizations in the ipsilateral median crescent (MC), ULAL, WED, posterior lateral protocerebrum (PLP), and epaulet (EPA) and varicose ramifications in the contralateral MC, ULAL, WED, PLP, vest and EPA. (e) Merged image stack of fine arborizations in the ipsilateral MC, superior to the glomerular lobe (GLO). (f) Merged image stack of fine arborizations in posterior regions of the ipsilateral ULAL. (g) Merged image stack of varicose arborizations in posterior regions of the contralateral ULAL. a, anterior; CBL, lower division of the central body; CBU, upper division of the central body; LALC, LAL commissure; MALT, medial antennal lobe tract. Scale bars = 100  $\mu$ m (a,d), 50  $\mu$ m (b,c, e,f,g) [Color figure can be viewed at [wileyonlinelibrary.com](http://wileyonlinelibrary.com)]

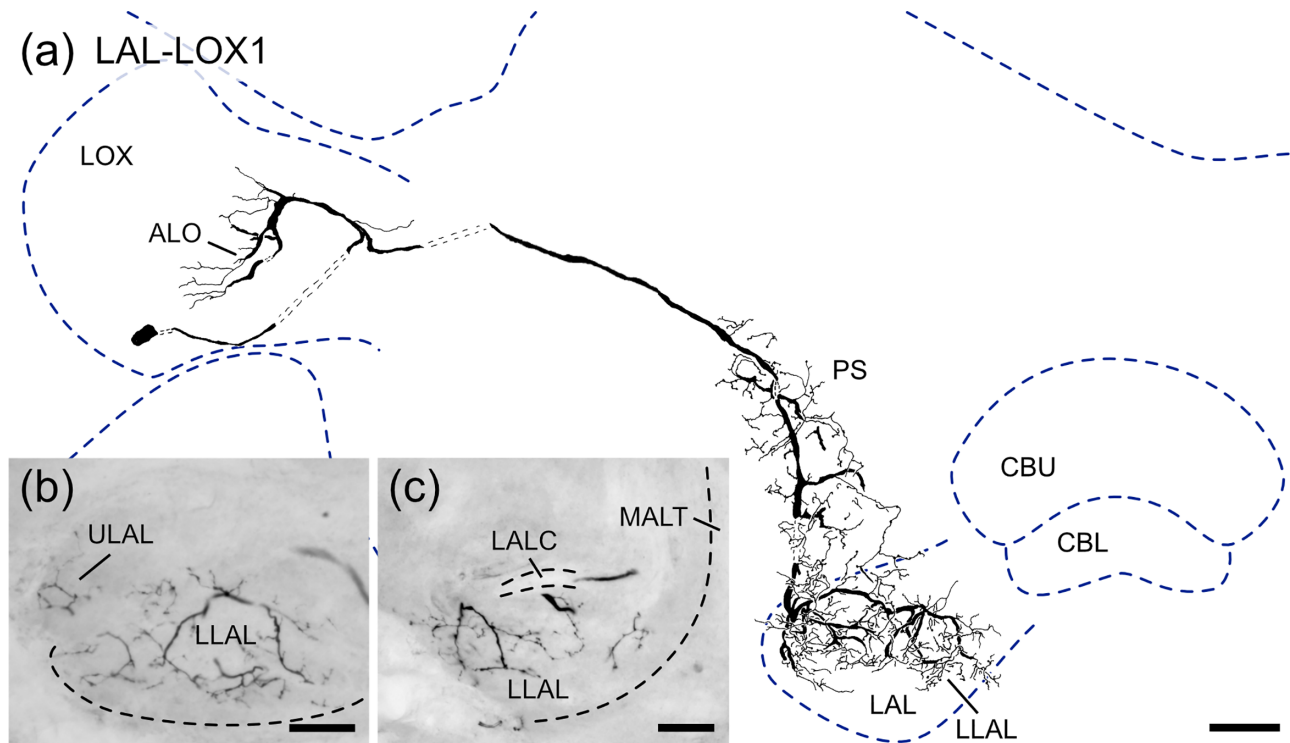


**FIGURE 11** Neuron of the lateral accessory lobe (LAL) with soma near the lobula complex (LOX). (a) 2D-reconstruction from microtome sections of the LAL-LOX1 neuron with fine arborizations in the anterior lobe of the lobula (ALO) and varicose arborizations in the ipsilateral upper LAL (ULAL) and lower LAL (LLAL), the wedge, and the posterior slope (PS). Dotted lines indicate likely connections that could not be reconstructed owing to a missing brain section. (b) Merged image stack of varicose arborizations in anterior regions of the ULAL and LLAL. (c) Merged image stack of varicose arborizations in posterior regions of the LLAL. CBL, lower division of the central body; CBU, upper division of the central body; LALC, LAL commissure; MALT, medial antennal lobe tract. Scale bars = 50  $\mu\text{m}$  [Color figure can be viewed at [wileyonlinelibrary.com](http://wileyonlinelibrary.com)]

loses some of its posterior-dorsal volume to the ULAL (Figure 1c). Posterior-medially and posteriorly the border of the LX remains delimited by the medial antennal lobe tract (MALT) and by the epaulet, the vest, and the wedge, respectively. Medially the LX is bordered by the medial accessory lobe (MAL, Figure 1b,c) and the CBU. Neurons that connect both LALs cross the midline of the brain via the LALC (Figure 1b,c,g), corresponding to commissure PC XI of Boyan et al. (1993) or via a commissure that is situated more dorsally and anteriorly, close to the ALI, the anterior LAL commissure (aLALC, Figure 1h), termed commissure PC III by Boyan et al. (1993).

### 3.2 | The gall and a potential feedback loop

Columnar neurons with ramifications in the PB and CBL, termed CL1 (equivalent to P-EG and E-PG neurons in flies) are key elements of the internal sky compass within the locust CX (Heinze & Homberg, 2009; Pegel et al., 2018; Zittrell et al., 2020). These neurons connect single columns of the CBL and PB, and have axonal terminals in a small area within the LAL, termed gall (GA) in *Drosophila* (Ito et al., 2014; Wolff & Rubin, 2018), the dung beetles, *Scarabaeus lamarckii* and *Scarabaeus satyrus* (el Jundi et al., 2018), the bogong moth, *Agrotis infusa* (Adden,

Wibrand, et al., 2020), and the honeybee *A. mellifera* (Hensgen et al., 2021), or anterior loblet in the monarch butterfly *D. plexippus* (Heinze & Reppert, 2012). In the locust a corresponding brain area has not been identified. Here axons of CL1 neurons have been reported to target the LBU or adjacent areas of the LAL (Müller et al., 1997; Heinze & Homberg, 2009; Figure 3A in Pegel et al., 2018). To further clarify their axonal projection sites, we analyzed the morphology of individual CL1 neurons in more detail (Figure 2a–c). All data were obtained from a particular subtype of CL1 neurons, termed CL1a. These neurons have, like E-PG neurons in flies, fine, dendritic ramifications in the CBL and beaded axonal terminals in the PB (Heinze & Homberg, 2008). 3D-reconstructions of axonal terminals of nine neurons show that CL1a neurons arborize in an area at the anterior surface of the LBU. Although in some preparations the region appears weakly stained by anti-synapsin compared to surrounding tissue, no clear boundaries could be defined.

Three additional types of neuron, columnar neurons of the PB, termed CP2, tangential neurons of the CBL termed TL1, and a newly identified cell type termed TL7, have projections in a similar area and were, therefore, also analyzed in detail. CP2 neurons are a second type of columnar neuron involved in sky compass signaling (Pegel et al., 2018; Vitzthum et al., 2002); they connect single slices of the PB to a region



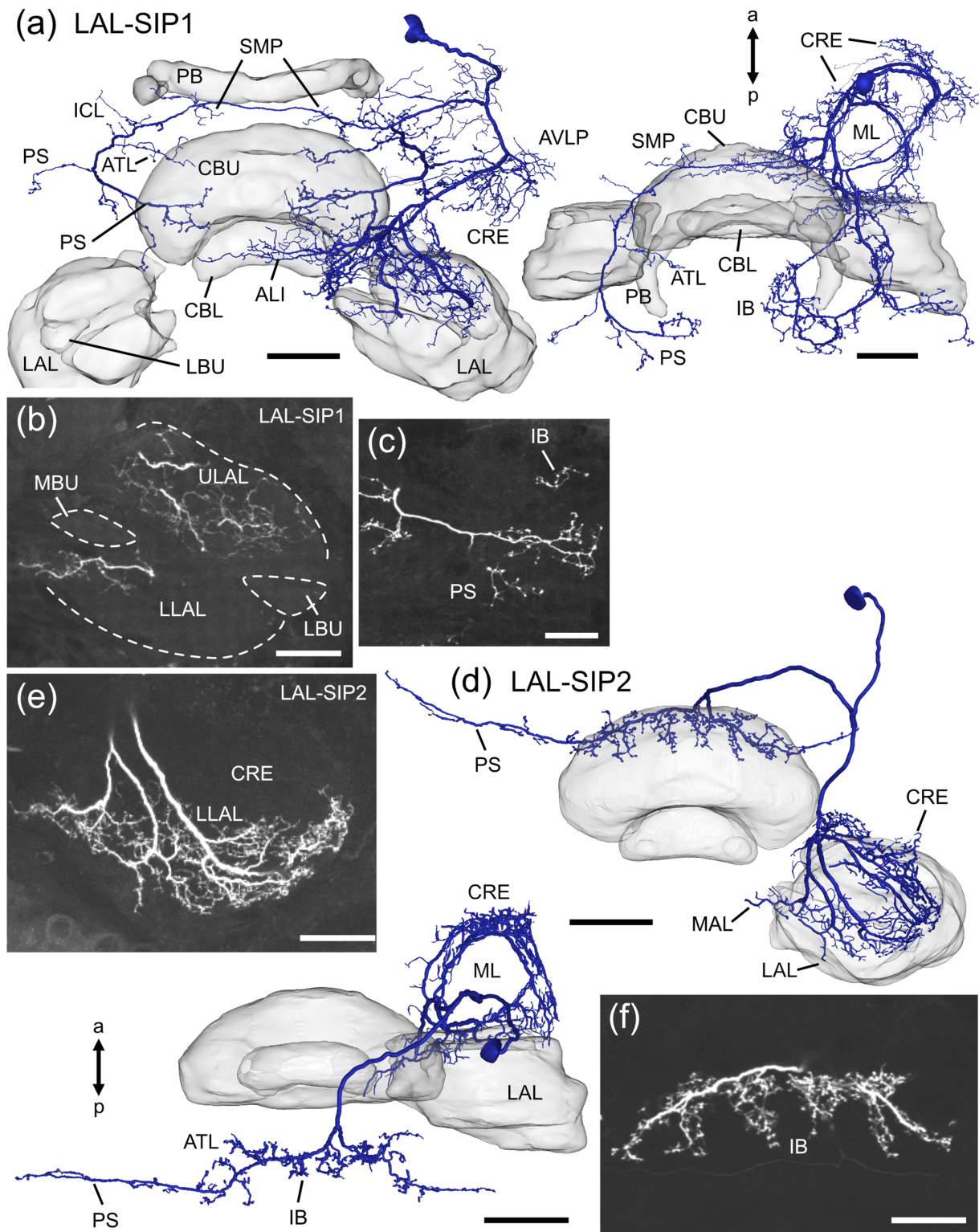


**FIGURE 12** Neurons of the lateral accessory lobe (LAL) with somata near the superior intermediate protocerebrum (SIP). (a) 3D-reconstruction of the LAL-SIP1 neuron with fine arborizations in the ipsilateral crepine (CRE), LAL, upper division of the central body (CBU), anterior ventrolateral protocerebrum (AVLP), superior clamp, inferior clamp (ICL), and medial accessory lobe, and the ipsi- and contralateral SMP, ICL, antler (ATL), and posterior slope (PS). (b) Merged image stack of fine arborizations in the ipsilateral upper (ULAL) and lower (LLAL) LAL, medial accessory lobe (MAL), and CBU. (c) Merged image stack of varicose arborizations in the IB and PS. (d) 3D-reconstruction of the LAL-SIP2 neuron with fine arborizations in the ipsilateral CRE, LLAL, and MAL and bilateral varicose arborizations in the IB, ATL and PS. (e) Merged image stack of fine arborizations in the CRE and anterior regions of the LLAL. (f) Merged image stack of varicose arborizations in the IB. a, anterior; CBL, lower division of the central body; LBU, lateral bulb; MBU, medial bulb; ML, medial lobe of the mushroom body; p, posterior; PB, protocerebral bridge. Scale bars = 100  $\mu\text{m}$  (a,d), 50  $\mu\text{m}$  (b,c,e,f) [Color figure can be viewed at [wileyonlinelibrary.com](http://wileyonlinelibrary.com)]

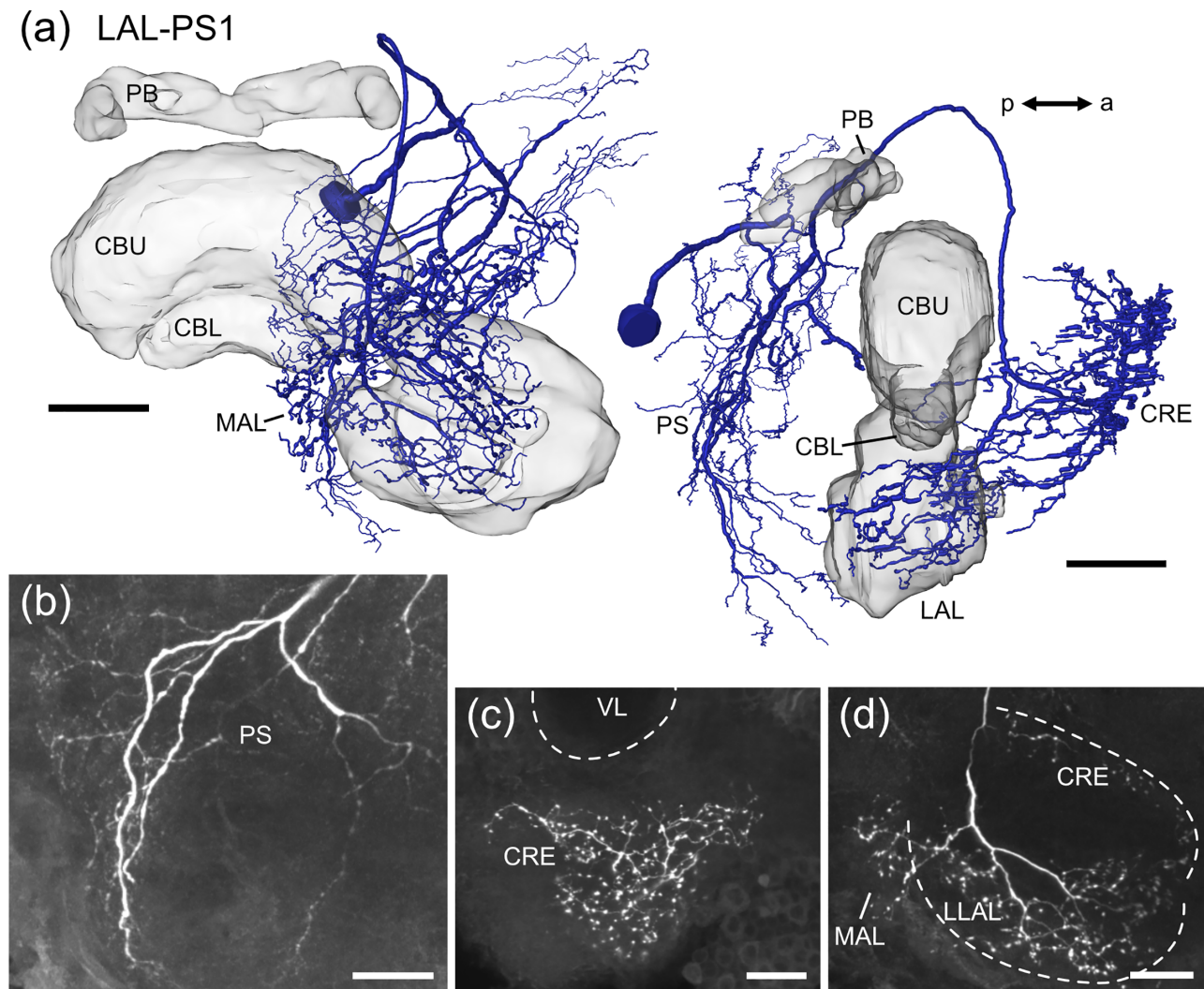


**FIGURE 13** Neuron of the lateral accessory lobe (LAL) with soma near the posterior slope (PS). (a) 3D-reconstruction of the LAL-PS1 neuron with fine arborizations in the ipsilateral PS, inferior bridge, antler, vest, and neck and varicose ramifications in the ipsilateral crepine (CRE), LLAL and medial accessory lobe (MAL). (b) Merged image stack of fine arborizations in the PS. (c) Merged image stack of varicose arborizations in the CRE, LLAL and MAL. (d) Merged image stack of varicose arborizations in the CRE. a, anterior; CBL, lower division of the central body; CBU, upper division of the central body; LLAL, lower LAL; p, posterior; PB, protocerebral bridge; VL, vertical lobe of the mushroom body. Scale bars = 100  $\mu\text{m}$  (a), 50  $\mu\text{m}$  (b–d) [Color figure can be viewed at [wileyonlinelibrary.com](http://wileyonlinelibrary.com)]

close to the LBU. 3D-reconstructions of two CP2 neurons showed that some terminals of CP2 neurons lie anterior to the LBU but a larger number in regions posterior and dorso-lateral to the LBU (Figure 2a,d,e). TL1 neurons are tangential neurons that project from the LX into layers 1–5 of the CBL (von Hadeln et al., 2020). Unlike the more numerous TL2 neurons that innervate the microglomeruli of the LBU, their dendritic ramifications in a similar but slightly larger area are fine without indications of condensations in microglomeruli (Müller et al., 1997). 3D-reconstructions showed that the dendritic ramifications of TL1 neurons form a dense mesh of fine processes that covers the LBU anteriorly, dorsally and posteriorly, extends into adjacent regions of the LAL (Figure 2a, f,g), but does not invade the microglomerular LBU.

Another, hitherto undescribed type of TL neuron (TL7, Figure 3) shows arborizations around the LBU (Figure 3a,c,e) that occupy

positions similar to those of the TL1 neuron, but its terminals are a mixture of fine smooth and fine beaded specializations. Cell body position and the course of the primary neurite of the TL7 neuron, however, are similar to those of TL2 and TL3 neurons. Ventrally to the CBL, side branches of the neuron extend dorsally into layer 1 and layer 6 (Figure 3b,c). Notably, at least one side branch on each side of the CBL projects laterally and gives rise to varicose arborizations outside the CBL, close to the MBU and ovoid body (OB, see below) of the LX (Figure 3b–d,f).

Taken together, at least four types of neuron, CL1-, CP2-, TL1- and TL7 neurons, have ramifications in a small region anterior to the LBU that likely corresponds to the GA in other insects. These morphological features, including their presumed polarity, point to a potential feedback loop between outputs (CP2/CL1) and inputs (TL1/TL7) of the CX.



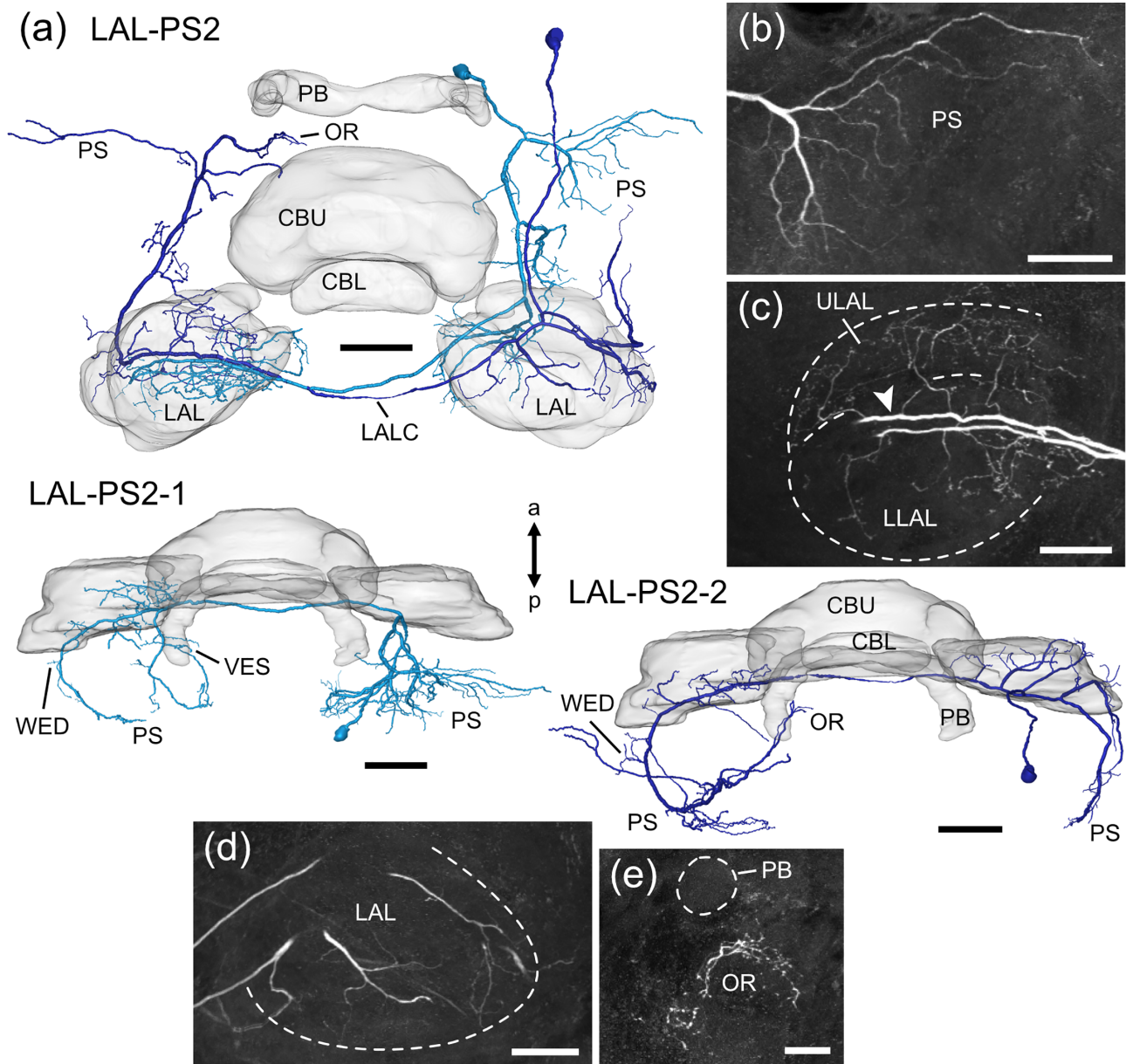


**FIGURE 14** Neurons of the lateral accessory lobe (LAL) with somata near the posterior slope (PS). (a) 3D-reconstruction of the LAL-PS2-1 neuron (light blue) and the LAL-PS2-2 neuron (dark blue). The LAL-PS2-1 neuron has fine arborizations in the ipsilateral PS and varicose arborizations in the contralateral lower LAL (LLAL), vest (VES), wedge (WED) and PS. The LAL-PS2-2 neuron has fine arborizations in the ipsilateral PS, WED and LAL and varicose arborizations in the contralateral upper LAL (ULAL), WED, PS, and ocellar root (OR). (b) Merged image stack of fine arborizations of the LAL-PS2-1 neuron in the PS. (c) Merged image stack of varicose arborizations in posterior regions of the contralateral ULAL and LLAL. The LAL-PS2-2 neuron (arrowhead) innervates the ULAL, and the LAL-PS2-1 neuron innervates the LLAL. (d) Merged image stack of fine arborizations of the LAL-PS2-2 neuron in the ipsilateral LAL. (e) Merged image stack of varicose arborizations of the LAL-PS2-2 neuron in the contralateral OR. a, anterior; CBL, lower division of the central body; CBU, upper division of the central body; LALC, LAL commissure; p, posterior; PB, protocerebral bridge. Scale bars = 100  $\mu$ m (a), 50  $\mu$ m (b-d), 30  $\mu$ m (e) [Color figure can be viewed at [wileyonlinelibrary.com](http://wileyonlinelibrary.com)]

### 3.3 | The ovoid body and a potential second feedback loop

Similar to CP2 neurons, CP1 neurons innervate the PB and a small region within the LAL that has been assumed to be the MBU, previously termed median olive (Heinze & Homberg, 2008; Müller et al., 1997). More detailed analysis of their LX arborizations

showed that they arborize in a distinct area posterior to the MBU that we named ovoid body (OB) (Figure 4a-d). In contrast to LBU and MBU that have a prominent microglomerular organization, the OB appears smoother in anti-synapsin staining (Figure 4c). Its borders can be fairly well delimited against the surrounding LAL tissue. A thin fiber tract, presumably containing the axons of CP1 neurons, enters the neuropil medially (Figure 4c, arrowhead). Beaded

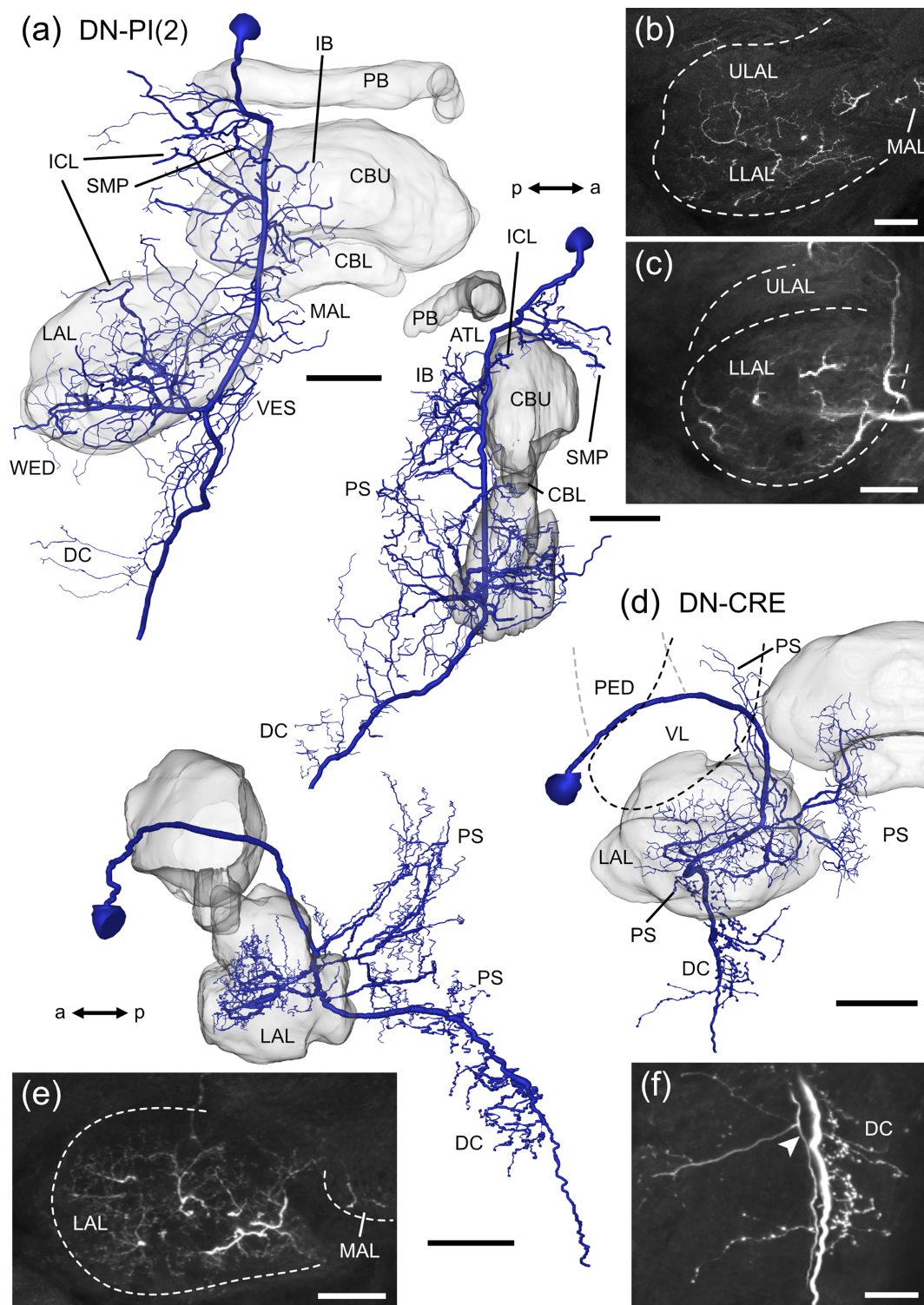


**FIGURE 15** Descending neurons with innervation in the lateral accessory lobe (LAL). (a) 3D-reconstruction of the DN-PI(2) neuron with soma in the PI, fine arborizations in the ipsilateral superior medial protocerebrum (SMP), inferior clamp (ICL), LAL, medial accessory lobe (MAL), vest (VES), wedge (WED), inferior bridge (IB), antler (ATL), and posterior slope (PS) and varicose ramifications in the ventral PS and the deutocerebrum (DC). (b) Merged image stack of fine arborizations in the MAL and in anterior regions of the upper (ULAL) and lower LAL (LLAL). (c) Merged image stack of arborizations in posterior regions of the LLAL. (d) 3D-reconstruction of the DN-CRE neuron with soma near the CRE, fine arborizations in the ipsilateral PS, VES, MAL, and LAL and varicose ramifications in the ipsilateral PS and DC. The cell body fiber of the neuron runs medially between the vertical lobe (VL) and the pedunculus (PED) of the mushroom body. (e) Merged image stack of fine arborizations in the ipsilateral MAL and LAL. (f) Merged image stack of varicose arborizations in the ipsilateral DC. Arrowhead points to a colabeled neuron. a, anterior; CBL, lower division of the central body; CBU, upper division of the central body; p, posterior; PB, protocerebral bridge; ULAL, upper LAL. Scale bars = 100 μm (a,d), 50 μm (b,c,e), 40 μm (f) [Color figure can be viewed at [wileyonlinelibrary.com](http://wileyonlinelibrary.com)]

arborizations of CP1 neurons ( $n = 3$ ) are homogeneously distributed within the OB (Figure 4b,d).

A novel, hitherto undescribed subtype of TL3 neuron (TL3c,  $n = 3$ ) innervates the OB and specifically targets layer 6 and 2 of the CBL (Figure 4a,e,f). Within the CBL endings have a beaded appearance, suggestive of presynaptic endings. Whereas arborizations in the OB of one TL3c neuron (Figure 4e,f) had a microglomerular appearance like the endings of TL2- and TL3 neurons in the LBU and MBU, respectively, arborizations of another TL3c neuron appeared less microglomerular (Figures 4g and 5d,e).

Double labeling experiments revealed dense staining of the OB by an antiserum against anti-Asn<sup>13</sup>-orcokinin and showed innervation of the OB by serotonin-immunoreactive fibers (Figure 5a–c). These markers confirm that TL3c neurons project into the OB, as their processes intermingle with orcokinin- and serotonin-positive structures within this region (Figure 5d,e). Moreover, we reanalyzed the arborizations of a leucokinin-immunoreactive neuron with dendritic ramifications in the lobula, that was described to innervate the MBU (Homberg et al., 2003). We found that its ramifications are, instead, located in the OB illustrated in Figure 5f together with the arborizations of a CP1 neuron.

Our data indicate that the OB is an additional, distinct neuropil within the LX, posterior to the MBU. It houses the presynaptic ramifications of CP1- and postsynaptic sites of TL3c neurons of the CX, and might thus be a second site of feedback connections between outputs and inputs of the CX compass network. In addition, the OB is innervated by leucokinin-positive neurons with dendrites in the lobula and serotonin-immunolabeled neurons with unknown input sites.

### 3.4 | Neurons of the lateral accessory lobe

The ULAL and LLAL constitute the largest volume of the LX. They house arborizations of neurons from the anterior optic tubercle (Homberg et al., 2003), to and from the CX (Heinze & Homberg, 2008; von Hadeln et al., 2020), and connections to other brain areas or the contralateral LAL (Heinze & Homberg, 2009; Homberg, 1991). Here, we present 16 types of LAL neuron to complement the data on the overall connectivity of this neuropil. Among these are three types of neuron (DN-PI(2), LAL-CRE3-2, and LAL-CRE4) that have already been characterized by Homberg (1994), and Vitzthum et al. (2002). We renamed these neurons according to the position of their cell bodies resulting in seven different groups of LAL neuron. LAL-CRE neurons have their cell bodies near the crepine (CRE), LAL-LAL neurons have cell bodies medial to the LAL, LAL-SIP neurons have their somata near the superior intermediate protocerebrum (SIP), one LAL-LOX neuron has its soma near the lobula complex (LOX), and LAL-PS neurons have their somata in the posterior brain near the posterior slope (PS). Two descending neurons with innervations in the LAL were named DN-PI(2) neuron (according to Homberg, 1994), and DN-CRE neuron, as they have their somata in the pars intercerebralis and near the CRE, respectively.

Based on differences in the trajectories of cell body fibers, we further subdivided LAL-CRE neurons into LAL-CRE1, LAL-CRE2, LAL-CRE3, and LAL-CRE4, LAL-LAL neurons into LAL-LAL1 and LAL-LAL2, LAL-SIP neurons into LAL-SIP1 and LAL-SIP2, and LAL-PS neurons into LAL-PS1 and LAL-PS2.

### 3.5 | LAL-CRE neurons

LAL-CRE neurons (Figures 6–9) have their somata in the anterior brain near the CRE, superior to the antennal lobe and lateral to the medial lobe of the mushroom body. All neurons have ramifications in both brain hemispheres.

LAL-CRE1 neurons (Figure 6) project along the anterior surface of the medial lobe and cross the midline of the brain via the aLALC. The LAL-CRE1-1 and LAL-CRE1-2 neuron have smooth ramifications in the ipsilateral CRE (Figure 6b,c,g) and LAL. Few processes of the LAL-CRE1-2 neuron also extend into the vest. Within the LAL, smooth ramifications of the LAL-CRE1-1 neuron are sparse and restricted to anterior regions of the LLAL (Figure 6c), whereas arborizations of the LAL-CRE1-2 neuron are more abundant and occupy the LLAL and anterior regions of the ULAL (Figure 6h). Varicose, and thus putatively axonal terminals are present in the contralateral CRE and LAL, and, additionally, in the contralateral epaulet (LAL-CRE1-1 neuron) or in the MAL of both hemispheres (LAL-CRE1-2 neuron). Axonal processes of the LAL-CRE1-1 neuron innervate the contralateral ULAL anteriorly, and the contralateral LLAL (Figure 6d,e). Compared to the LAL-CRE1-1 neuron, the LAL-CRE1-2 neuron has only few axonal endings in the contralateral LAL, which are predominantly concentrated in the LLAL (Figure 6i).

In contrast to LAL-CRE1 neurons, which project anteriorly around the medial lobe, the LAL-CRE2 neuron (Figure 7) projects posteriorly around the medial lobe before its main fiber crosses the brain midline via the aLALC. The neuron has smooth arborizations mainly in the ipsilateral LLAL. Axonal terminals are concentrated in the contralateral ULAL anteriorly, and in the contralateral LLAL (Figure 7b).

LAL-CRE3 neurons (Figure 8) cross the midline of the brain via the LAL commissure (LALC). The LAL-CRE3-1 neuron has smooth ramifications within the ipsilateral ULAL and LLAL (Figure 8b) and beaded arborizations mainly within the contralateral LLAL (Figure 8c), vest, wedge and PS. The LAL-CRE3-2 neuron has even more extensive ramifications outside the LAL, with several side branches giving rise to smooth ramifications in the ipsilateral CRE, MAL, superior medial protocerebrum (SMP), inferior bridge, inferior clamp, posterior ventrolateral protocerebrum (PVLP) and vest. Ramifications within the LAL are restricted to most anterior regions of the LLAL (Figure 8f). The axon bifurcates medial to the LLAL (Figure 8d, red arrows and circles). One branch gives rise to varicose arborizations in the ipsilateral PVLP, anterior ventrolateral protocerebrum (AVLP) and vest. The other branch projects via the LALC and has mirror-symmetric axonal endings in the contralateral PVLP, AVLP (Figure 8e) and vest.

The polarization-sensitive LAL-CRE4 neuron (Figure 9; termed LAL2 neuron in Vitzthum et al., 2002) crosses the midline of the brain

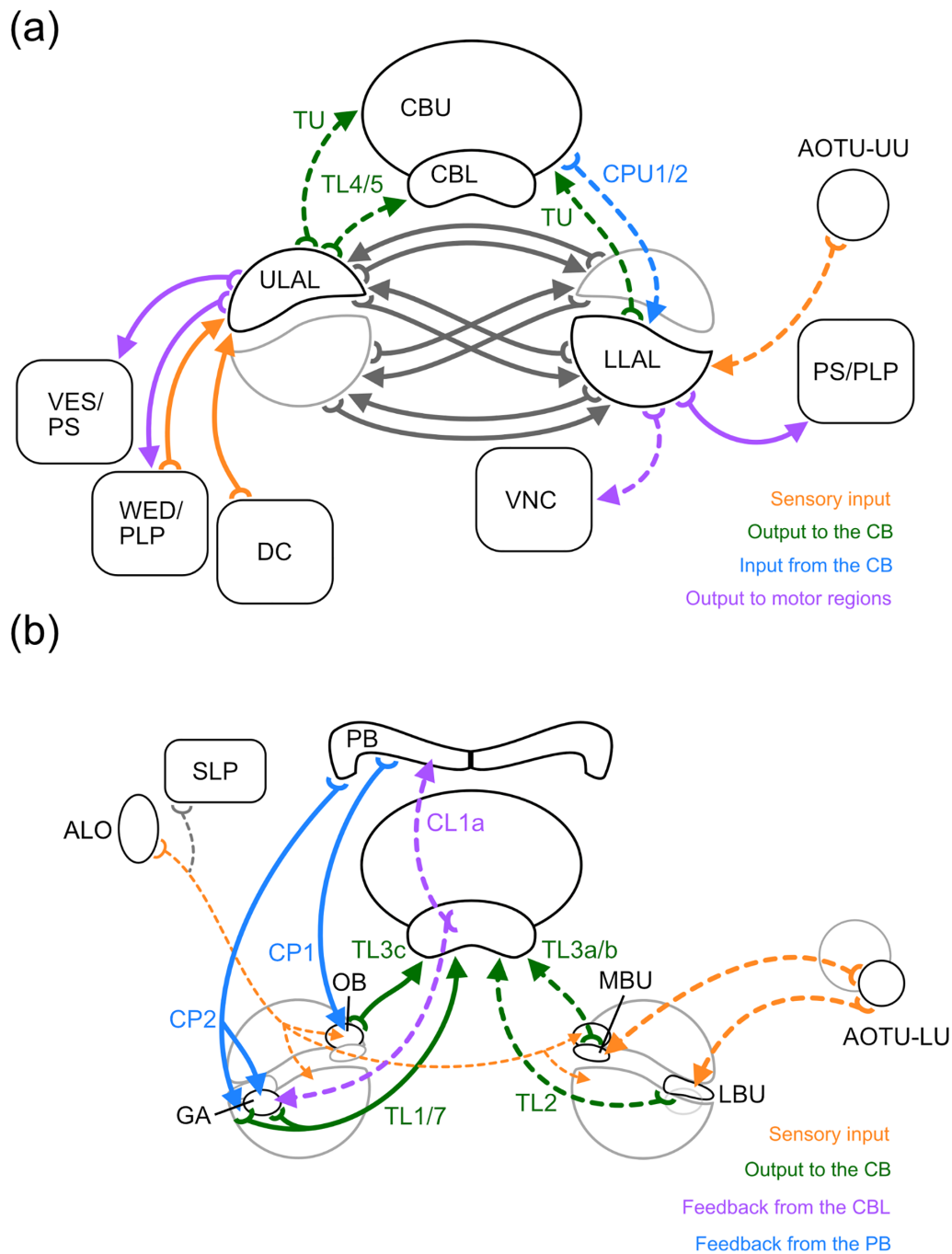


**FIGURE 16** Diagrams illustrating connections between the lateral complex and other brain areas in the desert locust. (a) Most prominent connections of the upper (ULAL) and lower (LLAL) lateral accessory lobe with other brain areas and the ventral nerve cord (VNC). Each arrow represents at least five labeled neurons, except for connections with the VNC (three stained neurons). Connections with the upper and lower division of the central body (CBU, CBL), the deutocerebrum (DC) and the upper unit of the anterior optic tubercle (AOTU-UU) consist of substantially larger cell numbers. (b) Connections of the lateral (LBU) and medial (MBU) bulb, the ovoid body (OB) and gall (GA). Thick lines indicate connections by sets of neurons, thin lines, connections by few individual neurons. Sensory input from the lower unit of the anterior optic tubercle (AOTU-LU) is transmitted via the LBU and MBU into the CBL. Feedback loops between the PB and CBL are established via the OB and the GA. The OBs get additional input from the superior lateral protocerebrum and anterior lobe of the lobula (ALO). CL, columnar neurons of the PB and CBL; CP, columnar neurons of the PB; CPU, columnar neurons of the PB and CBU; PLP, posterior lateral protocerebrum; PS, posterior slope; SLP, superior lateral protocerebrum; TL, tangential neurons of the CBL; TU, tangential neurons of the CBU; WED, wedge; VES, vest. Solid lines indicate findings of this study, dashed lines, data from Homberg (1991, 1994), Homberg et al. (2003), Heinze and Homberg (2008, 2009), von Hadeln et al. (2020), and Homberg et al. (2020) [Color figure can be viewed at [wileyonlinelibrary.com](https://onlinelibrary.wiley.com)]



**TABLE 1** Neurons of the lateral accessory lobes in the locust *Schistocerca gregaria*, presented in this study and their putative input and output domains

| Cell type  | Input domains                             | Output domains                              | Midline crossing        | Corresponding neurons in other studies and species   |
|------------|---|---|-------------------------|--|
| TL3c       | OB  | CBL layer 6, 2                              | Ventral face of the CBL | ER3a subtypes (Hulse et al., 2020; <i>Drosophila melanogaster</i> ) <sup>a</sup>   |
| TL7        | LAL, GA                                   | CBL layer 1, 6, LAL                         | Ventral face of the CBL | ER6 (Hulse et al., 2020; <i>D. melanogaster</i> ) <sup>a</sup>   |
| LAL-CRE1-1 | LLAL, CRE                                 | <b>LAL, CRE, EPA</b>                        | aLALC                   |  |
| LAL-CRE1-2 | LAL, CRE, VES                             | <b>LLAL, CRE, VES, MAL</b>                  | aLALC                   |  |
| LAL-CRE2   | LLAL                                      | <b>LAL</b>                                  | aLALC                   |  |
| LAL-CRE3-1 | LAL                                       | <b>LLAL, VES, WED, PS</b>                   | LALC                    |  |
| LAL-CRE3-2 | LLAL, CRE, SMP, MAL, IB, ICL, PVLP, VES   | PVLP, AVLP, VES                             | LALC                    | Figure 10 (Homberg, 1994; <i>S. gregaria</i> )   |
| LAL-CRE4   | LAL, AOTU-UU, CRE, ICL, WED               | <b>LAL, CRE, AOTU-UU, ICL, WED, VES, PS</b> | aLALC                   | LAL2 (Vitzthum et al., 2002; <i>S. gregaria</i> )  |
| LAL-LAL1   | LAL, MAL, WED                             | <b>LLAL, WED, PS</b>                        | LALC                    | S6 (Homberg, 1991; <i>S. gregaria</i> ), p1BN (Figure 3, Iwano et al., 2010; <i>Bombyx mori</i> )                            |
| LAL-LAL2   | ULAL, MC, PLP, WED, EPA                   | <b>ULAL, MC, VES, WED, PLP, EPA</b>         | LALC                    | 107a,b,c (Boyan et al., 1993; <i>S. gregaria</i> ), WL-L (Hulse et al., 2020; <i>D. melanogaster</i> ) <sup>a</sup>          |
| LAL-LOX1   | ALO                                       | LAL, WED, PS                                | –                       | LC33b (Hulse et al., 2020; <i>D. melanogaster</i> ) <sup>a</sup>   |
| LAL-SIP1   | LAL, CRE, AVLP, SCL, ALI, MAL, ICL, CBU   | MAL, N, IB, SMP, ICL, ATL, PS               | Superior commissure     |  |
| LAL-SIP2   | LLAL, CRE, MAL                            | IB, ATL, PS                                 | IB                      |  |
| LAL-PS1    | PS, ATL, IB, VES, N                       | LLAL, MAL, CRE                              | –                       |  |
| LAL-PS2-1  | PS  | <b>LLAL, VES, WED, PS</b>                   | LALC                    |  |
| LAL-PS2-2  | LAL, WED, PS                              | <b>ULAL, WED, PS, OR</b>                    | LALC                    |  |
| DN-PI(2)   | LAL, SMP, ICL, MAL, ATL, IB, VES, WED, PS | PS, DC                                      | –                       | DN-PI(2) (Homberg, 1994; Williams, 1975; <i>S. gregaria</i> )  |
| DN-CRE     | LAL, MAL, VES, PS                         | PS, DC                                      | –                       | i5-type (Staudacher, 2001; <i>Gryllus bimaculatus</i> ), DNa01-10 (Hulse et al., 2020; <i>D. melanogaster</i> ) <sup>a</sup> |

Notes: Italic: ipsilateral neuropils. Bold: contralateral neuropils. Regular: ipsi- and contralateral neuropils.

Abbreviations: aLALC, anterior LAL commissure; ALI, anterior lip; ALO, anterior lobe of the lobula complex; AOTU-UU, upper unit of the anterior optic tubercle; ATL, antler; AVLP, anterior ventrolateral protocerebrum; CBU, upper division of the central body; CRE, crepine; DC, deutocerebrum; EPA, epaulet; IB, inferior bridge; ICL, inferior clamp; LAL, lateral accessory lobe; LALC, LAL commissure; LLAL, lower LAL; MAL, medial accessory lobe; MC, median crescent; N, neck; OR, ocellar root; PLP, posterior lateral protocerebrum; PS, posterior slope; PVLP, posterior ventrolateral protocerebrum; SIP, superior intermediate protocerebrum; SCL, superior clamp; SLP, superior lateral protocerebrum; SMP, superior medial protocerebrum; ULAL, upper LAL; VES, vest; WED, wedge.

<sup>a</sup>Likely candidates.

via the aLALC. From its cell body near the CRE the cell body fiber projects posterior-medially and splits into three branches. One branch runs laterally toward the anterior optic tubercle and gives rise to a dense mesh of fine arborizations within the upper unit of the anterior optic tubercle (Figure 9b). Some processes also extend into the CRE. Another branch projects into the ipsilateral LAL, inferior clamp and wedge. Fine arborizations are distributed anteriorly in the ULAL and in the whole LLAL (Figure 9c). The third branch projects anteriorly around the medial lobe of the mushroom body toward the brain midline. Before crossing the brain midline via the aLALC one side branch splits off, projects posteriorly and innervates the vest and PS with varicose terminals. After crossing the brain midline, the neuron gives rise to varicose arborizations in the contralateral CRE, the upper unit of the anterior optic tubercle, the LAL (Figure 9a,d),

inferior clamp, wedge, vest and PS. Again, ramifications are concentrated anteriorly in the ULAL and throughout the whole LLAL (Figure 9d).

### 3.6 | LAL-LAL neurons

LAL-LAL neurons (Figure 10) have their somata medial from the antennal lobe and LAL. The LAL-LAL1 neuron has smooth ramifications in the ipsilateral LAL (Figure 10b), the MAL and the wedge. Ramifications are distributed throughout the LLAL, whereas only few processes project into anterior regions of the ULAL (Figure 10b). Midline crossing occurs via the LALC. Axonal terminals are present in the contralateral LLAL (Figure 10c), wedge and PS.

Ionophoretic dye injection via electroporation led to labeling of about 14 neurons of the same type, termed LAL-LAL2 (Figure 10d–g). Their somata are located medial from the antennal lobe and LAL. Smooth arborizations are present in the ipsilateral median crescent (Figure 10e), ULAL (Figure 10f), wedge, posterior lateral protocerebrum and epaulet. The median crescent is a crescent-shaped area in the posterior medial part of the antennal lobe (von Hadeln et al., 2018) that has not been described in other insects. Fibers run through the LALC into the contralateral hemisphere, where varicose ramifications occupy the ULAL (Figure 10g), the median crescent, vest, wedge, posterior lateral protocerebrum and epaulet.

### 3.7 | LAL-LOX neuron

The LAL-LOX1 neuron (Figure 11) connects the ipsilateral lobula complex (LOX) to the ipsilateral LAL. Its soma is located ventrally near the LOX. The neuron has smooth ramifications in the anterior lobe of the lobula complex and varicose arborizations in the PS, wedge and LAL. Within the LAL arborizations are mainly confined to the LLAL with only few processes reaching into the anterior ULAL (Figure 11b,c).

### 3.8 | LAL-SIP neurons

LAL-SIP neurons (Figure 12) have their somata in the dorsal brain anterior (LAL-SIP1) or posterior (LAL-SIP2) to the SIP. The main neurites of both neurons split into two branches, one of which gives rise to smooth arborizations in the anterior brain and the other, to varicose arborizations in posterior brain regions. The LAL-SIP1 neuron has smooth processes in the ipsilateral CRE, AVLP, superior clamp, LAL and anterior lip. Innervation within the LAL is restricted to anterior regions and is more abundant in the ULAL than the LLAL (Figure 12b). A few fine processes of the neuron extend into the CBU, MAL, inferior clamp, and the contralateral anterior lip. Varicose terminals of the LAL-SIP1 neuron are ipsilaterally in the MAL and neck and bilaterally in the SMP, inferior clamp, antler, inferior bridge and PS (Figure 12a,c). The LAL-SIP2 neuron (Figure 12d–f) has smooth arborizations in the ipsilateral CRE, LLAL and MAL. Only anterior regions of the LLAL are innervated (Figure 12e). Varicose arborizations of the neuron are present bilaterally in the inferior bridge (Figure 12f), antler, and a dorsal band of the PS.

### 3.9 | LAL-PS neurons

LAL-PS neurons (Figures 13 and 14) have their somata close to the PS. The LAL-PS1 neuron (Figure 13) has its soma near the brain midline at the posterior surface of the brain and ramifies in the ipsilateral hemisphere only. The neuron has wide dendritic ramifications throughout the PS (Figure 13b) with some processes extending into the antler, the inferior bridge, the vest, and the neck. An axonal fiber projects dorsally around the central body and gives rise to axonal terminals in

the MAL, the LLAL, and the CRE (Figure 13c,d). The LAL-PS2-1 and LAL-PS2-2 neuron (Figure 14) were labeled in the same preparation. The cell bodies of both neurons are located more dorsally and laterally at the posterior surface of the brain than that of the LAL-PS1 neuron. Smooth arborizations of the LAL-PS2-1 neuron invade the ipsilateral PS (Figure 14b). A major neurite crosses the brain midline via the LALC and ramifies with beaded terminals in posterior regions of the contralateral LLAL (Figure 14c). Some processes extend further posterior into the vest, wedge, and PS. The LAL-PS2-2 neuron has few, fine branches in the ipsilateral LAL (Figure 14d), wedge and PS. It crosses the brain midline in the LALC and has axonal terminals in posterior regions of the contralateral ULAL (Figure 14c, arrowhead), the wedge, PS and ocellar root (Figure 15e).

### 3.10 | Descending neurons

Two descending neurons with ramifications in the LAL were encountered (Figure 15). The soma of the DN-PI(2) neuron (Figure 15a–c) is located anteriorly in the pars intercerebralis, medially to the calyx of the mushroom body. The main neurite runs ventrally along the MALT and gives off side branches with smooth endings in the SMP, inferior clamp, MAL, LAL, antler, inferior bridge, vest, wedge, and PS. Fine processes mainly innervate anterior regions of the ULAL and the whole LLAL (Figure 15b,c). The ventral tip of the PS and the deutocerebrum house varicose ramifications. The DN-CRE neuron (Figure 15d–f) has its soma near the CRE. Its main neurite projects posterior-medially in an arc between the vertical lobe and the pedunculus of the mushroom body toward the posterior surface of the LX. Several prominent side branches extend from the main neurite and form smooth ramifications within anterior regions of the ULAL and in the LLAL (Figure 15e), MAL, vest, and PS. As the main neurite runs further ventrally, several varicose processes innervate ventral regions of the PS and deutocerebral areas (Figure 15f).

## 4 | DISCUSSION

The lateral complex (LX), found in the brain of all insects, can be regarded as the most important interface in the communication between the CX and other brain areas. The LXs are involved in the transfer of orientation-related sensory information to the CX and play a crucial role in the control of goal-directed steering behavior (Namiki & Kanzaki, 2016; Pfeiffer & Homberg, 2014; Steinbeck et al., 2020). We have characterized novel subdivisions of the LX in the brain of the desert locust, likely involved in feedback loops within the sky compass network of the CX, and show that the lateral accessory lobes (LALs), beyond their strong mutual connections with the CX, are widely connected with each other, numerous other brain areas, and, through descending neurons, with the ventral nerve cord (Figure 16; Table 1). These data add substantial insights into the role of these brain areas in sensory integration and motor control.

The LX consists of two distinct areas, the bulbs (BUs) and the LAL (Ito et al., 2014). The BUs are clusters of microglomerular complexes that relay spatial visual information from the lower unit of the anterior optic tubercle to the CBL (Hardcastle et al., 2021; Held et al., 2016; Mota et al., 2016; Omoto et al., 2017; Seelig & Jayaraman, 2013, 2015; Shiozaki & Kazama, 2017; Träger et al., 2008). The LAL mediates various other sensory input, such as optic flow information toward the noduli (Stone et al., 2017), wind direction signals to the central body (Currier et al., 2020; Okubo et al., 2020), and self-generated proprioceptive information to the central body (Homberg, 1994; Hulse et al., 2020). In addition, the LALs are also the main targets of output commands from the CX and use these to control goal-directed steering via bilateral interactions and contacts to descending pathways as shown in the locust, silk moth, cockroach, and fruit fly (Namiki, Dickinson, et al., 2018; Namiki & Kanzaki, 2016; Namiki, Wada, & Kanzaki, 2018; Rayshubskiy et al., 2020; Steinbeck et al., 2020).

#### 4.1 | Recurrent feedbacks via the GA and OB

Detailed analysis of the arborization areas of CL1a-, CP1-, CP2-, and TL1 neurons and two new types of TL neuron (TL3c, TL7) in the LX revealed anatomical evidence for feedbacks within the navigation network of the CX via two small compartments in the LX, the gall (GA) and the ovoid body (OB) (Figure 16b). Unlike in the fly (Ito et al., 2014) and monarch butterfly (Heinze & Reppert, 2012), but similar to bees (Hensgen et al., 2021), the GA of the locust, defined as the projection site of CL1 neurons in the LAL, has poorly defined borders and, therefore, cannot be recognized as a distinct area by synapsin labeling. Reanalysis of the projections of a population of CL1 neurons, labeled by an antiserum against locustatachykinin (Vitzthum & Homberg, 1998) might help in the future to better define the GA in the locust. Together with CL1a neurons, CP2-, TL1-, and TL7 neurons arborize in the GA anterior to the LBU. Whereas ramifications of CL1a neurons are restricted to the GA, ramifications of CP2, TL1 and TL7 neurons occupy a larger area surrounding the LBU also posteriorly and dorsally. These overlapping arborization domains in the LX suggest not only recurrent loops between neurons of the same type but also the existence of feedback loops between columnar and tangential neurons. In *Drosophila* (Hulse et al., 2020) E-PG (CL1a) neurons connect onto P-EG (CL1b/d) neurons in the GA. Both types of neuron are recurrently connected with ER6 neurons, that show morphological similarities to the newly identified TL7 neuron, in the EB (CBL) and the GA. P-EG and E-PG neurons also synapse onto ExR4 neurons, likely homologous to TL1 neurons (von Hadeln et al., 2020) in the GA (Hulse et al., 2020). These findings support the idea that similar connections between CL1-, TL1- and TL7 neurons in the GA also exist in the locust. However, whether the TL7 neuron is a homologue of the ER6 neuron remains unclear, because the neurons differ in their projections in the CBL and in their ramifications bilateral to the CBL, that are conspicuous in the TL7 neuron but are lacking in the ER6 neuron. Apparently, there are no homologues of CP2 neurons in the fruit fly.

However, two types of neuron in the fly, EL and P-FGs, arborize in an undefined region around the GA, called the GA surround (GAs; Hulse et al., 2020). EL neurons arborize in the ellipsoid body and the GAs, whereas the P-FGs neurons have arborizations in the PB, fan-shaped body (CBU), and GAs. Whether the GAs corresponds to the region around the LBU innervated by CP2 neurons is not clear. If so, TL1- and TL7 neurons would also innervate the GAs, but this has not been reported for the corresponding ring neurons (ExR4 and ER6) in *Drosophila*.

Analysis of ramifications of CP1 neurons and TL3c neurons in the LX of the locust revealed a distinct region posterior to the MBU, the OB (Figure 16b). TL3c neurons show a distinct pattern of innervation in the CBL, ramifying in layer 2 and layer 6. In the OB their arborizations appear to be a mixture of microglomerular structures and fine processes. TL3c neurons might correspond to ER3a\_b (two per hemisphere) or ER3a\_c neurons (two per hemisphere) in *Drosophila* (Table 1; Hulse et al., 2020) as they have ramification areas outside, but close to the BU, too. These projection sites in *Drosophila* might thus correspond to the locust OB but there is no evidence that ER3a\_b/c are prominently involved in a CX feedback loop. As for the CP2 neurons, there appear to be no homologues to CP1 neurons in *Drosophila*. In the fruit fly two neuropils were identified in close proximity to the BU and GA that are not known in the locust; the round body (ROB) and the rubus (RUB). Both structures are innervated by columnar neurons of the fan shaped body. PFR neurons innervate the ROB and FR neurons arborize in the RUB. PFR neurons have been assumed to be homologues of CPU1 neurons in the locust and other insects (Honkanen et al., 2019), whereas FR neurons, arborizing in the fan-shaped body (CBU) and in the RUB could be homologues to certain types of CU neurons in the locust. Based on this, the OB would neither correspond to the ROB nor the RUB in the fly brain. In addition to a possible connection between CP2- and TL3c neurons in the OB there are additional inputs to the OB by other neurons. Among them is a bilateral innervation of the two OBs by a leucokinin-positive projection neuron from the lobula (Homberg et al., 2003), schematically illustrated in Figure 16b and a pair of serotonin-positive neurons (Homberg, 1991).

The functional significance of these two recurrent loops is presently unclear. TL1-, CL1a-, CP1-, and CP2 neurons are part of the sky compass network in the CX (Bockhorst & Homberg, 2015; Heinze & Homberg, 2007; Pegel et al., 2018; Vitzthum et al., 2002; Zittrell et al., 2020). Because projection neurons from the lower unit of the anterior optic tubercle exclusively target the BUs, but do not innervate the GA, the relatively weak polarization sensitivity of TL1 neurons might result exclusively from convergence of synaptic input from contralateral CL1a- and CP2 neurons.

#### 4.2 | Sensory input to the LAL

Besides its strong mutual connections with the CX, in particular the CBU (Heinze & Homberg, 2008; von Hadeln et al., 2020), the LAL houses a variety of neurons that provide connections to other brain

areas (Figure 16a; Table 1). In addition to previously characterized input from the upper unit of the anterior optic tubercle, likely providing visual input (Homberg et al., 2003), the LAL-LOX neuron described here, provides an even more direct visual input to the LAL. In *Drosophila* around 77 individual neurons connect the lobula with the ipsilateral LAL (Scheffer et al., 2020). Although most of those neurons show some similarities to the LAL-LOX neuron, perhaps closest to LC33b (Table 1; Scheffer et al., 2020; Hulse et al., 2020) complete matching was not found. The LAL-CRE4 neuron, which is weakly sensitive to polarization angle (Vitzthum et al., 2002), provides bilateral connections between both anterior optic tubercles, LALs and posterior brain regions, and thus further strengthens the connectivity between the upper unit of the anterior optic tubercle and LAL. Numerous neurons connecting the larger subunit of the anterior optic tubercle to the LAL are, likewise, present in *Drosophila* and, judged from physiological data on anterior optic tract neurons, might be involved in object detection and figure-ground discrimination (Aptekar et al., 2015; Collett, 1972).

Another neuropil associated with putative sensory input into the LAL is the wedge. In silkmoths the ventral protocerebrum, likely corresponding to the wedge, is closely connected via feedback loops to the LAL (Iwano et al., 2010). In *Drosophila*, the wedge is targeted by neurons of the antennal mechanosensory and motor center and integrates information about the displacement of both antennae upon wind stimulation (Patella & Wilson, 2018; Suver et al., 2019). Neurons connecting the wedge to a narrow dorsal strip of the LAL (WL-L neurons) and postsynaptic cells connecting this strip to the noduli (LNa neurons) and ellipsoid body (R1 and R3a neurons) provide directional wind input to the central body (Currier et al., 2020; Okubo et al., 2020). A similar pathway appears to be present in the locust. As shown here, a group of more than a dozen LAL-LAL2 neurons (Figure 10d–g) connects the median crescent, an antennal neuropil, bilaterally to the wedge and the ULAL (Figure 10d–g). As in the fly, these neurons extensively innervate the small posterior region of the ULAL superior to the LALC, that is omitted by several other LAL neurons described here, but is innervated by TL4 neurons of the CBL (likely homologous to R1/R3a neurons in the fly) as well as TN1 neurons (corresponding to LNa neurons in the fly), that project to the noduli (Homberg et al., 2020; von Hadeln et al., 2020). The median crescent is a small neuropil posterior-medially attached to the antennal lobe (Kurylas et al., 2005). Its sensory input has not been determined, but it is not innervated by flagellar afferents of the antenna (von Hadeln et al., 2018).

### 4.3 | Motor output from the LAL

Three classes of LAL neurons, widely found across insect species, were proposed to serve a direct role in motor control networks: (i) neurons connecting the two LALs bilaterally, (ii) neurons projecting from the LAL to other brain areas, in particular the PS, and (iii) descending neurons with inputs in the LAL (Adden, Stewart, et al., 2020; Namiki & Kanzaki, 2016; Steinbeck et al., 2020). The bilateral LALs are densely connected by commissural interneurons; in

the silk moth, as many as 60 fibers were counted in the LAL commissure (Namiki & Kanzaki, 2016), and in *Drosophila*, at least 57 commissural neurons (LAL073 – LAL122) show similarly restricted arborizations to the LAL as some neurons described here (Table 1; Scheffer et al., 2020). These neurons are believed to provide mutual inhibition of the two LALs and thereby play an essential role in integrating direct sensory signals and compass output from the CX into steering commands (Adden, Stewart, et al., 2020; Iwano et al., 2010). Descending neurons of the LAL show activity correlated with pheromone-triggered turning behavior in the silk moth (Kanzaki et al., 1994; Mishima & Kanzaki, 1999), compass-directed steering in the fruit flies (Rayshubskiy et al., 2020), and phonotactic steering in the cricket (Zorović & Hedwig, 2011, 2013). In the locust activity of individual descending LAL neurons, including the DN-PI(2) neuron, precedes flight activity (Homberg, 1994). The newly identified DN-CRE neuron (Figure 15d) is highly similar to i5-type descending neurons in the cricket, *Gryllus bimaculatus* (Table 1; Staudacher & Schildberger, 1998; Staudacher, 2001). These neurons responded to air puffs delivered to the cerci, ipsilaterally moving gratings, and the conspecific calling song, however only during walking, indicating strong dependence on behavioral context (Staudacher, 1998; Staudacher, 2001).

Although these findings point to the LAL as directly relaying locomotor commands to thoracic motor centers, descending LAL neurons, including the neurons shown here, generally receive additional input in other brain areas, in particular the PS (Homberg, 1994; Namiki, Dickinson, et al., 2018; Namiki & Kanzaki, 2016; Namiki, Wada, et al., 2018; Staudacher, 2001). In fact, only a small fraction of descending neurons innervates the LAL, but most receive input in the PS and adjacent areas in the posterior brain (Namiki, Dickinson, et al., 2018; Namiki, Wada, et al., 2018). As shown here and in previous accounts (Heinze & Homberg, 2009; Homberg, 1994), the LAL is strongly connected to the PS by different types of neuron, which provide information flow from the LAL to the PS (Figure 16a) and to a lesser extent vice versa (Figure 14). In addition to direct input to descending neurons, the LAL, therefore, likely exerts its role in motor control largely via indirect connections with descending neurons from other brain areas such as the PS. Accordingly, two descending neurons in the locust sensitive to polarization angle had dendritic ramifications in the PS but not in the LAL (Träger & Homberg, 2011).

### 4.4 | Connections of the LAL with the crepine and superior protocerebrum

In addition to the PS, many neurons of the LAL made connections with the CRE and some with the SMP. CRE and LAL appear to be connected mostly in parallel, that is, they appear to be either parallel input sites or parallel output sites of the respective neuron (or both). Likewise, many tangential inputs from the LAL to the CBU have dendritic trees extending to the CRE (von Hadeln et al., 2020). This has also been found in *Drosophila* (Hulse et al., 2020). Although the CRE



constitutes a large portion of the anterior brain, little is known about its functional role. In *Drosophila* the CRE, together with the SIP and SMP, is strongly innervated by output neurons of the mushroom body (Li et al., 2020), and even direct projections of mushroom body output neurons to the LAL have been encountered (Li et al., 2020). As proposed by Hulse et al. (2020) these neurons might provide valence signals to the CBU, related to sleep or navigation.

As reviewed by Namiki and Kanzaki (2016) the SMP has various connections with the LAL in different insect species, including the silk moth, fruit fly, monarch butterfly, flesh fly, and desert locust. In each species, at least some of these neurons are tangential neurons of the CBU. Von Hadeln et al. (2020) and el Jundi et al. (2018) have described additional types of tangential neuron of the CBU with arborizations in the SMP in the locust and the dung beetle, respectively. In *Drosophila* the SMP is, like the CRE, densely targeted by output neurons of the mushroom body (Aso et al., 2014; Li et al., 2020), and both areas are likely involved in relaying learned associations from the mushroom body to the CBU.

#### 4.5 | Modular organization of the LAL

In several insect species the LAL is divided into two major subdivisions, the ULAL and LLAL (Ito et al., 2014) that differ in innervation of certain cell types, for example, classes of bilateral LAL neurons or types of CX neurons, suggesting different functional roles (Namiki & Kanzaki, 2016). In the locust, arborizations of most neurons extend across both compartments, however, with higher density of ramifications in the LLAL or ULAL. Data from this and previous studies (Heinze & Homberg, 2008, 2009; Homberg et al., 2003; Homberg et al., 2020; von Hadeln et al., 2020) show that, in addition to wide connections of both compartments with many brain areas, the ULAL receives prominent input from antennal neuropil (Figure 10d–g) and provides predominantly input to the CBL and CBU via tangential neurons (Figure 16a). The LLAL, on the other hand, receives the majority of visual input from the upper unit of the anterior optic tubercle (and lobula), is bilaterally connected with the CBU via tangential and columnar neurons, and largely provides output from the LAL to the PS/posterior lateral protocerebrum and ventral nerve cord (Figure 16a). Both LLAL and ULAL are, furthermore, strongly connected with their contralateral counterparts by large numbers of commissural neurons (Figure 16a). These data indicate a bias between both compartments in funneling antennal and visual input to the CX and suggest a closer association of the LLAL with motor control. Interestingly, these functional differences between the two LAL compartments may not be shared across species as pointed out by Namiki and Kanzaki (2016). In the fruit fly, monarch butterfly, silk moth, and dung beetle, both tangential and columnar neurons of the CX ramify in dorsal aspects of the LAL, while arborizations of descending neurons in the fly and silk moth are concentrated like in the locust in ventral parts (el Jundi et al., 2018; Heinze et al., 2013; Hulse et al., 2020; Namiki & Kanzaki, 2016; Scheffer et al., 2020). Whether these differences reflect stronger feedback between CX

inputs and outputs in holometabolous species than in the locust, or reflect other differences in the internal organization of the LALs, awaits further analysis.

#### ACKNOWLEDGMENTS

We are grateful to Tobias Bockhorst, Ulrike Haberland, Anja Nohe, Sabine Thiel, and Frederick Zittrell for contributing the preparations of Figures 9 (A.N.), 10a–c (F.Z.), 10d–g (U.H.), 12a–c (S.T.), and 12d–f (T.B.). We thank Drs. Christian Wegener and Erich Buchner for providing anti-synapsin antibodies, Dick Nässel for donating anti-leucokinin antiserum, Heinrich Dirksen for providing anti-orcokinin antiserum, and Jutta Seyfarth for technical assistance. Funding was obtained from Deutsche Forschungsgemeinschaft, grant number: HO 950/26-1 and HO 950/28-1.

Open access funding enabled and organized by Projekt DEAL.

#### CONFLICT OF INTEREST

The authors declare no conflict of interest.

#### AUTHOR CONTRIBUTIONS

Study concept and design: Uwe Homberg, Ronja Hensgen; acquisition of data: Ronja Hensgen, Jonas Göthe, Stefanie Jahn, Sophie Hümmert, Kim Lucia Schneider, Naomi Takahashi, Uta Pegel, Sascha Gotthardt; data analysis and interpretation: Ronja Hensgen, Jonas Göthe, Stefanie Jahn, Sophie Hümmert, Kim Lucia Schneider; drafting the manuscript: Ronja Hensgen; review and editing: Uwe Homberg, Ronja Hensgen.

#### PEER REVIEW

The peer review history for this article is available at <https://publons.com/publon/10.1002/cne.25209>.

#### DATA AVAILABILITY STATEMENT

Three-dimensionally reconstructed models and confocal image stacks of all fluorescently labeled neurons are freely available from the InsectBrainDatabase (Heinze et al., 2020). All data that support the findings of this study are available from the corresponding author.

#### ORCID

Ronja Hensgen  <https://orcid.org/0000-0002-4876-9084>

Uwe Homberg  <https://orcid.org/0000-0002-8229-7236>

#### REFERENCES

- Adden, A., Wibrand, S., Pfeiffer, K., Warrant, E., & Heinze, S. (2020) The brain of a nocturnal migratory insect, the Australian Bogong moth. *Journal of Comparative Neurology*, 528, 1942–1963.
- Aptekar, J. W., Keleş, M. F., Lu, P. M., Zolotova, N. M., & Frye, M. A. (2015). Neurons forming optic glomeruli compute figure-ground discriminations in *Drosophila*. *Journal of Neuroscience*, 35(19), 7587–7599. <https://doi.org/10.1523/JNEUROSCI.0652-15.2015>
- Aso, Y., Hattori, D., Yu, Y., Johnston, R. M., Iyer, N. A., Ngo, T.-T. B., Dionne, H., Abbott, L. F., Axel, R., Tanimoto, H., & Rubin, G. M. (2014). The neuronal architecture of the mushroom body provides a logic for associative learning. *eLife*, 3, e04577. <https://doi.org/10.7554/eLife.04577>

- Bender, J. A., Pollack, A. J., & Ritzmann, R. E. (2010). Neural activity in the central complex of the insect brain is linked to locomotor changes. *Current Biology*, 20(10), 921–926. <https://doi.org/10.1016/j.cub.2010.03.054>
- Bockhorst, T., & Homberg, U. (2015). Amplitude and dynamics of polarization-plane signaling in the central complex of the locust brain. *Journal of Neurophysiology*, 113(9), 3291–3311. <https://doi.org/10.1152/jn.00742.2014>
- Bockhorst, T., & Homberg, U. (2017). Interaction of compass sensing and object-motion detection in the locust central complex. *Journal of Neurophysiology*, 118(1), 496–506. <https://doi.org/10.1152/jn.00927.2016>
- Bodian, D. (1936). A new method for staining nerve fibers and nerve endings in mounted paraffin sections. *Anatomical Record*, 65(1), 89–97. <https://doi.org/10.1002/ar.1090650110>
- Boyan, G., Williams, L., & Meier, T. (1993). Organization of the commissural fibers in the adult brain of the locust. *Journal of Comparative Neurology*, 332(2), 358–377. <https://doi.org/10.1002/cne.903320308>
- Bungart, D., Dirksen, H., & Keller, R. (1994). Quantitative determination and distribution of the myotropic neuropeptide orcokinin in the nervous system of astacidean crustaceans. *Peptides*, 15(3), 393–400. [https://doi.org/10.1016/0196-9781\(94\)90194-5](https://doi.org/10.1016/0196-9781(94)90194-5)
- Clements, A. N., & May, T. E. (1974). Studies on locust neuromuscular physiology in relation to glutamic acid. *Journal of Experimental Biology*, 60, 673–705.
- Collett, T. (1972). Visual neurones in the anterior optic tract of the privet hawk moth. *Journal of Comparative Physiology*, 78, 396–433. <https://doi.org/10.1007/BF01417943>
- Currier, T. A., Matheson, A. M. M., & Nagel, K. I. (2020). Encoding and control of airflow orientation by a set of *Drosophila* fan-shaped body neurons. *eLife*, 9, e61510. <https://doi.org/10.7554/eLife.61510>
- el Jundi, B., Baird, E., Byrne, M. J., & Dacke, M. (2019). The brain behind straight-line orientation in dung beetles. *Journal of Experimental Biology*, 222, jeb192450. <https://doi.org/10.1242/jeb.192450>
- el Jundi, B., Heinze, S., Lenschow, C., Kurylas, A., Rohlfing, T., & Homberg, U. (2010). The locust standard brain: A 3D standard of the central complex as a platform for neural network analysis. *Frontiers in Systems Neuroscience*, 3, 21. <https://doi.org/10.3389/neuro.06.021.2009>
- el Jundi, B., Warrant, E. J., Pfeiffer, K., & Dacke, M. (2018). Neuroarchitecture of the dung beetle central complex. *Journal of Comparative Neurology*, 526(16), 2612–2630. <https://doi.org/10.1002/cne.24520>
- Evers, J. F., Schmitt, S., Sibila, M., & Duch, C. (2005). Progress in functional neuroanatomy: Precise automatic geometric reconstruction of neuronal morphology from confocal image stacks. *Journal of Neurophysiology*, 93(4), 2331–2342. <https://doi.org/10.1152/jn.00761.2004>
- Green, J., Vijayan, V., Mussells Pires, P., Adachi, A., & Maimon, G. (2019). A neural heading estimate is compared with an internal goal to guide oriented navigation. *Nature Neuroscience*, 22(9), 1460–1468. <https://doi.org/10.1038/s41593-019-0444-x>
- Gregory, G. E. (1980). The Bodian Protogol technique. In N. J. Strausfeld & T. A. Miller (Eds.), *Neuroanatomical techniques: Insect nervous system* (pp. 75–95). Springer. [https://doi.org/10.1007/978-1-4612-6018-9\\_6](https://doi.org/10.1007/978-1-4612-6018-9_6)
- Hardcastle, B. J., Omoto, J. J., Kandimalla, P., Nguyen, B.-C. M., Keleş, M. F., Boyd, N. K., Hartenstein, V., & Frye, M. A. (2021). A visual pathway for skylight polarization processing in *Drosophila*. *eLife*, 10, e63225. <https://doi.org/10.7554/eLife.63225>
- Harley, C. M., & Ritzmann, R. E. (2010). Electrolytic lesions within central complex neuropils of the cockroach brain affect negotiation of barriers. *Journal of Experimental Biology*, 213, 2851–2864. <https://doi.org/10.1242/jeb.042499>
- Heinze, S., el Jundi, B., Berg, B. G., Homberg, U., Menzel, R., Pfeiffer, K., Dacke, M., Warrant, E., Pfuhl, G., Rybak, J., & Tedore, K. (2020). InsectBrainDatabase—A unified platform to manage, share, and archive morphological and functional data. *bioRxiv*, 2020.11.30.397489. <https://doi.org/10.1101/2020.11.30.397489>
- Heinze, S., Florman, J., Asokaraj, S., el Jundi, B., & Reppert, S. M. (2013). Anatomical basis of sun compass navigation II: The neuronal composition of the central complex of the monarch butterfly. *Journal of Comparative Neurology*, 521(2), 267–298. <https://doi.org/10.1002/cne.23214>
- Heinze, S., & Homberg, U. (2007). Maplike representation of celestial E-vector orientations in the brain of an insect. *Science (New York, N.Y.)*, 315(5814), 995–997. <https://doi.org/10.1126/science.1135531>
- Heinze, S., & Homberg, U. (2008). Neuroarchitecture of the central complex of the desert locust: Intrinsic and columnar neurons. *Journal of Comparative Neurology*, 511(4), 454–478. <https://doi.org/10.1002/cne.21842>
- Heinze, S., & Homberg, U. (2009). Linking the input to the output: New sets of neurons complement the polarization vision network in the locust central complex. *Journal of Neuroscience*, 29(15), 4911–4921. <https://doi.org/10.1523/JNEUROSCI.0332-09.2009>
- Heinze, S., & Reppert, S. M. (2012). Anatomical basis of sun compass navigation I: The general layout of the monarch butterfly brain. *Journal of Comparative Neurology*, 520(8), 1599–1628. <https://doi.org/10.1002/cne.23054>
- Held, M., Berz, A., Hensgen, R., Muenz, T. S., Scholl, C., Rössler, W., Homberg, U., & Pfeiffer, K. (2016). Microglomerular synaptic complexes in the sky-compass network of the honeybee connect parallel pathways from the anterior optic tubercle to the central complex. *Frontiers in Behavioral Neuroscience*, 10, 186. <https://doi.org/10.3389/fnbeh.2016.00186>
- Hensgen, R., England, L., Homberg, U., & Pfeiffer, K. (2021). Neuroarchitecture of the central complex in the brain of the honeybee: Neuronal cell types. *Journal of Comparative Neurology*, 529, 159–186. <https://doi.org/10.1002/cne.24941>
- Hofer, S., Dirksen, H., Tollbäck, P., & Homberg, U. (2005). Novel insect orcokinins: Characterization and neuronal distribution in the brains of selected dicondylarian insects. *Journal of Comparative Neurology*, 490(1), 57–71. <https://doi.org/10.1002/cne.20650>
- Homberg, U. (1991). Neuroarchitecture of the central complex in the brain of the locust *Schistocerca gregaria* and *S. americana* as revealed by serotonin immunocytochemistry. *Journal of Comparative Neurology*, 303(2), 245–254. <https://doi.org/10.1002/cne.903030207>
- Homberg, U. (1994). Flight-correlated activity changes in neurons of the lateral accessory lobes in the brain of the locust *Schistocerca gregaria*. *Journal of Comparative Physiology A*, 175, 597–610.
- Homberg, U., Hensgen, R., Rieber, E., Seyfarth, J., Kern, M., Dippel, S., Dirksen, H., Spänig, L., & Kina, Y. P. (2020). Orcokinin in the central complex of the locust *Schistocerca gregaria*: Identification of immunostained neurons and colocalization with other neuroactive substances. *Journal of Comparative Neurology*, 529, 1876–1894. <https://doi.org/10.1002/cne.25062>
- Homberg, U., Hofer, S., Pfeiffer, K., & Gebhardt, S. (2003). Organization and neural connections of the anterior optic tubercle in the brain of the locust, *Schistocerca gregaria*. *Journal of Comparative Neurology*, 462(4), 415–430. <https://doi.org/10.1002/cne.10771>
- Honkanen, A., Adden, A., da Silva Freitas, J., & Heinze, S. (2019). The insect central complex and the neural basis of navigational strategies. *Journal of Experimental Biology*, 222, jeb188854. <https://doi.org/10.1242/jeb.188854>
- Hulse, B. K., Haberkern, H., Franconville, R., Turner-Evans, D. B., Takemura, S., Wolff, T., Noorman, M., Dreher, M., Dan, C., Parekh, R., Hermundstad, A. M., Rubin, G. M., & Jayaraman, V. (2020). A connectome of the *Drosophila* central complex reveals network motifs suitable for flexible navigation and context-dependent action selection. *bioRxiv*. <https://doi.org/10.1101/2020.12.08.413955>
- Ito, K., Shinomiya, K., Ito, M., Armstrong, J. D., Boyan, G., Hartenstein, V., Harzsch, S., Heisenberg, M., Homberg, U., Jenett, A., Keshishian, H., Restifo, L. L., Rössler, W., Simpson, J. H., Strausfeld, N. J., Strauss, R., &

- Vosshall, L. B. (2014). A systematic nomenclature for the insect brain. *Neuron*, 81(4), 755–765. <https://doi.org/10.1016/j.neuron.2013.12.017>
- Iwano, M., Hill, E. S., Mori, A., Mishima, T., Mishima, T., Ito, K., & Kanzaki, R. (2010). Neurons associated with the flip-flop activity in the lateral accessory lobe and ventral protocerebrum of the silkworm moth brain. *Journal of Comparative Neurology*, 518(3), 366–388. <https://doi.org/10.1002/cne.22224>
- Kanzaki, R., Ikeda, A., & Shibuya, T. (1994). Morphological and physiological properties of pheromone-triggered flipflopping descending interneurons of the male silkworm moth, *Bombyx mori*. *Journal of Comparative Physiology A*, 175, 1–14. <https://doi.org/10.1007/BF00217431>
- Kim, S. S., Hermundstad, A. M., Romani, S., Abbott, L. F., & Jayaraman, V. (2019). Generation of stable heading representations in diverse visual scenes. *Nature*, 576, 126–131. <https://doi.org/10.1038/s41586-019-1767-1>
- Klagges, B. R., Heimbeck, G., Godenschwege, T. A., Hofbauer, A., Pflugfelder, G. O., Reifegerste, R., Reisch, D., Schaupp, M., Buchner, S., & Buchner, E. (1996). Invertebrate synapsins: A single gene codes for several isoforms in *Drosophila*. *Journal of Neuroscience*, 16(10), 3154–3165. <https://doi.org/10.1523/JNEUROSCI.16-10-03154.1996>
- Kurylas, A. E., Ott, S. R., Schachtner, J., Elphick, M. R., Williams, L., & Homberg, U. (2005). Localization of nitric oxide synthase in the central complex and surrounding midbrain neuropils of the locust *Schistocerca gregaria*. *Journal of Comparative Neurology*, 484(2), 206–223. <https://doi.org/10.1002/cne.20467>
- Kurylas, A. E., Rohlfig, T., Kroczyk, S., Jenett, A., & Homberg, U. (2008). Standardized atlas of the brain of the desert locust, *Schistocerca gregaria*. *Cell and Tissue Research*, 333, 125–145. <https://doi.org/10.1007/s00441-008-0620-x>
- Leitinger, G., Pabst, M. A., Rind, F. C., & Simmons, J. P. (2004). Differential expression of synapsin in visual neurons of the locust *Schistocerca gregaria*. *Journal of Comparative Neurology*, 480(1), 89–100. <https://doi.org/10.1002/cne.20333>
- Li, F., Lindsey, J. W., Marin, E. C., Otto, N., Dreher, M., Dempsey, G., Stark, I., Bates, A. S., Pleijzier, M. W., Schlegel, P., Nern, A., Takemura, S. Y., Eckstein, N., Yang, T., Francis, A., Braun, A., Parekh, R., Costa, M., Scheffer, L. K., ... Rubin, G. M. (2020). The connectome of the adult *Drosophila* mushroom body: Implications for function. *eLife*, 9, e62576. <https://doi.org/10.7554/eLife.62576>
- Martin, J. P., Guo, P., Mu, L., Harley, C. M., & Ritzmann, R. E. (2015). Central-complex control of movement in the freely walking cockroach. *Current Biology*, 25(21), 2795–2803. <https://doi.org/10.1016/j.cub.2015.09.044>
- Mishima, T., & Kanzaki, R. (1999). Physiological and morphological characterization of olfactory descending interneurons of the male silkworm moth, *Bombyx mori*. *Journal of Comparative Physiology A*, 184(2), 143–160. <https://doi.org/10.1007/s003590050314>
- Mota, T., Kreissl, S., Durán, A. C., Lefer, D., Galizia, G., & Giurfa, M. (2016). Synaptic organization of microglomerular clusters in the lateral and medial bulbs of the honeybee brain. *Frontiers in Neuroanatomy*, 10, 103. <https://doi.org/10.3389/fnana.2016.00103>
- Müller, M., Homberg, U., & Kühn, A. (1997). Neuroarchitecture of the lower division of the central body in the brain of the locust (*Schistocerca gregaria*). *Cell and Tissue Research*, 288, 159–176. <https://doi.org/10.1007/s004410050803>
- Namiki, S., Dickinson, M. H., Wong, A. M., Korff, W., & Card, G. M. (2018). The functional organization of descending sensory motor pathways in *Drosophila*. *eLife*, 7, e34272. <https://doi.org/10.7554/eLife.34272>
- Namiki, S., Iwabuchi, S., Pansopha Kono, P., & Kanzaki, R. (2014). Information flow through neural circuits for pheromone orientation. *Nature Communications*, 5, 5919. <https://doi.org/10.1038/ncomms6919>
- Namiki, S., & Kanzaki, R. (2016). Comparative neuroanatomy of the lateral accessory lobe in the insect brain. *Frontiers in Physiology*, 7, 244. <https://doi.org/10.3389/fphys.2016.00244>
- Namiki, S., Wada, S., & Kanzaki, R. (2018). Descending neurons from the lateral accessory lobe and posterior slope in the brain of the silkworm *Bombyx mori*. *Scientific Reports*, 8(1), 9663. <https://doi.org/10.1038/s41598-018-27954-5>
- Nässel, D. R. (1993). Insect myotropic peptides: Differential distribution of locustatachykinin- and leucokinin-like immunoreactive neurons in the locust brain. *Cell and Tissue Research*, 274, 27–40. <https://doi.org/10.1007/BF00327982>
- Nässel, D. R., Cantera, R., & Karlsson, A. (1992). Neurons in the cockroach nervous system reacting with antisera to the neuropeptide leucokinin I. *Journal of Comparative Neurology*, 322(1), 45–67. <https://doi.org/10.1002/cne.903220105>
- Ofstad, T. A., Zuker, C. S., & Reiser, M. B. (2011). Visual place learning in *Drosophila melanogaster*. *Nature*, 474(7350), 204–207. <https://doi.org/10.1038/nature10131>
- Okubo, T. S., Patella, P., D'Alessandro, I., & Wilson, R. I. (2020). A neural network for wind-guided compass navigation. *Neuron*, 107(5), 924–940.e18. <https://doi.org/10.1016/j.neuron.2020.06.022>
- Omoto, J. J., Keles, M. F., Nguyen, B.-C. M., Bolanos, C., Lovick, J. K., Frye, M. A., & Hartenstein, V. (2017). Visual input to the *Drosophila* central complex by developmentally and functionally distinct neuronal populations. *Current Biology*, 27, 1098–1110. <https://doi.org/10.1016/j.cub.2017.02.063>
- Omoto, J. J., Nguyen, B.-C. M., Kandimalla, P., Lovick, J. K., Donlea, J. M., & Hartenstein, V. (2018). Neuronal constituents and putative interactions within the *Drosophila* ellipsoid body neuropil. *Frontiers in Neural Circuits*, 12, 103. <https://doi.org/10.3389/fncir.2018.00103>
- Patella, P., & Wilson, R. I. (2018). Functional maps of mechanosensory features in the *Drosophila* brain. *Current Biology*, 28(8), 1189–1203. <https://doi.org/10.1016/j.cub.2018.02.074>
- Pegel, U., Pfeiffer, K., & Homberg, U. (2018). Integration of celestial compass cues in the central complex of the locust brain. *Journal of Experimental Biology*, 221, jeb171207. <https://doi.org/10.1242/jeb.171207>
- Pegel, U., Pfeiffer, K., Zittrell, F., Scholtyssek, C., & Homberg, U. (2019). Two compasses in the central complex of the locust brain. *Journal of Neuroscience*, 39(16), 3070–3080. <https://doi.org/10.1523/JNEUROSCI.01940-18.2019>
- Pfeiffer, K., & Homberg, U. (2014). Organization and functional roles of the central complex in the insect brain. *Annual Review of Entomology*, 59, 165–184. <https://doi.org/10.1146/annurev-ento-011613-16203>
- Pfeiffer, K., Kinoshita, M., & Homberg, U. (2005). Polarization-sensitive and light-sensitive neurons in two parallel pathways passing through the anterior optic tubercle in the locust brain. *Journal of Neurophysiology*, 94(6), 3903–3915. <https://doi.org/10.1152/jn.00276.2005>
- Aleksandr, Rayshubskiy, Stephen L. Holtz, Isabel D'Alessandro, Anna A. Li, Quinn X. Vanderbeck, Isabel S. Haber, Peter W. Gibb, Rachel I. Wilson *bioRxiv* 2020.04.04.024703; doi: <https://doi.org/10.1101/2020.04.04.024703>
- Rosner, R., & Homberg, U. (2013). Widespread sensitivity to looming stimuli and small moving objects in the central complex of an insect brain. *Journal of Neuroscience*, 33(19), 8122–8133. <https://doi.org/10.1523/JNEUROSCI.5390-12.2013>
- Rosner, R., Pegel, U., & Homberg, U. (2019). Responses of compass neurons in the locust brain to visual motion and leg motor activity. *Journal of Experimental Biology*, 222(Pt. 8), jeb196261. <https://doi.org/10.1242/jeb.196261>
- Scheffer, L. K., Xu, C. S., Januszewski, M., Lu, Z., Takemura, S., Hayworth, K. J., Huang, G. B., Shinomiya, K., Maitlin-Shepard, J., Berg, S., Clements, J., Hubbard, P. M., Katz, W. T., Umayam, L., Zhao, T., Ackerman, D., Blakely, T., Bogovic, J., Dolafi, T., ... Plaza, S. M.

- (2020). A connectome and analysis of the adult *Drosophila* central brain. *eLife*, 9, e57443. <https://doi.org/10.7554/eLife.57443>
- Schmitt, S., Evers, J. F., Durch, C., Scholz, M., & Obermayer, K. (2004). New methods for the computer-assisted 3-D reconstruction of neurons from confocal image stacks. *NeuroImage*, 23(4), 1283–1298. <https://doi.org/10.1016/j.neuroimage.2004.06.047>
- Seelig, J. D., & Jayaraman, V. (2013). Feature detection and orientation tuning in the *Drosophila* central complex. *Nature*, 503(7475), 262–266. <https://doi.org/10.1038/nature12601>
- Seelig, J. D., & Jayaraman, V. (2015). Neural dynamics for landmark orientation and angular path integration. *Nature*, 521(7551), 186–191. <https://doi.org/10.1038/nature14446>
- Shiozaki, H. M., & Kazama, H. (2017). Parallel encoding of recent visual experience and self-motion during navigation in *Drosophila*. *Nature Neuroscience*, 20(10), 1395–1403. <https://doi.org/10.1038/nn.4628>
- Shiozaki, H. M., Ohta, K., & Kazama, H. (2020). A multi-regional network encoding heading and steering maneuvers in *Drosophila*. *Neuron*, 106(1), 126–141.e5. <https://doi.org/10.1016/j.neuron.2020.01.009>
- Staudacher, E. (1998). Distribution and morphology of descending brain neurons in the cricket *Gryllus bimaculatus*. *Cell and Tissue Research*, 294, 187–202. <https://doi.org/10.1007/s004410051169>
- Staudacher, E., & Schildberger, K. (1998). Gating of sensory responses of descending brain neurones during walking in crickets. *Journal of Experimental Biology*, 201, 559–572.
- Staudacher, E. M. (2001). Sensory responses of descending brain neurons in the walking cricket, *Gryllus bimaculatus*. *Journal of Comparative Physiology A*, 187(1), 1–17. <https://doi.org/10.1007/s003590000171>
- Steinbeck, F., Adden, A., & Graham, P. (2020). Connecting brain to behaviour: A role for general purpose steering circuits in insect orientation? *Journal of Experimental Biology*, 223, jeb212332. <https://doi.org/10.1242/jeb.212332>
- Stone, T., Webb, B., Adden, A., Weddig, N. B., Honkanen, A., Templin, R., Wcislo, W., Scimeca, L., Warrant, E., & Heinze, S. (2017). An anatomically constrained model for path integration in the bee brain. *Current Biology*, 27(20), 3069–3085.e11. <https://doi.org/10.1016/j.cub.2017.08.052>
- Strauss, R. (2002). The central complex and the genetic dissection of locomotor behaviour. *Current Opinion in Neurobiology*, 12(6), 633–638. [https://doi.org/10.1016/S0959-4388\(02\)00385-9](https://doi.org/10.1016/S0959-4388(02)00385-9)
- Suver, M. P., Matheson, A. M. M., Sarkar, S., Damiata, M., Schoppik, D., & Nagel, K. I. (2019). Encoding of wind direction by central neurons in *Drosophila*. *Neuron*, 102(4), 828–842. <https://doi.org/10.1016/j.neuron.2019.03.012>
- Träger, U., & Homberg, U. (2011). Polarization-sensitive descending neurons in the locust: Connecting the brain to thoracic ganglia. *Journal of Neuroscience*, 31(6), 2238–2247.
- Träger, U., Wagner, R., Bausenwein, B., & Homberg, U. (2008). A novel type of microglomerular synaptic complex in the polarization vision pathway of the locust brain. *Journal of Comparative Neurology*, 506(2), 288–300. <https://doi.org/10.1002/cne.21512>
- Triphan, T., Poeck, B., Neuser, K., & Strauss, R. (2010). Visual targeting of motor actions in climbing *Drosophila*. *Current Biology*, 20(7), 663–668. <https://doi.org/10.1016/j.cub.2010.02.055>
- Turner-Evans, D., Wegener, S., Rouault, H., Franconville, R., Wolff, T., Seelig, J. D., Druckmann, S., & Jayaraman, V. (2017). Angular velocity integration in a fly heading circuit. *eLife*, 6, e23496. <https://doi.org/10.7554/eLife.23496>
- Vitzthum, H., & Homberg, U. (1998). Immunocytochemical demonstration of locust tachykinin-related peptides in the central complex of the locust brain. *Journal of Comparative Neurology*, 390(4), 455–469. [https://doi.org/10.1002/\(sici\)1096-9861\(19980126\)390:4<455::aid-cne1>3.0.co;2-#](https://doi.org/10.1002/(sici)1096-9861(19980126)390:4<455::aid-cne1>3.0.co;2-#)
- Vitzthum, H., Müller, M., & Homberg, U. (2002). Neurons of the central complex of the locust *Schistocerca gregaria* are sensitive to polarized light. *Journal of Neuroscience*, 22(3), 1114–1125. <https://doi.org/10.1523/JNEUROSCI.22-03-01114.2002>
- von Hadeln, J., Althaus, V., Häger, L., & Homberg, U. (2018). Anatomical organization of the cerebrum of the desert locust *Schistocerca gregaria*. *Cell and Tissue Research*, 374, 39–62. <https://doi.org/10.1007/s00441-018-2844-8>
- von Hadeln, J., Hensgen, R., Bockhorst, T., Rosner, R., Heidasch, R., Pegel, U., Quintero Pérez, M., & Homberg, U. (2020). Neuroarchitecture of the central complex of the desert locust: Tangential neurons. *Journal of Comparative Neurology*, 528(6), 906–934. <https://doi.org/10.1002/cne.24796>
- Williams, J. L. D. (1975). Anatomical studies of the insect central nervous system: A ground-plan of the midbrain and an introduction to the central complex in the locust, *Schistocerca gregaria* (Orthoptera). *Journal of Zoology*, 176, 67–86. <https://doi.org/10.1111/j.1469-7998.1975.tb03188.x>
- Wolff, T., & Rubin, G. M. (2018). Neuroarchitecture of the *Drosophila* central complex: A catalog of nodulus and asymmetrical body neurons and a revision of the protocerebral bridge catalog. *Journal of Comparative Neurology*, 526(16), 2585–2611. <https://doi.org/10.1002/cne.24512>
- Zittrell, F., Pfeiffer, K., & Homberg, U. (2020). Matched-filter coding of sky polarization results in an internal sun compass in the brain of the desert locust. *Proceedings of the National Academy of Sciences of the United States of America*, 117(41), 25810–25817. <http://doi.org/10.1073/pnas.2005192117>
- Zorović, M., & Hedwig, B. (2011). Processing of species-specific auditory patterns in the cricket brain by ascending, local, and descending neurons during standing and walking. *Journal of Neurophysiology*, 105(5), 2181–2194. <https://doi.org/10.1152/jn.00416.2010>
- Zorović, M., & Hedwig, B. (2013). Descending brain neurons in the cricket *Gryllus bimaculatus* (de Geer): Auditory responses and impact on walking. *Journal of Comparative Physiology A*, 199(1), 25–34. <https://doi.org/10.1007/s00359-012-0765-7>

**How to cite this article:** Hensgen, R., Göthe, J., Jahn, S., Hümmert, S., Schneider, K. L., Takahashi, N., Pegel, U., Gotthardt, S., & Homberg, U. (2021). Organization and neural connections of the lateral complex in the brain of the desert locust. *Journal of Comparative Neurology*, 529(15), 3533–3560. <https://doi.org/10.1002/cne.25209>

## Appendix

### Zusätzliche Publikationen

Die nachstehenden Veröffentlichungen und Manuskripte sind nicht Teil meiner Dissertation, sollen hier jedoch auch Erwähnung finden, da ich während meiner Zeit als Doktorandin meinen Beitrag zu diesen leistete.

#### **A three-dimensional atlas of the honeybee central complex, associated neuropils and peptidergic layers of the central body**

Kaiser, A., **Hensgen, R.**, Tschirner, K., Beetz, E., Wüstenberg, H., Pfaff, M., Mota, T., Pfeiffer, K.

Eingereicht am 11.03.2022 beim *Journal of Comparative Neurology*

Mein Beitrag:

- Durchführung der immunhistochemischen Färbungen für die Erstellung des 3D Standards des Zentralkomplexes der Honigbiene

#### **Receptive field structures for two celestial compass cues at the input stage of the central complex in the locust brain (2022)**

Takahashi, N., Zittrell, F., **Hensgen, R.**, Homberg, U.

*Journal of Experimental Biology*, 225:jeb243858. doi: 10.1242/jeb.243858

Mein Beitrag:

- Durchführung von sieben intrazellulären Ableitungen zur morphologischen Auswertung und statistischen Analyse der Physiologie

#### **A unified platform to manage, share, and archive morphological and functional data in insect neuroscience (2021)**

Heinze, S., el Jundi, B., Berg, B. G., Homberg, U., Menzel, R., Pfeiffer, K., **Hensgen, R.**, Zittrell, F., Dacke, M., Warrant, E., Pfuhl, G., Rybak, J., Tedore, K.

*eLife*.10:e65376. doi: 10.7554/eLife.65376

Mein Beitrag:

- Bereitstellung von morphologischen Datensätzen und Testung der Datenbank

**Orcokinin in the central complex of the locust *Schistocerca gregaria*: Identification of immunostained neurons and colocalization with other neuroactive substances (2020)**

Homberg, U., **Hensgen, R.**, Rieber, E., Seyfarth, J., Kern, M., Dippel, S., Dirksen, H., Spänig, L., Kina, Y. P.

*Journal of Comparative Neurology* 529:1876-1894. doi: 10.1002/cne.25062

Mein Beitrag:

- Mitentwicklung und Auswertung von immunzytochemischen Färbungen für Abbildung 8c-e, 10 und 11
- Anfertigung von Abbildung 8c-e und 9-11

**Neuroarchitecture of the central complex in the brain of the honeybee: Neuronal cell types (2020)**

**Hensgen, R.**, England, L., Homberg, U., Pfeiffer, K.

*Journal of Comparative Neurology* 529:159-186

Mein Beitrag:

- Anfertigung des Manuskriptes in Zusammenarbeit mit Prof. Dr. Keram Pfeiffer auf der Basis von Daten, die ich größtenteils während meiner Masterarbeit erhoben habe

**Neuroarchitecture of the central complex of the desert locust: Tangential neurons (2019)**

von Hadeln, J., **Hensgen, R.**, Bockhorst, T., Rosner, R., Heidasch, R., Pegel, U., Quintero Pérez, M., Homberg, U.

*Journal of Comparative Neurology* 528:906-934

Mein Beitrag:

- Anfertigung von 2-dimensionalen Rekonstruktionen für Abbildung 3c,d,f, 4a, 6e, 7f, 8c, 11a, 13b, 15c,d
- Anfertigung von 3-dimensionalen Darstellungen für Abbildung 15c,d



## Curriculum vitae

Name Ronja Hensgen  
Address Hochstr. 31  
61130 Nidderau  
Germany  
Email ronja.hensgen@gmail.com  
Phone +49 177 3143936

### *Education*

---

- Since 12/2015**      **Philipps-University Marburg**  
Graduate student in Animal Physiology  
Laboratory of Prof. Dr. Uwe Homberg
- 10/2011-09/2014**    **Philipps-University Marburg**  
Master of Science in Molecular and Cellular Biology  
Laboratory of Dr. Keram Pfeiffer  
Title of thesis: "The morphology of neurons of the central complex of the honeybee *Apis mellifera*"
- 10/2008-09/2011**    **Philipps-University Marburg**  
Bachelor of Science  
Laboratory of Dr. Christian Wegener  
Title of thesis: "Anatomical identification and characterization of CCAP neurons in the brain of *Drosophila melanogaster*"

### *Work experience (scientific assistance)*

---

- 10/2021-current**    **Lund University**  
Project assistant  
Functional Zoology and Lund Vision Group  
Data administration and analysis
- 06-07/2016**        **Philipps-University Marburg**  
Graduate assistant  
Laboratory of Prof. Dr. Uwe Homberg  
Supervision of master students during their practical courses
- 10/2014 –02/2015**   **Johannes-Gutenberg University of Mainz**  
Graduate assistant  
Laboratory of Dr. Werner Kilb  
Performing whole-cell patch-clamp recordings from acute brain slices of mice



**04/2011, 04/2014**     **Philipps-University Marburg**  
Graduate assistant  
Laboratory of Prof. Dr. Uwe Homberg  
Supervision of bachelor students during their practical courses

**11/2011**             **Philipps-University Marburg**  
Graduate assistant of Dr. Carsten Heuer  
Supervision of bachelor students during their practical courses

### *Methodological expertise*

---

|                           |   |
|---------------------------|---|
| <b>Computer software</b>  | Amira 3D visualization<br>ImageJ<br>Adobe Photoshop & Illustrator<br>Affinity Photo & Design<br>Microsoft office  |
| <b>Laboratory methods</b> | Intracellular recordings in insects<br>Iontophoretic dye injections in insects<br>Confocal laser scanning microscopy<br>Immunofluorescence staining<br>Patch-clamp recordings in acute brain slices of mice |

### *Additional qualifications*

---

**06-07/2017**             Completion of a two-month practical course: Neural Systems & Behavior at MBL, Woods Hole, MA, USA

**09/2014**                Completion of a 40-hour course on Laboratory Animal Science (category B–FELASA)

### *Publications*

---

**Hensgen, R.**, Zittrell, F., Pfeiffer, K., Homberg, U. (2022). Performance of polarization-sensitive neurons of the locust central complex at different degrees of polarization. *J Comp Physiol A Neuroethol Sens Neural Behav Physiol*. Advance online publication. doi: 10.1007/s00359-022-01545-2

Takahashi, N., Zittrell, F., **Hensgen, R.**, Homberg, U. (2022) Receptive field structures for two celestial compass cues at the input stage of the central complex in the locust brain. *J Exp Biol*. 225:jeb243858. doi: 10.1242/jeb.243858

Heinze, S., el Jundi, B., Berg, B. G., Homberg, U., Menzel, R., Pfeiffer, K., **Hensgen, R.**, Zittrell, F., Dacke, M., Warrant, E., Pfuhl, G., Rybak,

J., Tedore, K. (2021) A unified platform to manage, share, and archive morphological and functional data in insect neuroscience. *eLife*. 10:e65376. doi: 10.7554/eLife.65376

**Hensgen, R.**, Göthe, J., Jahn, S., Hümmert, S., Schneider, K. L. Takahashi, N., Pegel, U., Gotthardt, S., Homberg, U. (2021) Organization and neural connections of the lateral complex in the brain of the desert locust. *J Comp Neurol*. 529:3533-3560. doi: 10.1002/cne.25209

Homberg, U., **Hensgen, R.**, Rieber, E., Seyfarth, J., Kern, M., Dippel, S., Dircksen, H., Spänig, L., Kina, Y. P. (2020) Orcokinin in the central complex of the locust *Schistocerca gregaria*: Identification of immunostained neurons and colocalization with other neuroactive substances. *J Comp Neurol*. 529:1876-1894. doi: 10.1002/cne.25062

**Hensgen, R.**, England, L., Homberg, U., Pfeiffer, K. (2020) Neuroarchitecture of the central complex in the brain of the honeybee: Neuronal cell types. *J Comp Neurol*. 529:159-186. doi:10.1002/cne.24941

Von Hadeln, J., **Hensgen, R.**, Bockhorst, T., Rosner, R., Heidasch, R., Pegel, U., Quintero Pérez, M., Homberg, U. (2019) Neuroarchitecture of the central complex of the desert locust: Tangential neurons. *J Comp Neurol*. 528:906-934. doi: 10.1002/cne.24796

Selcho, M., Mühlbauer, B., **Hensgen, R.**, Shiga, S., Wegener, C., Yasuyama, K. (2018) Anatomical characterization of PDF1-tri neurons and peptidergic neurons associated with eclosion behavior in *Drosophila*. *J Comp Neurol*. 526:1307-1328. doi: 10.1002/cne.24408

Held, M., Berz, A., **Hensgen, R.**, Muenz, T. S., Scholl, C., Rössler, W., Homberg, U., Pfeiffer, K. (2016) Microglomerular synaptic complexes in the sky-compass network of the honeybee connect parallel pathways from the anterior optic tubercle to the central complex. *Front Behav Neurosci*. 10:186. doi: 10.3389/fnbeh.2016.00186

### ***Conference contributions***

---

**Hensgen, R.**, Jahn, S., Schneider, K. L., Homberg, U. (2019) Organization of the lateral complex in the brain of the desert locust *Schistocerca gregaria* – single-cell analyses and neuropil structure. 13<sup>th</sup> Meeting of the German Neuroscience Society, Poster T14-3B

**Hensgen, R.**, Pfeiffer, K., Homberg, U (2018) Temporal dynamics of *E*-vector responses in neurons of the central

complex of the desert locust *Schistocerca gregaria*. Spring Meeting of the Arthropod Neuroscience Network, Altleiningen, Poster 60

**Hensgen, R., Pfeiffer, K., Homberg, U. (2017)**

Temporal dynamics of E-vector responses of CL1 neurons of the desert locust *Schistocerca gregaria*. 12<sup>th</sup> Göttingen Meeting of the German Neuroscience Society, Poster T14-2D

**Hensgen, R., Pfeiffer, K (2016)**

Morphological characterization of neurons of the central complex of the honeybee *Apis mellifera*, 109. Annual Meeting of the German Zoological Society, Kiel, Poster PP-NB-18

Selcho, M., Yasuyama, K., **Hensgen, R.**, Wegener, C (2012)

Anatomy of peptidergic neurons involved in *Drosophila* eclosion. 2012 European Fly Neurobiology Meeting, Padua, Italy, Poster 199

**Hensgen, R., Selcho, M., Wegener, C (2011)**

Anatomical identification and characterization of CCAP neurons in the brain of *Drosophila melanogaster*, 104. Annual Meeting of the German Zoological Society, Saarbrücken, Poster NB.25

## Danksagung

An dieser Stelle möchte ich allen danken, die mich während der Arbeit an meiner Promotion unterstützt und begleitet haben.

Zunächst möchte ich mich bei Prof. Dr. Uwe Homberg und Prof. Dr. Keram Pfeiffer für die Bereitstellung des Promotionsthemas und die Möglichkeit zur Promotion bedanken. Ich danke Euch herzlich für die gute Zusammenarbeit und die Unterstützung bei der Ausgestaltung der verschiedenen Projekte. Uwe, vielen Dank für das Teilen Deines immensen Wissensschatzes, Deine unbeirrbare Geduld und dafür, dass ich Teil Deiner fantastischen Arbeitsgruppe sein durfte. Keram, vielen Dank, dass Du mir die wundervolle Welt der Elektrophysiologie näher gebracht hast, für Dein Vertrauen in meine Fähigkeiten, die Hilfe bei jeglichen Fragen und die Ermutigungen auch in frustrierenden Zeiten.

Ich danke Prof. Dr. Monika Hassel und Prof. Dr. Christian Helker herzlich für die Bereitschaft Mitglieder meiner Prüfungskommission zu sein und meine Arbeit zu begutachten.

Besonderer Dank gilt allen Mitgliedern der Arbeitsgruppe Homberg, Schachtner und Pfeiffer für den fachlichen und freundschaftlichen Austausch der letzten Jahre, der zum Gelingen dieser Arbeit beigetragen hat. Großer Dank gilt Dr. Frederick Zittrell für die Bereitstellung der Auswerteskripte. Ohne ihn wäre meine Arbeit in dieser Form nicht möglich gewesen. Zudem möchte ich Martina Kern herzlich für ihre Hilfe bei der Laborarbeit, und Dr. Joss von Hadeln für seine Unterstützung bei der Auswertung anatomischer Daten danken. Viel Dank gilt auch Dr. Erich Staudacher und Dr. Björn Trebels für ihre Hilfe bei der Bewältigung technischer Probleme. Stefanie Jahn und Vanessa Althaus möchte ich herzlich für die Unterstützung jeglicher Art und die zahlreichen Gespräche danken. Ihr seid mir alle nicht nur wunderbare Kollegen gewesen, sondern auch Freunde geworden und dafür danke ich Euch sehr.

Bei meinen Freundinnen, Dr. Martina Held, Dr. Annuska Berz und Tanja Heinloth möchte ich mich herzlichst für ihre Unterstützung während der letzten Jahre bedanken. Ich danke Dir, Tina, auch für das Korrekturlesen dieser Arbeit und ich danke Euch von Herzen für die Motivation, Eure Ermutigungen und Eure Hilfe bei der Klärung allerlei Fragen. Für das Einbringen einer anderen Sichtweise und für seine Geduld möchte ich zudem meinem Freund, Philipp Kooock, danken.

Schließlich gilt mein größter Dank meinen Eltern und meinen Geschwistern. Danke, dass Ihr auch dann an mich geglaubt habt, wenn ich es nicht tat. Vielen Dank für Eure grenzenlose Unterstützung während der letzten Jahre und für all die schönen Ablenkungen.

## Erklärung

Ich versichere hiermit, dass ich meine Dissertation

### **Anatomical and functional characterization of the orientation network in the central and lateral complex of the desert locust *Schistocerca gregaria***

Anatomische und funktionelle Charakterisierung des Orientierungsnetzwerkes im Zentralkomplex und lateralen Komplex der Wüstenheuschrecke (*Schistocerca gregaria*)

selbstständig, ohne unerlaubte Hilfe angefertigt und mich dabei keiner anderen als der von mir ausdrücklich bezeichneten Quellen und Hilfsmittel bedient habe.

Diese Dissertation wurde in der jetzigen oder einer ähnlichen Form noch bei keiner anderen Hochschule eingereicht und hat noch keinen sonstigen Prüfungszwecken gedient.

---

Ort, Datum

---

Ronja Hensgen, M.Sc.